NUCLEATION MECHANISM OF CRYSTAL FORMATION DURING ANTISOLVENT OR COOLING INDUCED CRYSTALLISATION

Anna Jawor-Baczynska

"Thesis submitted to Chemical and Process Engineering Department University of Strathclyde in accordance with the requirements for degree of Doctor of Philosophy".

2010

This thesis is the result of the author original research. It has been composed by the author and has been previously submitted for examination which has led to the award of a degree.

Signed:

Date:

Acknowledgements

I would like to express my grateful thank to all people who I met and worked with during my PhD project.
My supervisor dr Jan Sefcik for all his support and supervision through the process of this work.
My special gratitude goes to dr Barry Moore for his support, guidance and useful discussions.
All my colleagues and friends from Chemical Engineering Department Fiona, Andrew, Kasia, Karina, Peter, Alexander, Rui, Nadeem and Chemistry Department Anna, Cheska, Ahmed and Lee. Thanks to them time which I spent in Strathclyde was wonderful.

I would like to thank all my friends and family in Poland, especially my parents for their love and moral support during my study.
Finally, I would like to thank my husband Dariusz for his help, moral support and faith in me during my PhD experience.

List of abbreviations used in the text

A - Absorbance
CIJ - Confined Impinging Jet mixer
c - Speed of light (300 000 km/s)
DLS - Dynamic Light Scattering
DOSY - Diffusion Ordered Spectroscopy
D - Diffusion coefficient (m^2/s)
ΔG - Gibbs free energy (J/mol)
HPLC - High Performance Liquid Chromatography
H - Planck constant (6.626×10^{-34} J·s)
J - Rate of nucleation (number of nuclei formed per unit time per unit volume)
k_B - Boltzmann constant (1.3805×10^{-23} J/K)
NMR - Nuclear Magnetic Resonance
PCMCs - Protein Coated Microcrystals
PFG NMR - Pulsed-field Gradient NMR
PS - Polystyrene
PTFE - Polytetrafluoroethylene
SAXS - Small Angle X-ray Scattering
SEM - Scanning Electron Microscopy
SLS -Static Light Scattering
S - Supersaturation
WAXD - Wide Angle X-ray Scattering
γ - Interfacial tension
λ - Wavelenght (nm)
η - Viscosity (Pa*s)

Abstract

This project studied the nucleation mechanism of crystal formation during antisolvent or cooling crystallisation of simple amino acids: D,L-valine and glycine. These amino acids can co-precipitate with proteins to form Protein Coated Microcrystals (PCMCs) in which the crystals create a solid support and the biomacromolecules cover their surface while remaining in a native state. The understanding of the formation mechanism of small microcrystals would help to better control and manage the process which leads to ordered attachment of biomacromolecules on their surfaces.

Spectrophotometry, ^{1}H nuclear magnetic resonance (NMR), dynamic light scattering (DLS) and optical microscopy were used to probe the evolution of the system from the transparent solution to a suspension of microcrystals.

The nucleation mechanism of antisolvent crystallisation was found to involve formation of a transparent nanoemulsion composied of sub-micron valine-rich liquid nanodroplets with an average size and size distribution depending on supersaturation and the mixing conditions used during sample preparation. The supersaturated solutions prepared by cooling crystallisation, without agitation produced smaller nanodroplets and resulted in formation of only a few large crystals with an extremely slow crystallisation rate compared to samples with identical composition prepared by antisolvent crystallisation.

The following nucleation mechanism of amino acids crystals is proposed:

- dissolution of amino acid into an aqueous/2-propanol mixture at concentration close to saturation results in spontaneous formation of a thermodynamically stable system consisting of amino acid rich liquid nanodroplets dispersed in amino acid solution,
- above a particular amino acid composition (consistent with the crystal solubility limit) the dispersed nanodroplets become metastable and shear induced coalescence of nanodroplets can provide access to a fast crystallisation pathway (non-classical),
- in the absence of shear the nanodroplets are colloidally-stable and crystallisation follows a much slower pathway (classical).

The spontaneous formation of solute-rich nanodroplets below the crystalline saturation limit as well as formation of metastable solute–rich nanodroplets above this limit provides a paradigm shift which can be potentially used to develop fundamental understanding of non-classical crystallisation phenomena. It will be crucial for better design and control of crystallisation processes in pharmaceutical applications.

TABLE OF CONTENTS

LIST OF FIGURES

LIST OF TABLES

1. Introduction.

Crystallisation processes are widely used for particle formation, purification and separation in the chemical and pharmaceutical industry. Phase separation of a solute from supersaturated solution to form a crystalline phase is a basic premise of equilibrium thermodynamics and is commonly proposed to involve two main steps: nucleation, the birth of a stable crystal nucleus, and crystal growth, the addition of material onto an existing crystal lattice. The supersaturation is an essential requirement for all crystallisation operations and a solution can only nucleate when it is supersaturated. A supersaturated solution is one in which the concentration of solute in solution exceeds its thermodynamic solubility limit. The solubility represents the maximum concentration of crystalline solute that can be dissolved in a specific solvent at a given temperature and pressure. The supersaturation S can be expressed as a ratio of the actual concentration C to the solubility (equilibrium) concentration C_{eq}: $S = \frac{C}{C_{eq}}$.

Figure1.1 shows a hypothetical solubility-supersolubility diagram which is divided into three regions:

- the undersaturated (stable) region where present crystals will dissolve,
- the supersaturated (metastable) region in which crystals will grow but nucleation is kinetically controlled and may be negligible close to solubility line,
- the supersaturated (labile) region in which a crystals will nucleate spontaneously.

The supersaturated metastable region (Figure 1.1) is sometimes divided by a so-called supersolubility line into two areas: a) extremely slow nucleation (below the supersolubility, but above the solubility line, often called “metastable zone”), and b) appreciable nucleation (above the supersolubility line, but still kinetically controlled, i.e. below the metastability line). The supersolubility line is a kinetically described and depends on sample preparation methods, mixing conditions etc. ***(Jones 2002).***

A solution with starting composition at point A (undersaturated) can crystallise by following three main pathways (Figure 1.1):

a) changing temperature – e.g. cooling crystallisation without loss of solvent,
b) changing solute concentration –e.g. solvent evaporation at constant temperature,
c) changing solvent composition – e.g. antisolvent crystallisation, which changes solubility of solute in the new solvent mixture.

In practice, a combination of all these techniques is commonly employed ***(Davey and Garside 2000; Jones 2002; Mullin 1993).***

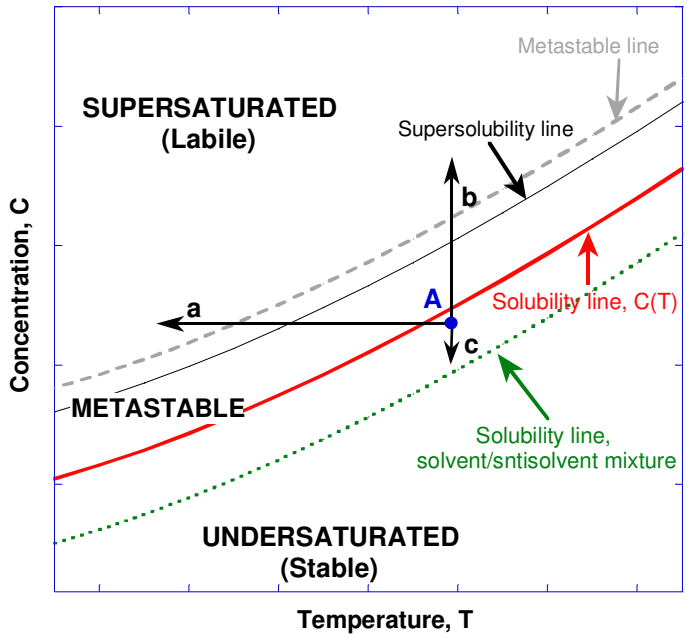

Figure 1.1 The solubility-supersolubility diagram.

Nucleation is a central part of all types of crystallisation processes and commonly is divided into two classes: ***primary***, when the supersaturated system does not contain any crystalline matter, and ***secondary,*** when nuclei are generated in the vicinity of crystals present in a supersaturated solution. The primary nucleation process can be broken into two main categories: ***homogeneous*** and ***heterogeneous***. Homogeneous primary nucleation occurs only in the absence of any solid matter in the supersaturated solution whereas foreign particles induce heterogeneous nucleation. The structure of critical nucleus is generally unknown. It could be a miniature crystal, nearly perfect in form (as predict by classical nucleation theory). Or it could be a rather diffuse body with molecules or solvated ions in a

state not too different from that in the bulk solution, with no clearly defined surface (non-classical nucleation theory) ***(Davey and Garside 2000; Erdemir et al. 2009; Mullin 1993).*** The small size of a critical nucleus, which is thought to typically contain from 100 to 1000 units (atoms, ions, molecules) is not easly accessible by most current experimental techniques. This makes it difficult to study nucleation mechanisms and develop more accurate description of the process ***(Erdemir et al. 2009).***

1.1 Classical nucleation theory

The classical theory of nucleation is based on the condensation of a vapour to a liquid and is the simplest and most widely used theory that describes nucleation mechanisms. Although nucleation has been studied since the 18th century, the theoretical formulation and understanding of this process was found surprisingly difficult. According to the classical nucleation theory in the superasturation region the first short-lived sub-nuclei are formed, which eventually will transform and build up a crystalline lattice structure. The sub-nuclei are extremely unstable (high free energy structure) and many of them fail to achieve stability and simply redisolve. However, if the sub-nuclei grow beyond a certain size (critical size), it becomes stable and continue to grow. The classical theory of nucleation was formulated at the end of the 19th century by Gibbs, who defined the free energy change required for nucleus formation (ΔG) as the sum of the free energy change for the phase transformation (ΔG_v) and the free energy change for the formation of a surface (ΔG_s) (equation 1.1).

$$\Delta G = \Delta G_v + \Delta G_s \qquad (1.1)$$

ΔG_s is a positive quantity and is related to the nucleus size by the relationship $\Delta G_s = 4\pi r^2 \gamma$, where γ is the interfacial tension (between the developing crystalline surface and the superastaurated solution), and r is the radius of the nucleus.

ΔG_v is a negative quantity in supersaturated solution and is realated to the nucleus size by the relationship $\Delta G_v = \frac{4}{3}\pi r^3 \Delta G_v$ where ΔG_v is the free energy change of the transformation per unit of volume, and r is the radius of the nucleus. So, the free energy required for phase transformation (critical nucleus formation) can be expressed by equation 1.2:

$$\Delta G = 4\pi r^2 \gamma + \frac{4}{3}\pi r^3 \Delta G_v \qquad (1.2)$$

For a small aggregate (sub-nucleus) the free energy *(ΔG)* increases as the size of nucleus *(r)* increases until a maximum in Gibbs energy *(ΔG_{crit})* is reached, which represents the formation of the "critical nucleation entity" (Figure 1.2). The maximum value of ΔG_{crit} for a spherical cluster is obtained by maximizing the equation (1.2), $\frac{\partial(\Delta G)}{\partial(r)} = 0$.

$$\frac{\partial(4\pi r^2\gamma + \frac{4}{3}\pi r^3 \Delta G_v)}{\partial(r)} = 8\pi r\gamma + 4\pi r^2 \Delta G_v = 0 \qquad (1.3)$$

The critical size which represents the minimum size of the stable nucleus and could be obtained from equation (1.3) is:

$$r_c = \frac{-2\gamma}{\Delta G_v} \qquad (1.4)$$

where ΔG_v is negative quantity.

The critical free energy of the system could be calculated from equation (1.2) and (1.4)

$$\Delta G_{crit} = \frac{4}{3}\pi \cdot \gamma \cdot r_c^2 \qquad (1.5)$$

Nucleus smaller than critical size *(r_c)* will dissolve and particles larger than a critical size *(r_c)* will continue to grow because this leads to a reduction in their free energy ***(Davey and Garside 2000; Erdemir et al. 2009; Mullin 1993).***

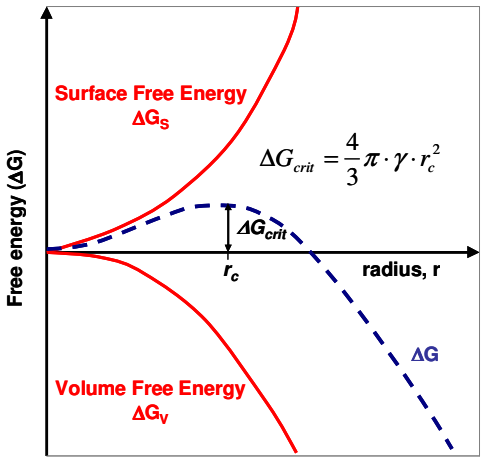

Figure 1.2 The classical nucleation process, free energy diagram.

The main assumption of the classical nucleation theory is that the small nucleus has the same thermodynamic properties as the final crystallised product (crystal) and is created by

attachment of atoms/ions/molecules to a primary particle (nucleus) forming a single crystal (Figure 1.3).

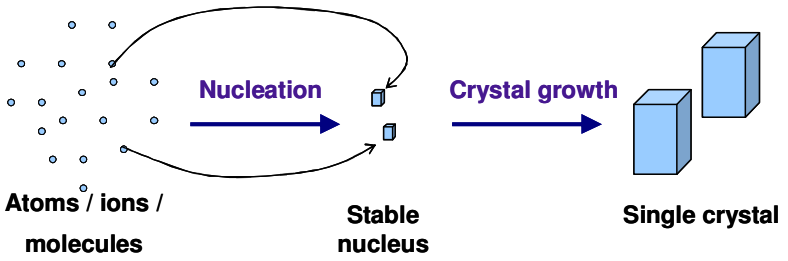

Figure 1.3 Schema of the classical nucleation mechanism.

According to equation (1.6) the volume free energy and then the free energy of nucleus formation (*ΔG*) also depend on the temperature of supercooling ΔT :

$$\Delta G_v = \frac{\Delta H_f \Delta T}{T^*} \qquad (1.6)$$

where, T^* is the solid-liquid equilibrium temperature expressed in kelvins, ΔH_f is the latent heat of fusion and $\Delta T = T^* - T$ is the supercooling. The relationships between the size of the critical nucleus (r_c) and the free energy (ΔG_V) for two different temperatures are shown in Figure 1.4.

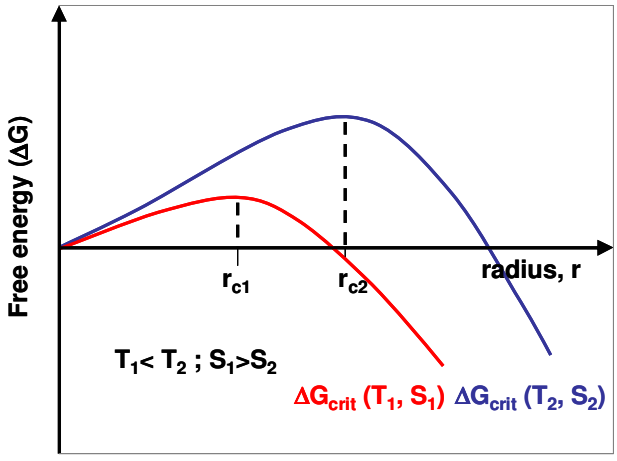

Figure 1.4 Effect of temperature and supersaturation on the size and free energy of formation of a critical nucleus.

The size of the critical nucleus increases with temperature in accordance with $r_c \propto (\Delta T)^{-1}$ and $\Delta G_{crit} \propto (\Delta T)^{-2}$. However, there is an optimum temperature for nucleation of a given system and excessive supercooling does not help nucleation. The physical properties of a solution change with temperature (e.g. density, viscosity) and when the system is highly viscous further cooling may not lead to nuclei formation. To induce nucleation the temperature would typically have to be increased to a value in the optimum region ***(Mullin 1993).***

The rate of nucleation, J, which is equal to the number of nuclei formed per unit time per unit volume, can be expressed in the form of the Arrhenius reaction rate equation as:

$$J = A \exp\left(\frac{-\Delta G_{crit}}{k_B T} \right) \qquad (1.7)$$

where k_B is the Boltzmann constant and A is the pre-exponential factor.
For homogeneous nucleation the pre-exponential factor derives form molecular collision frequency and in theory it is of the order of 10^{30} $cm^{-3}s^{-1}$ but in reality it is very difficult to determine. Since the molecular mobility changes rapidly with temperature, the temperature dependence of the pre-exponential factor can be quite significant ***(Erdemir et al. 2009; Fokin and Zanotto 2000; Oxtoby and Kashchiev 1994).***

While classical nucleation theory allows (at least theoretically) calculation of nucleation rate and the critical size of a nucleus it does not consider molecular self-organisation. Since this is required for nucleus formation, it can be crucial for understanding and controlling the quality of the final crystalline product and size, purity, morphology, polymorphism and crystal structure ***(Davey and Garside 2000; Erdemir et al. 2009; Mullin 1993).***

1.2 Non-classical nucleation theory

Non-classical, two-step nucleation theory assumes large composition (density) fluctuations which cause the formation of a new liquid-like phase. The formation of a liquid-like intermediate phase is the first step of a nucleation process which decreases the free energy of the system (Figure 1.5). The liquid phase which is first created in solution can be in the form of droplets, small aggregates or amorphous domains, which rearrange subsequently to make more complex structures.

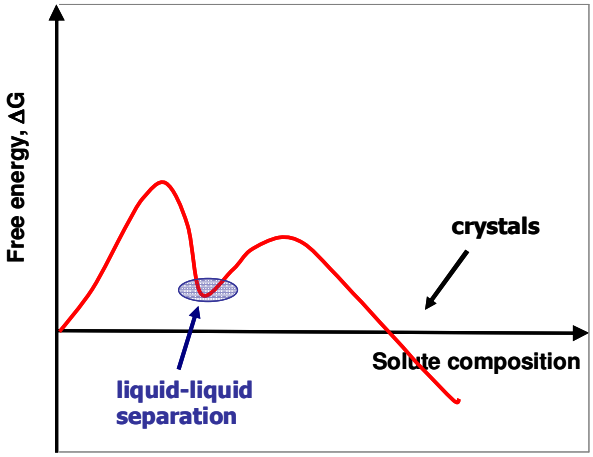

Figure 1.5 The non-classical (liquid-liquid separation) nucleation process, free energy diagram.

This two step non-classical nucleation pathway involves firstly a density fluctuation which creates a region of higher solute concentration leading to liquid-liquid separation (liquid-droplet, amorphous layers), secondly a series of complicated processes such as liquid droplet coalescence, aggregation, surface or volume nucleation and finally crystal growth (Figure 1.6).

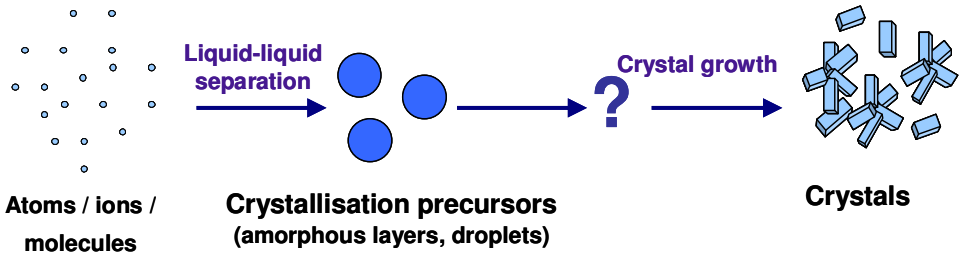

Figure 1.6 Schema of the non-classical (liquid-liquid separation) nucleation mechanism.

The intermediate pseudo-equilibrium steps of crystal formation mechanism (e.g. formation of stable nucleus “classical crystallisation theory” or stable dense – liquid phase “non-classical crystallisation theory”) should of course folow both the thermodynamic equilibrium theory.
If the system exists in equilibrium the chemical potential of a compound must be equal in every phase and system should agree with the Gibb’s phase rule. The thermodynamic phase equilibrium rule was proposed by Gibbs in the 1870s and describes the possible number of degrees of freedom *(F)* in a closed of system in terms of the maximum number of phases *(P)* and the number of compounds *(C)* equation 1.8.

$$P+F = C+2 \qquad (1.8)$$

The number of compounds *(C)* of the system is the minimum number of the chemical compounds required to define the composition of all phases in the system.
The number of phases *(P)* is the number of homogeneous, uniform state of the system.
The number of degrees of freedom *(F)* is variables like: pressure, temperature and composition of the system, which could be changed without changing the number of phase in the system.

In the one compound system *C=1*, the number of degrees of freedom *(F)* according to equation 1.8 is *F=3-P*. When the one compound *(C=1)* system exists only in one phase *(P=1),* the two variables (pressure and temperature) can be varied independently *(F=2).* If the system contains two phases *(P=2),* the number of degrees of freedom is reduced to one *(F=1)* and it is not possible to control temperature and pressure independently. For one component *(C=1)* and three phases system *(P=3)* the number of degrees of freedom is *0 (F=0),* and the three phases system exists only at a specific temperature and pressure (Figure 1.7a).

In the two compounds system *C=2* the number of degrees of freedom calculated from equation 1.8 is *F=4-P*. In the one phase system *(P=1)* in equilibrium three variables (temperature, pressure and composition) could be change independently *(F=3).* When the number of phases is increased to two (*P=2*) the number of degrees of freedom is 2 *(F=2)* and from this point only two variables can be controlled independently (Figure 1.5b).
When a liquid of composition a_1 is cooled to a_2, it enters to the two phase region 'Liquid + A'. At this temperature almost pure solid A begins to come out of solution and remaining liquid becomes richer in B. At point a_3 more of the solid A precipitates and the relative amount of the solid and liquid are given by the level of rule. At point a_4 there is less liquid than at a_3, and phase composition is given by eutectic point. At eutectic point liquid is freezes to give a two-phase system of almost pure A and almost pure B. At point a_5 the composition of the two-phases are given by a_5' and a_5''.

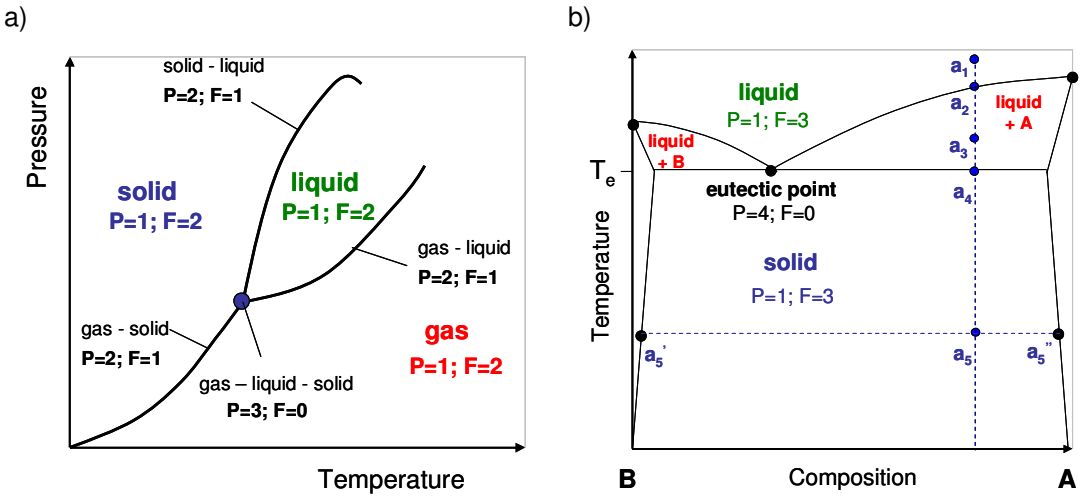

Figure 1.7 The equilibrium phase diagram, a) one compound system, b) two compounds system.

For the three compounds system *C=3* and number of degrees of freedom calculated from equation 1.8 is *F=5-P*. It means that two phases can exist in equilibrium and three variables can be changed in this system without changing the number of phases (temperature, pressure or composition of one compound) ***(Atkins 1986).***

In a typical crystallisation processes three or four component systems are widely used. The three components phase diagrams are usually presented as a triangular phase diagram (where every apex represents the pure compound) (Figure 1.8a), or a temperature /composition diagram (Figure 1.8b)

Figure 1.8a shows the three components system with one or two phases present in equilibrium ***(Atkins 1986).***

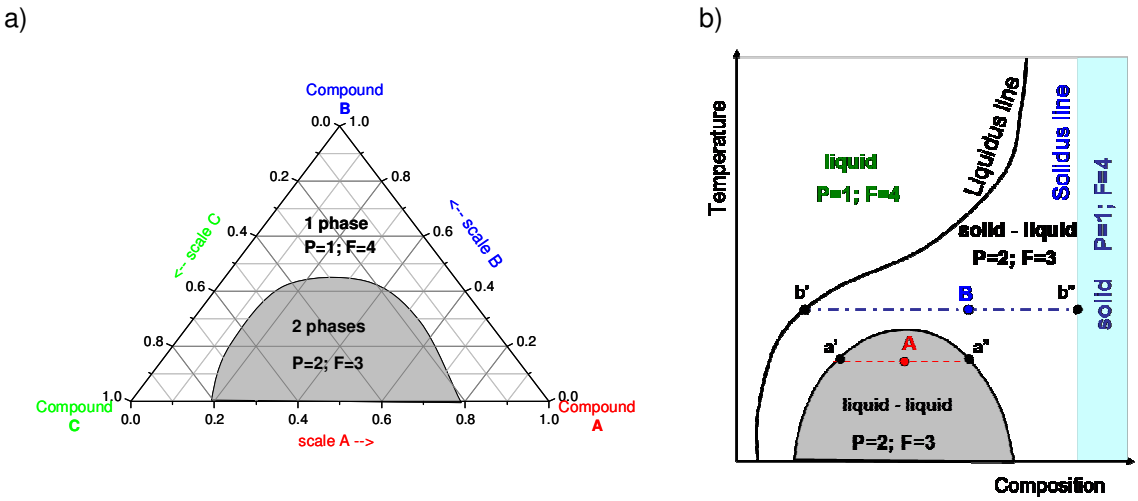

Figure 1.8 The equilibrium phase diagram, three compounts system, a) ternary diagram, b) temperature-composition diagram.

Figure 1.8 b shows a two phase system where a liquid-liquid split into two heterogeneous liquids occurs with one liquid phase of composition a' in equilibrium with a second liquid of composition represents by point a''. The point B represents the system in which the liquid phase with composition b' is in equilibrium with the crystalline b''. The crystallisation of protein is very often presented using temperature-composition graphs, with liquid-liquid separation region ***(Atkins 1986).***

1.3 Crystal nucleation mechanism

In the last twenty years significant effort has been made to better understand the mechanism of the nucleation process and scientists have used a wide variety of techniques to probe the relationship between molecular self-organization in solution and melts, formation of nuclei and the resulting crystal polymorphs. One of the first experimental results which seemed not to follow the classical nucleation theory was observed as a concentration gradient in supersaturated aqueous solutions of citric acid held in an isothermal column. Higher concentrations were measured at the bottom than the top ***(Mullin and Leci 1969).*** The authors suggested molecular clustering in the solution which preceded crystal formation (nucleation and growth). A two-step nucleation mechanism was proposed by Wolde and Frenkel who theoretically studied homogeneous nucleation in a Lennard-Jones system of short-range attraction using Monte Carlo technique. The authors found that far from the metastable critical point in the colloidal system the critical nucleus appearance followed a classical nucleation mechanism. However, around the metastable critical point large density fluctuations were observed, which caused formation of highly disordered liquid droplets and then formation of a crystalline nucleus inside droplets with a certain critical size ***(Rein den Wolde and Frenkel 1997).*** The two-step nucleation mechanism started to be a more popular theory and more theoretical studies have been reported in which a liquid-liquid separation intermediate pathway is revealed as a potential in crystallisation mechanism. The theoretical study of critical density fluctuations on the structure of the critical nucleus by Talanquer et al. revealed that characteristic temperatures close to the critical point are very sensitive to the structure of a phase diagram. Results have showed that at temperatures, slightly above the metastable critical point, nucleation proceeds through the formation of crystal-like nucleus, while at lower temperatures liquid-like phase separation occurs. Thus experiments carried out at temperatures slightly above the metastable critical point can speed up the rate of nucleation processes, but not the rate of crystal growth, and lowering temperatures will increase crystal growth more then the nucleation rate ***(Talanquer and Oxtoby 1998).*** Lomakin et al. studied liquid-solid transition in nuclei of protein crystals by

numerical simulation and showed that protein crystals nucleate by a two-step process. A nucleus first forms and grows as a disordered liquid-like aggregate. When the aggregate cluster reaches a critical size, crystal nucleation becomes possible ***(Lomakin et al. 2003).***

A further theoretical investigation of the kinetics of nucleation processes was reported by Kashchiev at al. The authors proposed the existence of a two step nucleation mechanism: involving firstly formation of a droplet of dense liquid and secondly crystallisation within the droplet upon ordering of a critical number of molecules. Their results revealed that crystal nucleation can be strongly delayed by the slow growth of the droplets and/or by the slow nucleation of the crystals in them and that the formation rate of the intermediate phase determined the number of nucleated crystals ***(Kashchiev et al. 2005).***

The non-classical pathway was also proposed for the crystallisation mechanism of small molecules and because a metastable dense-liquid state was found to be energetically favoured relative to the classical path it was suggetsted that intermediate liquid separation may be a generic phenomenon ***(Lutsko and Nicolis 2006).*** The rate of the steps: formation of an intermediate liquid phase and nucleation of crystalline particles depends on their respective free-energy barriers. Filobelo at al. studies revealed that crystal nucleation is 8-10 orders of magnitude slower than the formation of dense liquid droplets ***(Filobelo et al. 2005).*** Drews et al. proposed a mathematical model which described the kinetics of nucleation and crystal growth in the presence of non-ordered precursor particles. The authors made a simple model involving the formation of intermediate disordered particles followed by the nucleation of an ordered crystalline nucleus gradually within the primary particles ***(Drews et al. 2005).***

Liquid-liquid separation as a crystallisation intermediate step was first experimentally observed in the crystallisation of large molecules such as proteins. Vekilov et al. experimentally studied the nucleation rate of lysozyme crystals from supersaturated solution ***(Galkin and Vekilov 2000; Galkin and Vekilov 2001).*** The results showed the existence of a liquid phase at high protein concentration which strongly affected crystal nucleation kinetics. Nucleation rates under conditions that are close to the liquid-liquid separation boundary in the phase diagram of the protein solution are lower than expected for the given protein concentration and temperature. However, the nucleation kinetics for an experiment in the area slightly above this phase boundary are higher by up to a factor of 20 than the expected rate ***(Galkin and Vekilov 2000; Galkin and Vekilov 2001).*** Further investigation of metastable liquid protein clusters in super- and undersaturated solutions were studied using dynamic light scattering and atomic force microscopy. Results have demonstrated the existing submicron size clusters of dense liquid, metastable not only with respect to the solid phase, but also with respect to the low-concentration protein solution. In undersaturated solutions the clusters have a limited lifetime of several seconds, after which they decay into

the low-concentration solution. In supersaturated solution the clusters are metastable with respect to the crystalline solid phase and are a precursor to the formation of ordered structures. The size of the clusters seemed not to depend on protein concentration but increasing protein concentration increased the frequency of cluster detection. This suggests that a preferred cluster size exists ***(Gliko et al. 2005; Gliko et al. 2007; Vekilov 2009).*** Existence of the liquid-liquid separation process during the aggregation of lysozyme in aqueous solution was also observed experimentally using multi-angle static light scattering, dynamic light scattering, optical microscopy and diffusivity measurements ***(Heijna et al. 2007; Onuma and Kanzaki 2007; Poznanski et al. 2005).***

Aggregation of lysozyme in supersaturated solution using small angle neutron scattering (SANS) was studied by Niimura et al. The results showed two groups of aggregates in supersaturated lysozyme solution. The first with a radius greater than several hundreds Å and a second much smaller with a radius around 25-40Å. The structure of large aggregates did not change with time while the radius of the second aggregates increased with time and stopped when nucleation occurred, after which the size decreased ***(Niimura et al. 1995).***
The phase diagram of the protein-water system incluading the liquid-liquid phase was studied by Hass and Drenth. The phase diagram showed a metastable liquid-liquid immiscibility region, for certain parameters, and nucleation proceeds in two steps: first formation of small liquid droplets with high protein concentration and then small crystalline nuclei grow inside these droplets. The final protein form crystals covered by a thin liquid film containing a high protein concentration ***(Haas and Drenth 1999).***

As crystallisation process on small molecules have been studied in greater detail there have been an increasing number of reports of supersaturated systems that produce phases with liquid-like properties ***(Chen et al. 1998; Soh et al. 1995).*** A common finding from these studies has been that solutes associate to form clusters in supersaturated solutions. Davey et al. used SAXS and WAXD to study nucleation of molecular crystals from under-cooled benzamide and para-azoxyanisole melts and supersaturated aqueous solutions of urea, sucrose and citric acid in order to obtain evidence for the onset of long-range ordering before the appearance of crystallised structures. The results for melts revealed rapid formation of unstable but kinetically accessible phases. These were dimers, ribbons or ordered layers and were found to rapidly transform into the stable form providing a possible link between long-range position ordering observed in a liquid crystal and a nucleating crystal. Preassembled structures were not observed in supersaturated aqueous solutions of urea, sucrose and citric acid and the authors suggested that this could be because such states only have a very short life-time or else pass through a different

nucleation mechanism ***(Davey et al. 2002b).*** A combination of thermodynamic, structural and modelling approaches were used to better understand the solvent dependence of the nucleation of saccharin from acetone and ethanol solvents. These studies concluded that, in acetone solution, sacharin nucleation most likely arises from a monomeric species, while in ethanol it involves the assembly of dimers. The nature of solute-solvent interactions were shown to significantly impact upon the initial association of solute molecules providing evidence for a direct link between molecular self -association in solution and the crystallized solid phase ***(Davey et al. 2002a).***

Small Angle Neutron Scattering revealed that colloidal structures or clusters (metastable and labile) of vanillin formed in aqueous alcoholic solutions. It was proposed that two different phenomena resulted in phase separation with one population undergoing liquid-liquid phase separation by spinodal decomposition and the other undergoing crystallization ***(Sorensen et al. 2003).*** Bonnett et al. have studied the liquid-liquid phase separation and appearance of small liquid droplets during cooling induced crystallization of (methyl-(E)-2-.-3-methoxyacrylate) from water-methanol solvent mixtures. The composition of the separated liquid phases was determined and the transformation of the macroscopic liquid droplets into a crystalline material monitored using an optical microscope ***(Bonnett et al. 2003).*** A question about the role of solvent-solute interactions in polymorph nucleation processes still remains open. Georgalis et al. studied super- and undersaturated solutions of NaCl, $(NH_4)SO_4$ and Na-citrate using dynamic light scattering. The results revealed that both solution contain two predominant components, small particles with radii below 1nm (corresponding to solvated ions) and larger particles with radii between 50-500nm (corresponding to ion clusters). ***(Georgalis et al. 2000)*** Veesler et al. investigated the phase diagram of a pharmaceutical compound irbesartan ($C_{35}H_4Cl_2N_3O_2$) in a mixture of ethanol/water. Irbesartan possess two polymorphs with the solubility of both polymorphs high in ethanol and very low in water. Static light scattering, HPLC measurements and video microscopy were used for investigation of the phase diagram and monitoring liquid-liquid separation. They concluded that the crystallisation mechanism and kinetics are different depending on the starting position in the phase diagram, and as a consequence the final product can have different solid phase, crystal habit, morphology and size. It was also observed that liquid-liquid phase separation changes the medium and conditions of crystallisation and hinders the nucleation for several hours ***(Lafferrere et al. 2004a; Lafferrere et al. 2004b; Veesler et al. 2003; Veesler et al. 2006).*** Liquid-liquid phase separation of another pharmaceutical compound from a water-ethanol mixture was observed by Deneau and Steele. The authors showed that during the crystallisation process at first small droplets are formed, then the droplets subsequently grow / coalescence into large droplets which finally crystallised. The droplets grow through coalescence without

agitation to form two liquid layers. Analysis of these layers revealed that each phase contains ethanol, water and crystallising compound in different amounts. The droplet phase contained higher concentrations of the pharmaceutical compound ***(Deneau and Steele 2005)***. Nuclear Magnetic Resonance spectroscopy was used to study crystal nucleation of a novel acaricide, amidoflument and simple amides. The results showed that the structures of the aggregates formed in the solution were similar to the structures of dimer motifs found in final solid material and the cluster structure changed depending on the mole fraction of compound ***(Kimura 2006; Spitaleri et al. 2004).*** Formation of liquid droplets in aqueous solutions of insulin by varying pH and Zn^{2+} concentrations of the mother solutions was studied by Waizmumi et al. They observed nucleation and growth of insulin crystal on the surface of droplets and concluded that this novel pH-dependent nucleation and growth process via liquid droplets would be applicable to control nucleation of crystals and their micro assembly ***(Waizumi and Eguchi 2005).***

Proton solution NMR was used for detection of self-association of inosine in aqueous solution during initial nucleation of a metastable polymorph, and it was proposed that nucleation of a metastable polymorph is directed by an initial dimeric self-association ***(Chiarella et al. 2007).***

Nucleation mechanism of a well known, simple amino acid, glycine, have been widely studied due to its molecular simplicity and three existing glycine polymorphic forms. Glycine exists in three distinct polymorphic forms: α, β and γ with thermodynamic stability under ambient conditions: $\gamma > \alpha > \beta$. α-glycine polymorph is crystallised from neutral aqueous solution, γ-glycine is obtained from basic (pH>8.9) or acidic (pH<3.8) aqueous solution and from deuterated aqueous solution at neutral pH. The metastable β-form crystallises from water-ethanol solution or by freezing of aqueous solution ***(Akers et al. 1995; Hughes et al. 2007; Hughes and Harris 2009; Itaka 1961; Weissbuch et al. 2005).*** The polymorph formation process seems to be more complicated than originally thought and three polymorphs of glycine has been found in the same solution preparation described as concomitant polymorphs ***(Bernstein et al. 1999; Boldyreva et al. 2003).***

Myerson et al. studied diffusion coefficients of supersaturated solutions of glycine and concluded that clusters formed were mainly dimers and trimers, although a few contained hundreds of molecules ***(Myerson and Lo 1990).*** Further SAXS studies of the nucleation process of glycine suggested that the first step of glycine crystallization involves the formation of the liquid-like clusters of solute molecules, while the second involves the reorganization of such clusters into an ordered crystalline structure ***(Chattopadhyay et al. 2005; Erdemir et al. 2007).*** The authors suggested the existence of mass fractals in

natural aqueous solution, even before supersaturation is achieved, then formation of liquid-like clusters in supersaturated solution and finally reorganisation of these clusters leading to nucleation of α-glycine crystals. In an acidic aqueous solution existing of glycine molecules mostly the monomers were found. The dimer structures in aqueous solution of glycine and the growth of α-form the glycine by assembly of cyclic dimers were detected by Gidalevitz ***(Gidalevitz et al. 1997).***

The SAXS results presented in the paper show also data which could correspond to larger structures present in crystallising aqueous solution of glycine, with a size of few hundreds nanometers. These larger clusters could be recognized as dense glycine-rich liquid clusters which make the first step in crystallisation pathway and they could be compared to dense liquid protein clusters reported by Vekilov ***(Gliko et al. 2005; Gliko et al. 2007; Vekilov 2009).*** Further experimental studies of supersaturated glycine solution by Davey et al. showed the solute molecules in the solution also existed as clusters corresponding in structure to each of the known polymorphs ***(Davey et al. 2002a).***

The existence of monomers as the main population in supersaturated aqueous solution of glycine was tested by measuring freezing-point depression and diffusion. The authors concluded that glycine supersaturated solution mostly contains monomers, up to 70%, with the rest of the glycine molecules estimated to exist as dimers ***(Huang et al. 2008).*** Hamad et al. used Molecular Dynamic simulation to study nucleation of glycine from aqueous solution and concluded that glycine molecules exist mostly as monomers. However, some population of dimers were observed in solution as well as trimers and larger clusters which could involve a greater number of molecules like tetramer or pentamers ***(Hamad et al. 2008).***

The nucleation process of glycine still remains unclear, and the difference in interpretation of glycine clusters existing in under- and supersaturated solution is probably due to applying different experimental techniques. Light scattering techniques are more sensitive to larger particles even when they are less populated.The exact distribution of the clusters could also be distorted by larger dense-liquid clusters whose presence is not consider in these papers, where the authors have concentrated on small glycine molecular clusters.

This overview shows that in the last decade a massive amount of work was directed towards understanding crystal nucleation phenomenon. Advanced experimental techniques such as SAXS, DLS, NMR etc. allow monitoring of molecular interaction in undersaturated, saturated and supersaturated solutions of large and small molecules, as well as direct relationship between molecular self-assembly in solution and the subsequent solid phase. The results show that a commonly proposed mechanism of nucleation involves a two-step pathway: dense liquid precursor formation (liquid-liquid separation) and then subsequent solid nuclei appearance. However, the liquid-liquid separation is still poorly understood and

often is thought to be undesirable in crystallisation applications, as it leads to slow crystal growth and uncontrollable crystal morphology. It is therefore essential to better understand the liquid-liquid phase separation phenomena and conditions under which a liquid-liquid split occurs. This may allow better control those processes that lead to formation of desirable crystal products.

1.4 Mesocrystals and iso-oriented self-assembly

Further investigations of crystallisation mechanisms have also revealed oriented attachment and mesocrystal formation pathways which are not consistent with classical crystallisation theory. These non-classical crystallisation mechanisms are closely connected with biomineralization and seem to be frequently applied by natural organisms. Non-classical oriented attachment theory assumes that instead of ions/molecules arranging to produce a single crystal, primary nanoparticles attach in crystalographic orientation making an iso-oriented crystal. The crystal composed of nanocrystalline units lock in and fuse to make a single crystal (Figure 1.9). The driving force for this spontaneous orientated attachment is elimination of pairs of high energy surfaces which lead to substantial reduction of the crystal free energy.

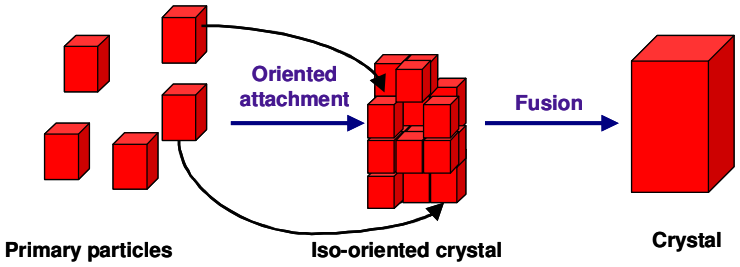

Figure 1.9 Iso-oriented crystal formation, oriented attachment of primary nanoparticles forming an iso-oriented crystal, non-classical crystallisation mechanism.

If the primary nanoparticles are covered by some organic compounds (e.g. polymer) they can form an iso-oriented crystal (mesocrystal) with macromolecules making a bridge (amorphous layer) between individual building units (Figure 1.10). As the nanoparticle units are already organized (mesocrystal), crystal fusion is thermodynamically favoured and eventually the organic compound (e.g.polymer) forms part of the organic coating in the single crystal ***(Cölfen and Mann 2003; Niederberger and Cölfen 2006; Xu et al. 2007).***

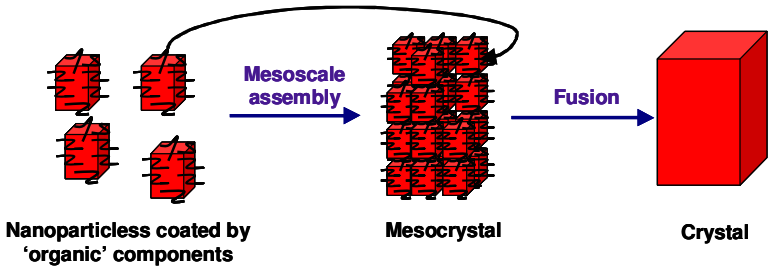

Figure 1.10 Mesocrystal formation, self-assembly of primary nanoparticles covered with organics, non-classical crystallisation mechanism.

Mesocrystal structures of the small organic molecule D,L-alanine, synthesized from aqueous solution in absence of any additives were studied by Cölfen et al. Depending on supersaturation, which was controlled either by temperature or by pH, iso-oriented attachment of nanoparticles leading to D,L-alanine mesocrystals formation was found over a wide range of conditions. Time-resolved conductivity measurements and dynamic light scattering experiments have revealed colloidal structures with a radius around 40-100nm, presumably amorphous nanoparticles or liquid droplets. These liquid precursors partially crystallised and grew via colloidal aggregation to the final mesocrystal form. Small angle neutron scattering experiments have shown clearly that the final crystals were composed of subunits first, which later transformed into a compact structure ***(Ma et al. 2006; Schwahn et al. 2007).*** Further investigation of the crystallisation of D,L-alanine from water/alcohol supersaturated solutions also showed formation of alanine mesocrystals composed of three-dimensional, rod-like nanocrystals and amorphous material ***(Medina and Mastai 2008).***

Mesoscale self-assembly of nanoparticles and formation of controlled organized structures have been widely studied. Mann et al have used stearic acid monolayers in the controlled crystallisation of $CaCO_3$ from supersaturated solution. The presence of the monolayer can determinate the structure, morphology and crystallographic orientation of final product. In the absence of a monolayer, rhombohedral calcite crystals were formed, in the presence of fully or partially compressed monolayers, crystallisation was confined to the organic surface and the crystal structure was exclusively vaterite ***(Mann et al. 1988).***

Li et al studied the mesoscale assembly of superstructures by using surfactant coated nanopartilces with high shape anisotropy. This have shown that the interfacial activity of reverse micelles and microemulsions can be exploited to couple nanoparticle synthesis and self-assembly over a range of length scale to produce materials with complex organization (nanorods of $BaCrO_4$) ***(Li et al. 1999).***

1.5 Protein Coated Microcrystals (PCMCs)

Protein Coated Microcrystals (PCMCs) provide a new and innovative way for stabilizing bio-molecules (e.g. proteins ***(Kreiner et al. 2005a; Kreiner et al. 2001)*** nanoparticles ***(Murugesan et al. 2005),*** and nucleic acids ***(Kreiner et al. 2005b)***), at the surface of excipient crystals. The rapid coprecipitation of bio-molecules and excipient into solvent/antisolvent mixtures (antisolvent for bio-molecules and excipient) results in fast formation of fine powder of excipient particles coated by bio-molecules. In the coprecipitation process simultaneously excipient crystals are created and the bio-molecules are bound to the crystal surface which provides a stable solid support for these molecules. The fast dehydratation process allows the bio-molecules to remain in a native structure with full retention of bioactivity. Free-flowing powders are produced with a specific particle size and morphology which can be used to provide a range of delivery options for variety of modern biotherapeutics. PCMC thus represent a novel technology platform for formulating a wide range of biomolecules including: proteins, peptides, DNA/RNA and vaccines.

PCMCs may be prepared by dissolving biomolecules in a concentrated aqueous solution of an excipient such as amino-acid (e.g. D,L-valine) and rapidly mixing the resulting solution with a water miscible solvent in which both the carrier and biomiolecules are poorly soluble (e.g.2-propanol).

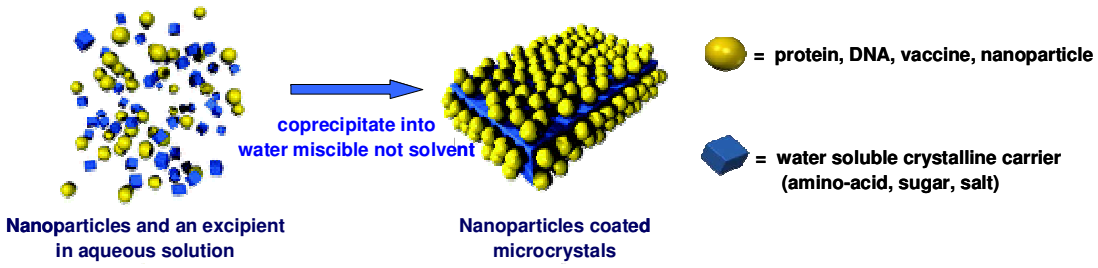

Figure 1.11 Precipitation in non-solvent results in self-assembly of PCMCs with protein located on the surface of carrier crystals.

Although a lot of work has been done to understand this self-assembly precipitation process, the formation mechanism which leads to dehydration of proteins and self-organization at the surface of excipiant crystal still remains unclear. PCMC formation was the inspiration for deeper investigation of the antisolvent crystallisation mechanism of pure excipient in order to better understand the coprecipitation mechanism.

Crystallisation of D,L-valine following addition of an aqueous solution to a 9 fold excess of 2-propanol was previously studied using Small Angle Static Light Scattering and turbidimetry measurements. The results showed that the kinetics of valine precipitation were strongly dependent on the pathway by which the supersaturated solution had been prepared even though there were no visible particles formed immediately upon mixing the aqueous and propanol. It was suggested there may be an intermediate phase separation of precursors with negligible scattering, such as very small nanoparticles or droplets with a refractive index closely matching the continuous phase ***(Variny et al. 2008).***

There are two known polymorphs of D,L-valine: monoclinic ($P2_1/c$ 5.21, 22.10, 5.41, beta =109.2 ***(Mallikarjunan and Thyagaraja 1969)***) and triclinic (P-1, 5.222, 5.406, 10.835, 90.89, 92.34, 110.2 ***(Dalhus and Gorbitz 1996)***).
The D,L-valine crystals precipitated from water -2-propanol solutions was found to be the monoclinic form ***(Vos 2006).***

1.6 Controlled continuous mixing

Interactions between mixing and crystallisation can affect every aspect of the crystallisation processes including nucleation kinetics, final particle size and distribution. Successful operations depend on identifying the mixing parameters which can help to control crystallisation process. Common crystallisers widely employed in the fine chemical and pharmaceutical industries are different types of stirred vessels used in batch and semi-batch operations ***(Paul et al. 2004).*** Confined Impinging Jet reactor (CIJ) is a well controlled, continuous mixer developed by Johnson and Pru'homme and used for mixing of approximately equal volumetric flow streams ***(Johnson and Prud'homme 2003).*** In the CIJ mixer two streams of fluid are mixed in a very small cylindrical chamber placed in the central part of the mixer where the turbulent energy of each stream is dissipated due to fluid collision and redirection, inducing very rapid mixing. The mixing characteristic times for CIJ mixer were studied by Johnson and Pru'homme ***(Johnson and Prud'homme 2003).*** They used highly sensitive homogeneous competitive parallel chemical reactions. The fast reaction was the neutralisation of sodium hydroxide and slow reaction acid catalyzed hydrolysis of 2,2-di-methoxypropane to form acetone and methanol. For a fast enough mixing the fast reaction will finish before the slow reaction begins and will not consume the chemical reagent for the slow reaction:

$$A + B \xrightarrow{k_1} P$$

$$D + B \xrightarrow{k_2} Q + P + B$$

$$k_2 << k_1$$

where *(A)* is sodium hydroxide, NaOH, *(B)* is hydrochloric acid, HCl, *(D)* is 2,2-di-methoxypropane, *(Q)* is acetone and *(P)* is methanol ***(Wang and Kirwan 2006).*** The characteristic mixing time was found to be of the order of milliseconds and the dependence of the stream velocity, fluid viscosity and chamber dimensions on mixing conditions were also studied ***(Johnson and Prud'homme 2003).***

The CIJ mixer could be successfully employed for fast precipitation systems where fast mixing helps to produce final product with small diameters and narrow size distribution. Use of a CIJ mixer in systems with slow nucleation kinetics and liquid-liquid separation pathways (oiling out, solute rich droplets formation) should be tested. Fast mixing on a time-scale of milliseconds may be not sufficient for dense liquid phase transformation in low supersaturated systems. The nucleation kinetics could be faster in batch stirred vessels due to better coalescence of dense rich-solute liquid-droplets. Different types of mixing conditions (batch (stirrer beaker) and continuous (Confined Impinging Jet CIJ)) during antisolvent precipitation of small organic molecules in the liquid-liquid separation region were studied by Kirwan et al. It was found that the size of liquid droplets can be changed by employing different agitation systems and the mixing conditions have different effects on crystal nucleation and growth process. The results showed that stationary solutions of the pharmaceutical compound (e.g. methylparaben, p-aminobenzoic acid and sulfabilamide), which precipitated through liquid-liquid separation, form the stable polymorph whereas rapid mixing induces formation of the metastable polymorph. Authors suggested that polymorph formation can be highly mixing sensitive ***(Wang et al. 2006; Wang and Kirwan 2006; Wang et al. 2005).***

2. Experimental techniques.

2.1 Dynamic Light Scattering (DLS)

Dynamic Light Scattering (DLS) is the most common technique for direct determination of particle size in the submicron region. During the experiment the investigated sample is illuminated by monochromatic laser light (in our case with 632nm wavelength). Scattered laser light radiation is only observed when the investigated sample is **heterogeneous** and it can be either:

- pure compound, where the local density fluctuations can lead to scattering of incident radiation, or
- multicomponent system, where the main scattered signal is due to the difference in optical properties, (namely the difference in refractive index) between the dispersion medium and the dispersed phase.

In the perfectly **homogeneous** and isotropic sample the radiation scattered by individual atoms or molecules interferes destructively and no scattering radiation is observed **(Brown 1993).**

The particles dispersed in the sample scatter light in all directions producing the light scattering intensity signal. The scattered light intensity fluctuates due to particles movement resulting from collisions with the surrounding solvent molecules – Brownian motion. Because smaller particles move quicker then the larger ones, the analysis of scattering intensity fluctuations signal over time gives the information about movement of the particles in solution, which is in turn related to the size of the particles.

The scattered light intensity signal is collected by a detector placed in fixed position (173° in our case –namely back scattering conditions). The back scattering set-up minimises multiple scattering effects (where the scattered light from one particles is subsequently scattered by other particles) and enhances the sensitivity (helping to measure smaller particle size at lower concentration).

The signal from the detector is sent to a correlator which takes the fluctuating intensity signal and turns it into the intensity autocorrelation function: $G_2(\tau)$.

$$G_2(\tau) = \langle I(t) \cdot I(t+\tau) \rangle$$

The autocorrelation function of the scattered intensity $G_2(\tau)$ is the average value of the intensity registered at certain observation time $I(t)$ multiplied by the intensity registered at time delay later, $I(t+\tau)$ (Figure 2.1a).

$$G_2(\tau) = A\left[1 + g_1(\tau)^2\right] \quad ; \quad g_2(\tau) = \frac{G_2(\tau)}{A} \text{ , where}$$

$$A = \left\langle I(t)^2 \right\rangle \quad ; \quad g_1(\tau) = \sqrt{g_2(\tau) - 1} \text{ , and}$$

The autocorrelation function $g_1(\tau)$ is then used to calculate the size distribution of the particles in sample as follows. For mono-dispersed particles in solution, the autocorrelation function $g_1(\tau)$ due to they Brownian motion decays exponentially $g_1(\tau) = B\exp(-\Gamma\tau)$ (Figure 2.1a) with a decay rate of $\Gamma = D \cdot q^2$, where *B* is the intercept equal $g_1(0)$, *D* is the diffusion coefficient of the particles and *q* is the scattering wave vector, $q = \left(\frac{4\pi n}{\lambda}\right)\sin\left(\frac{\theta}{2}\right)$, where *n* is the refractive index of the solvent, λ the wavelength of the laser in vacuum, and θ the scattering angle. Finally, from the Stokes-Einstein equation $D = \frac{k_B T}{3\pi\eta d_H}$ the average hydrodynamic diameter of the particles d_H is calculated, where k_B is Boltzmann's constant, *T* is the absolute temperature and η is the viscosity of the dispersing liquid at the given temperature.

For poly-disperse samples the autocorrelation function $g_1(\tau)$ decays as follows:

$$g_1(\tau) = \sum_i \left\langle I_i(t) \right\rangle e^{-\Gamma_i \tau} \quad ; \quad \Gamma_i = D_i q_i$$

i.e., $g_1(\tau)$, is the intensity weighted sum of all exponential decays due to diffusion of particles of various sizes contained in the sample (Figure 2.1b).

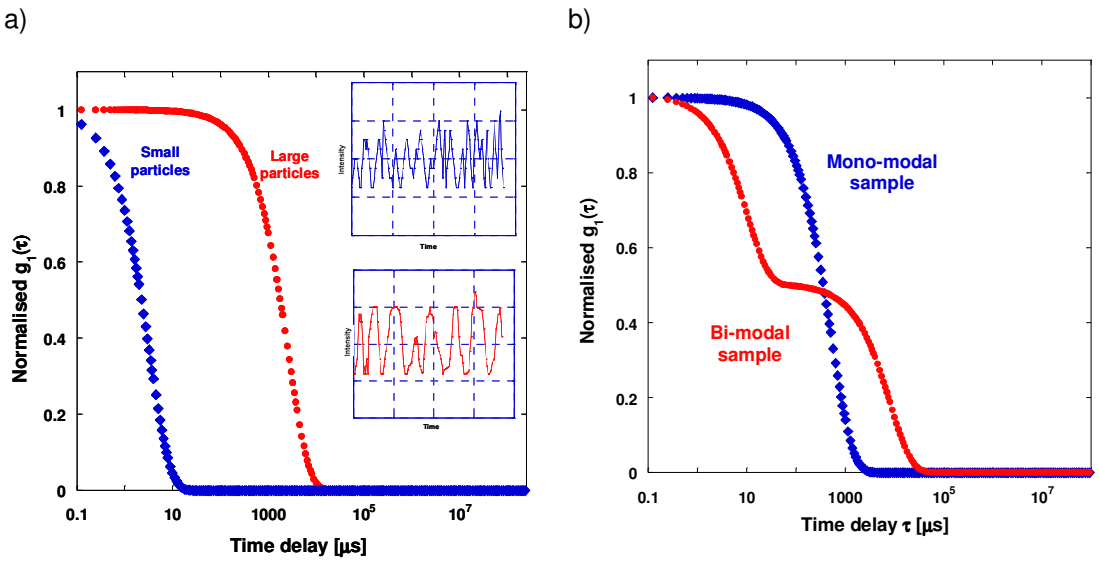

Figure 2.1 Typical autocorrelation graphs for a) mono-disperse sample of either small or large particles, shown together with corresponding scattered intensity fluctuations b) mono and poly-disperse sample.

The analysis of the autocorrelation function can be done using different mathematical fitting methods e.g., Cumulant or Contin, which are typically used for estimation of particle size and their distributions from DLS measurements ***(Brown 1993; Finsy 1994; ISO13321 1996; Linder et al. 2002a; Linder et al. 2002b).***

Dynamic Light Scattering has been used for monitoring of molecular clustering of protein during aggregation process ***(Onuma and Kanzaki 2007; Poznanski et al. 2005).*** As well as for determining protein (pre-)crystallisation parameters or conditions ***(Moreno et al. 2000).*** The presence of dense liquid clusters in undersaturated and supersaturated protein solutions was detected by DLS and reported by Vekilov and co-workers. Two-exponential decay of the autocorrelation function was observed, which indicates that two populations of scattering entities existing in the investigated proteins solutions: protein molecules and larger liquid clusters ***(Gliko et al. 2005; Gliko et al. 2007; Vekilov 2009).*** Sub-micrometer size liquid clusters were also found in aqueous solution of NaCl, $(NH_4)_2SO_4$ and Na-citrate. Two-exponential decays of the autocorrelation function correspond to the presence of solvated ions with small radii ~1nm accompanied by larger clusters with a radii between 50-500nm, ion clusters ***(Georgalis et al. 2000).***

2.1.1 DLS – data acquisition and analysis

All DLS measurements of hydrodynamic diameter of particles during antisolvent and cooling crystallisation process were preformed using HPPS from Malvern Instruments, model number HPP5001, equipped with temperature control unit, using laser light (He-Ne, 3.0mW) wavelength of 632nm with detection in backscattering mode (scattering angle of 173°). Recorded autocorrelation data are displayed and recorded as $g_2(\tau)=1$.

The cumulant analysis of the autocorrelation function is a simple and widely used method for determination the average particle size from DLS measurements. Generally, it consists of fitting of the initial decay of the autocorrelation function by a polynomial of up to the third order to the function $\ln(g_1(\tau))$, where $g_1(\tau)=\sqrt{g_2(\tau)-1}$, $g_1(\tau)=\left(e^{-\Gamma\cdot\tau}\right)$, so $\ln(g_1(\tau))\approx-\Gamma\cdot\tau$. The cumulant method can be straightforwardly used for mono-exponential decay function $g_1(\tau)=\left(e^{-\Gamma\cdot\tau}\right)$, so $\ln(g_1(\tau))\approx-\Gamma\cdot\tau$, where the graph of $\ln(g_1(\tau))$ vs. τ is a straight line with a constant slope proportional to the decay rate, which is inversely proportional to the particle size (Figure 2.2a). So the average diffusion coefficient *D* and the corresponding average hydrodynamic diameter d_H can be determined from $\Gamma=D\cdot q^2$ and $D=\frac{k_B T}{3\pi\eta d_H}$. For poly-disperse samples the graph, $g_1(\tau)$ is a multi-exponential and the graph of $g_1(\tau)$ vs. τ is no longer linear, so it can be fitted by a polynomial of up to the third order, and the initial decay rate is determined from the linear term coefficient b and $\ln(g_1(\tau))$ is no longer linear ***(Figure2.2b) (Linder et al. 2002a; Linder et al. 2002b).***

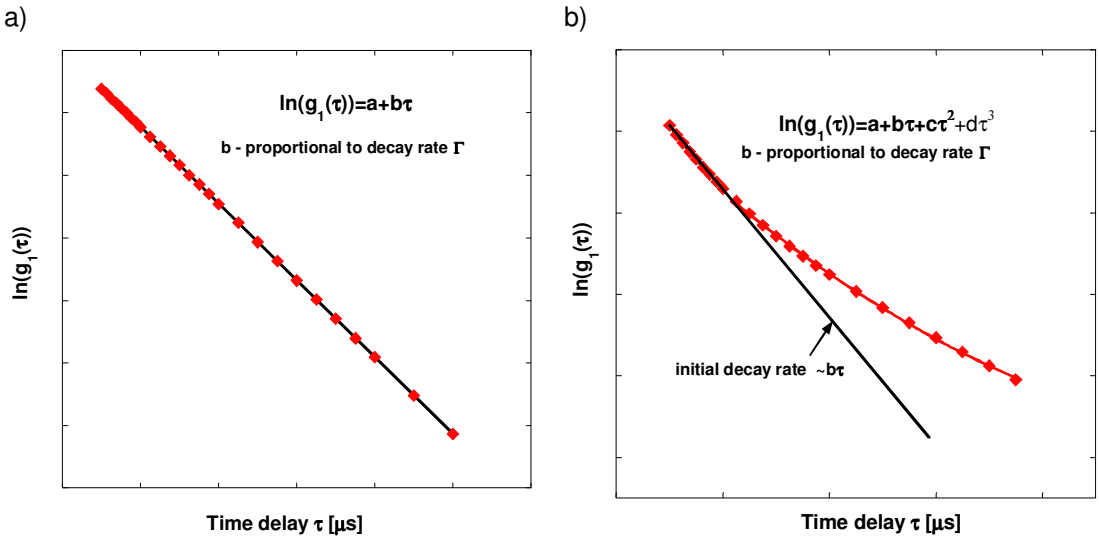

Figure 2.2 Example of fitting autocorrelation function $g_1(\tau)$ with polynomial a) mono-disperse sample, b) poly-disperse sample.

Figure 2.3 shows an example of the autocorrelation function $g_2(\tau)-1$ obtained for a sample prepared by mixing together pre-filtered aqueous D,L-valine solution and 2-propanol, using a magnetic stirrer with the resulting valine concentration of 16mg/ml. Two different kinds of scattering species can be clearly detected in the apparently clear solution.

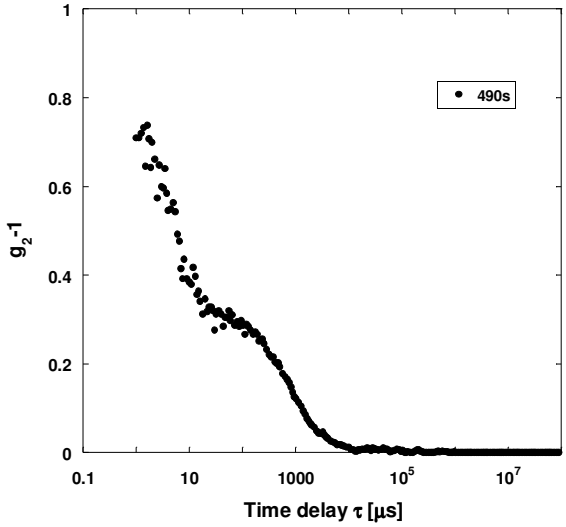

Figure 2.3 Autocorrelation function $g_2(\tau)-1$ for sample at t=490s with C_{Val}=**16mg/ml**, magnetic mixer 90s, 2-propanol/water, 1:1.

From the fitting of the two separate decay parts of $\ln(g_1(\tau))$ the average size of a small (first decay at smaller (τ) and large (second decay at larger (τ)) species can be estimated using the cumulant analysis. The example of fitting $\ln(g_1(\tau))$ autocorrelation data from Figure 2.3 is shown in Figure 2.4. The mean diameter calculated from fitting of the first decay of autocorrelation data using 1st and 2nd order polynomials is around 2.3 nm and 2.2 respectively, (Figure 2.4a). From fitting the second decay part of $\ln(g_1(\tau))$ autocorrelation function the mean diameter is calculated as 202nm and 157nm using 1st and 2nd order polynomials respectively (Figure 2.4b). Since experimental data are quite noisy (especially the first decay), the higher order polynomial fits data are less valuable and were not used here. The mean diameter calculated using 1st order polynomial fits were found to be systematically larger compared to those estimated from 2nd order fits which is expected for polydispersed size distributions.

a) b)

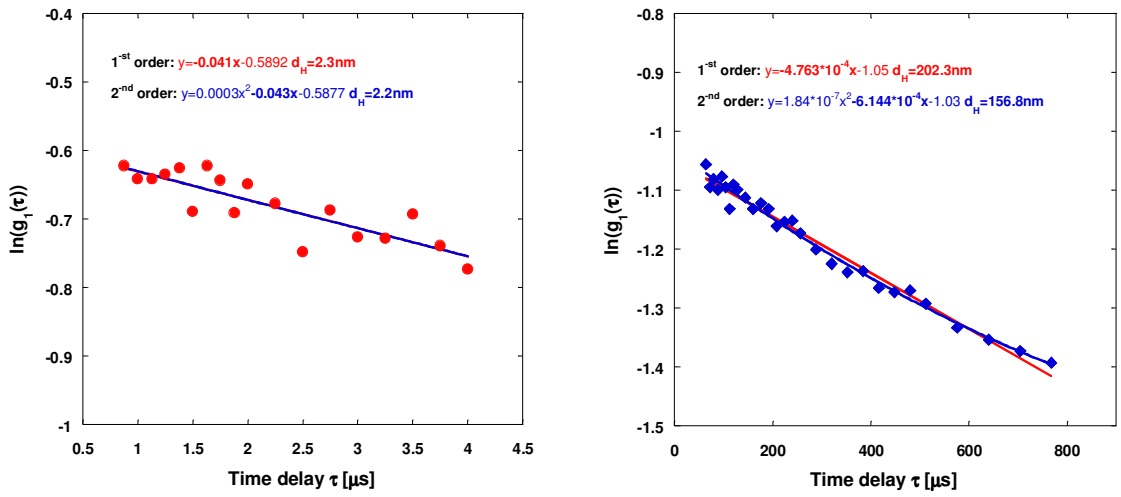

Figure 2.4 Correlation function ln(g_1(τ)) fitted with 1st and 2nd order polynomial for sample at t=490s with **C_{Val}=16mg/ml**, magnetic mixer 90s, 2-propanol/water, 1:1, a) first decay of autocorrelation function, b) second decay of autocorrelation function.

Confidence intervals for estimated hydrodynamic diameter were obtained as follows. The 95% confidence intervals of parameter '*a*' from the first order fitting function ($y = ax + b$) was calculated using t-student distribution statistics: $a_{t-student} = t_{\frac{\alpha}{2},n-2} \cdot \frac{\sigma}{\sqrt{S_{xx}}}$, where $t_{\frac{\alpha}{2},n-2}$ is t-distribution value for *n-2* degrees of freedom and 95% confidence, σ is the mean error of

fitting and S_{xx} was calculated from equation $S_{xx} = \sum x^2 - \frac{\left(\sum x\right)^2}{n}$ where *n* is the number of *x* variables. The mean error of fitting was calculated from the formula $\sigma^2 = \frac{\sum e^2}{n-2}$, where *e* is the residual which expresses the total variability and was determined from $e = \sum y - \hat{y}$ where $\hat{y}$ are predicted values of *y* variable.

The hydrodynamic diameter is calculated from Stokes-Einstein equation: $D = \frac{k_B T}{3\pi\eta d_H}$ where D is: $D = \frac{\Gamma}{q^2}$. The calculated size of particles depends on decay rate of autocorrelation function $\ln(g_1(\tau)) = -\Gamma\tau$ according to relation: $d_H = \frac{k_B T q^2}{3\pi\eta\Gamma}$.

Using the error propagation formula, $md_H = \sqrt{\left(f(a)' \cdot a_{t-student}\right)^2}$, the relative error of the mean hydrodynamic diameter was calculated, where $f(a)'$ is the derivative of the Stokes-Einstein relation, $\frac{\partial\left(\frac{k_B T}{3\pi\eta a}\right)}{\partial(a)} = \frac{-k_B T}{3\pi\eta a^2}$, *a* is the best estimated parameter, and $a_{\text{t-student}}$ is confidence interval of estimated diameter calculated using t-student distribution.

For the second order fitting the error of calculated diameters was determined using the same error propagation formula and instead of student distribution error $a_{t\text{-}student}$, the mean error of parameter *'b'* from second order function $y = ax^2 + bx + c$ was used. The mean error of parameter *'b'* was calculated from equation $\sigma_b = \sigma \cdot \sqrt{\frac{1}{\sum\left(x - \bar{x}\right)^2}}$ where σ is the mean error of fitting and $\bar{x}$ is average value from *x* variables. Table 1.1 shows results of cummulant method fitting using 1st and 2nd order polynomials with errors estimated as discussed above ***(Wadsworth 1990).***

Table 2.1 Hydrodynamic diameter of poly-disperse sample calculated using 1st and 2nd order polynomial. t=490s, C_{Val}=**16mg/ml**, magnetic mixer 90s, 2-propanol/water, 1:1.

Time [s]	First decay of correlation function Hydrodynamic diameter [nm]		Second decay of correlation function Hydrodynamic diameter [nm]	
	1-st order fit	**2-nd order fit**	**1-st order fit**	**2-nd order fit**
490	**2.3**± 0.7	**2.2**± 1.9	**202**± 12	**157**± 12

Figure 2.5a shows the measured autocorrelation function $g_2(\tau)-1$ at time 490s and two theoretical autocorrelation function curves for particles with hydrodynamic diameter d_{H1}=2.2nm and d_{H2}=180nm (calculated using 2-nd order polynomial). Theoretical autocorrelation functions were calculated using the same physical parameters (viscosity η, temperature T, refractive index of solvent n, scattering angle θ) that were used for estimation of mean hydrodynamic diameters from experimental data. The calculated autocorrelation functions for two populations (d_{H1}=2.2nm and d_{H2}=180nm) agree well with experimental data when considered separately. However, since autocorrelation decay in polydisperse samples is equal to intensity weighted sum of decays due to respective populations, the overall decay should be calculated as follows:

$$\left(g_2(\tau)-1\right)^{1/2} = g_1(\tau) = I_1 e^{-\Gamma_1 \tau} + I_2 e^{-\Gamma_2 \tau}, \text{ where}$$

I_i are time average scattering intensity and $\Gamma_i = -D_i q$ are decay rate due to present species.

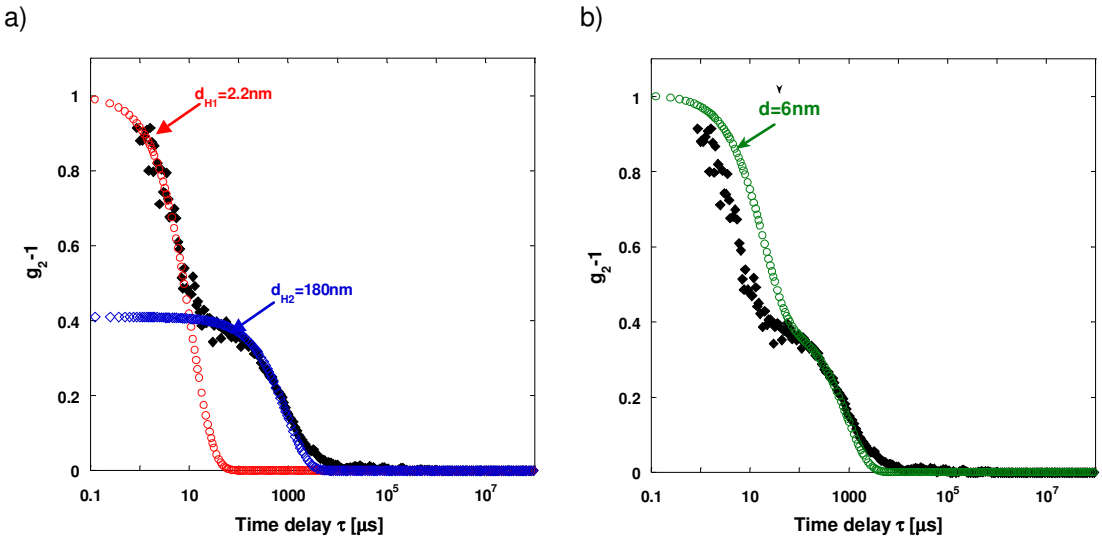

Figure 2.5 Correlation function $g_2(\tau)-1$ at time 490s, **C_{Val}=16mg/ml**, magnetic mixer 90s, 2-propanol/water, 1:1, plotted with a) standard correlation function correspond to size 2.2nm and 180nm, b) the normalised sum of autocorrelation functions correspond to mean diameter of 2.2nm+180nm.

The sum of theoretical autocorrelation functions corresponding to the particle size obtained from separate fitting of correlation data of presented example (2.2nm and 180nm) is plotted in Figure 2.5b. First decay of correlation data plotted as a sum of correlation function for particle size of 2.2nm and 180nm clearly shows a significantly overestimated size, with diameter around 6nm. So, the real diameter of small species should be about 2.7 times smaller than obtained from separate fitting of autocorrelation decay parts ($6.0nm/2.2nm = 2.7$). This allows us to estimate the actual diameter of small particles as 0.8nm ($2.2nm/2.7 = 0.8nm$).

The fitting of the whole autocorrelation data curve with the function calculated as a sum of standard correlation data for small and large particles shows that the first decay corresponds to smaller particles (d_{H1}=0.8nm), whereas the size of particles from the second decay is the same (d_{H2}=180nm) (Figure 2.6).

However, the size of large particles is the same in both cases and does not depend on the fitting method. We note that, there are variations of software which can be use for calculation of the mean hydrodynamic diameter from autocorrelation functions, using Cumulant or Contin method, usually applied with Dynamic Light Scattering instruments. However, software often is typically set up to fit data assuming that the sample is mono-disperse, or

alternatively tries to fit a polydisperse distribution, which often leads to ill-defined problems resulting in suggestive but unreliable particle size distribution. Thus, the calculation of the particle size was done as described above, by fitting the two decay parts of autocorrelation function separately.

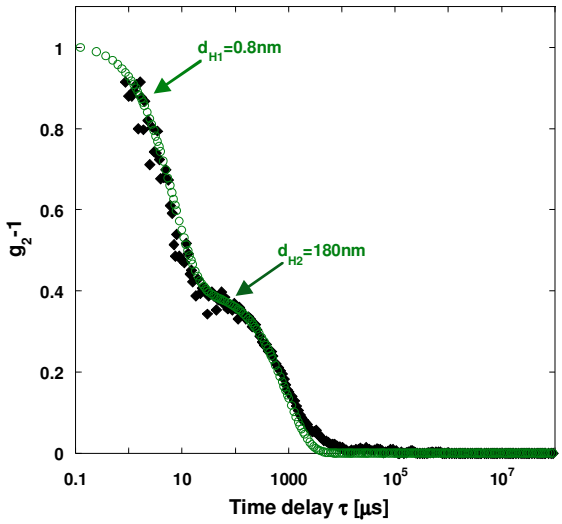

Figure 2.6 Correlation function $g_2(\tau)-1$ of given example at time 490s, **C_{Val}=16mg/ml**, magnetic mixer 90s, 2-propanol/water, 1:1, plotted with the normalized sum of standard correlation functions correspond to 0.8nm+180nm.

Another issue is, that the autocorrelation function is obtained on the basis of light scattering intensity. The scattering intensity signal is proportional to the six-th power of particle size e.g. intensity signal ~ d^6. This means, that for the same number of particles with size for example 1 and 10nm the intensity signal from the larger particles will be 10^6 times stronger than from smaller particles. 1 particle with size 10nm will give the same intensity signal as 10^6 particles with size 1nm. DLS lets us monitor a small population of large particles even if they number is very low.

2.2 Spectroscopic techniques

Spectroscopic techniques are used for qualitative and quantitative analysis of molecular structure of matter based on differences in absorption, emission or scattering of electromagnetic radiation. The matter can be atoms, molecules, ions (atomic or molecular) or solid. Figure 2.7 summarizes the regions of the electromagnetic spectrum and the types of energy transition observed into respective region. Although there are many types of spectroscopy four are used more often in chemistry: Nuclear Magnetic Resonance spectroscopy (NMR), Ultraviolet / Visible spectroscopy (UV/ Vis), infrared spectroscopy (IR) and mass spectroscopy (MS) ***(Harwood and Claridge 1997).***

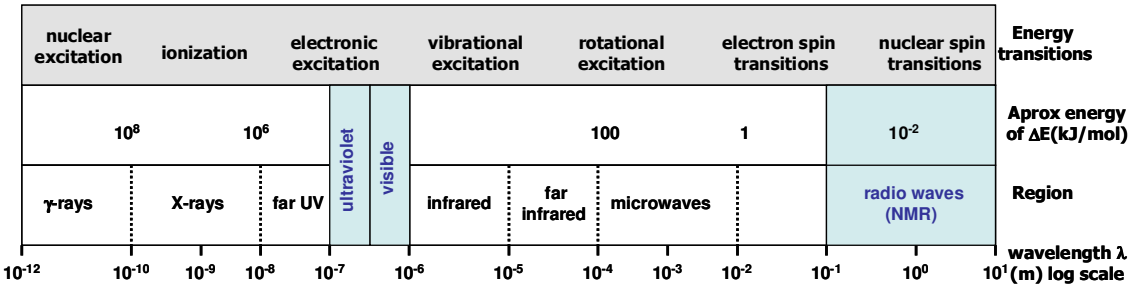

Figure 2.7 The electromagnetic spectrum.

NMR and UV/Vis spectroscopy techniques were used to study the liquid precursor of antisolvent and cooling crystallisation process of amino acids (D,L-valine, glycine). These two techniques were also used for determination of D,L-valine solubility in water/2-propanol solvent.

2.2.1 Nuclear Magnetic Resonance (NMR)

Nuclear Magnetic Resonance (NMR) is a powerful analytical technique for determination of the structure of organic and inorganic compounds as well as various properties of solution phase (solution state NMR) where molecular interactions lead to aggregation, self-association or molecular clustering. NMR phenomenon is based on behaviour of atomic nucleus in external magnetic field. An atomic nucleus has the properties of mass, electric charge, magnetism and spin. Magnetism of a nucleus implies interaction

with magnetic fields; spin is a form of angular momentum and is a characteristic for specific nucleus. Both of these properties are essential to NMR.

According to quantum mechanics nuclei with spin, S, have 2S+1 possible orientations (a nuclei with a spin ½ (^{1}H, ^{13}C, ^{19}F, ^{31}P) have two orientations), which are degenerate in the absence of an external field. In the presence of an external field (B_o), two spin states exist: +½ and - ½ .The magnetic moment of the lower energy + ½ is aligned with the external field, but that of higher energy - ½ state is opposite to the external field.

The difference in energy between the two spin levels is constant and dependent on the external magnetic filed strength B_0 and is calculated from the relation: $\Delta E = \frac{\mu B_0}{S}$, where μ is the magnetic moment of nuclei in the external field, *S* is the spin (for proton *S=½*) (Figure2.8).

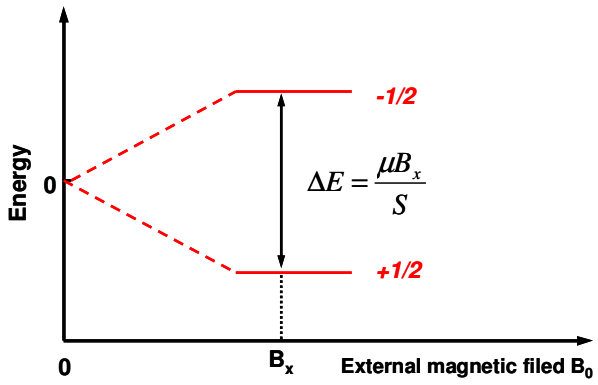

Figure 2.8 The nuclear spin energy for single nucleus with S=1/2 plotted as a function of magnetic filed B_0.

The magnetic field, B_0, is specified in units of Tesla. The natural magnetic field at the surface of the earth is ~50μT, compared with modern NMR spectrophotometers operating up to 21.14T. In NMR the small energy difference (ΔE) is usually given as a frequency ν in units of MHz and it depends on the magnetic field strength and specific magnetic properties of the nucleui according to the equation: $\Delta E = h\nu = \frac{\mu B_0}{S}$. Because angular momentum of nucleus is quantized in unit of $\frac{h}{2\pi}$, the final equation has form $\nu = \frac{\gamma B_0}{2\pi}$ where, ν is a frequency in Hz, h is the Planck's constant (h=6.626x10^{-34}J·s), γ is a gyromagnetic ratio (for proton γ=42.58MHz/T). The nucleus of a hydrogen atom (the proton) has a magnetic moment μ=2.7927 J/T, and has been studied more than any other nucleus. Since protons all

have the same magnetic moment, we might expect all hydrogen atoms to give resonance frequency signal at the same values. However, different local environment of protons according to the molecular structure (e.g. electrons surrounding the protons) exist at different resonance frequencis at which energy is absorbed. The spectrum of resonance frequency is obtained which reflects the differences in the specific proton environment and this provides very detailed information about molecular structure of compounds.

The chemical shift is the frequency difference between the absorption of a particular proton and the absorption from a standard compound (reference signal e.g. TMS Tetramethylsilane, where the methyl 'singlet' for ^{1}H nuclei is defined as 0ppm). The actual chemical shift can be expressed by the relation; $\delta_{ppm} = \frac{\nu_0 - \nu_{ref}}{\nu_{ref}} \times 10^6$ where ν_{ref} is a resonance frequency of a reference substance, and ν_0 is a measured frequency of nuclei in a sample. Because the difference in the resonance frequency is very small, it is usually expressed in 'parts per million' (ppm) with 0 ppm defined for each nucleus by a reference compound ***(Akitt 1992; Canat 1991; Harwood and Claridge 1997; Parkinson 2003).***

The magnitude of the NMR resonance signal is proportional to the number of nucleus (e.g. protons) contributing to a signal. The determination of the absolute concentration requires a reference compound of known concentration to be added to the sample and then determination of unknown concentration of the investigated sample can be calculated by comparison of the integrals in one spectrum ***(Akitt 1992; Harwood and Claridge 1997).***

The chemical shift of a nucleus is very sensitive to its electronic environment, and molecular interactions in solution can produce changes in chemical shifts and lead to deformation of the signals (broad peaks, splitting of peaks). The initial stage of the spontaneous emulsification of trans-anethole was studied using solution state ^{1}H NMR and as a result two separate signals were obtained, one for free molecules in aqueous phase anda second for aggregated trans-anathole molecules ***(Carteau et al. 2007)***. Solution state NMR was also successfully used for monitoring molecular interactions in solutions: the aggregation of dye molecules in aqueous solution ***(Asakura and Ishida 1989; Hamada et al. 1986)*** self-association of pharmaceuticals ***(Ding et al. 2004)*** and the clustering of steroid compounds ***(Shikii et al. 2004).*** Proton NMR was used for detection of self-association of inosine in aqueous solution during initial nucleation of a metastable polymorph, and it was proposed that nucleation of a metastable polymorph is directed by an initial dimeric self-association ***(Chiarella et al. 2007).***

Crystal nucleation and characterisation of the dense liquid precursor of acaricide, amidoflument ***(Kimura 2006)*** and simple amides ***(Spitaleri et al. 2004)*** using ^{1}H solution state NMR was investigated and formation of small molecular clusters during the first step of nucleation process was reported.

In the case of antisolvent or cooling crystallisation of valine from a water/2-propanol mixture no visible shifting or deformation of valine peaks indicating molecular association was observed. However, D,L-valine is a small molecule without any polariesable aromatic rings, which seems to be a common feature of systems where molecular self-association effects have been observed in ***(Kimura 2006; Spitaleri et al. 2004)***.

- ^{1} H NMR data analysis

The concentration of D,L-valine during antisolvent and cooling crystallisation processes as well as D,L-valine solubility measurement in water/2-propanol solvent was determined using a TSP (3-(trimethylsilyl)-1-propanesulfonic acid sodium salt) reference solution. The addition of a reference compound directly into the tested crystallising sample could change the kinetics and thermodynamics of the crystallisation process and so to avoid this problem an NMR coaxial insert tube was used. The main sample tube used was: Wilmad 535-PP 7" NMR 5mm, 600MHz, internal reference tube: Wilmad coaxial insert, stem L32mm. The influence of the double tube on the strength of the TSP signals was tested by placing the reference sample of known concentration into the internal and external tube in turn. As a second reference sample aqueous solutions of D,L-valine of known concentration were used. Figure 2.9 shows the scheme of a double NMR tube and spectrum obtained from D,L-valine and TSP reference placed in external and internal tubes respectively.

a) b)

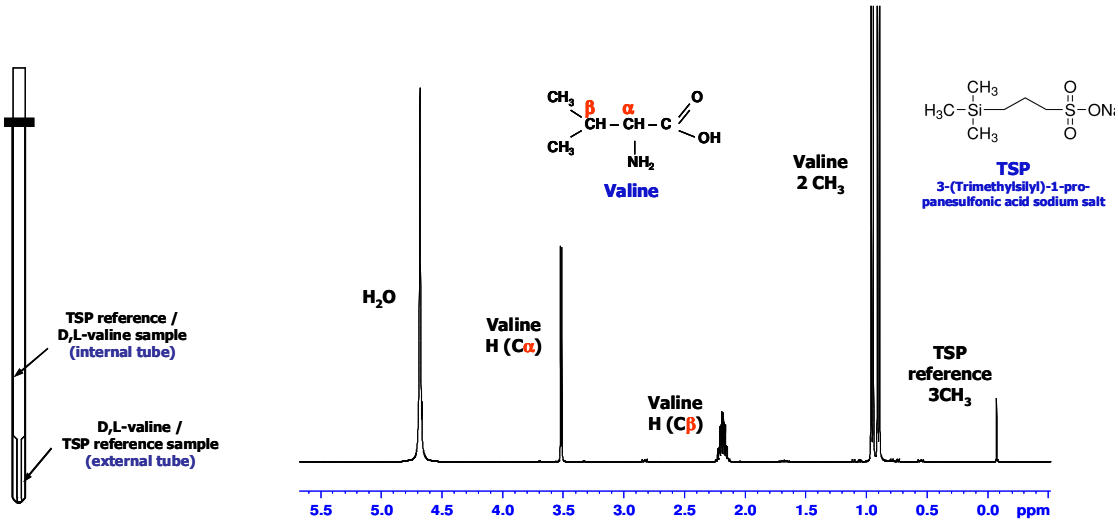

Figure 2.9 NMR experiment a) standard and coaxial insert NMR tubes, b) NMR spectrum obtained from TSP reference and D,L-valine samples placed into internal/ external tubes respectively.

All NMR experiments were done on Bruker (400MHz) instrument with the following specification: 0.4T Oxford unshielded magnet, B-ACS 60 autosampler, 2 Channel H/X Console, DQD and Waveform –equipped, BBFO-z-ATMA-probe [^{31}P- ^{109}Ag/ ^{1}H/^{19}F]. Number of scan collected was 32, number of dummy scan was 2 and relaxation delay was 10s.

The quantification of TSP standard signal in the internal tube was preformed as follows. Two solutions were prepared:

a) D,L-valine in deuterium oxide (D_2O), at concentration $C_{Val} = 0.1716 mol/dm^3$.

b) TSP in deuterium oxide (D_2O), $C_{TSP} = 0.0957 mol/dm^3$.

If the concentration and volume of TSP and valine solutions were equal, then the ratio between integrated peak areas (number of protons contributing to the peaks: TSP 0ppm and D,L-valine 1.1ppm ($2CH_3$)) should be $\frac{6(valine)}{9(TSP)}$.

a) TSP solution sample was placed in the internal tube and valine solution in the external tube.

The measured ratio between valine and TSP signals was: $\frac{369.68(Valine)}{9(TSP)}$.

So, the area under the valine peak is 61.6 times bigger than in the case when the concentration of valine and TSP will be equal ($\frac{369.68(Valine)}{6(Valine)} = 61.6$). On the assumption that concentration of valine is unknown, this value can be calculated from the equation:

$$C_{Val} = C_{TSP} \cdot 61.6 = 0.0957 mol/dm^3 \cdot 61.6 = 5.89 mol/dm^3$$

However, valine concentration is known and this calculation shows that the TSP signal from internal tube is around 34.32 times weaker ($\frac{5.89 mol/dm^3}{0.1716 mol/dm^3} = 34.32$).

b) Valine solution was placed in the internal tube and TSP solution in the external tube.

The measured ratio between valine and TSP signals was $\frac{6(Valine)}{173.85(TSP)}$.

So, the area under the TSP peak is 19.32 times larger than in the case when the concentration of Valine and TSP will be equal ($\frac{173.85(TSP)}{9(TSP)} = 19.32$). On the assumption that concentration of TSP is unknown, this value can be calculated from the equation:

$$C_{TSP} = C_{Val} \cdot 19.32 = 0.1716 mol/dm^3 \cdot 19.32 = 3.31 mol/dm^3$$

However, TSP reference concentration is known and this calculation shows that the valine signal from internal tube is around 34.58 times weaker ($\frac{3.31 mol/dm^3}{0.0957 mol/dm^3} = 34.58$).

Four repetitions of these experiments were done and it was found that the volume per unit of length from samples placed in internal tube is 34.3 times smaller (on average) than that in the external tube. This was taken into account during interpretation of NMR results.

2.2.2 Diffusion ordered spectroscopy (DOSY) NMR

Pulsed-field gradient spin-echo (PGSE) NMR is a powerful technique for measuring diffusion coefficient. The measurement of diffusion is carried out by observing the exponential decay of the NMR signal during a pulsed field gradient experiment. Compounds with smaller hydrodynamic diameter move faster and have larger diffusion coefficients. The diffusion coefficient is related to properties of an individual molecule such as size, shape, mass and charge as well as surrounding solution properties as temperature and viscosity. Assuming a spherical size of the molecule the diffusion coefficient *D* is described by the Stokes-Einstein relation $D = \frac{k_B T}{3\pi\eta d_H}$ where, k_B is the Boltzmann's constant, T is the absolute temperature, η is the viscosity of the surrounding liquid and d_H is the hydrodynamic diameter of the molecule. NMR diffusion experiment provide a way to pseudo-separate the different species in a mixture based on the difference in their diffusion coefficient. Calculating the diffusion coefficient for each component in a sample allows obtain a two-dimensional DOSY NMR spectrum where one dimension is for the conventional chemical shift and the other dimension is for the diffusion coefficient ***(Huo et al. 2003)***.

PGSE NMR diffusion measurement has been recently applied to study the molecular self-organisation during aggregation of lysozyme ***(Poznanski et al. 2005; Price et al. 1999; Price et al. 2001)*** and the first step on the crystallisation process of the amino acid (glycine) ***(Huang et al. 2008).*** Diffusion experiment of glycine aqueous solution has indicated that glycine molecules exist mostly as a monomer (based on number weighted diffusion coefficients) in supersaturated solutions. DOSY measurements of the initial stage of the spontaneous emulsification of trans-anethole have shown that at first a large number of small aggregates are formed which immediately begin to coalescence to generate larger droplets ***(Carteau et al. 2007).***

Diffusion ordered spectroscopy technique can be used for size determination of species in solution, similarly to Dynamic Light Scattering. However, it should be stressed that the intensity of the scattered light is proportional to the second power of the mass of the scattering aggregates, and so scattering is dominated by larger particles, even if their populations are very low. In contrast, DOSY NMR technique, because of relaxation restrictions can only detect a small molecular species, and this could be affected by molecular exchange with larger aggregate population.

- DOSY NMR data analysis.

Dynamic characterisation of antisolvent and cooling crystallisation processes of D,L-valine from water/2-propanol solvent was carried out. Measurement of diffusion coefficients allows us to calculate the hydrodynamic diameter of diffusing particles using the Stokes-Einstein equation $D = \frac{k_B T}{3\pi\eta d_H}$, where D is the diffusion coefficient, k_B is Boltzmann's constant, T is the absolute temperature, η is the viscosity of the dispersing liquid at the corresponding temperature and d_H is the hydrodynamic diameter of the particles. Figure 2.10 shows the two-dimensional DOSY NMR spectrum obtained for D,L-valine /2-propanol/water sample prepared by mixing together aqueous valine and 2-propanol to generate a valine concentration 17.5mg/ml.

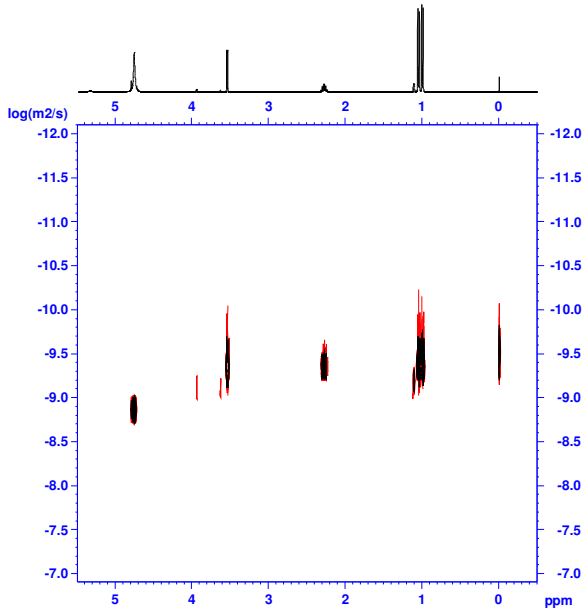

Figure 2.10 DOSY NMR two dimensional spectrum, antisolvent crystallisation of D,L-valine from water/2-propanol solution, **C_{Val}=17.5mg/ml**.

The spectrum shows values of diffusion coefficients for all molecular spaces existing in the sample (valine, water, 2-propanol and TSP reference). The hydrodynamic diameter of valine calculated on the base of diffusion coefficient measurement is 0.58nm, as determined by the Stokes-Einstein relation:

$$d_H = \frac{k_B \cdot T}{3\pi \cdot \eta \cdot D} = \frac{1.38 \cdot 10^{-23} J/K \cdot 298K}{3\pi \cdot 0.003 Pa \cdot s \cdot 2.51 \cdot 10^{-10} m^2/s} = 5.8 \cdot 10^{-10} m = 0.58nm$$

This calculated size corresponds to single D,L-valine molecules present in solution, where,

$k_B = 1.38 \cdot 10^{-23} J/K$ - Boltzmann's constant,

$T = 298K$ -absolute temperature,

$\eta = 0.003 Pa \cdot s$ -viscosity of solvent,

$D = 10^{-9.6} m^2/s$ - diffusion coefficient.

2.2.3 UV / Vis spectrophotometry

UV/Vis spectrophotometry is a method for determination of transmittance of light at given wavelength by a sample. Transmittance is the fraction of incident light at specified wavelength which passes through the sample and is expressed by equation: $T = \frac{I_1}{I_0}$ where

I_0 is an intensity of incident light and I_1 is an intensity of transmitted light. Absorbance $A = I_0 - I_1$, is a fraction of light absorbed or scattered by the sample. Transmittance (T) is related to absorbance (A) according to Beer-Lambert Law: $A = -\ln(T) = -\ln\left(\frac{I_1}{I_0}\right)$.

The absorption of UV/Vis (Ultraviolet/Visible) radiation results from transitions in the electronic energy levels of the bonds of a molecule and lead to excitation of electrons from ground state into en excited state. Figure 2.11 shows the various types of electronic transitions of π, σ and n electrons which can occur ***(Harwood and Claridge 1997).***

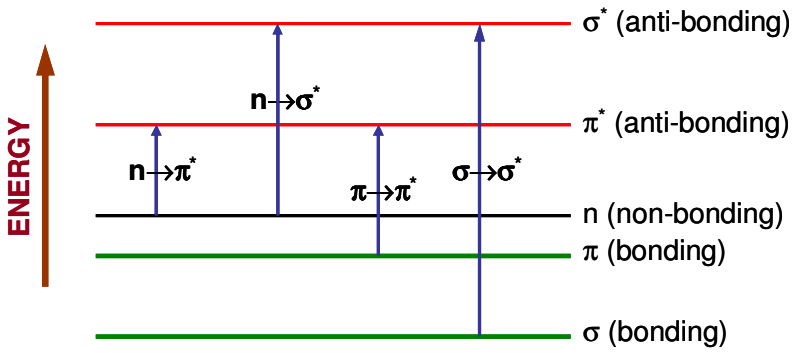

Figure 2.11 Molecular electronic transitions.

According to equation $\Delta E = \frac{h \cdot c}{\lambda}$ where, h is the Planck's constant, c is the speed of light and λ is a wavelength, the higher energy corresponds to smaller wavelength which is required for excited an electron form one orbital to another. The $\sigma \rightarrow \sigma^*$ transitions are required the highest energy and the absorption is at 125nm wavelength. These transitions are not seen in typical UV-Vis spectrum. The $n \rightarrow \sigma^*$ transitions are required less energy compare to $\sigma \rightarrow \sigma^*$, and can be initiated by light with wavelength in range 150-250nm. The absorption peaks for $n \rightarrow \pi^*$ and $\pi \rightarrow \pi^*$ transitions are fallen in the spectrum with region between 200-700nm. Most organic compounds have an absorption spectrum based on $n \rightarrow \pi^*$ and $\pi \rightarrow \pi^*$ electrons transitions ***(Harwood and Claridge 1997).***

UV spectroscopy gives two important information, first is a position of absorption peak (λ_{max}, nm), and second is the value of molar absorptivity (ε). The molar absorptivity is a measure of how strongly a molecule absorbs light at a given wavelength and is a constant value for a given molecule at a given wavelength. The relationship between molar absorptivity and concentration is expressed by the Beer-Lambert Law assuming that not scattering is present: $A = \varepsilon \cdot c \cdot l$ where A is an absorbance so the final equation is often stated as: $\varepsilon = \frac{A}{c \cdot l}$ where, I_0 is an intensity of incident light, I_1 is an intensity of transmitted light, c is a concentration in *mol/dm*^{3}, *A* is a absorbance and l is the path length of absorbing solution in cm. Absorbance is therefore directly related to concentration and can be plotted against concentration on linear graph. However, absorbance may result from scattering as well, in which case the Beer-Lambert law is as follows (assuming no absorption is present): $A \approx \tau \cdot l$ where τ is turbidity. Spectrophotometry is a good technique for measurement of the turbidity of a sample, which is "an expression of the optical properties of a liquid that causes light rays to be scattered and absorbed rather than transmitted in straight lines trough a sample" ***(ASTM_Standards 2003).***

UV spectrophotometry was used as an one of method for determination of D,L-valine solubility in different ratios of water-2-propanol solvents mixture. All measurements were done using single beam DU800 spectrophotometer from Beckmann Coulter, quartz covered cuvette. During the measurements the temperature inside the UV sample chamber was kept constant at 25°C. The absorption values were read at 210nm wavelength for D,L-valine in water/2-propanol solvent with ratio 1:3, v/v, for solvents ratios 1:1 and 1:0 (pure water), max absorption was at 220nm and 230nm respectively. Figure 2.12 shows D,L-valine calibration curves for three different solvents mixtures.

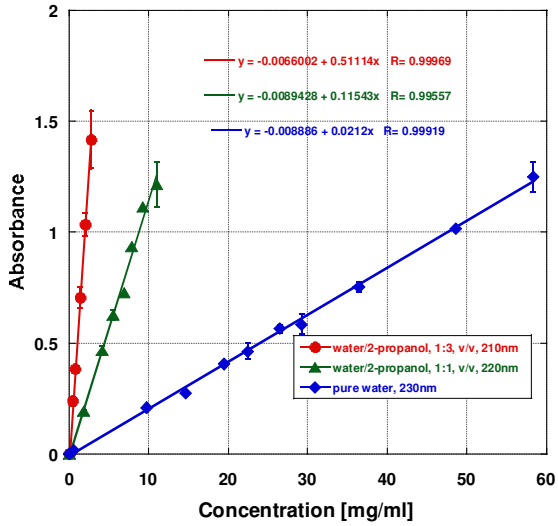

Figure 2.12 The UV calibration curves for D,L-valine in water/2-propanol solvents, solvent (water/2-propanol) ratios, 1:0, 1:1, 1:3, v/v.

On the basis of calibration curves the solubility of D,L-valine were determined (see ''Solubility of D,L-valine" chapter for details).

Visible light spectrophotometry was used for measurement the turbidity of a D,L-valine crystallise solution at wavelength 600nm. All measurements were done in quartz covered cuvette to prevent sample evaporation during measurement. From turbidity, plotted vs absorbance and transmitted light vs time in Figure 2.13, the kinetics of the crystallisation process can be monitored.

a) b)

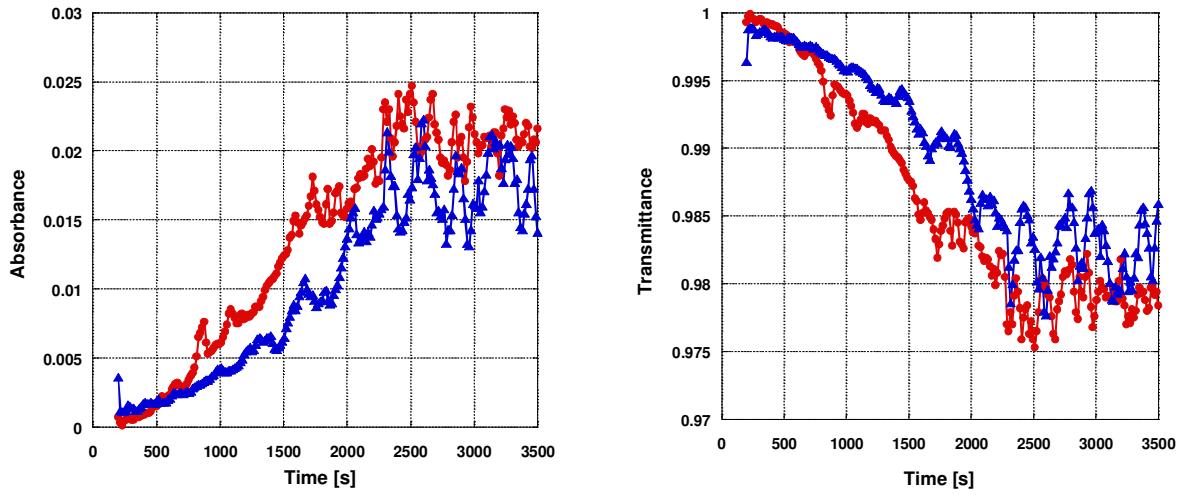

Figure 2.13 Turbidity measurements of D,L-valine crystallise samples at 25°C, C_{Val}**=18mg/ml**, water-2-propanol, 1:1, v/v, at 600nm wavelength, a) Absorbance vs time, b) Transmittance vs time.

This method can not be used for direct kinetics measurement, however by comparison of the results from the same analysis conditions, information about crystallisation process can be obtained. Absorbance and transmittance light can be interpreted as a light absorbed or scattered by some particles in solution which can be already formed crystals or some crystallisation precursors.

2.3 High Performance Liquid Chromatography (HPLC)

High Performance Liquid Chromatography (HPLC) is an analytical technique widely used for separation, identification and quantification of chemical compounds which involves mass transfer between a stationary and mobile phase ***(Kazakevich and LoBrutto 2007).*** The stationary phase is defined as the immobile packing material in the column. Silica and modified silica are the most popular, but alumina, magnesium oxide and calcium phosphate are also used often. The composition of mobile phase is important and has a large influence on the separation process ***(Meyer 2004).*** The interactions of the compounds of an analyte mixture with mobile and stationary phase can be manipulated through various choices of solvents and stationary phase composition.

Separation of compounds is based on an adsorption process where molecules, while moving through the porous stationary phase material tend to interact with surface adsorption sites. Depending on the types of adsorption processes three different variances of HPLC modes are used:

- normal-phase HPLC, stationary phase is polar (silica particles), non-polar solvents are used as mobile phase, good for separation of polar molecules.

- reversed-phase HPLC, where reversed-phase means that the stationary phase is non-polar (it is a long –usually C_{18} – hydrocarbon chain covalently bonded to the silica) and polar solvents are used as mobile phase (usually a mixture of water and an alcohol), good for separation of non-polar molecules.

- ion-exchange chromatography, stationary phase contains ionic groups (e.g. $–NH_3^+$ or $–SO_3^{2-}$), based on interaction between solute ions in the mixture to be separated and charged sites bound to the stationary phase, good for protein separation.

HPLC instrument contain a detector (e.g. UV, Fluorometry, Refractive Index (differential refractometry)), which analyse the composition of the mixture passing through, and as a result a series of peaks are typically recorded. Both the peak height and peak area may be used as a measure of the concentration of a component in the sample ***(Kazakevich and LoBrutto 2007; Meyer 2004).***

Reversed-phase HPLC technique was used for determination of D,L-valine solubility in water/2-propanol solvents with different ratios. Prepared samples were injected into a Waters 2697 Separations Module with a 2487 Dual Wavelength detector (UV detector) using Waters Symmetry C18 3.8x150mm column. Valine molecules were eluted with 98% solvent B (water) and 2% solvent A (HPLC grate acetonitrile) for 20 minutes at a flow rate of 1ml/min, injected volume was 100µl. Detection of D,L-valine molecules was measured at 210, 220 and 230nm, depending on the solvent (water/2-propanol) ratio.

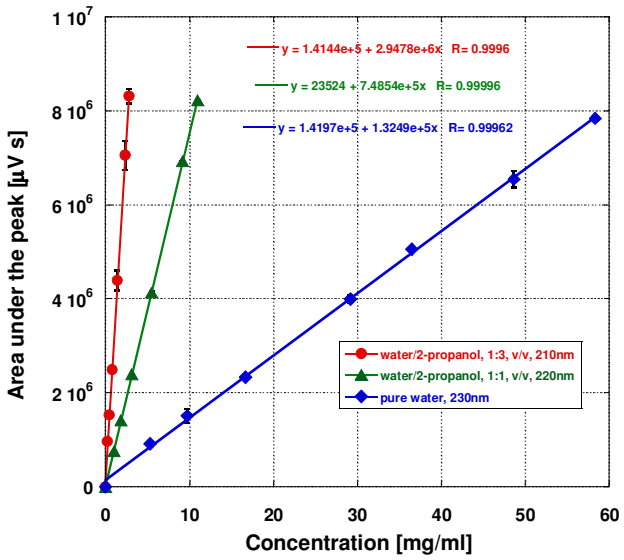

Figure 2.14 The HPLC calibration curves for D,L-valine in water/2-propanol solvents, solvent (water/2-propanol) ratios, 1:0, 1:1, 1:3, v/v.

The concentration calibration curves were determined at first for three different ratios water/2-propanol solvent, and then on the basis of these curves the concentration of D,L-valine saturated sample was measured (see “Solubility of D,L-valine” chapter for more details).

2.4 Optical and Scanning Electron Microscopy (SEM)

- Optical microscopy

The optical microscope uses visible light and a system of lenses to magnify images of small samples. Two kinds of optical microscopy were used to study antisolvent and cooling crystallisation process of D,L-valine from water/2-propanol solvent. Valine crystals morphology was studied using an OLYMPUS Vanox optical microscopy using a variety of magnifications between M5 – M100. All pictures were done with dry valine crystals and at room temperature around 23°C.

Liquid droplets were observed using a BX51 OLYMPUS optical microscopy with oil immersed lens 100x1.4 NA. All liquid-droplets pictures were done at room temperature around 23°C.

- Scanning Electron Microscopy (SEM)

Scanning Electron Microscopy (SEM) is a type of microscopy which uses a focused high-energy electron beam to generate a variety of signals at the surface of solid specimens that make it possible to examine objects on a very small scale. The signals obtained from electron-sample interactions give information about: morphology, topography, composition and crystallographic information. All SEM pictures were done with gold coated dry valine crystals using a Jeol JSM 6400 Scanning Electron Microscopy. Using a 6kV acceleration potential, samples were imaged using a variety of magnifications between 100-2000x. Samples were mounted on aluminium stubs, and a gold coat applied via sputter coating, prior to analysis.

3. Experimental methods.

3.1 D,L-valine solubility measurements

All chemicals and solvents were of laboratory reagent grade and used without further purification. The suppliers used were:

- 2-propanol, puriss.≥99.5% (Sigma Aldrich),
- D,L-valine, puriss. ≥ 99.0%, NT (Fluka),
- 3-(trimethylsilyl)-1-propanesulfonic acid sodium salt, puriss. ≥ 97.0% (Sigma Aldrich),
- 2-propanol-d^8, isotopic purity 99.9% (Alfa Aesar),
- Deuterium Oxide, isotopic purity 99.9% (Alfa Aesar),
- Deionised water was supplied from a in-house Milipore Water System.

3.1.1 Solubility measurement: GRAVIMETRIC METHODS

- Filtration.

A weighed excess of the crystalline phase was agitated with a small volume of solvent for at least 24 h at the constant temperature of 23°C. Next, the remaining amount of undissolved crystalline material was separated by filtration using a pre-weighted 0.45μm PVDF membrane filter (Durapore HV) and then the filter with the filtered cake was held for at least 3 days at laboratory temperature until it was completely dry (so that its mass remained unchanged). The dry filter with the filtration cake was weighted and the mass of dissolved valine was calculated from an overall material balance.

- Dissolution of crystals.

A solution with a weighed excess of crystalline material was prepared at constant temperature of 23°C and then the small volume (~1ml) of solvent was added gradually. Every time after addition of a new portion of solvent the solution was mixed for at least 1 hour and the presence of valine crystals was observed. This step was repeated until the last noticeable valine crystal was dissolved and then on the basis of this observation the saturation concentration was calculated.

3.1.2 Solubility measurement: HPLC

The solubility of D,L-valine in water/2-propanol mixtures was determined by allowing an excess of crystalline valine to equilibrate with solvent under agitation for at least 24h at the constant temperature of 23°C. Supernatant solutions were separated by filtration using disposable 0.2µm PP filters, diluted and analysed for solute concentration by HPLC. The saturation concentrations (solubility) of valine were determined by using appropriate calibration curves. HPLC was performed using a UV detector and reversed phase liquid chromatography column (RPLC) in stationary phase (Phenomenex Gemini 5µm, C18, 110A, 00G-4435-E0, 250mm x 4.60mm x 5microns). Mobile phases B and C were pure water and acetonitrile, respectively. The column was pre-equilibrated with 98% solvent B (HPLC grade water) and 2% solvent C (HPLC grade acetonitrile). All D,L-valine was eluted with a linear 98% to 2% gradient of solvent C for 20min at a flow rate of 1ml/min. Detection of valine molecules was measured at 210-230nm.
The thermostat temperature was 30°C. Injection volume was 100µl, and after each injection the needle was washed with water. The run time was 30min.

3.1.3 Solubility measurement: UV spectroscopy

The solubility of D,L-valine in water/2-propanol mixtures was determined by allowing an excess of crystalline valine to equilibrate with the solvent under agitation for at least 24h at the constant temperature of 23°C. Supernatant solutions were separated by filtration using disposable 0.2µm PP filters, diluted and analysed for solute concentration by UV spectroscopy, scanning over the wavelength range 195-400nm.

3.1.4 Solubility measurement: NMR

The solubility of the D,L-valine in Deuterium Oxide D_2O/2-propanol-d^8 mixture was determined by allowing an excess of crystalline phase to equilibrate with the D_2O/2-propanol-d^8 solvent with agitation for at least 24 hours at the constant temperature 25°C. Next, the supernatant solution was separated by filtration using a disposable 0.1µm PTFE syringe filter and glass syringe preheated to 25°C, diluted and analysed for solute by NMR using standard solution (TSP) placed into coaxial insert tube.

3.2 Antisolvent crystallisation – batch system

All chemicals and solvents were of laboratory reagent grade and used without further purification. The suppliers used were:

- 2-propanol, puriss. ≥ 99.5%, (Sigma Aldrich),
- D,L-valine, puriss. ≥ 99.0%, NT (Fluka),
- Glycine, puriss. ≥99.0%, NT (Fluka),
- L-histidine, puriss. ≥ 99.0%, (Sigma Aldrich),
- 3-(trimethylsilyl)-1-propanesulfonic acid sodium salt, puriss. ≥ 97.0% (Sigma Aldrich),
- 2-propanol-d^8, isotopic purity 99.9% (Alfa Aesar),
- Deuterium Oxide, isotopic purity 99.9% (Alfa Aesar),
- Deionised water was supplied from a in-house Milipore Water System.

3.2.1 2-propanol saturated with amino acid (D,L-valine)

2-propanol saturated with amino acid (D,L-valine) was prepared by intense mixing of 2-propanol and solute (2-3g solute in 1-2 l of solvent) for at least 6 hours in a glass bottle. Then the solution was filtered by 0.1μm (PTFE) syringe filter using a glass syringe and stored in a glass bottle. Before using these solutions, filtration was applied again to remove any newly formed crystals (in case laboratory temperature changed over time).

3.2.2 Aqueous solutions of amino acid (D,L-valine)

Aqueous solutions of amino acid (D,L-valine) were prepared by dissolution of a predetermined weighed amount of valine in distilled water, filtered by 0.2μm PP syringe filter using glass syringe, and stored in a glass bottle. Fresh aqueous solutions were prepared at least once a week in order to avoid bacterial contamination.

3.2.3 Standard solutions of 3-(trimethylsilyl)-1-propanesulfonic acid sodium salt (TSP)

A standard solution of 3-(trimethylsilyl)-1-propanesulfonic acid sodium salt (TSP) was prepared for NMR valine concentration measurement. 3ml of 2-propanol-d8/deuterium oxide solvent was placed into a small glass bottle and then the predetermined 3-(trimethylsilyl)-1-propanesulfonic acid sodium salt (weighed carefully) was added. The solution was mixed with a magnetic mixer for 24 hours at 25°C (dissolving all TSP standard), and then was transferred into NMR coaxial insert tube (Wilmad coaxial insert, stem L32mm, reference capacity 40µl, sample capacity 339µl). The tube with standard was precisely closed with a cap and parafilm. The five different standards were prepared with appropriate pure D_2O, 2-propanol-d_8 and 1:1, (v/v), ratio D_2O:2-propanol-d_8.

3.2.4 Batch antisolvent crystallisation

All batch antisolvent precipitation experiments were prepared at 25°C in small glass vials (diameter 25mm), with volume 5ml and mixing 180, 90 or 60 seconds with a magnetic mixer set to speed 975rpm, (MINI MR Standard IKA® WARKE, 1500 1/min Ident.No 00.250604, magnetic stirrer bar: 12mmx4.5mm; octagonal) or with a vortexer (Model: Lab dancer S2, IKA®, fixed speed 2800rpm, Ident.No. 3365000) (Figure 3.1). Appropriate volumes of aqueous solution were added to antisolvent solution (2-propanol saturated with D,L-valine) with a volumetric pipette (RAININ), and after mixing the sample was transported with a pipette into a quartz cuvette or NMR tube. Where samples were prepared differently it will be indicated in the results and discussion.

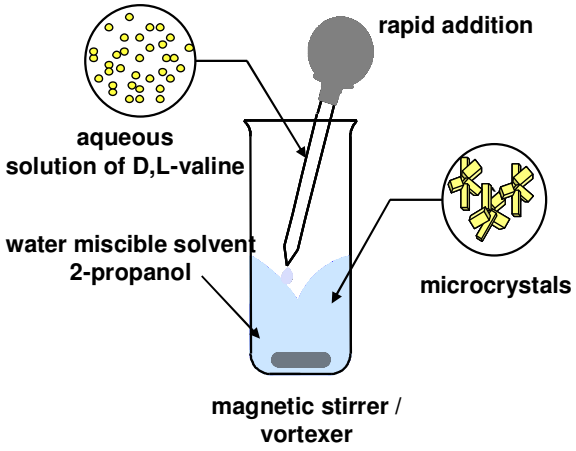

Figure 3.1 Schematic of batch apparatus using in antisolvent crystallisation processes.

3.3 Antisolvent crystallisation – continuous system

All chemicals and solvents were of laboratory reagent grade and used without further purification. The suppliers used were:

- 2-propanol, puriss. ≥ 99.5%, (Sigma Aldrich),
- D,L-valine, puriss. ≥ 99.0%, NT (Fluka),
- Deionised water was supplied from a in-house Milipore Water System.

3.3.1 2-propanol saturated with amino acids (D,L-valine)

Saturated isopropanol solutions were prepared by intense mixing of isopropanol and valine (about 2-3g solute in 1-2 l of solvent) for at least 6 hours. Then the solution was filtered by 0.45μm membrane filter (Millipore, Durapore HV) and stored in a glass bottle. Before using these solutions, filtration was applied again to remove any newly formed crystals (in case that laboratory temperature changes over time).

3.3.2 Aqueous solutions of amino acids (D,L-valine)

Aqueous solutions were prepared by dissolution of a predetermined weighed amount of valine in deionised water, filtered by 0.45μm membrane filter (Millipore, Durapore HV) and stored in a glass bottle. Fresh aqueous solutions were prepared at least once a week in order to avoid bacterial contamination.

3.3.3 Continuous antisolvent crystallisation

In continuous antisolvent crystallisation experiments the crystallising solutions were prepared using a Confined Impinging Jet mixer. The CIJ mixer contains the two inlet streams of aqueous solution (solvent) and 2-propanol saturated with D,L-valine (antisolvent) which are mixed in a very small volume of a cylindrical chamber placed in the central part of mixer, where a region characterized by fast flows and dissipation of turbulent kinetic energy is created. The diameters of inlet and outlet channels were 1mm and 2mm respectively. Figure 3.2 shows the scheme of the CIJ mixer used in experiments with dimensions. The solutions

(aqueous solution of D,L-valine and 2-propanol saturated with D,L-valine) were placed in glass bottle and the two gear pumps (Micropump magnetically coupled gear pumps, model GB-P35 JKSB form *ISMATEC®*) used to generate a required flow rate in the inlet streams. The pumps were calibrated and the mean error between solvent and antisolvent ratio was not larger than 5%. A sample of about 10ml was collected directly from the outlet of the CIJ mixer into a small glass vial. Then 1-2ml of sample was placed into a quartz cuvette for particles size measurement.

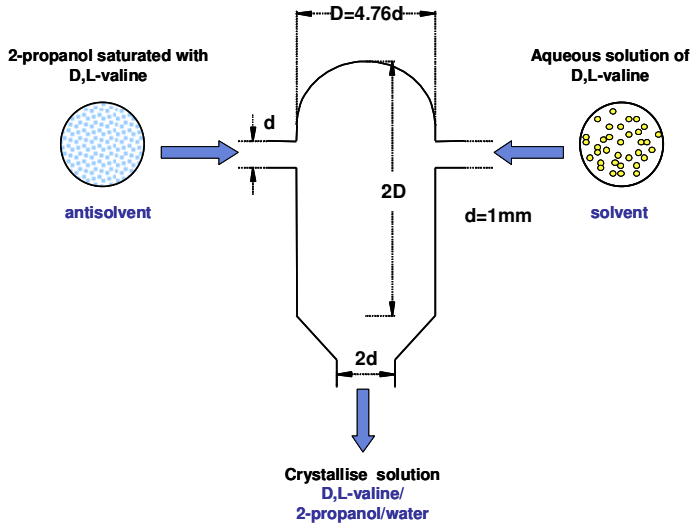

Figure 3.2 Schematic of Continuous Impinging Jet (CIJ) mixer.

The Reynolds number is the most common number used for characterisation of flow and is defined as a ratio of inertial forces, or those that give rise to motion of the fluid, to frictional forces, or those that tend to slow the fluid down. The Reynolds number is determined as: $\mathrm{Re} = \frac{\rho \cdot u \cdot d}{\eta}$ where, ρ is the density of the fluid, u is the velocity of the fluid in a pipe, d is the pipe diameter and η is the dynamic viscosity of the fluid. Based on the value of Reynolds number the characteristic flow could be specified as laminar (when Re is smaller than 2000) or as a turbulent flow (when Re is larger than 4000) ***(Paul et al. 2004).***

The inlet streams characteristic Reynolds numbers were calculated on the basis of the physical parameters of water and 2-propanol at 25°C (WATER: $\rho = 0.998$ g/cm^3, $\eta = 8.94 \cdot 10^{-4}$ Pa · s; 2-PROPANOL: $\rho = 0.787$ g/cm^3, $\eta = 2.044 \cdot 10^{-3}$ Pa). The Reynolds number of solvent in a jet with diameter 1mm and flow rate 60ml/min is 4465, and with flow rate 125ml/min Re=9303.

The Reynolds number of antisolvent in the inlet jet with diameter 1mm and flow rate 60ml/min is around 1540, and with flow rate 125ml/min Re=3208.

3.4 Cooling crystallisation of D,L-valine

All chemicals and solvents were of laboratory reagent grade and used without further purification. The suppliers used were:

- 2-propanol, puriss. ≥ 99.5%, (Sigma Aldrich),
- D,L-valine, puriss. ≥ 99.0%, NT (Fluka),
- 3-(trimethylsilyl)-1-propanesulfonic acid sodium salt, puriss. ≥ 97.0% (Sigma Aldrich),
- 2-propanol-d^8, isotopic purity 99.9% (Alfa Aesar),
- Deuterium Oxide, isotopic purity 99.9% (Alfa Aesar),
- Deionised water was supplied from a in-house Milipore Water System.

3.4.1 Cooling crystallisation

The supersaturated solution of D,L-valine was prepared by dissolution of predetermined weighed amount of solid valine in distilled water, filtered by 0.2μm PP syringe filter (using glass syringe), in a small glass vial with a screw-on cap, at 50°C for few hours. Then the valine aqueous solution was mixed with 2-propanol preheated to 50°C and filtered using a 0.1μm PTFE syringe filter using glass syringe and left 24hours, 2-propanol/water solvents ratio in the prepared solution was 1:1, (v/v). The syringes, filters, cuvettes and NMR tubs were placed in an incubator at 50°C beforehand to prevent the solution from crystallising. NMR and DLS sample holders were preheated to 50°C before solution was inserted. Data collection was started immediately and the temperature was reduced: from 50°C to 20-15°C. Dynamic Light Scattering measurements mostly were carried out with standard solvents: deionised water and 2-propanol, (some control DLS measurement was also done with deuterated solvents), and Nuclear Magnetic Resonance analysis with NMR solvents, using Deuterium Oxide and 2-propanol-d_8.

3.4.2 Cooling crystallisation – D,L-valine microcrystals filtration for SEM

D,L-valine crystals were isolated by filtration of crystallising mixtures on a 0.45μm membrane filter (Millipore, Durapore HV) with applied vacuum.

3.5 Cooling crystallisation of glycine

All chemicals and solvents were of laboratory reagent grade and used without further purification. The suppliers used were:

- glycine puriss. ≥ 99.0% (NT) (Fluka),
- 3-(trimethylsilyl)-1-propanesulfonic acid sodium salt, puriss. ≥ 97.0% (Sigma Aldrich),
- 2-propanol-d^8, isotopic purity 99.9% (Alfa Aesar),
- Deuterium Oxide, isotopic purity 99.9% (Alfa Aesar),
- Deionised water was supplied from a in-house Milipore Water System.

3.5.1 Cooling crystallisation

The supersaturated solution of glycine was prepared by dissolution of predetermined weighed amount of solid glycine in distilled water, filtered by 0.2μm PP syringe filter (using a glass syringe), in a small glass vial with a screw-on cap, at 55ºC for few hours. The syringes, filters, cuvettes and NMR tubs were placed in an incubator at 55ºC beforehand to prevent the solution from crystallising. NMR and DLS sample holders were preheated to 55ºC before solution was inserted. Data collection was started immediately and the temperature was reduced: from 55°C to 10°C.
Dynamic Light Scattering measurements were done with normal solvents (deionised water), and Nuclear Magnetic Resonance analysis with NMR solvents, using Deuterium Oxide. The control DLS sample with deuterated solvent was also prepared.

3.5.2 Cooling crystallisation – glycine microcrystals filtration for SEM

Glycine crystals were isolated by filtration of crystallising mixtures on a 0.45μm membrane filer (Millipore, Durapore HV) with applied vacuum.

4. SOLUBILITY of D,L-valine.

The solubility represents the maximum (saturated) concentration of the solute that can be dissolved in a given solvent at a given temperature and pressure. Design of crystallisation processes needs to be based on solubility data which are used to predict the theoretical yield or choose the most suitable crystallisation method (e.g. cooling, evaporation, antisolvent) for a certain system ***(Mullin 1993).***

It could be expected that non-polar D,L-valine molecules will be more soluble in non-polar solvent than in polar one (e.g. water). However, the amino acids generally are more soluble in water and poorly soluble in non-polar organic solvents. This reflects the presence of the zwitterions (molecules which contain acidic and bases groups at the same time). In polar solvent the ionic attractions between the ions in a solid amino acid are replaced by strong solvation interaction of zwitterions.

The solubility can be measured using several standard analytical techniques such as High Performance Liquid Chromatography (HPLC), Spectroscopy, such as UV, IR, NMR MS and thermogravimetric analysis etc.***(Mullin 1993)***. In all these techniques it is necessary to prepare a calibration curve. The calibration curve can be constructed from data which can be obtained by measurement of concentrations of a series of solution of known composition. Thus, the composition of unknown solution is then determined on the basis of the calibration curve.

The solubility of D,L-valine in 2-propanol/water solvents at different solvent ratios (1:3, 1:1, 3:1 H_2O/2-propanol, v/v) was measured using gravimetric techniques, HPLC, UV spectroscopy and NMR.

4.1 Solubility measurement: GRAVIMETRIC METHODS

Gravimetric methods are among the fastest and simplest ways to determinate the solubility of a solute. However, the methods require a precise procedure in sample preparation to minimize the errors of measurement. The solubility of D,L-valine was measured at the constant temperature of 23°C and three different solvents ratios: 1:3, 1:1, 3:1 2-propanol/water, v/v. Table 4.1 and Figure 4.1 show the solubility data determined with

the gravimetric methods. The data for solubility in pure water and 2-propanol was taken from literature.

Table 4.1 Solubility of D,L-valine in 2-propanol/water at 23°C, GRAVIMETRIC METHODS.

Mass fraction of 2-propanol		Mass fraction of water		Solubility [mg/ml]		Mass fraction of D,L-valine	
Filtration	Crystals dissolving	Filtration	Crystals dissolving	Filtration	Crystals dissolving	Filtration	Crystals dissolving
(0)*		(0.934)*		(70.00)*		(0.066)*	
0.202	0.202	0.768	0.769	29.13	28.70	0.030	0.029
0.434	0.435	0.551	0.552	13.17	11.67	0.015	0.013
0.700	0.700	0.296	0.297	3.26	2.63	0.004	0.003
(0.999)*		(0)*		$(5.0 \cdot 10^{-4})$*		$(6.37 \cdot 10^{-6})$*	

* data in parentheses are taken from literature ***(Vos 2006; Yalkowsky and He 2003)***.

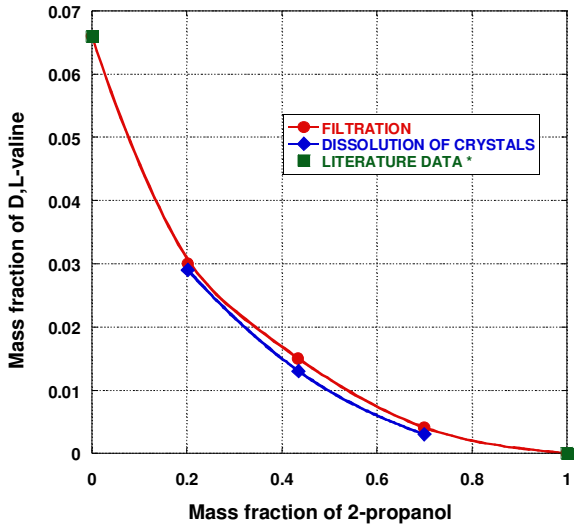

Figure 4.1 Solubility curve for different 2-propanol/water ratios at 23°C measured with GRAVIMETRIC METHOD, mass fraction of D,L-valine as a function of mass fraction of 2-propanol.

4.2 Solubility measurement: UV SPECTROSCOPY

Solubility measurement was done at the constant temperature of 23℃ and three different solvent ratios: 1:3, 1:1, 1:0 2-propanol/water, v/v. The saturated concentration was calculated on the basis of calibration curves plotted in Figure 2.12, which was determined from the series of solutions with different D,L-valine concentration prepared without filtration before UV absorbance measurements.

The calibration curves for D,L-valine/water/2-propanol solutions filtered through 0.45μm PTFE filter was also done, however, these data showed large deviations. Figure 4.2 shows calibration curves for filtered and unfiltered solution for solvent ratio 3:1, 2-propanol/ water, v/v measured at 210nm wavelength.

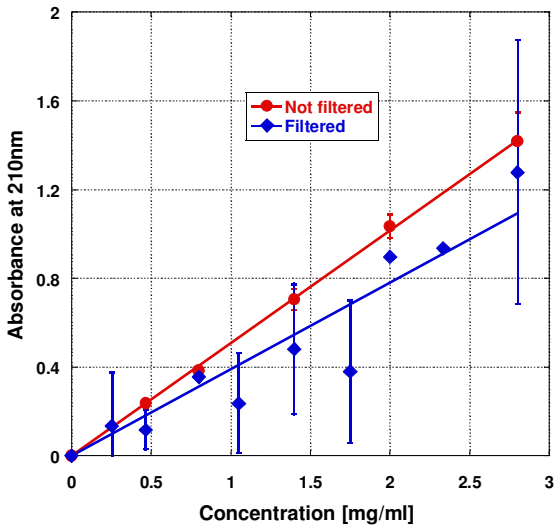

Figure 4.2 UV spectroscopy calibration curves for series of solutions with different D,L-valine concentrations **filtered** through 0.45 μm PTFE filter and **not filtered**, solvent ratio 3:1, 2-propanol/ water, v/v at 210nm.

Filtered solutions showed lower absorbance values for higher concentration than expected if we take into consideration that all prepared solutions were undersaturated in D,L-valine. Filtration may have removed subvisible particles which contribiute the absorbance value, and the presence of scattering particles in the investigated samples could lead to increasing the measured absorbance ***(Vekshin 2002).*** This point will be explained better following the results and discussion of Dynamic Light Scattering measurements. Table 4.2 shows the

solubility data determined with UV spectroscopy- using the calibration cuve obtained for unfiltered solutions.

Table 4.2 Solubility of D,L-valine in 2-propanol/water at 23°C, UV SPETROSCOPY.

Mass fraction of 2-propanol	Mass fraction of water	Solubility [mg/ml]	Mass fraction of D,L-valine
0	0.936	68.33	0.064
0.433	0.551	14.57	0.016
0.700	0.296	3.26	0.004

4.3 Solubility measurement: HPLC

HPLC was another technique used for solubility measurement of D,L-valine. Similarly to the previous solubility experiments, samples were prepared at constant temperature of 23°C with three different solvent ratios: 1:3, 1:1, 1:0 2-propnol/water, v/v. The saturation concentration was determined on the basis of the calibration curves plotted in Figure 2.14. The calibration curves were also determined for valine filtered solutions (0.45 μm PTFE) and HPLC data look more consistent compared to the data obtained using UV spectroscopy (Figure 4.3). However, still filtered solution has smaller values of area under the peak than a solution with the same concentration but not filtered, especially with higher valine concentration samples. One explanation of these results could be that scattered species present in the solution (detected by UV spectrophotometer) now could be stuck to the column and only small fraction of valine from them could be eluated. It could be also possible that the eluants diluted the tested sample with the scattering species and even though the same detector was applied (UV) a different result are obtained for exactly the same samples. The number of scattering species still is unknown and this point will be better explained in the results and discussion of Dynamic Light Scattering measurements.

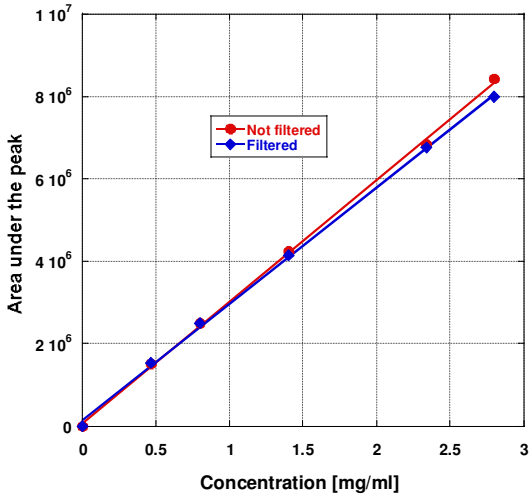

Figure 4.3 HPLC calibration curves for series of solutions with different D,L-valine concentrations **filtered** through 0.45 μm PTFE filter and **not filtered**, solvent ratio 3:1, 2-propanol/ water, v/v at 210nm.

Table 4.3 shows the solubility data determined using HPLC.

Table 4.3 Solubility of D,L-valine in 2-propanol/water at 23°C, HPLC.

Mass fraction of 2-propanol	Mass fraction of water	Solubility [mg/ml]	Mass fraction of D,L-valine
0	0.935	69.03	0.065
0.433	0.550	15.23	0.017
0.700	0.296	3.33	0.004

4.4 Solubility measurement: NMR

The solubility of the crystalline D,L-valine in deuterium oxide 2-propanol-d_8 /D_2O mixtures with a 0:1, 1:3, 1:1, 3:1, 1:0 solvent ratios at 25°C using NMR. The saturation concentrations were determined on the basis of data from the reference sample with known concentration (see Experimental Techniques and section for details). Since kinetic experiments on antisolvent and cooling crystallisation processes were done using NMR, the solubility data for deuterated solvents were measured. Table 4.4 shows the solubility data measured at constant temperature of 25°C using NMR and deuterated solvents.

Table 4.4 Solubility of D,L-valine in 2-propanol-d_8/D_2O at 25°C, NMR.

Mass fraction of 2-propanol-d_8	Mass fraction of deuterium oxide (D_2O)	Solubility [mg/ml]	Mass fraction of D,L-valine
0	0.938	73.01	$6.20 \cdot 10^{-2}$
0.207	0.763	32.74	$3.01 \cdot 10^{-2}$
0.443	0.543	14.54	$1.43 \cdot 10^{-2}$
0.708	0.290	2.69	$2.82 \cdot 10^{-3}$
0.999	0	0.022	$2.50 \cdot 10^{-5}$

The solubility data obtained using different techniques are plotted in Figure 4.4.
Figure 4.4a shows the solubility data measured using three different methods: gravimetric, UV spectroscopy and HPLC. All measurements were done at 23°C and using hydrogen oxide (H_2O) and 2-propanol. Figure 4.4b shows additional data obtained using NMR and deuterated solvents (D_2O and 2-propanol-d_8) prepared at 25°C.

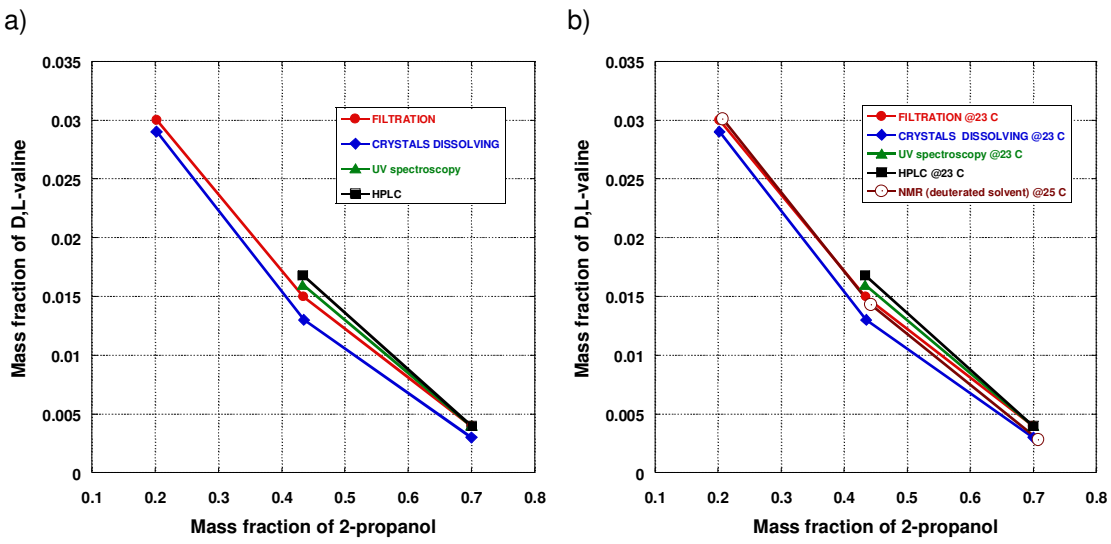

Figure 4.4 Solubility data obtained using different techniques: gravimetric methods, UV spectroscopy, HPLC and NMR, mass fraction of D,L-valine plotted as a function of mass fraction of 2-propanol a) solubility in hydrogen oxide (H_2O) and 2-propanol at 23°C , b) solubility in hydrogen oxide (H_2O) and 2-propanol at 23°C, and data obtained using NMR, deuterium oxide (D_2O) and 2-propanol-d_8 at 25°C. Solvent ratio: 3:1, 1:1, 1:3 2-propanol (2-propanol-d_8)/H_2O (D_2O).

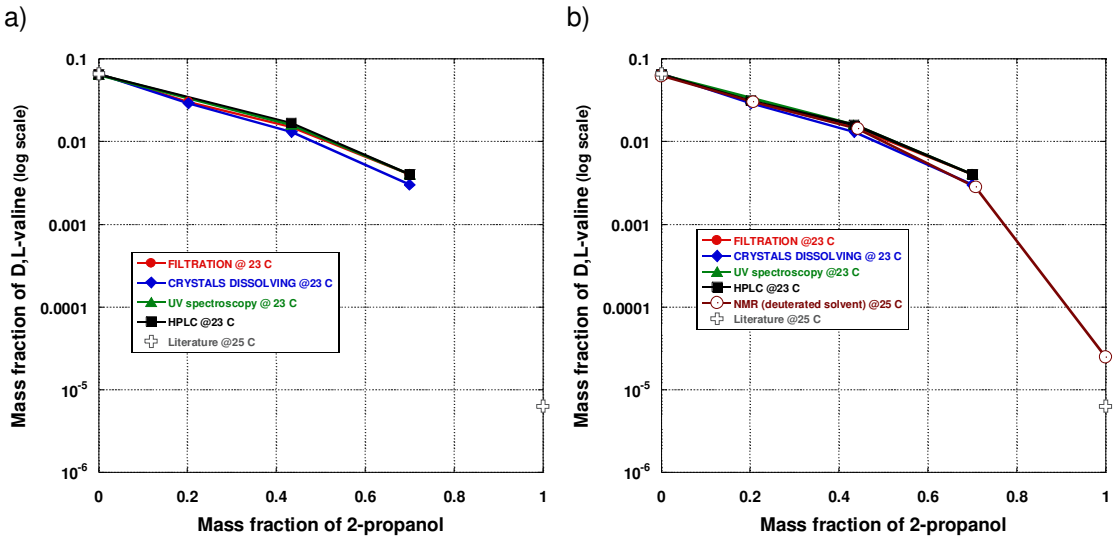

Figure 4.5 Solubility data obtained using different techniques: gravimetric methods, UV spectroscopy, HPLC, NMR and data from literature, mass fraction of D,L-valine plotted as a function of mass fraction of 2-propanol a) solubility in hydrogen oxide (H_2O) and 2-propanol at 23°C and at 25°C (literature data) , b) solubility in hydrogen oxide (H_2O) and 2-propanol at 23°C and 25°C (literature data) and deuterium oxide (D_2O) and 2-propanol-d_8 at 25°C. Solvent ratio: 1:0, 3:1, 1:1, 1:3, 0:1 2-propanol (2-propanol-d_8)/H_2O (D_2O).

Figure 4.5 shows the data obtained for whole measured range of solvent ratio using different methods and with some data which were taken from literature.

In spite of difficulties with UV spectroscopy and HPLC measurements the solubility data seem not to be different and same variations could be due to removal of scattering species from measured samples. Better explanation of this point will be in later sections.

5. ANTISOLVENT CRYSTALLISATION of D,L-valine –batch system.

In this chapter the extensive experimental study of the antisolvent crystallisation of D,L-valine initiated by mixing an aqueous solution of D,L-valine with 2-propanol alcohol (saturated with valine) is presented. The composition and kinetics of the system were particularly well suited to study by complementary techniques: including spectrophotometry, NMR spectrometry and dynamic light scattering (DLS). Four different ratios of 2-propanol (antisolvent)/water (solvent) were investigated (3:1, 1:1, 1:3, 9:1), and some preliminary results for other amino acids (glycine, histidine) will be also presented.

5.1 Antisolvent (2-propanol) – solvent (H_2O) ratio 1:1, v/v

Crystallisation of the amino-acid, D,L-valine, can be achieved rapidly by vigorously mixing an aqueous valine solution with the water miscible solvent, 2-propanol, a poor solvent (or antisolvent) for valine. During studies of the kinetics of this process it was observed that the time taken for microcrystals to appear from a clear undisturbed homogeneous solution was a strong function of the type, intensity and period of mixing originally used to prepare it. In order to investigate this phenomenon further, a number of complementary techniques were used to monitor the time evolution of the mixed solution including spectrophotometry, nuclear magnetic resonance (NMR) and dynamic light scattering (DLS), see Figure 5.1.

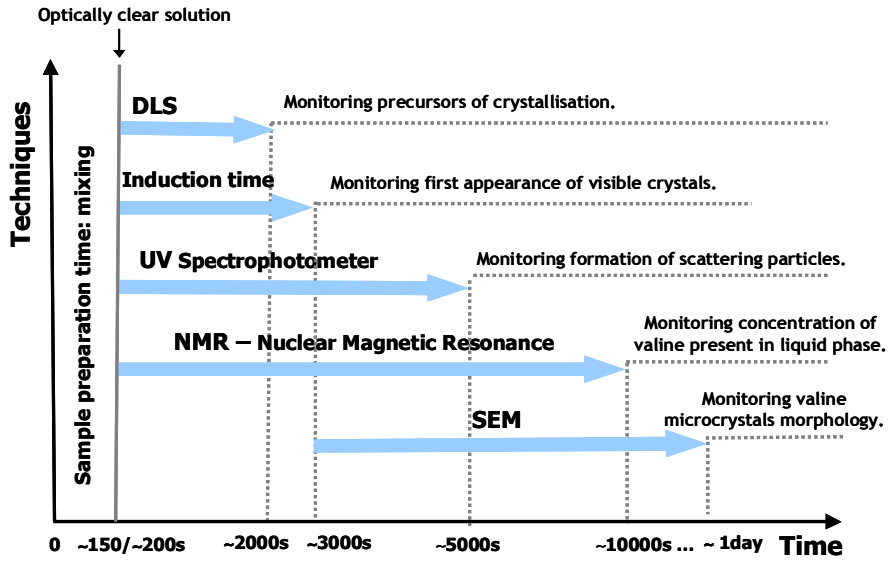

Figure 5.1 Monitoring Techniques and Experimental time-scales.

Samples for antisolvent crystallisation study were prepared by mixing an aqueous valine solution with an equal volume of 2-propanol in a small glass vial, using either a magnetic stirring bar or a vortex mixer. This mixing process was carefully controlled and a clear apparently homogeneous solution was typically generated in less than 5 s. The mixing was then continued for measured periods to give total agitation times of between 60 and 180 s. Previous studies showed that the vortex mixer (vortexing) provided more intense shearing of the mixture than the use of the magnetic stirrer (stirring) ***(Baldyga and Bourne 1999; Bourne et al. 1981; Johnson and Prud'homme 2003; Paul et al. 2004; Paul and Treybal 1971).*** Typically, 2.56 ml of an aqueous valine solution of known concentration was rapidly admixed with 2.5 ml of 2-propanol in a 20 ml vial to give a solution of specified supersaturation. The time before appearance of the first crystals (induction time), was found to vary as a function of the period and type mixing as well as the supersaturation.

5.1.1 Induction times

Induction times were determined by visual inspection of the standing solutions and plots of induction time as a function of valine supersaturation made for different mixing methods and mixing periods (Figure 5.2, Table 5.1). Supersaturated S was calculated using relation $S = \frac{C_{Val}}{C_{Val,eq}}$ where, C_{Val} is a actual valine concentration in sample and $C_{Val,eq}$ is the solubility equilibrium ($C_{Val,eq}$ = *14.54mg/ml*, water/2-propanol, 1:1, v/v). In general it was

observed that mixing conditions had a large impact on the time appearance of the first crystals. For higher valine concentrations (> 19mg/ml) crystal formation was always relatively fast and the first crystals could be observed in solutions mixed for less than 60s. At lower valine concentrations, induction times were slow enough to allow the effects of different mixing regimes to be seen. For example with an 18 mg/ml valine solution, initially stirred for 60 s, the first crystals were visually observed 420s later, while for the same composition initially stirred for 180s crystals started to appear after only 60 s. When the initial mixing period was kept constant at 90s, but different types of mixers were used, further effects on induction time were revealed. With the stirred samples, the first crystals were observed 270 s later, with the vortexed samples they appeared 150 s later.

In all these experiments actual formation of the supersaturated solution was very rapid, since it required only seconds to achieve complete mixing of the two fully miscible solvents. Variations in the induction times were therefore influenced by mixing processes carried out over periods 30-50 times greater than this. Such behaviour clearly does not fit with a classic crystallisation mechanism because, once a supersaturated solution is produced, the process of molecular association to form critical nuclei should not be affected by the period or intensity of mixing, unless mixing promotes heterogeneous nucleation. Furthermore when the initial mixing conditions were kept identical but the supersaturation varied, a standard plots of log induction time versus log reciprocal of supersaturation squared was not linear, as would be predicted by classical theory, see Figure 5.2. To better understand the kinetics of the crystallisation process it was decided to use spectrophotometry to monitor the rate of formation of scattering particles following the initial mixing step. The plot of induction times (t_{ind}) as a function of initial supersaturation (log $(S)^{-2}$) of D,L-valine is attached in Appendix (Figure 11.1).

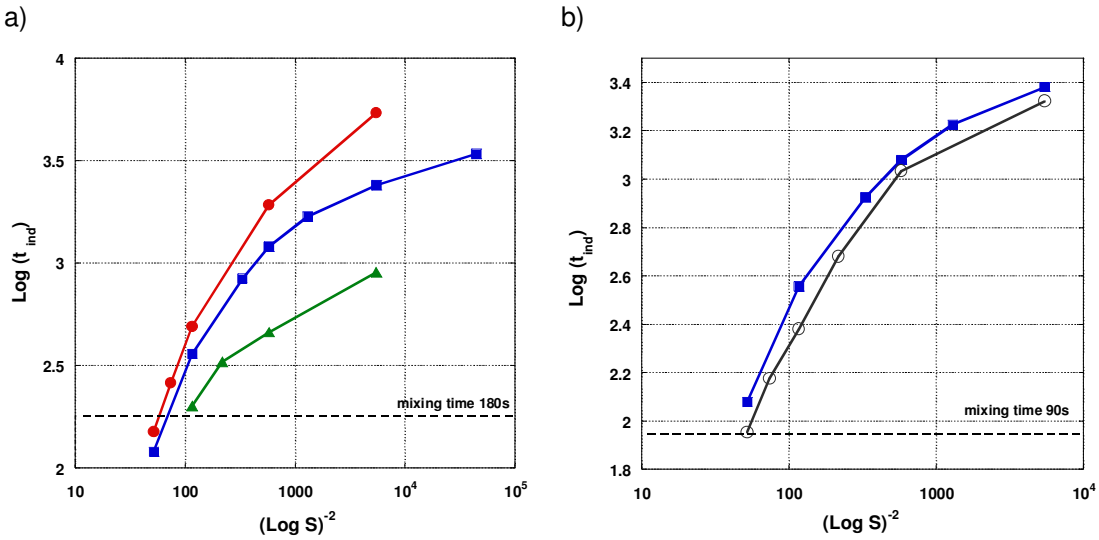

Figure 5.2 Plot of induction times (Log (t_{ind})) as a function of initial supersaturation (Log S)$^{-2}$ for D,L-valine: a) **magnetic mixer**, mixing time: 60s (red circles), 90s (blue squares), 180s (green triangles), b) **mixing time 90s**, magnetic mixer (blue squares), vortexer (opened black circles), 2-propanol/water, 1:1, v/v.

Table 5.1 Induction times for different mixing conditions and valine concentrations, substracted mixing times, 2-propanol/water, 1:1, v/v.

	Induction times [s]			
Concentration [mg/ml]	Magnetic mixer 60s	Magnetic mixer 90s	Magnetic mixer 180s	Vortexer 90s
14.7	-	3330	-	-
15	5340	2310	720	2010
15.5	-	1590	-	-
16	1860	1110	280	990
16.5	-	750	-	-
17	-	-	150	390
18	420	270	60	150
19	200	-	-	60
20	90	60	-	-

5.1.2 Spectrophotometry

This technique was used to monitor changes of absorbance within stationary pre-mixed solutions at a fixed wavelength of 600nm. As the number (or size) of scattering particles increased there was an apparent increase in the absorbance of a sample due to scattering of the incident light and this was used to monitor the crystallisation process.

Unfortunately, because the intensity of scattering is a strong function of the number and the size of particles, both of which were likely to be changing, spectrophotometry can only be used to extract qualitative kinetic data. However, it was reasoned that because identical starting compositions were to be used it may be possible to make useful comparisons of the effect mixing had on the process. Samples were prepared by vortexing or stirring, transferred to a quartz cuvette and introduced into the spectrophotometer. The lag time prior to data collection was 150 s and 200 s for samples initially mixed for 90 s and 180 s respectively. It was observed that repeat runs of the same sample were not very reproducible and hence conditions were chosen such that the differences between mixing regimes were large enough for conclusions to be drawn. Representative data are shown in Figure 5.3 and Figure 5.4. The maxima that were typically observed in the absorbance-time plot are interpreted as arising because flocculation leads to sedimentation of crystals out of the optical path. From Figure 5.3a it can be seen that samples that were initially stirred for longer, 180 s versus 90s, showed significantly increased absorbance and this persisted right out to 2000 s. The effect of preparing samples by vortexing was even more striking (Figure 5.3b and Figure 5.4).

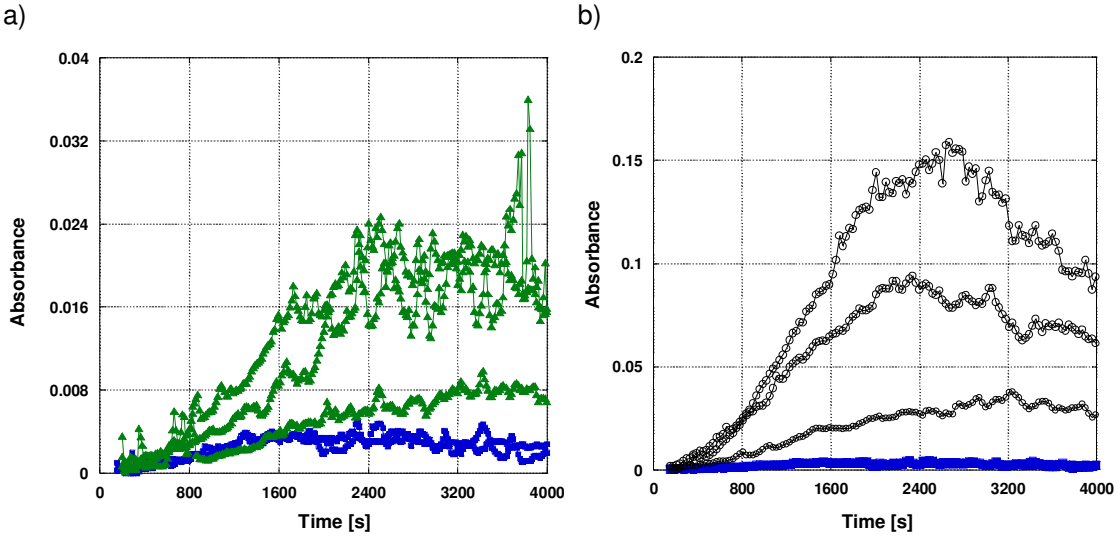

Figure 5.3 Turbidity measurement: a) **effect of mixing time** using magnetic mixer, 90 seconds (blue squares), 180 seconds (green triangles), b) **effect of mixer type**, mixing time 90seconds, magnetic mixer (blue squares), vortexer (opened black circles), $\mathbf{C_{val}}$**=18mg/ml**, 2-propanol/water, 1:1, v/v.

Vortexed samples exhibited an up to ten-fold increase in absorbance, relative to the stirred samples, and tended to show a more pronounced intensity maximum for higher (18mg/ml Figure 5.3b) and lower (16mg/ml and 17mg/ml Figure 5.4) valine concentration.

This reinforces the observation that an initial period of high intensity mixing increases the subsequent crystallisation rates. In order to better distinguish whether the higher absorbance should be attributed to a greater number of scattering particles or to the formation of much larger particles, scanning electron microscopy (SEM) was used to image the crystals formed.

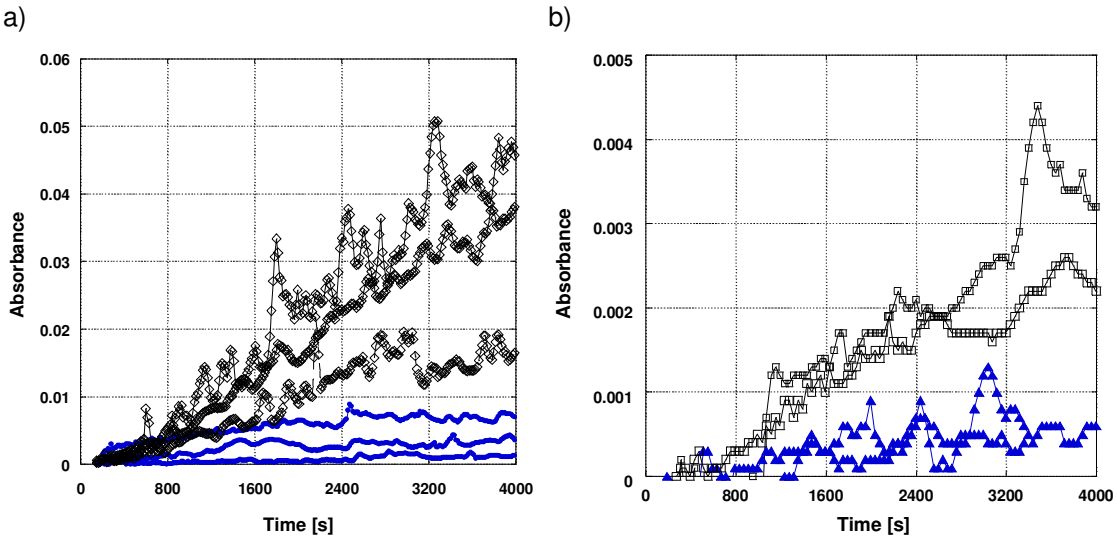

Figure 5.4 Turbidity measurement: **effect of type of mixer**, mixing time 90 seconds, a) C_{val}**=17mg/ml**, magnetic mixer (blue circles), vortexer (opened black rhombus), b) C_{val}**=16mg/ml**, magnetic mixer (blue triangles), vortexer (opened black squares) 2-propanol/water, 1:1, v/v.

5.1.3 Scanning Electron Microscopy (SEM)

Valine crystals were isolated by rapid filtration of the crystallising mixtures on a membrane with applied vacuum. Samples were filtered after ~2800 and ~7200 seconds and representative SEM images of the collected microcrystals are shown in Figure 5.5. D,L-valine crystallises in the form of thin rhombohedral-shaped plates, typically with well defined edges and vertices. Publised powder XRD experiments on valine microcrystals of very similar appearance, precipitated by mixing a 1:9 v/v mix of aqueopus solution with 2-propanol, showed the presence of a single monoclinic $P2_1/c$ polymorph ***Vos 2006***. The average size of the crystals was very comparable for samples prepared using either form of mixing but the vortexed samples appeared to contain a second population of needle-like crystals. Since the particles were generally of similar size the much higher scattering intensities observed with the vortexed samples can be confidently assigned to production of greater number of crystals. Indeed filtration actually directly showed that the mass of crystals isolated from the vortexed sample was much greater than the stirred sample. Because the

high variability of this spectrophotometric data made it difficult to extract precise kinetic information it was decided to probe the kinetics of the crystallisation process using ^{1}H NMR.

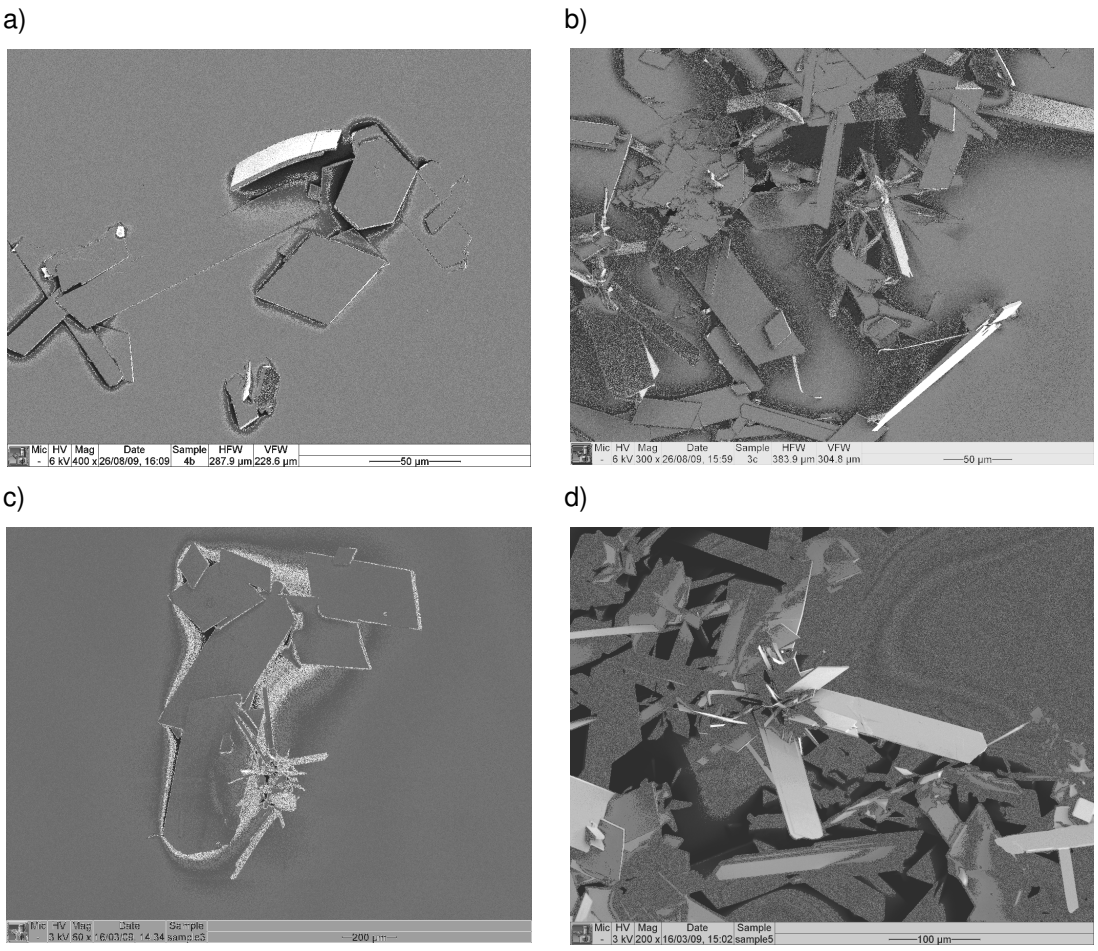

Figure 5.5 SEM images of valine microcrystals,mixing time 90s a) magnetic mixer, b) vortexer, **C_{val}=18mg/ml, filtered after 2800s**, c) magnetic mixer, d) vortexer, **C_{val}=17mg/ml, filtered after 7200s.**

5.1.4 ^{1}H Nuclear Magnetic Resonance (NMR)

The nuclear relaxation times for a substance in solution are considerably faster than in the solid state and hence it is possible to use solution-phase NMR to selectively determine the amount of solute remaining in the liquid phase throughout a crystallisation process. Within the NMR tube the solid phase is effectively invisible and sedimentation and changes in the size of and morphology of crystals will not impact on the data. One drawback is that the crystallisation needs to be carried out in deuterated solvents. However, this will typically only result in small differences in solubility and because the technique is quite sensitive only

small amounts of solvent are required. Samples were prepared by mixing deuterated aqueous valine and deuterated 2-propanol using different mixing regimes and transferred to an NMR tube in which was present a smaller tube containing an internal reference standard (TSP) of known concentration. The reference allowed the absolute concentration of valine remaining in solution to be monitored throughout the crystallisation process. Figure 5.6 shows the variation of valine concentration with time for samples prepared with a range of initial concentrations using either vortexing or stirrering. The dotted line at 14.54 mg/ml shows the experimentally determined solubility limit for valine crystals in a 1:1 v/v mixture of deuterated water and 2-propanol. An initiation period of 500-1000 s was observed for most samples during which the valine concentration remained approximately constant (a similar initiation period in which no scattering species could be seen occurred in the spectrophotometry experiments).The conversion of soluble valine to the solid-state could be followed much more precisely and reproducibly in the NMR experiments. Differences in the kinetics of the crystallisation process for the two mixing methods were very apparent, particularly at higher supersaturation. For the vortexed samples, the rate of loss of valine was a clear function of supersaturation with much higher initial crystallisation rates being observed above a threshold of about 16.5 mg/ml. Interestingly, the time to completion of the crystallisation process was similar whatever the starting concentration, taking around 10,000 seconds. With the stirred samples conversion of valine to the solid-state was found to be much slower at the higher concentrations (Figure 5.6b).

Linear regression of liquid phase concentration data were preformed as follows:

C_{Val}=15.7mg/ml; y= 16.44-**2.222e^{-4}**x; R^2=0.80

C_{Val}=15.9mg/ml; y= 16.09-**2.289e^{-4}**x; R^2=0.99

C_{Val}=16.6mg/ml; y= 16.95-**1.641e^{-4}**x; R^2=0.94

C_{Val}=17.6mg/ml; y= 17.63-**1.338e^{-4}**x; R^2=0.85

Crystallisation rates determinated from the slop of linear regression are shown in Figure 5.7.

Furthermore, after the initiation period the reductions in valine concentration appeared to very constant with time (Figure 5.7). These differences between the data for mixed and vortexed samples are striking and point to different limitations on the rate of crystal formation and growth depending on how the samples were prepared.

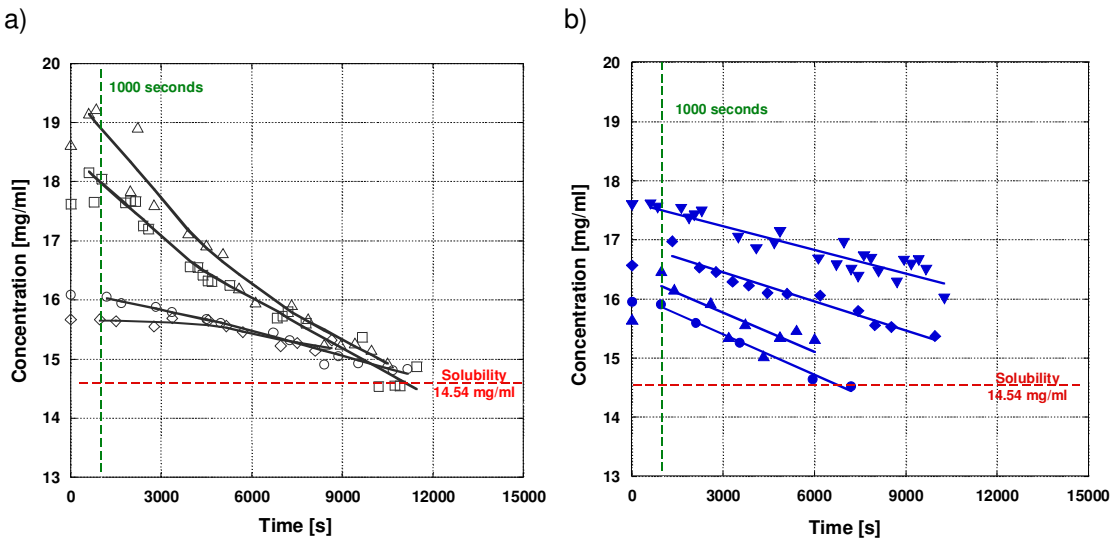

Figure 5.6 Kinetics of antisolvent crystallisation process determined using NMR, mixing time 90s, 2-propanol/water, 1:1, v/v, at 25°C, a) Vortexer, b) Magnetic mixer.

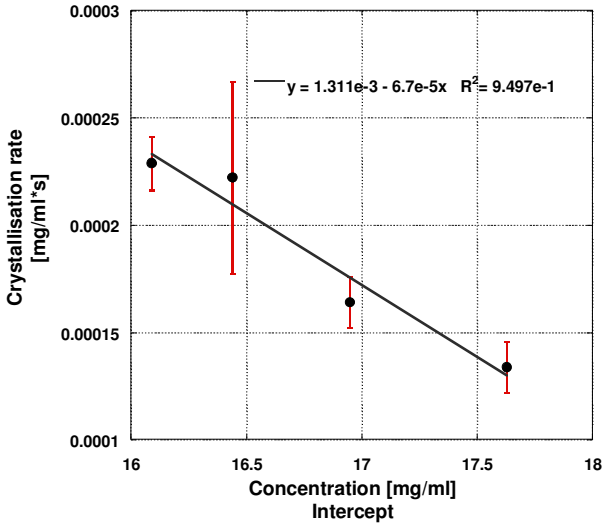

Figure 5.7 Crystallisation rate as a function of D,L-valine concentration determined using NMR, magnetic mixer 90s, 2-propanol/water, 1:1, v/v, at 25°C.

One plausible explanation of the results would be that nucleation takes place preferentially at the solvent-air interface. High intensity agitation will increase the area of this interface and hence the rate of crystallisation will be greatest in vortex solution because a larger number of nuclei will initially be formed. This explanation would be consistent with conventional theories of heterogeneous nucleation. An alternative more radical explanation

would be that within the supersaturated solution there are a sub-visible intermediate species which are sufficiently large to be affected by mixing processes. In order to probe for the possible presence of such species, dynamic light scattering (DLS) was used to monitor the crystallising solutions.

5.1.5 Dynamic Light Scattering (DLS)

DLS is a very useful experimental technique for characterising nanoscale particles in solution. By measuring the time-dependent fluctuations of scattered light, arising from Brownian motion of nanoscale particles, diffusion coefficients and particle size information can be extrapolated. For this study it was found that the technique could typically only be applied to study the first 2000 seconds because after this interference from larger scattering species (probably sedimenting crystals) became too intense. Figure 5.8 shows an example of the autocorrelation function g_2-*1* obtained for a sample prepared by mixing together pre-filtered aqueous valine and 2-propanol, with a magnetic stirrer to generate a valine concentration of 16mg/ml. Immediately following mixing two different kinds of scattering species could be detected in the visibly clear solution, very small molecular clusters (dimers, trimers) and larger nanoclusters. The presence of small molecular clusters has been reported previously and might be expected for a molecule with large nonpolar regions dissolved in a polar medium. The presence of the larger nanoclusters was much more surprising.

a) b)

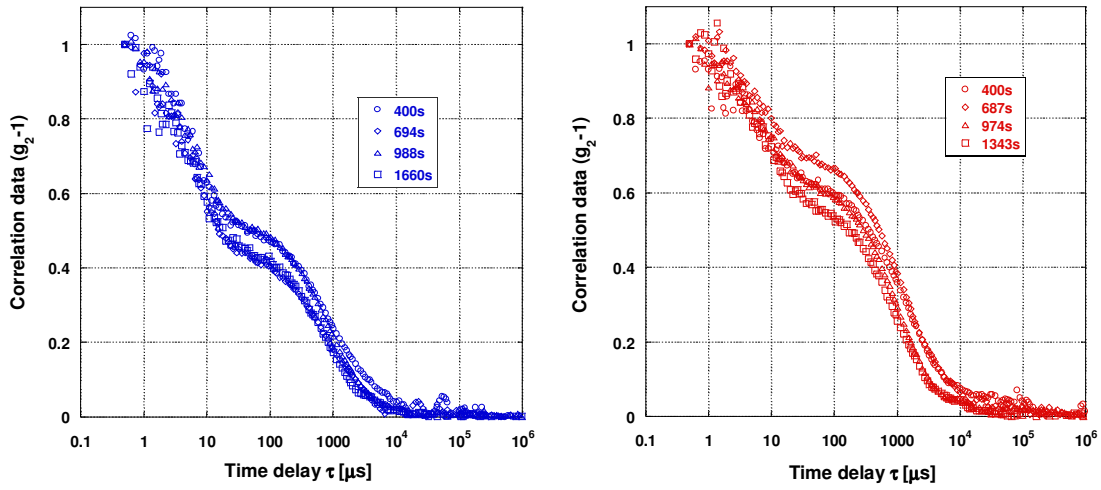

Figure 5.8 Light scattering autocorrelation function g_2-*1* of crystallising solutions, **Cval=16mg/ml**, data collecting time 400s – 1700s, a) 2-propanol/ water (H_2O), 1:1, v/v, b) 2-propanol/ Deuterium Oxide (D_2O), 1:1, v/v.

Control experiments showed that no scattering species were present in filtered aqueous valine solution or in filtered 2-propanol, prior to mixing, and none were formed in mixtures prepared at low valine concentrations (Figures 5.9 and Figure 5.10). They cannot therefore be ascribed to the formation of impurities or bubbles and must arise because of the presence of the supersaturated valine.

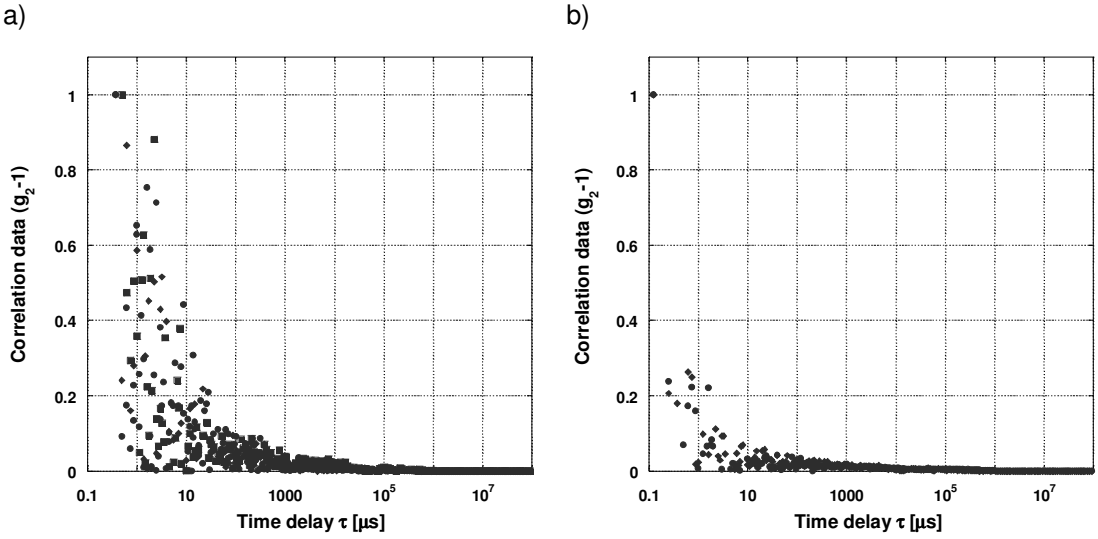

Figure 5.9 Light scattering autocorrelation function g_2-*1*, a) **water** filtered through 0.2μm PP filter, b) **2-propanol** filtered through 0.1 μm PTFE filter.

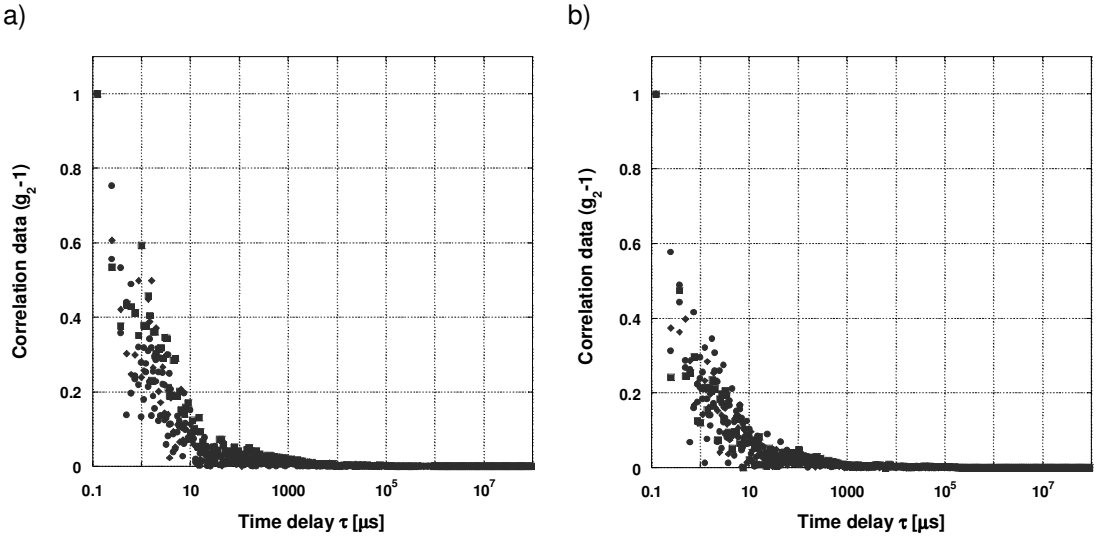

Figure 5.10 Light scattering autocorrelation function g_2-*1* of solvent: **2-propanol/water, 1:1, v/v**, mixing time 90s, a) vortexer, b) magnetic mixer.

The NMR results, described above, showed that for the first 1000s of the crystallization process there was an induction period during which all valine put into the system was in a liquid phase and no solid particles were present. The observed scattering must therefore be formed by separation of some fraction of the valine into liquid valine-rich nanodroplets which are dispersed throughout the saturated molecular valine solution. The size of the scattering species were determined by fitting two separate decay parts of the autocorrelation graph, $\ln(g_1)$ where, $g_1 = \sqrt{g_2 - 1}$, with 1^{-st} and 2^{-nd} order functions and from the fit parameters the diffusion coefficient, and subsequently the hydrodynamic diameters were calculated from the Stokes-Einstein equation (more details in Experimental Techniques chapter). The physical parameters used in hydrodynamic diameter calculations were taken from ***(Flick 1998)*** and for 2-propanol/water ratio 1:1, v/v were: viscosity η*=0.0033 Pa·s*, refractive index *n=1.365* and temperature *T=298K*. (Solvent viscosity and refractive index table in Appendix Table 11.1).

DLS analysis was carried out on mixtures prepared over a wide range of valine concentrations from undersaturated to supersaturated solutions. Unexpectedly these experiments revealed that molecular clusters and nanodroplets were present not only in saturated solutions but also in undersaturated solutions. Even at 7 mg/ml, well below the measured valine crystal solubility limit of 14.5 mg/ml, time fluctuating signals arising from nanodroplets could be observed. Figure 5.11a shows the average size of the scattering species within a 9 mg/ml solution over a period of 1140 s. Opened symbols indicate measurements which did not reveal scattering species or where the fitting analysis was very poor. It can be seen that nevertheless many data sets, collected from this undersaturated solution, could be fitted and showed the presence of nanodroplets (autocorrolation function g_2*-1* undersaturated solution C_{Val}=9mg/ml attached in Appendix Figure 11.2).

At higher concentration the signal from the scattering species was much more stable. As shown in Figure 5.11b, for a 16 mg/ml supersaturated valine solution, prepared by stirring, nanodroplets were present immediately on sampling and remained the same average size over the monitoring period.

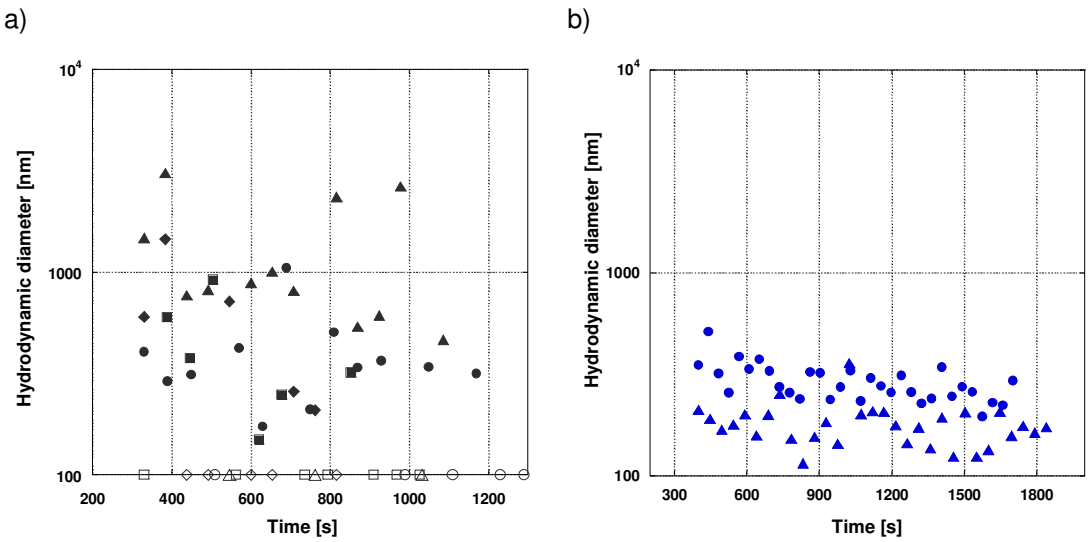

Figure 5.11 Time dependence of the droplets diameter in nanodispersion: magnetic mixer, mixing time 90s, 2-propanol/water, 1:1, v/v a) C_{val} **=9mg/ml** (undersaturated solution), three separate experiments, b) C_{val}**=16mg/ml** (supersaturated solution), two separateexperiments.

Table 5.2 shows the cluster and droplet hydrodynamic diameters calculated for undersaturated D,L-valine solutions. The autocorrelation functions obtained for those samples are very poor and from one set of data only a few curves could be fit (see autocorrelation data in Appendix). In spite of the quality of data problems it seems agree that some species with a size of a few hundreds nanometers exist even in undersaturated solution. However the precise size and number of them can not be obtained.

Table 5.3 summarises the nanospecies size in supersaturated solutions and how, as the valine concentration was increased, the average size of the nanodroplets varied according to the mixing method used to prepare them. Above the saturation limit differences between samples became more evident. Average hydrodynamic diameters of clusters and droplets as a function of D,L-valine concentration for undersaturated and supersaturated solutions calculated using first and second order function are shown in Figure 5.12 and Figure 5.13 respectively. The error bars represent the range of sizes i.e. the minimum and maximum values of diameter that occurred in series of samples with the same conditions (valine concentration, mixing type). Nanoprecursors size as a function of valine concentration with size distribution of clusters and droplets plotted together are presented in Appendix in Figure 11.3.

Table 5.2 Mean clusters and droplets diameters with different valine concentrations and types of mixing for **undersaturated D,L-valine solution**, 2-propanol/water, 1:1, v/v.

Concentration [mg/ml]	**Anstisolvent crystallisation -Magnetic mixer 90s-**				**Anstisolvent crystallisation -Vortexer 90s-**			
	Hydrodynamic CLUSTERS diameter [nm]		**Hydrodynamic DROPLETS diameter [nm]**		**Hydrodynamic CLUSTERS diameter [nm]**		**Hydrodynamic DROPLETS diameter [nm]**	
	1-st order fit	2-nd order fit	1-st order fit	2-nd order fit	1-st order fit	2-nd order fit	1-st order fit	2-nd order fit
2	-	-	-	-	**2.0** (± 0.3)	**1.6** (± 0.8)	**244** (± 78)	**239** (± 132)
4	-	-	-	-	**1.7** (± 0.5)	**1.4** (± 0.7)	**190** (± 86)	**129** (± 61)
7.5	**1.7** (±0.7)	**1.4** (±0.6)	**405** (±111)	**266** (±79)	**1.7** (± 0.6)	**1.2** (±0.6)	**680** (± 100)	**384** (±33)
9	**2.3** (±1.3)	**1.6** (±1.1)	**885** (±266)	**796** (±270)	**2.8** (±1.5)	**2.1** (±1.1)	**1593** (±333)	**1310** (±278)
10	**2.3** (± 0.6)	**1.8** (±0.7)	**441** (±74)	**333** (±90)	**2.1** (± 0.5)	**1.9** (±0.7)	**503** (±64)	**400** (±85)
11.5	**2.0** (± 0.8)	**1.8** (±0.7)	**485** (± 86)	**329** (±54)	**2.3** (± 1.3)	**1.8** (±0.4)	**570** (± 41.8)	**461** (±47)
12	**2.4** (± 1.6)	**1.3** (± 0.7)	**692** (± 144)	**858** (± 433)	**1.6** (± 0.9)	**0.9** (± 0.6)	**1557** (± 326)	**1475** (± 491)
13	-	-	-	-	**1.7** (± 0.5)	**1.4** (± 0.6)	**186** (± 33)	**318** (± 160)
14	-	-	-	-	**1.2** (± 0.7)	**0.8** (± 0.5)	**328** (± 100)	**401** (± 150)

Table 5.3 Mean clusters and droplets diameters with different valine concentrations and types of mixing for **supersaturated D,L-valine solution**, 2-propanol/water, 1:1, v/v.

Concentration [mg/ml]	**Anstisolvent crystallisation -Magnetic mixer 90s-**				**Anstisolvent crystallisation -Vortexer 90s-**			
	Hydrodynamic CLUSTERS diameter [nm]		**Hydrodynamic DROPLETS diameter [nm]**		**Hydrodynamic CLUSTERS diameter [nm]**		**Hydrodynamic DROPLETS diameter [nm]**	
	1-st order fit	2-nd order fit	1-st order fit	2-nd order fit	1-st order fit	2-nd order fit	1-st order fit	2-nd order fit
15.5	**3.8** (±0.6)	**2.6** (±0.6)	**215** (±33)	**231** (±47)	**2.4** (±0.3)	**1.7** (±0.3)	**404** (±40)	**458** (±126)
16	**3.3** (±0.5)	**2.3** (±0.5)	**234** (±19)	**216** (±28)	**1.7** (±0.2)	**1.3** (±0.3)	**612** (±104)	**599** (±184)
17	**3.3** (±1.3)	**1.9** (±0.9)	**575** (±86)	**439** (±99)	**4.4** (±1.5)	**2.7** (±1.2)	**1371** (±137)	**1347** (±308)
17.5	**5.4** (±3.4)	**2.4** (±1.5)	**612** (±89)	**645** (±294)	**2.9** (±1.4)	**1.9** (±1.1)	**3494** (±330)	**5088** (±662)
18.5	**5.7** (±2.6)	**2.5** (±1.7)	**672** (±36)	**722** (±83)	**19.8**(±12.2)	**10.5** (±8.4)	**1879** (±153)	**3467** (±703)

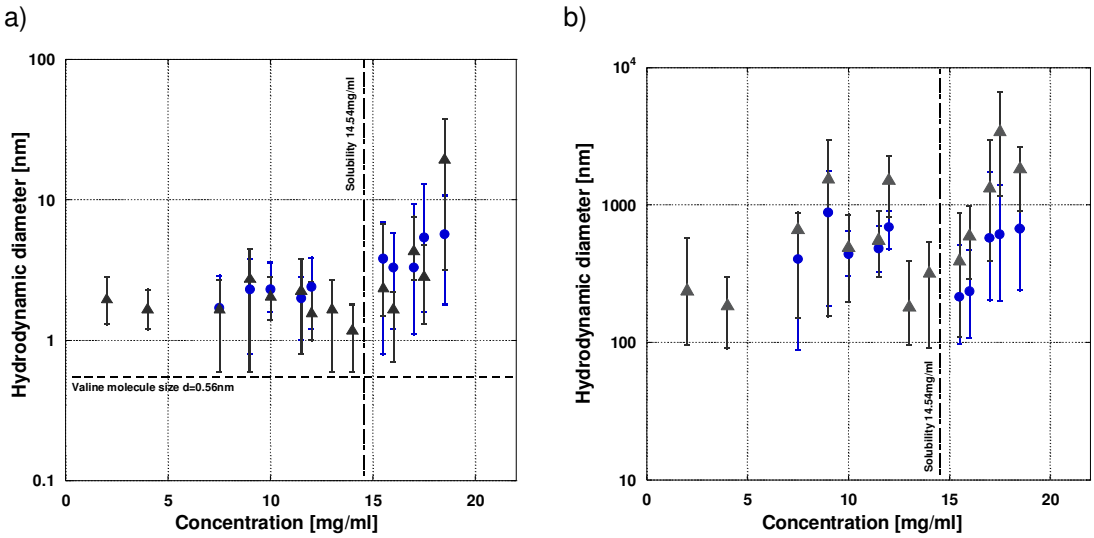

Figure 5.12 Nanoprecursors hydrodynamic diameter as a function of valine concentration with size distribution, blue symbols - magnetic mixer, black symbols - vortexer, **first order fit**, a) clusters, b) droplets, mixing time 90s, 2-propanol/water, 1:1, v/v.

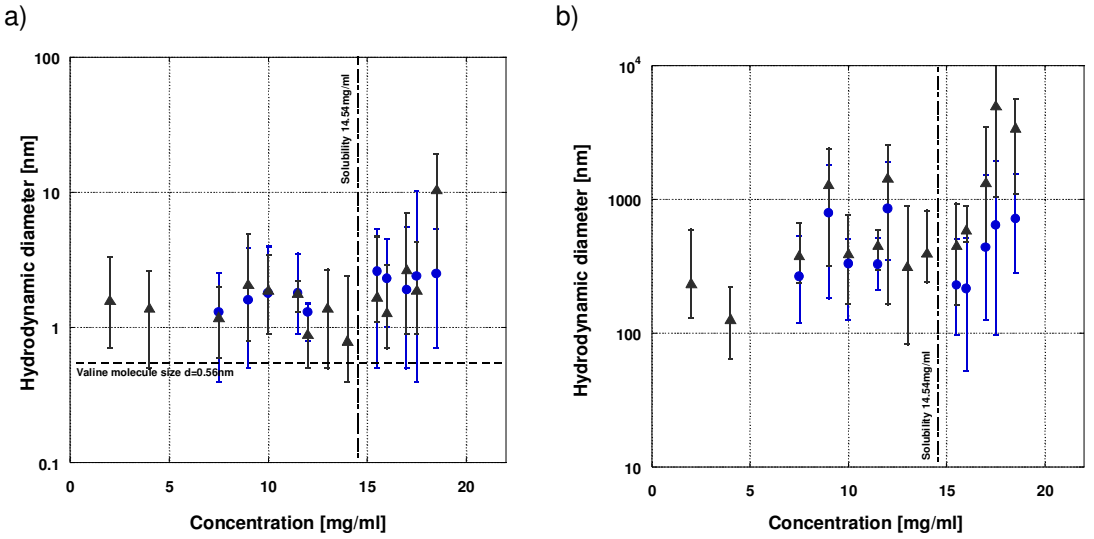

Figure 5.13 Nanoprecursors hydrodynamic diameter as a function of valine concentration with size distribution, blue symbols - magnetic mixer, black symbols - vortexer, **second order fit**, a) clusters, b) droplets, mixing time 90s, 2-propanol/water, 1:1, v/v.

Figure 5.14 and Figure 5.15 show the nanodroplet size distribution, for samples prepared at a valine concentration of 16mg/ml and 17mg/ml. The vortexed sample contained a heterogeneous distribution of nanodroplets with a significant population greater than 400 nm while the stirred sample was more homogeneous with an average size less than 400 nm. On increasing the valine concentration to 17mg/ml, and above, the nanodroplets obtained on vortexing were invariably found to be significantly larger (>1300 nm) than those obtained on stirring (<900 nm), see Table 5.3. Thus, subjecting a supersaturated solution to greater mixing intensities (or longer mixing periods) increased the extent of coalescence of nanodroplets. This is a significant observation because spectrophotometry and NMR data both demonstrated that valine crystallisation was much faster from samples prepared under more intense shearing mixing. Larger valine-rich droplets must therefore be the key intermediate species on the rapid crystallisation pathway. The greater the input of shear energy into the supersaturated solution the more of these species are formed. (Nanodispersion estimated size distribution calculated on the basis of 1-st order fit, valine concentration 16mg/ml and 17 mg/ml are attached in Appendix Figures 11.4-11.7)

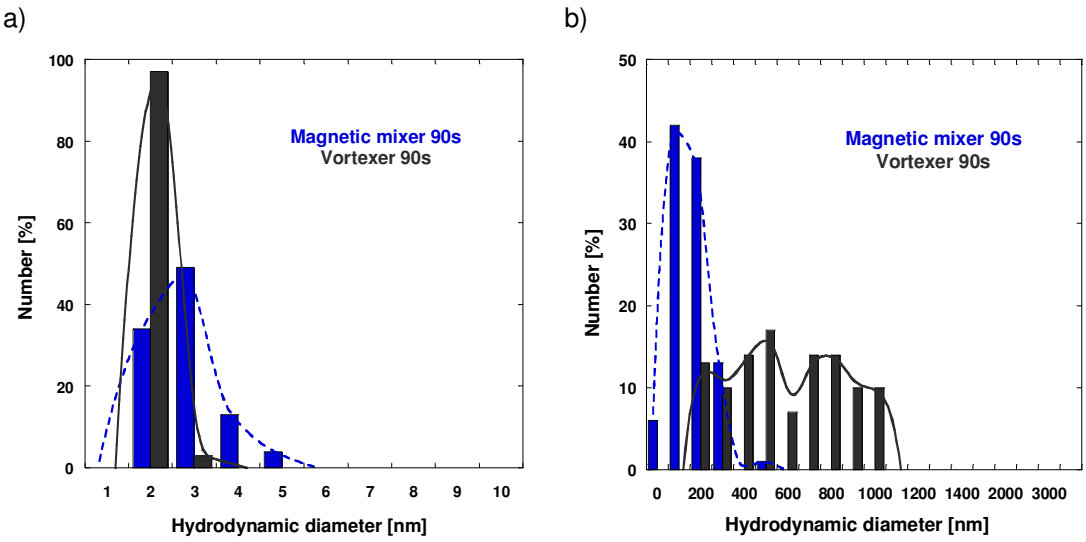

Figure 5.14 Nanodispersions estimated size distribution, mixing time 90s, **C $_{val}$=16mg/ml**, 2-propanol/water, 1:1, v/v, **second order fit** a) CLUSTERS, b) DROPLETS.

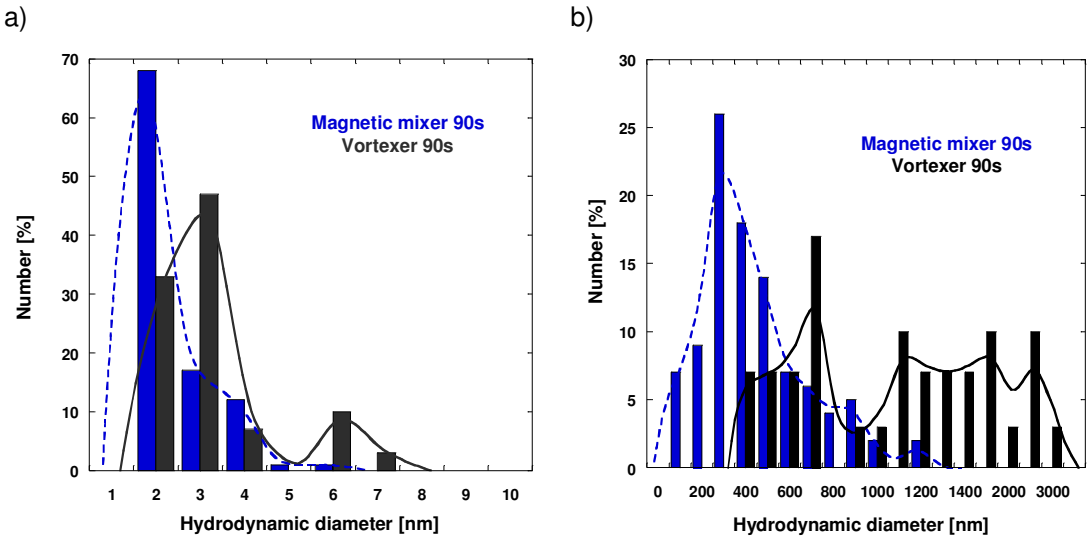

Figure 5.15 Nanodispersions estimated size distribution, mixing time 90s, **C $_{Val}$=17mg/ml**, 2-propanol/water, 1:1, v/v, **second order fit** a) CLUSTERS, b) DROPLETS.

5.1.5.a Nucleation mechanism – magnetic mixer, NMR-DLS results.

The NMR measurements of the crystallisation rate for samples prepared using magnetic stirrer (Figure 5.7) and DLS nanodroplets hydrodynamic diameter values for the same sample supersaturations and conditions of preparation (Table 5.3) are presented linear relationship (Figure 5.16). Figure 5.16 clearly shows that crystallised samples with larger nanospecies have slower kinetics and faster kinetics corresponds to smaller nanospecies.

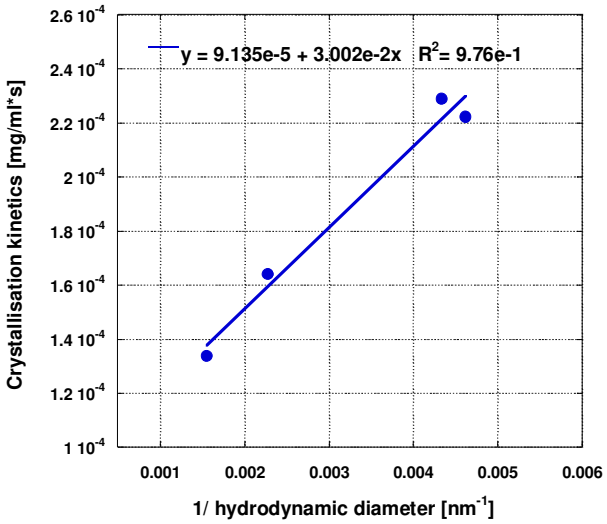

Figure 5.16 Crystallisation kinetics (NMR) as a function of nanodroplets hydrodynamic diameter (DLS, second order fit), **magnetic mixer**, mixing time 90s, 2-propanol/water, 1:1, v/v.

As already discussed, fewer valine microcrystals are formed in samples prepared using a magnetic mixer than from vortexing samples (spetrophotometry measurements and SEM pictures). This could also indicate that fewer metastable nanodroplets are able to crystallise in a mixture obtained by stirring than vortexing. When the first crystal (nuclei) is created the region around it becomes locally of low supersaturation. D,L-valine rich metastable nanodroplets will move toward the valine microcrystals via a diffusion process. According to Stokes-Einstein relation the diffusion coefficient is inversely proportional to the size of diffusing species: $D = \frac{k_B T}{3\pi\eta d_H}$ where d_H is the hydrodynamic diameter of the diffusing particles, k_B is Boltzmann's constant, T is the absolute temperature and η is the viscosity of the dispersing liquid at the corresponding temperature.

In the stirring samples only a few crystal nuclei are formed and crystals could only grow via a diffusion process of nanodroplets towards valine microcrystals. The larger nanodroplets diffuse slower than the smaller ones and the crystallisation kinetics depends on sample supersaturation (by the size of difuse nanoparticles). The samples with higher valine concentration (supersaturation) produce larger nanoparticles which eventually leads to decrease in the crystallisation kinetics (stirred experiment) (Figure 5.17). In the vortexing samples a larger number of crystal nuclei are formed (especially at higher supersaturations) and the kinetics at the beginning of process is considerably faster. However, when all local nanodroplets are exploited the later crystals grow the process is slows down and also depends on diffusion of the nanodroplets.

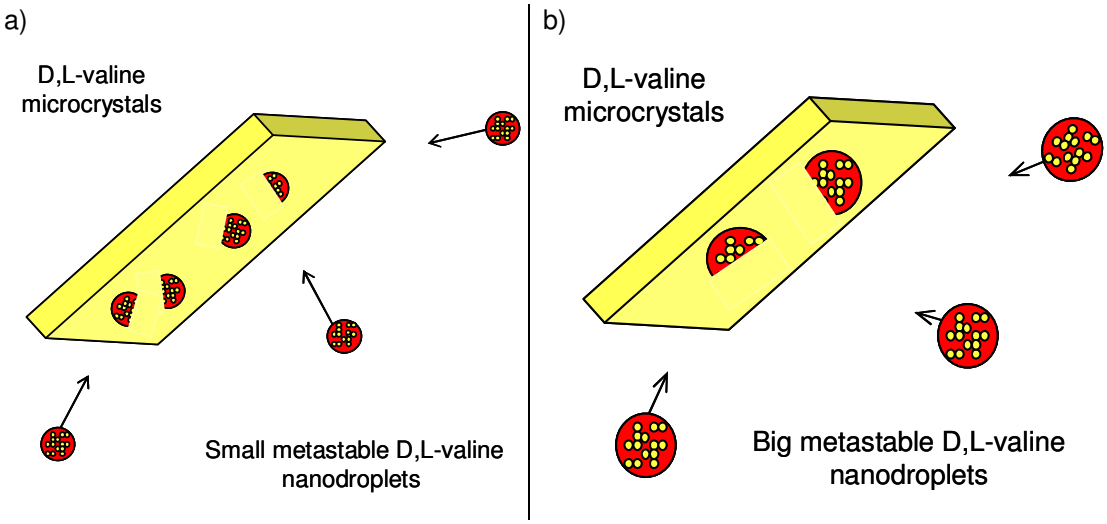

Figure 5.17 Diffusion process of D,L-valine nanodroplets, a) low supersaturations, b) high supersaturations, **magnetic mixer**, mixing time 90s, 2-propanol/water, 1:1, v/v.

5.1.6 Scanning Electron Microscopy (SEM)

Further SEM investigation of D,L- valine microcrystals prepared by antisolvent crystallisation with solvents 2-propanol/water ratio 1:1, has revealed that some droplets are present at the crystal surface after filtration and drying. SEM pictures of microcrystals prepared using magnetic stirrer, agitation time 90s, C_{Val} = 16mg/ml, and filtration after 24hours of crystallisation process are shown in Figure 5.18. The size of droplets is larger than can be expected on the basis of DLS characterisation of crystallising solution at certain time. However, this could be a result of droplet coalescence and attachment to crystals surface during the 24 hours standing in supersaturated solution. Presumably most nanodroplets existing in the crystallising supersaturated solution were used in crystal formation. However, some of them could coalesce but because the local supersaturation fallows too low for them to make new nucleus and to overcome the free energy barrier they instead stack to valine microcrystals during filtration and finally transform into solid valine form. Figure 5.18 shows the drying process of nanodroplets from valine crystal surface and to preclude the solvents effect during the crystals drying the control SEM was also done for D,L-valine powder used for aqueous solution preparation. Excess D,L-valine was dissolved in 2-propanol/water ratio 1:1, v/v, filtered and dried with the same procedure as an antisolvent crystallisation sample. The nanodroplets were not present on those crystals surface even when DLS showed valine nanodroplets in undersaturated solution. However, these nanodroplets could have different composition or be too small or alternative the surface of filtered valine crystals may be too rough to be possible to see them (see Appendix for SEM pictures of control sample Figure 11.8).

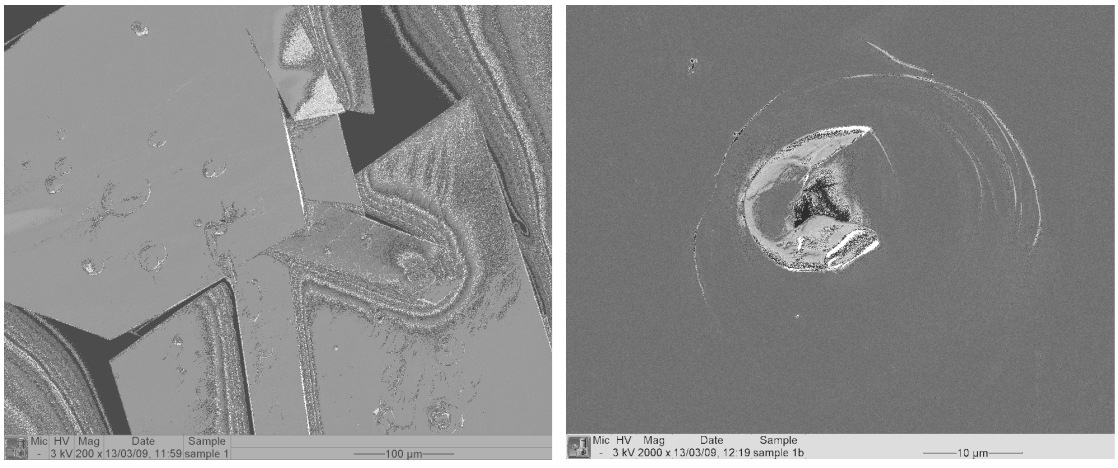

Figure 5.18 SEM images of the surface of D,L-valine microcrystals prepared using magnetic mixer, mixing time 90s, **C_{Val} = 16mg/ml**, filtered after 24hours, 2-propanol/water, 1:1, v/v.

Figure 5.19 shows the schema of deposition of valine from nanodroplets on the crystals surface. The metastable nanodroplets presumably during the filtration process attached to the crystalsand then during the drying process when the solvent is removed they make at the crystals surface the valine nanodroplets shell.

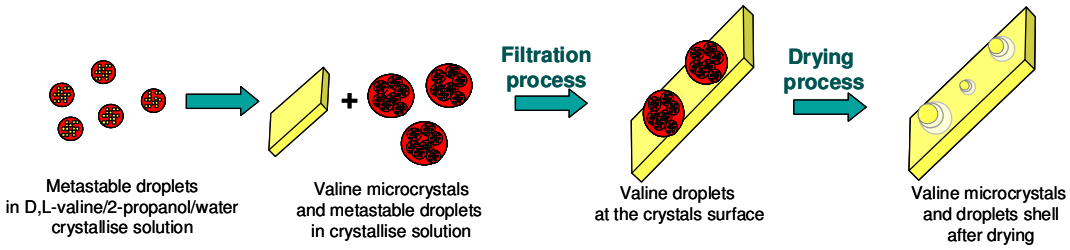

Figure 5.19 Schema of the deposition process of D,L-valine nanodroplets at the surface of valine microcrystals.

5.2 Antisolvent (2-propanol) – solvent (H_2O) ratio 1:3, v/v

The antisolvent crystallisation of the amino acid D,L-valine was also investigated using, 2-propanol/water solvent ratio 1:3, v/v. Typically, 3.75 ml of an aqueous valine solution of known concentration was rapidly admixed with 1.25 ml of 2-propanol in a 5 ml vial to give a solution of specified supersaturation. The samples were mixed using magnetic mixer and two different agitation times 35 and 90 seconds. Dynamic light scattering was employed for checking whether, similarly to water/2-propanol, 1:1 ratio, nanodispersions exist in pre-crystallised solution.

5.2.1 Induction times

Firstly, the induction times were determined to find a good solution composition for the dynamic light scattering technique and typically the samples with 30min induction times were used for characterisation of the pre-crystallisation nanodispersions. Induction times were determined by visual observation of standing solutions and a plot of induction times as a function of valine supersaturation S for samples prepared using a magnetic mixer and an agitation time 90 seconds is shown in Figure 5.20 and Table 5.4.

Supersaturation S was calculated using the relation $S = \frac{C_{Val}}{C_{Val,eq}}$ where, C_{Val} is a actual valine concentration in sample and $C_{Val,eq}$ is the solubility equilibrium ($C_{Val,eq}$ = *30.58mg/ml*, water/2-propanol, 3:1, v/v). The plot shows a curved relationship, what is different to classical crystallisation theory as was observed in previous experiments with solvents ratio 2-propanol/water 1:1, v/v.

The induction time experiments showed that solutions with a final valine concentration of around 35-36 mg/ml could be used in dynamic light scattering characterisation.

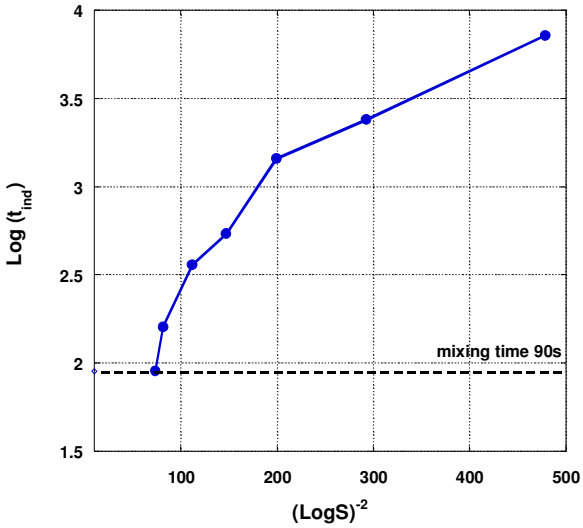

Figure 5.20 Plot of induction times as a function of initial supersaturation for D,L-valine, mixing type: magnetic mixer, mixing time 90s, 2-propanol/water, 1:3, v/v.

Table 5.4 Induction times and D,L-valine concentrations, 2-propanol/water, 1:3, v/v.

Induction times [s]	
Concentration [mg/ml]	Magnetic mixer 90s
34	7200
35	2400
36	1440
37	540
38	360
39.5	160
40	90

5.2.2 Dynamic Light Scattering (DLS)

The example of autocorrelation function g_2-1 obtained for a sample prepared by mixing together aqueous solutions of valine and 2-propanol using a magnetic stirrer to generate a valine concentration 36 mg/ml is plotted in Figure 5.21. Dynamic light scattering experiments were done for three different valine concentrations: 35.5, 36.0 and 36.5 mg/ml and two mixing times 35 and 90 seconds. DLS results have shown that immediately after mixing two different kinds of scattering species are present in a visibly clear solution, similar to previous experiments.

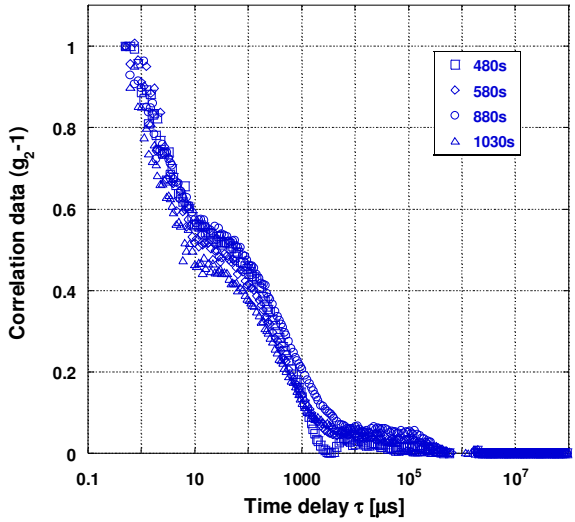

Figure 5.21 Light scattering autocorrelation function g_2-1 of solution with valine concentration C_{Val}**=36mg/ml**, data collecting time 480s-1030s, magnetic mixer, mixing time 90s, 2-propanol/water (H_2O), 1:1, v/v.

The small species with hydrodynamic diameters around a few nanometers, shown in the autocorrelation function as a first decay (Figure 5.21) correspond to molecular clusters existing in pre-crystallising solution. The second decay corresponds to larger nanoparticles (hundred nanometers) and they are presumably valine rich large liquid nanodroplets. The size of these nanodispersions was calculated by fitting two separate parts of the autocorrelation function $ln(g_1)$ and subsequently the diameters calculated using Stokes-Einstein relation (more details in Experimental Techniques chapter). The physical parameters used in hydrodynamic diameters calculations were taken from ***(Flick 1998)***, solvent viscosity and refractive index table in Appendix Table 11.1. The results show that the hydrodynamic diameter of nanodroplets is around 100-150nm and the size depends more on mixing time than the valine supersaturation. Samples prepared by mixing for 35 seconds

have slightly smaller nanodroplets than samples with the same final valine concentration prepared by mixing for 90 seconds (Figure 5.22, Table 5.5). For example, the hydrodynamic diameter of nanodroplets prepared by mixing valine solution with concentration 36mg/ml by 35 seconds is around 104.7nm, while in the same solution but mixed 90 seconds nanodroplets with size 134.4nm exist. The greater the input of shear energy by longer mixing, the greater the extent of coalescence of nanodroplets, finally resulting in faster crystallisation kinetics.

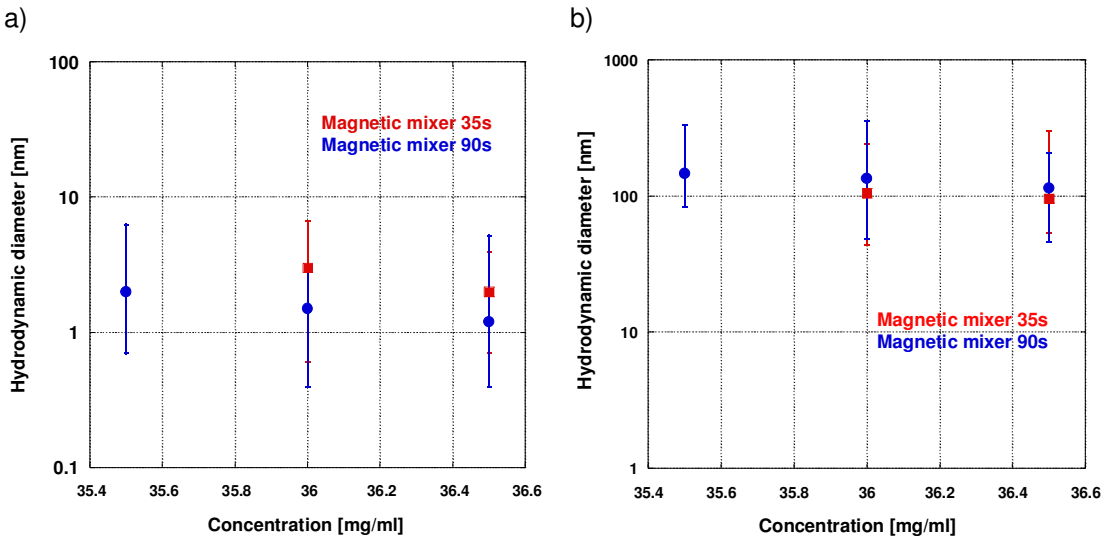

Figure 5.22 Nanoprecursors hydrodynamic diameter as a function of D,L-valine concentration with size distribution, a) clusters, b) nanodroplets, red symbols - magnetic mixer 35s, blue symbols – magnetic mixer 90s, **second order fit**, 2-propanol/water, 1:3, v/v.

Table 5.5 Mean clusters and droplets diameters with different D,L-valine concentrations and mixing times, magnetic mixer, 2-propanol/water, 1:3, v/v, antisolvent crystallisation.

Concentration [mg/ml]	**Anstisolvent crystallisation -Magnetic mixer 35s-**				**Anstisolvent crystallisation -Magnetic mixers 90s-**			
	Hydrodynamic CLUSTERS diameter [nm]		**Hydrodynamic DROPLETS diameter [nm]**		**Hydrodynamic CLUSTERS diameter [nm]**		**Hydrodynamic DROPLETS diameter [nm]**	
	1-st order fit	2-nd order fit	1-st order fit	2-nd order fit	1-st order fit	2-nd order fit	1-st order fit	2-nd order fit
35.5	-	-	-	-	**2.7** (± 0.6)	**2.0** (±1.3)	**156** (± 6)	**146** (±10)
36	**5.3** (± 0.9)	**3.0** (± 0.9)	**117** (± 5)	**105** (± 9)	**2.4** (± 0.6)	**1.5** (± 0.6)	**163** (± 13)	**134** (± 18)
36.5	**3.1** (± 0.5)	**2.0** (± 0.6)	**103** (± 5)	**96** (± 11)	**1.8** (± 0.6)	**1.2** (± 1.1)	**125** (± 7)	**114** (± 14)

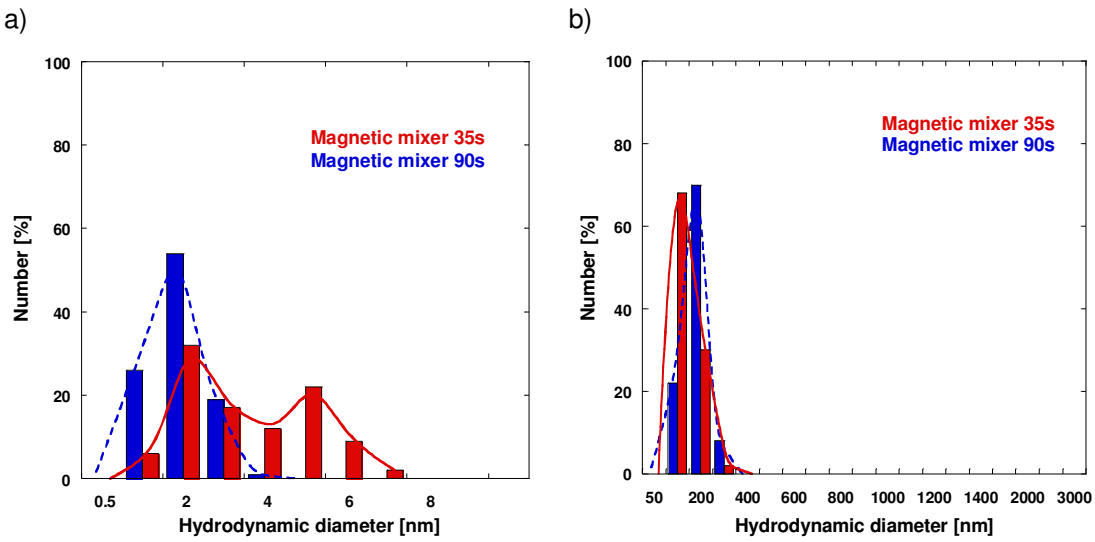

Figure 5.23 Nanodispersions estimated size distribution, magnetic mixer, mixing times 35s and 90s, **C $_{Val}$=36mg/ml**, 2-propanol/water, 1:3, v/v, **second order fit** a) CLUSTERS, b) DROPLETS.

Figure 5.23 shows the nanodispersions size distribution, for sample prepared at a valine concentration of 36mg/ml and mixing time 35 and 90 seconds and solvent ratio 2-propanol/water, 1:3. The size distribution shows that generally the droplets are small and they are slightly larger when the mixing time is extended.

The results showed that the samples with a higher content of water (solvents ratio 2-propanol/water 1:3) resulting in formation smaller valine-liquid nanodroplets compare to the equil solvents ratio samples, made using the same preparation method (magnetic mixer 90s) and similar supersaturations (around 1.1). The average hydrodynamic diameter of nanodroplets prepared using magnetic stirrer, mixing time 90 seconds and solutions supersaturation S=1.1 for solvent ratio 1:1, 2-propanol/water was d_h=216.5nm, whereas for samples with solvent ratio 1:3, 2-propanol/water was d_h=114.0nm. Supersaturation S was calculated using the relationship $S = \frac{C_{Val}}{C_{Val,eq}}$ where, C_{Val} is a actual valine concentration in sample and $C_{Val,eq}$ is the solubility equilibrium: $C_{Val,eq}$ = *14.54mg/ml*, 2-propanol/water, 1:1, v/v and $C_{Val,eq}$ = *32.74mg/ml*, 2-propanol/water, 1:3, v/v).

5.3 Antisolvent (2-propanol) – solvent (H_2O) ratio 3:1, v/v

The antisolvent crystallisation of D,L-valine using 2-propanol/water solvents with ratio 3:1 was also investigated using dynamic light scattering. Typically, 1.25 ml of an aqueous valine solution of known concentration was rapidly admixed with 3.75 ml of 2-propanol in a 5 ml vial to give a solution of specified supersaturation. The samples were prepared using magnetic mixer and agitation time 90 seconds.

5.3.1 Induction times

The induction times were determined by visual observation of the standing solutions. The plot of the induction time as a function of supersatuartion is shown in Figure 5.24 and Table 5.6. Supersaturated S was calculated using relation $S = \frac{C_{Val}}{C_{Val,eq}}$ where, C_{Val} is a actual valine concentration in sample and $C_{Val,eq}$ is the solubility equilibrium (in this case $C_{Val,eq}$=*3.3mg/ml*, water/2-propanol, 1:3, v/v). From the induction times experiments the most appropriate composition of crystallising solution for dynamic light scattering measurement was specified, and typically samples which crystallised after 30 minutes were most suitable.

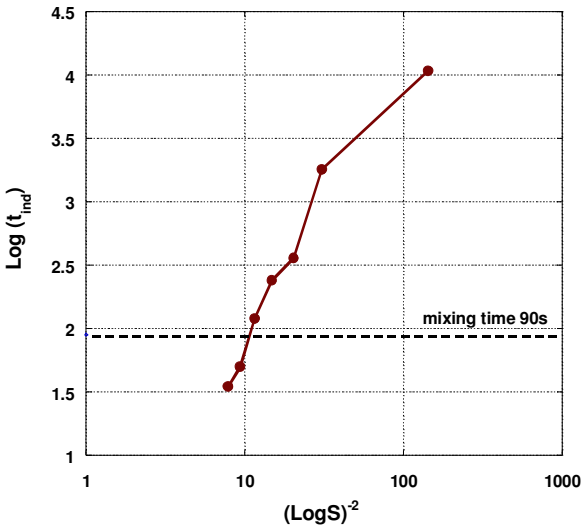

Figure 5.24 Plot of induction times as a function of initial supersaturation for D,L-valine, magnetic mixer, mixing time 90s, 2-propanol/water, 3:1, v/v.

Table 5.6 Induction times for different D,L-valine concentrations, magnetic mixer, mixing time 90s, 2-propanol/water, 3:1, v/v.

Induction times [s]	
Concentration [mg/ml]	Magnetic mixer 90s
4.5	10800
5	1800
5.5	360
6	240
6.5	120
7	50
7.5	35

5.3.2 Dynamic Light Scattering (DLS)

Dynamic light scattering experiments were done for samples of solvents ratio 3:1, 2-propanol/water and D,L valine concentrations 4.5, 4.0 and 3.7 mg/ml. The example of autocorrelation function g_2*-1* determined for crystallised solution of valine concentration 4.0mg/ml and prepared using a magnetic mixer with agitation time 90s is plotted in Figure 5.25. The autcorrelation functions immediately after mixing showed only one exponential decay part which corresponded to a few hundred nanometer particles. These nanoparticles are presumably the liquid nanodroplets observed previously, however the small molecular clusters were not observed with these conditions (solvent ratio 2-propanol/water, 3:1). This may be connected with the solvents polarity, which now is less polar than in all the previous cases, and probably the molecular clusters are less likely to form.

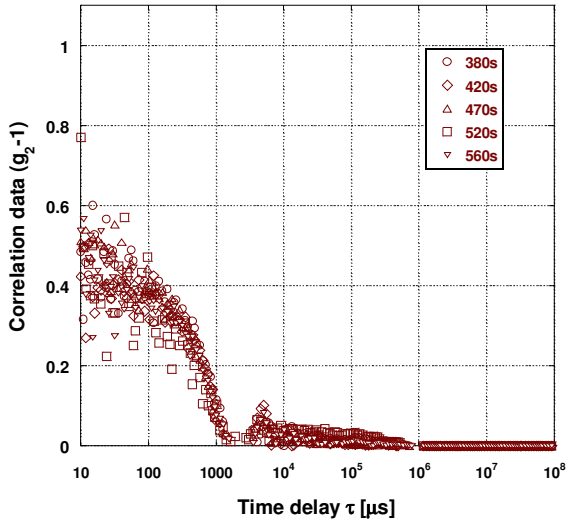

Figure 5.25 Light scattering autocorrelation function g_2-*1* of solution with D,L-valine concentration **C_{Val}=4.0 mg/ml**, magnetic mixer, mixing time 90s, data collection time 380s-560s, 2-propanol/water (H_2O), 3:1, v/v.

The size of these nanodroplets was calculated by fitting autocorrelation function *ln(g_1)* and subsequently from fitting parameters the diameters were calculated using Stockes-Einstein relation (more details in Experimental Techniques chapter). The physical parameters used in hydrodynamic diameters calculations were taken from ***(Flick 1998)*** and for 2-propanol/water ratio 3:1, v/v was: viscosity *η=0.0031 Pa·s*, refractive index *n=1.369* and temperature *T=298K*. (Solvent viscosity and refractive index table in Appendix Table 11.1). The results presented in Table 5.7 show that in this case of the nanodroplets diameter is strongly dependent on valine concentration. Changing the solution supersaturation from 1.21 (corresponds to 4.0 mg/ml D,L-valine concentration) to 1.36 (corresponds to 4.5 mg/ml D,L-valine concentration) the hydrodynamic diameter of nanodroplets increased from around 190nm to 530nm (first order fit).

Table 5.7 Mean droplets diameter with different D,L-valine concentrations, magnetic mixer 90s, 2-propanol/water, 3:1, v/v, antisolvent crystallisation.

Concentration [mg/ml]	**Anstisolvent crystallisation -Magnetic mixer 90s-**	
	Hydrodynamic DROPLETS diameter [nm]	
	1-st order fit	2-nd order fit
4	**193** (± 85)	**263** (± 148)
4.5	**528** (± 50)	**561** (± 184)

5.4 Antisolvent (2-propanol) - solvent (H_2O) ratio 9:1, v/v

The DLS characterisation of the crystallising D,L-valine solutions with solvents 2-propanol/water ratio 0.9/0.1 was also investigated. Typically, the solutions with volume fraction of 2-propanol more than 90% is used for Protein Coated Microcrystals formation, to prevent contamination (changing bioactive structure) of a bionanoparticles (such as proteins, vaccines, etc). Crystallised solutions were prepared by rapidly mixing 0.5 ml of an aqueous valine solution of known concentration with 4.5ml of 2-propanol in a 5ml vial to obtain a solution of specified supersaturation. The samples were prepared using magnetic mixer or vortexer with agitation time 90 seconds.

5.4.1 Dynamic Light Scattering (DLS)

The example of autocorrelation function g_2-1 for antisolvent crystallise solution of D,L-valine with concentration 0.69mg/ml, prepared by agitation 90 seconds using a magnetic stirrer is plotted in Figure 5.26a. Immediately following mixing scattering species with a size around few hundreds nanometers are formed (similar to the previous experiment, with solvents 2-propanol/water ratio 3:1). Differently from crystallised solutions with a larger volume fraction of water the small molecular clusters are not formed, and the autocorrelation function shows only one exponential decay part. This could be presumably connected with the solvent polarity which has changed from more to less polar as more 2-propanol was added (water polarity index 9.0, 2-propanol polarity index 3.9). The few hundreds nanometer species are presumably again liquid intermediate nanodroplets. Figure 5.26b shows the control autocorrelation function for 2-propanol/water 0.9:0.1 solvent and no scattering species were present in solvent prepared with the same procedure but without valine.

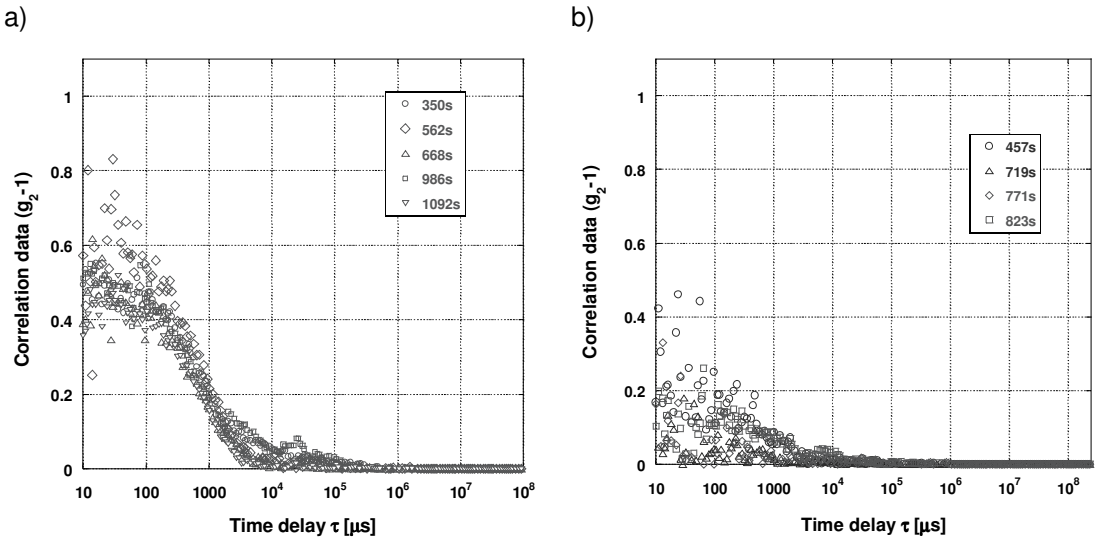

Figure 5.26 Light scattering autocorrelation function g_2-*1*, a) D,L-valine crystallise solution, **C_{Val}=0.69 mg/ml**, data collecting time 350s -1092s, b) solvent, 2-propanol/water (H_2O), data collecting time 460s - 830s, 2-propanol/water, 0.9:0.1, v/v, **magnetic mixer, mixing time 90s.**

The hydrodynamic diameters of nanodroplets were calculated using Stokes-Einstein equation and fitting parameters obtained from first and second order fit *of ln(g1)* correlation data, (more details in Experimental Techniques chapter). The physical parameters for 2-propanol/water ratio 0.9:0.1 were taken from ***(Flick 1998)*** and were: viscosity η*= 0.0031 Pa·s*, refractive index *n=1.366*, temperature *T=298K*. (Solvent viscosity and refractive index table in Appendix Table 11.1).

Table 5.8 summarises hydrodynamic diameters of nanodroplets calculated for different D,L-valine concentrations and mixing types. The supersaturation of crystallised solution has a large influence on nanoprecursor dimensions and increased from 200nm to 900nm when the D,L-valine concentration increased from 0.66mg/ml to 0.7mg/ml.

Table 5.8 Mean droplets diameters with different D,L-valine concentrations and mixing types, 2-propanol/water, 0.9:0.1, v/v, antisolvent crystallisation.

Concentration [mg/ml]	**Anstisolvent crystallisation -Magnetic mixer 90s-**		**Anstisolvent crystallisation -Vortexer 90s-**	
	Hydrodynamic DROPLETS diameter [nm]		**Hydrodynamic DROPLETS diameter [nm]**	
	1-st order fit	**2-nd order fit**	**1-st order fit**	**2-nd order fit**
0.66	-	-	**219** (± 64)	**175** (± 79)
0.67	-	-	**280** (± 58)	**273** (± 112)
0.69	**286** (± 103)	**192** (± 112)	**940** (± 189)	**843** (± 254)
0.70	-	-	**681** (± 41)	**819** (± 212)

The plot of the autocorrelation functions correspond to three different valine concentrations: 0.66, 0.67, 0.69mg/ml and hydrodynamic diameter as a function of D,L-valine concentration are shown in Figure 5.27. This diagram clearly shows that small changes in solution supersaturation change significantly the nanodroplet size and affected the induction times as well as crystallisation kinetics.

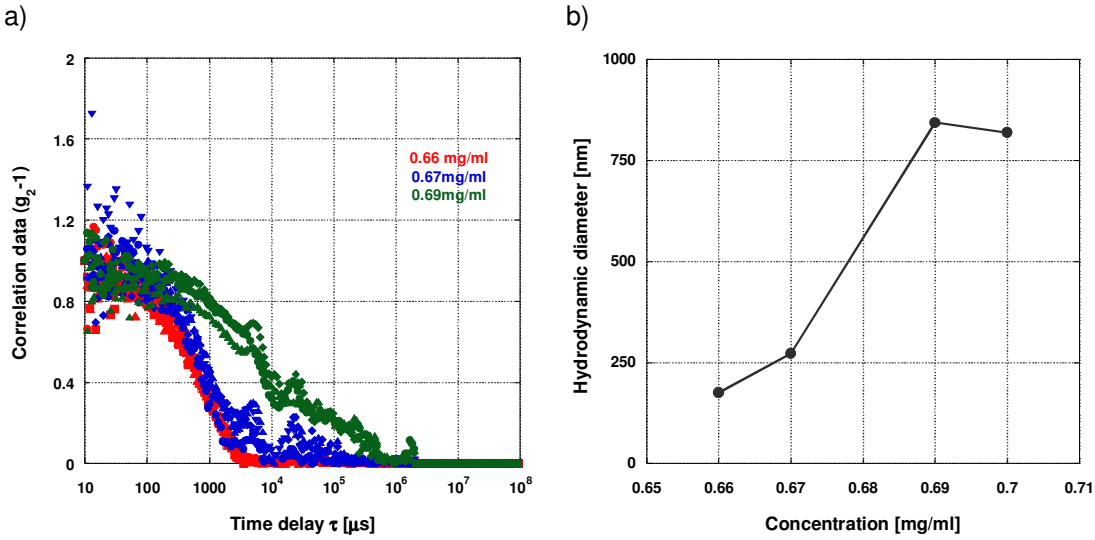

Figure 5.27 Antisolvent crystallization, vortexer,mixing time 90s, 2-propanol/water, 0.9:0.1, v/v.
a) light scattering autocorrelation function (g_2-1) for different D,L-valine concentrations in samples
b) nanoprecursors hydrodynamic diameter as a function of D,L-valine concentrations, **second order fit.**

Two different mixing types (magnetic mixer and vortexer) were tested for crystallising solution with D,L-valine concentration 0.69mg/ml. The results showed that supersaturation had also large impact on the size of the nanodipersions, smilar to mixing conditions. Magnetic stirrer samples produced smaller nanodproplets than solutions prepared using the vortexer, with the same agitation time. However, the mixing type did not change the final crystal morphology, which looked similar from solution prepared using magnetic mixer and vortexer. Figure 5.28 shows the optical microscopy pictures of D,L-valine microcrystals prepared using magnetic mixer and vortexer formed in a solution of 0.69mg/ml valine concentration where samples were filtered after 24hours.

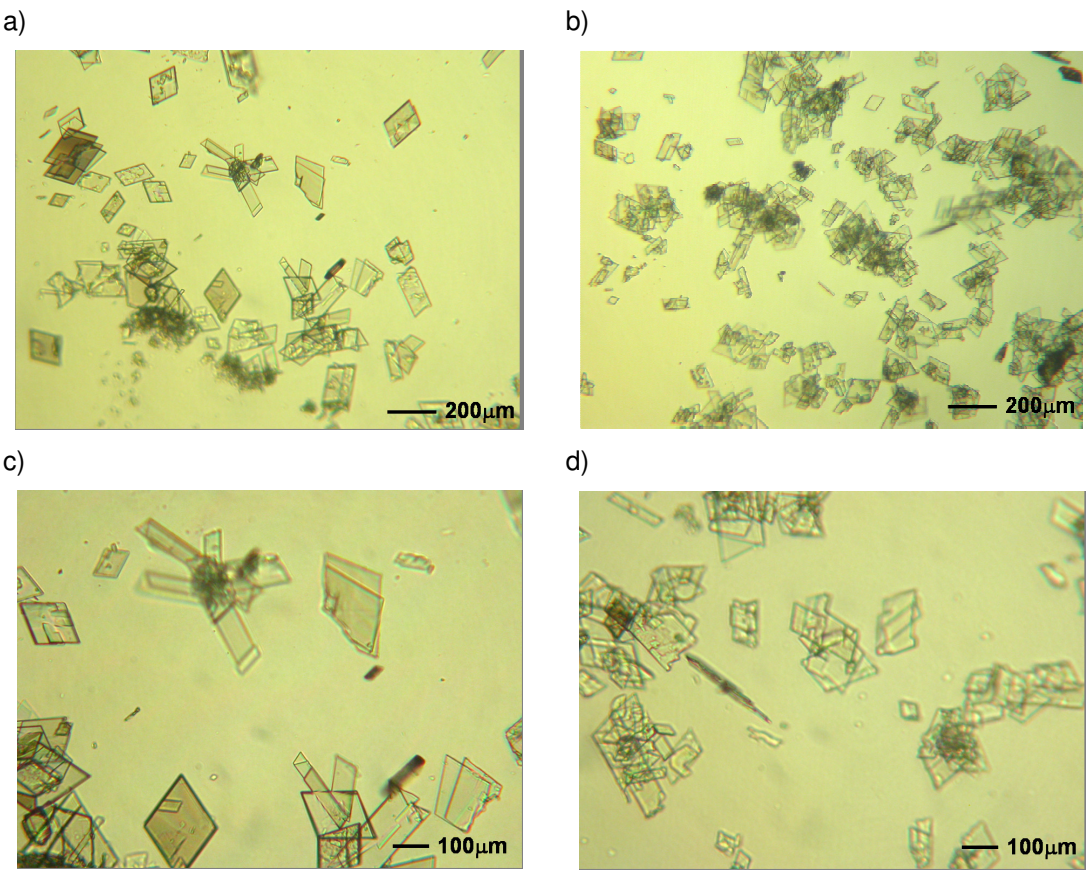

Figure 5.28 D,L-valine microcrystals, C_{val} **=0.69mg/ml**, a)- c)magnetic mixer, b) – d) vortexer, mixing time 90s, 2-propanol/water, 0.9:0.1, v/v.

5.5 Antisolvent crystallisation: glycine, histidine

A preliminary DLS characterisation of antsiolvent crystallisation solutions of two different amino acids glycine and L-histidine was also carried out. Aqueous solutions of amino acids were prepared and 2-propanol was used as an antisolvent. Typically samples were prepared by mixing 2.5 ml 2-propanol with 2.5ml of aqueous solution of the specified amino acid using a magnetic stirrer, with agitation time of 90 seconds. Final glycine concentration in crystallised samples was 30mg/ml and L-histidine concentration was 12mg/ml.

5.5.1 Dynamic Light Scattering (DLS)

The examples of autocorrelation function g_2-1 obtained from crystallised solution of glycine and L-histidine are plotted in Figure 5.29. Immediately after mixing two kinds of species were present in crystallised solution. The small molecular clusters (correspond to first correlation function decay) with size around 1-2nm and larger nanodroplets with a few hundred nanometres size (correspond to second correlation function decay).

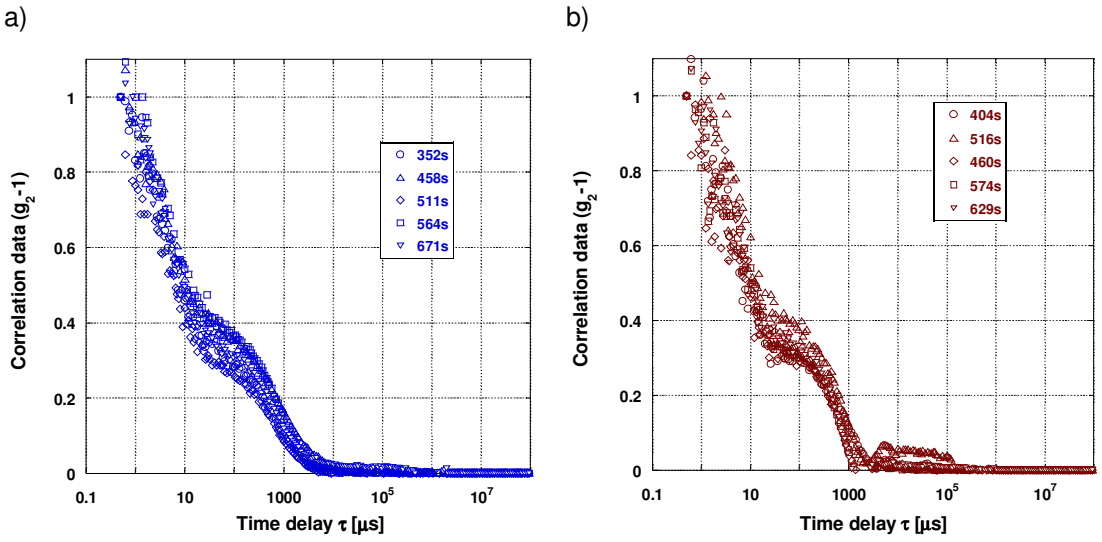

Figure 5.29 Light scattering autocorrelation function g_2-1, a) glycine, C_{Gly} = **30mg/ml**, data collecting time 350s - 670s, b) histidine, C_{His} = **12mg/ml**, data collecting time 400s - 630s, 2-propanol/water (H_2O), 1:1, v/v, magnetic mixer, mixing time 90s.

Using the first and second order fit two separate parts of autocorrelation functions were fitted and from fitting parameters and Stokes-Einstein relation the hydrodynamic diameters of molecular clusters and nanodroplets were calculated. The physical parameters for solvents were taken from ***(Flick 1998)*** and were: viscosity $\eta=0.0033\ Pa{\cdot}s$, refractive index $n= 1.365$ and temperature $T=298K$. (Solvent viscosity and refractive index table in Appendix Table 11.1). Table 5.9 shows estimated diameters of nanodispersions for antisolvent crystallisation of glycine and histidine.

Table 5.9 Mean clusters and droplets diameters for glycine and L-histidine antisolvent crystallisation, 2-propanol/water, 1:1, v/v.

	Anstisolvent crystallisation -Magnetic mixer 90s-		**Anstisolvent crystallisation -Magnetic mixer 90s-**	
	Estimated CLUSTERS diameter [nm]		**Estimated DROPLETS diameter [nm]**	
	1-st order fit	**2-nd order fit**	**1-st order fit**	**2-nd order fit**
Glycine 30mg/ml	**2.6** (± 0.3)	**1.9** (± 0.4)	**185** (± 11)	**156** (± 16)
L-histidine 12mg/ml	**2.8** (± 0.8)	**2.4** (± 1.3)	**148** (± 13)	**237** (± 83)

5.5.1.a Antisolvent crystallisation –batch system summary.

The study of antisolvent crystallisation of D,L-valine from 2-propanol/water solvent using different experimental techniques: spectrophotometry, NMR, DLS, SEM show that the process proceeds by formation of valine-rich liquid nanodroplets. The size of nanoprecursors changes with sample preparation methods, valine supersaturation and solvent ratios. Figure 5.30 shows the changes in hydrodynamic diameter of nanodroplets with increasing the volume fraction of 2-propanol and for similar valine supersaturation (S≈1.1-1.3) of crystallising solution. Supersaturated S calculated using equation $S = \frac{C_{Val}}{C_{Val,eq}}$ where, C_{Val} is a actual valine concentration in sample and $C_{Val,eq}$ is the solubility equilibrium.

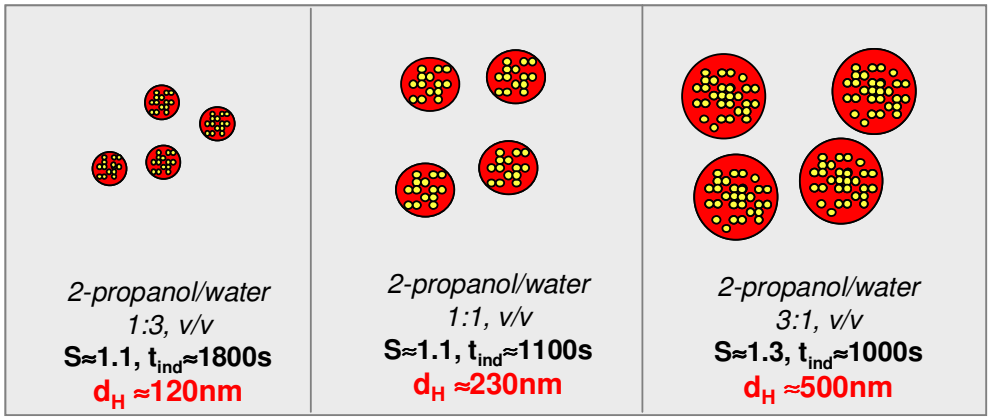

Figure 5.30 Hydrodynamic diameter of D,L-valine liquid nanodroplets for supersaturations around 1.1-1.3, prepared using magnetic mixer, mixing time 90s and different solvent ratios, 2-propanol/water, (1:3, 1:1, 3:1), v/v.

The mixing effect on antisolvent crystallisation of D,L-valine was tested using dynamic mixers: stirrer and vortexer. The former induces formation of smaller nanodroplets and finally less crystals product is produced. The latter helps to make larger nanoprecursors and crystallisation yield. Since the mixing type is important in valine microcrystal formation process, the continuous mixer (Confined Impinging Jet CIJ) was tested and results are presented in Chapter 6.

A preliminary result of antisolvent crystallisation process for two different amino acids: glycine and histidine also shows two-step crystallisation mechanism: the liquid nanoprecursors formation and liquid phase transformation to form solute microcrystals.

6. ANTISOLVENT CRYSTALLISATION of D,L-valine - continuous system.

Interactions between mixing and crystallisation are very important and can affect every aspect of crystallisation operation including crystal nucleation and growth. In the previous experiments two dynamic mixers: magnetic and vortexer were investigated and it was found that mixing conditions have a very big influence on induction times, nucleation kinetics and final microcrystals size. The mixing conditions determined the size of liquid-nanodroplets during the liquid-liquid separation process of antisolvent crystallisation of D,L-valine. The kinetics of the nucleation process as well as the final product properties depend on the mixing operation and subsequent nanodroplet characteristics.

In this chapter the Confined Impinging Jet (CIJ) mixer was used for determination of the liquid nanodroplet size and final valine microcrystal product morphology. In a CIJ mixer the two inlet streams: aqueous solution of valine and 2-propanol (antisolvent) were mixed in a very small volume at the centre of a cylindrical chamber, where as a consequence of their collision and impingement, turbulent kinetic energy is generated and then quickly dissipated, inducing very rapid mixing. The characteristic mixing times in this device were found to be in the order of magnitude of millisecond ***(Gavi et al. 2007; Marchisio et al. 2006).*** This technology is successfully employed to fast precipitation process where mixing times were found to be less than characteristic process times ***(Mahajan and Kirwan 1993; Mahajan and Kirwan 1994).*** Impinging crystallisation promotes the nucleation process by rapid mixing and finally leads to small final particle size and narrow particle size distribution ***(Paul et al. 2004).***

In this chapter some preliminary experiments using a CIJ mixer are presented. The liquid nanodroplet size and distribution were monitored using dynamic light scattering (DLS) and final crystals morphology was investigated using optical and scanning electron mictoscopy (SEM).

6.1 Dynamic Light Scattering (DLS)

The samples were prepared using a CIJ mixer with characteristic parameters presented in the experimental methods section. Two different flow rate of inlet streams: 60 and 125ml/min, and three different D,L-valine concentrations in the final solution: 15, 16 and 18mg/ml were used. Figure 6.1 shows an example of autocorrelation functions g_2*-1* obtained

for samples prepared using a CIJ mixer with inlet solutions (aqueous solution of valine and 2-propanol) both with flow rates: 60ml/min (Figure 6.1a),125ml/min (Figure 6.1b) valine concentration 16mg/ml.

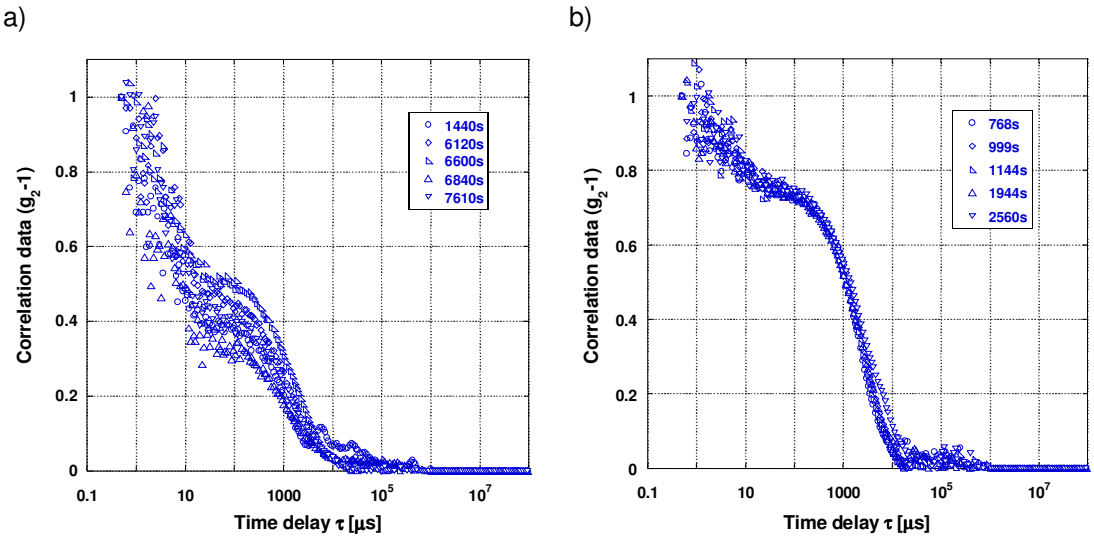

Figure 6.1 Light scattering autocorrelation function g_2-*1* of D,L-valine crystallising solutions, **Cval=16mg/ml**, CIJ mixer, a) Flow rate 60ml/min, data collecting time 1440s-7610s, b) Flow rate 125ml/min, data collecting time 770s-2560s, 2-propanol/ water (H_2O), 1:1, v/v.

The autocorrelation function is similar to previous experiments and shows two kind of species existing in crystallising solution, small molecular valine clusters (size of few nanometers) and larger nanodroplets (size of few hundreds nanometers). The shape of the correlation curves does not change with processing time and higher intercept values of the exponential decay functions correspond to droplets obtained in samples mixed with higher flow rate. This higher intercept values could presumably be due to the presence of a larger number of droplets in the investigated solutions.

The hydrodynamic diameter of molecular clusters and nanodroplets were calculated by fitting two separate parts of autocorrelation data $ln(g_1)$ using first and second polynomial, then from fitting parameters and Stokes-Einstein equation the nanospecies size was calculated. (See Experimental Techniques chapter for more details). Table 6.1 presents the average clusters and nanodroplets size calculated with using first and second polynomial for crystallised solution with different valine concentrations and inlet stream flow rates. The samples with valine concentration C_{Val}=15mg/ml prepared using solvents inlet flow rate 60ml/min resulting in formation smaller size nanodroplets compare to samples prepared using higher inlet flow rate 125ml/min. For low supersaturations: S=1.03 and S=1.1 (calculated as a ratio between

solution concentration, C and the equilibrium saturation, C^*, $S=C/C^*$, in this case $C_{Val,eq}$ = *14.54mg/ml*, water/2-propanol, 1:1, v/v) the nanodroplets size increased with valine concentration in the samples as well as with applied flow rate. However, when the supersaturatation of the crystallising solution is higher (S=1.23) the size of detected nanodroplets was smaller compare to the same flow rate (125ml/min) and lower valine concentration (15 mg/ml and 16mg/ml). It was also found that crystallisation kinetics in these samples was slower compare to batch system and it was made possible to monitor the crystallisation process (particles size monitoring) for longer than 2 hours.

Table 6.1 Mean clusters and droplets diameters with different D,L- valine concentrations and inlet streams flow rates, 2-propanol/water, 1:1, v/v.

Concentration	***Flow rate = 60ml/min***				***Flow rate = 125ml/min***			
	Hydrodynamic **CLUSTERS** diameter [nm]		Estimated **DROPLETS** diameter [nm]		Hydrodynamic **CLUSTERS** diameter [nm]		Estimated **DROPLETS** diameter [nm]	
	1-st order fit	**2-nd order fit**	**1-st order fit**	**2-nd order fit**	**1-st order fit**	**2-nd order fit**	**1-st order fit**	**2-nd order fit**
15	**1.9** (±1.0)	**0.8** (±0.5)	**354** (±89)	**300** (±94)	**4.5** (±1.4)	**3.1** (±1.7)	**414** (±24)	**404** (±44)
16	**2.7** (±1.5)	**1.4** (±0.9)	**299** (±39)	**363** (±108)	**6.4** (±4.5)	**2.1** (±1.4)	**503** (±10)	**522** (±19)
18	**-**	**-**	**-**	**-**	**5.7** (±1.7)	**3.5** (±1.7)	**284** (±7)	**304** (±29)

The droplets size did not change during monitoring times (Figure 6.2), however the inlet streams flow rates and valine concentrations impact on the average droplet size was observed. Figure 6.2 shows the time dependence on the diameter of droplets for solutions prepared using CIJ mixer with different inlet flow rates (60ml/min and 125ml/min) and valine concentrations (15mg/ml and 18mg/ml).

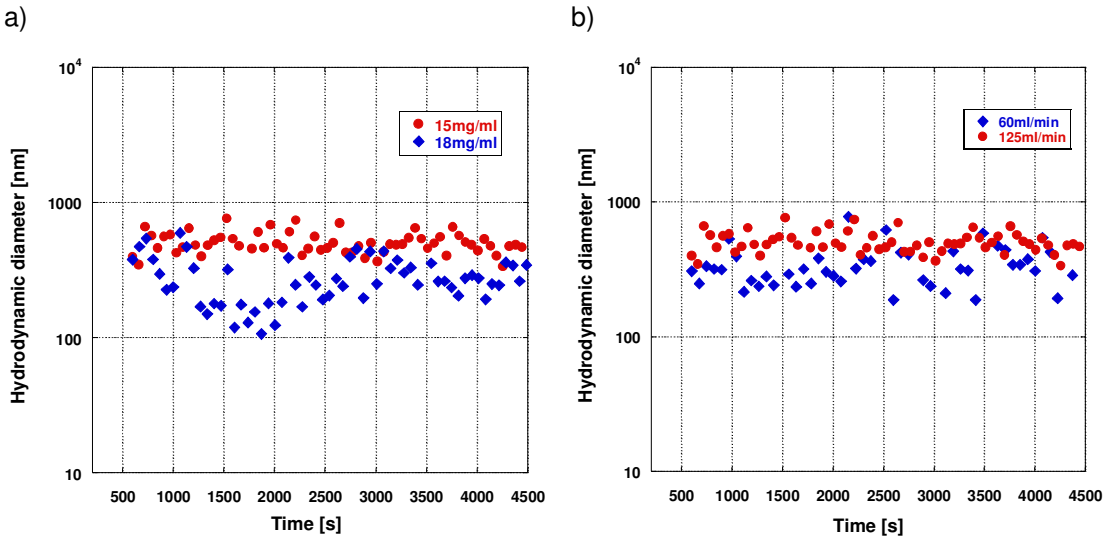

Figure 6.2 Time dependence of the diameter of droplets in samples prepared using CIJ mixer, calculated using **second order fit**, a) inlet streams flow rate 125ml/min, C_{val} =15mg/ml and C_{val} =18mg/ml, b) C_{val}=15mg/ml, inlet streams flow rates: 60ml/min and 125ml/min, 2-propanol/water, 1:1, v/v.

The plot of hydrodynamic diameter of liquid nanodroplets as a function of valine concentration in crystallising samples for different flow rates is shows in Figure 6.3. The diameter of nanodroplets was decreased for valine concentration in samples 18mg/ml and inlet streams flow rate 125ml/min. The samples with valine concentration 18mg/ml were tested only with one flow rate (125ml/min).

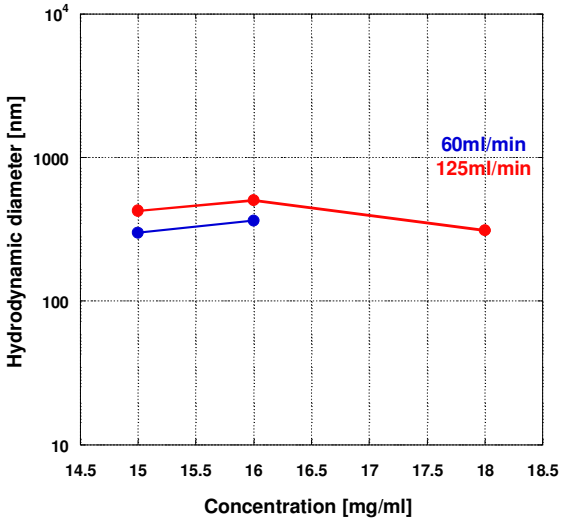

Figure 6.3 Nanoprecursors hydrodynamic diameter as a function of D,L-valine concentration, blue symbols – CIJ flow rate 125ml/min, red symbols – CIJ flow rate 60ml/min, **second order fit**, 2-propanol/water, 1:1, v/v.

Figure 6.4a shows the nanodroplets size distribution for samples prepared using CIJ mixer with inlet streams flow rate 125ml/min and valine concentrations 15mg/ml and 18mg/ml. It was found that droplets have narrow size distribution for these samples and their hydrodynamic diameters were not larger than 700nm. The main number of droplets are have hydrodynamic diameter range from 200nm to 500nm. In case of crystallising solutions with valine concentration 18mg/ml most droplets were had diameters between 200nm and 400nm, and actually only a small population of droplets with larger size existed, however they are not larger then 600nm. For lower valine concentration (15mg/ml) the droplets size distribution corresponded to larger nanodroplets, but still most number of droplets is with a size not larger than 500nm. The molecular cluster size distributions for these samples are broad with size range from 0.5nm to 9nm (Figure 6.4b). It was already discussed in the Experimental Techniques chapter how the cluster diameter could be affected by the presence of the second exponential decay of the autocorrelation function, and actually the real size may correspond to smaller clusters like valine dimers or trimers.

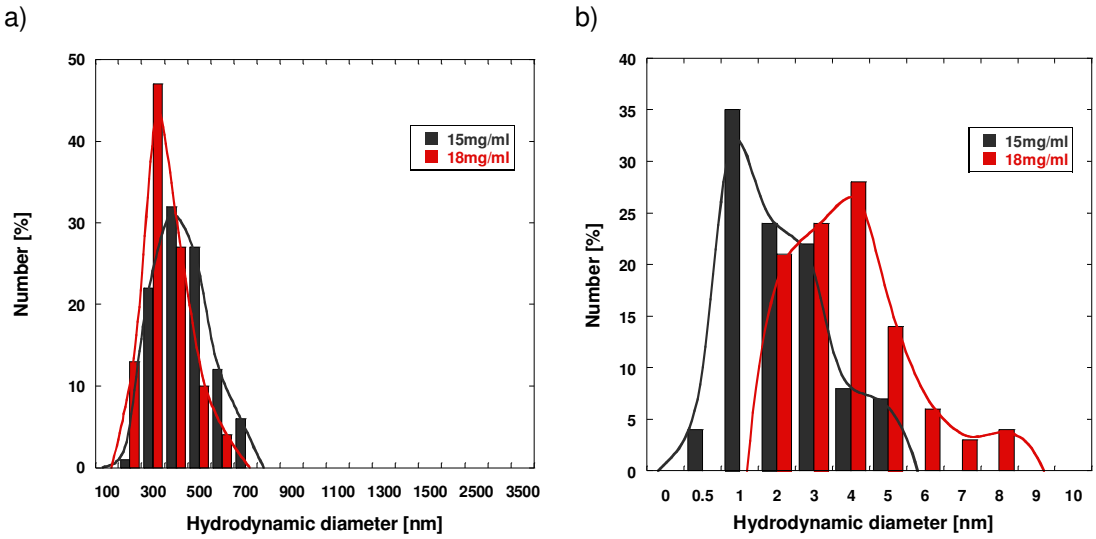

Figure 6.4 Clusters and nanodroplets estimated size distribution, CIJ mixer, inlet flow rate 125ml/min, **C_{val}=15mg/ml,** and **C_{val}=18mg/ml**, 2-propanol/water, 1:1, v/v, **second order fit** a) DROPLETS, b) CLUSTERS.

Figure 6.5a shows the impact of different inlet stream flow rates on droplet size distribution for crystallising samples with valine concentration 16mg/ml. For the lower flow rate (60ml/min) the droplets size is mostly in the range between 200nm and 400nm. A small population of larger droplets are present in sample, but they are not larger than700nm. If the

higher flow rate (125ml/min) was applied a narrow size distribution of droplets was observed but corresponded to the larger diameter range. The nanodroplets are mostly with hydrodynamic diameter between 400nm to 600nm, but they are not larger than 700nm. The SMALL molecular clusters size distribution is present in Figure 6.5B, and they size is also change with inlet streams flow rates, higher flow rate (125ml/min) produce larger clusters. This could be due to presence of different size nanodroplets (second decay in autocorrelation function) which have influence on the clusters size (first decay in autocorrelation function), disscused in Experimental Techniques section.

a) b)

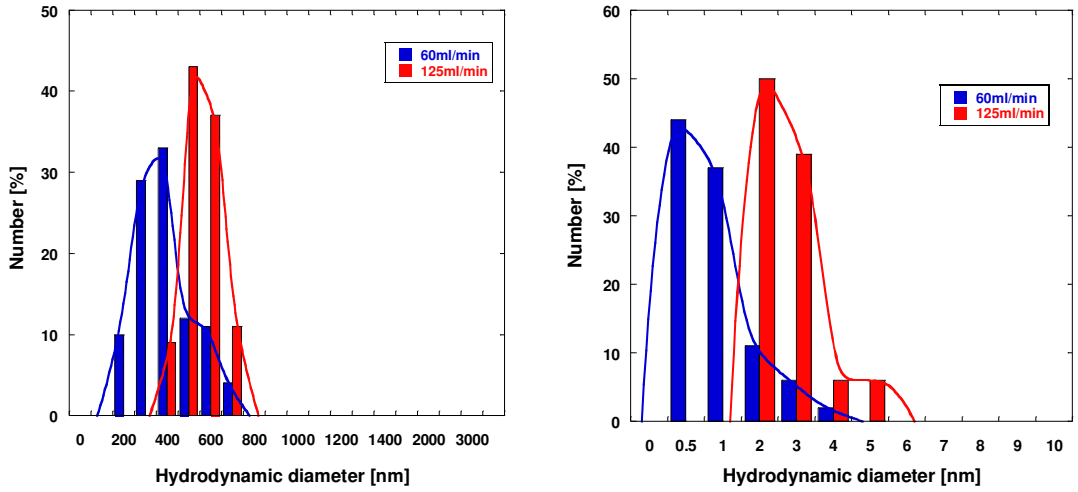

Figure 6.5 Clusters and nanodroplets estimated size distribution, CIJ mixer, inlet flow rates 125ml/min and 60ml/min, **C_{val}=16mg/ml**, 2-propanol/water, 1:1, v/v, **second order fit** a) DROPLETS, b) CLUSTERS.

In order to investigate how applying the CIJ mixer and different inlet stream flow rates could impact the final valine microcrystals morphology, optical and scanning electron microscopy were used.

6.2 Scanning Electron Microscopy (SEM)

SEM samples were prepared with a similar procedure like for DLS measurements and valine crystals were isolated by rapid filtration of the crystallising mixtures on a membrane with applied vacuum after 4 hours and 24 hours. Figure 6.6 shows the valine crystals produced using CIJ mixer with inlet streams flow rate 125ml/min and valine concentrations 16mg/ml (Figure 6.6a) and 18mg/ml (Figure 6.6b). The microcrystals were isolated from crystallising solution after 24 hours. The images show one population of crystals with rhombohedral-

shaped plates, typically with well defined edges and vertices, and a second population of needle-like crystals. The crystals prepared in samples containing lower valine concentration (16mg/ml) appeared to contain large crystals compared to microcystals produced in samples with higher solute concentration. It was also observed that samples prepared by applying higher flow rate produced a greater number of crystals.

a) b)

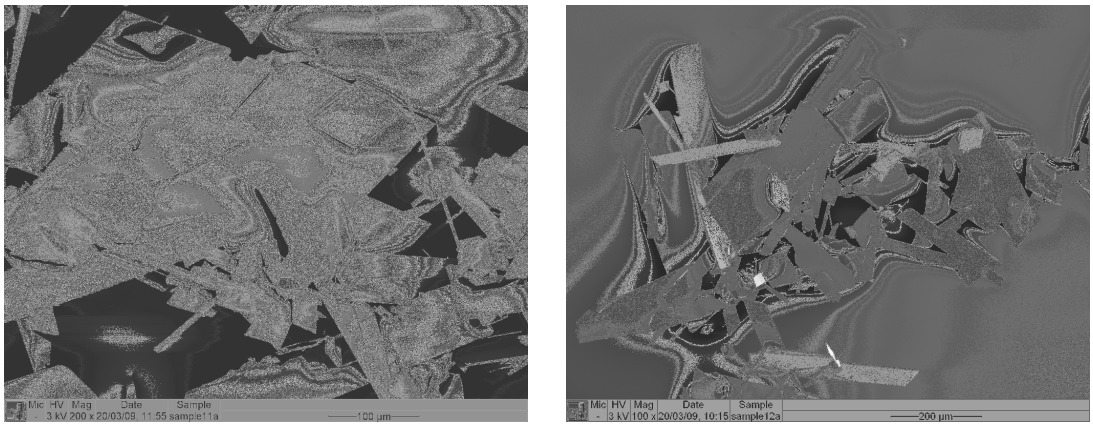

Figure 6.6 SEM images of valine microcrystals, CIJ mixer, inlet streams flow rate 125ml/min, **filtered after 24 hours**, 2-propanol/water, 1:1, v/v, a) **C_{Val}=16mg/ml**, b) **C_{Val}=18mg/ml.**

Figure 6.7 shows the valine microcrystals produced using the CIJ mixer with inlet streams flow rate 125ml/min and valine concentration 18mg/ml. The microrystals were isolated from solution after 4 hours (Figure 6.7a) and 24 hours (Figure 6.7b). The average size of crystals was very comparable in two samples filtered either after 4 hours or 24 hours, but samples filtered after 24 hours appeared to contain a biger number of the larger crystals. The pictures suggest that the number of crystals is determined during the first hours of the nucleation process which is crucial and then most part of the crystal growth takes place in the first 4 hours of crystallisation. During the next 20hours a small increase of crystals size was observed.

a) b)

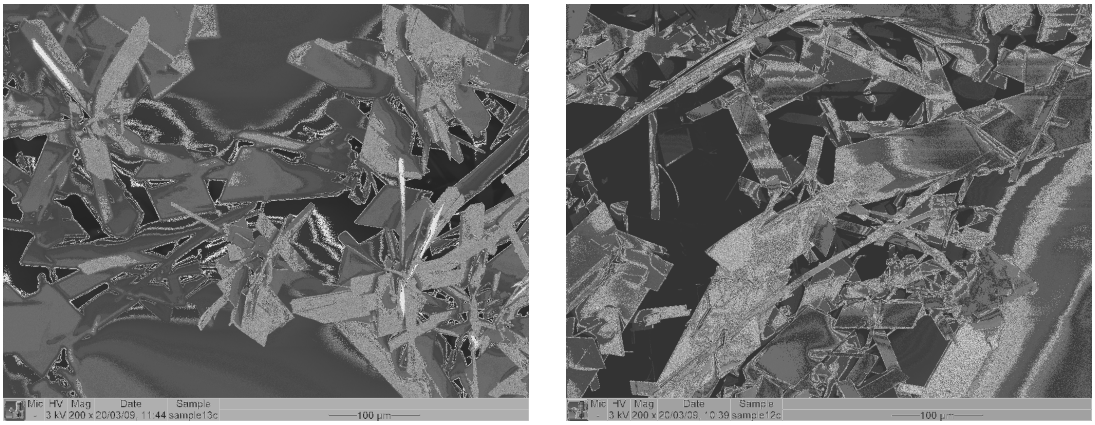

Figure 6.7 SEM images of valine microcrystals, CIJ mixer, inlet streams flow rate 125ml/min, **C_{Val}=18mg/ml**, 2-propanol/water, 1:1, v/v, a) sample filtered after 4hours, b) sample filtered after 24 hours.

Using the optical microscopy platelet crystals intergrown in rosette-like forms were observed in the samples filtered after 4 hours (Figure 6.8a). This could be due to crystal nucleation taking place inside of valine rich nanodroplets phase and subsequent crystal growth by nanodroplets attachment to the existing crystals surface (Figure 6.8b). The SEM sample preparation procedure probably destroyed most of those intergrown crystals structures, but they were easly observed in the same sample observed under optical microscopy. Figure6.8b shows macrodroplets at the surface of valine crystals isolated from samples after 24 hours and prepared using CIJ with inlet flow rate 125ml/min and with valine concentration 15mg/ml.

a) b)

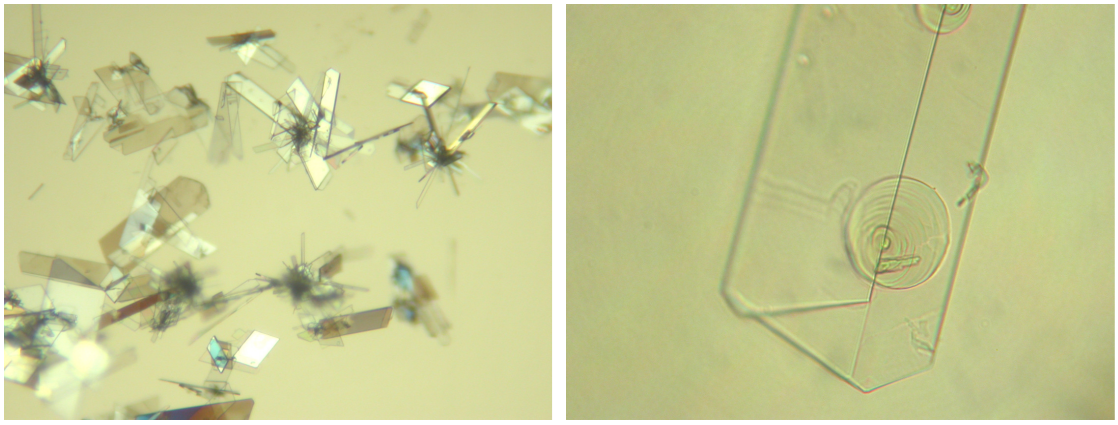

Figure 6.8 Optical microscopy images of valine microcrystals, CIJ mixer, inlet streams flow rate 125ml/min, 2-propanol/water, 1:1, v/v, a) **C_{Val}=18mg/ml,** sample filtered after 4hours, b) **C_{Val}=15mg/ml,** sample filtered after 24 hours.

7. COOLING CRYSTALLISATION of D,L-valine.

In this chapter the cooling crystallisation of D,L-valine from 2-propanol/water solution with ratio 1:1, v/v was studied. The antisolvent crystallisation experiments have shown that sample preparation has a big impact on the rate of crystal formation and growth. It was found that the greater the input of shear energy into the supersaturated solution the faster the kinetics and the more species is formed. To provide data for an undisturbed crystallising solution, samples of similar composition were prepared by mixing aqueous valine and 2-propanol at 50°C (undersaturated condition). These were then monitored during cooling experiments (cooling to 20-15°C Supersaturated condition) using NMR and DLS.

7.1 ^{1}H Nuclear Magnetic Resonance (NMR)

In a typical NMR experiment the samples were prepared by mixing aqueous solutions of valine and 2-propanol using a magnetic stirrer at 50°C (undersaturated condition), transferred to an NMR tube and cooled undisturbed to 20°C, in the tube. Figure 7.1 shows the variation in concentration of valine on cooling solutions of different supersaturations. Even at high supersaturation all of the valine remained in the liquid phase during these NMR cooling experiments and the undisturbed solution remained transparent for more than 24 hours. Large microcrystals were typically observed only after 2 days of keeping the samples at 25°C. Compared to the previous vortexed samples this represents a crystallisation rate which is about 500 fold slower and for the stirred sample around 50 fold slower. Surprisingly, when the cooled samples were agitated by swirling the NMR tube, a large number of crystals were observed to form within a few minutes. Therefore moderate input of shear energy into an aged supersaturated system at a later time can also be used to speed up the crystallisation process.
In order to probe for the possible presence of such species, dynamic light scattering (DLS) was used to monitor the crystallising solutions.

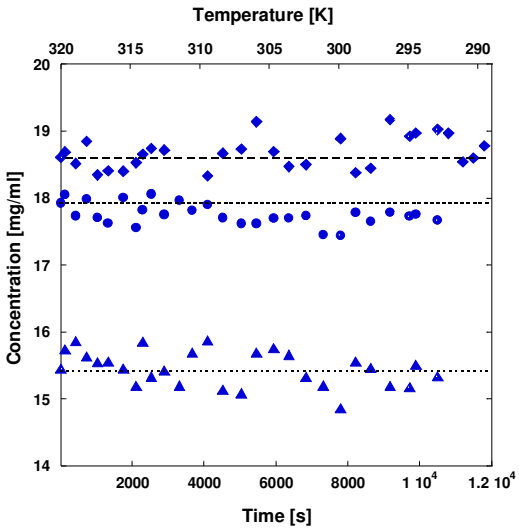

Figure 7.1 Kinetics of cooling crystallisation processes determinated using NMR, 2-propanol/water, 1:1, v/v.

7.2 Dynamic Light Scattering (DLS)

Dynamic light scattering technique was used to monitor the cooling crystallisation process of D,L-valine from 2-propanol/water solution. Typically the supersaturated samples were prepared by mixing filtered aqueous valine and 2-propanol at 50°C (where valine is fully soluble) and cooling it to 20°C. Figure 7.2 shows the sequence of autocorrelation functions g_2-*1* for different temperatures during the cooling crystallisation experiment with valine concentration 16mg/ml. At high temperature no scattering species could be observed, but below about 35°C nanodroplets were found to form spontaneously. The autocorrelation plots of cooling crystallisation samples with different valine concentrations (19, 25, 27mg/ml) are presented in Appendix (Fig. 11.9-11.11). The control cooling experiment of 2-propanol/water solvent was also done and scattering autocorrelation functions are plotted in Figure 7.3. The correlation functions for sample and solvent both show at higher temperature a noisy exponential decay in about 10^6μs, which is probably due to solution movement induced by changing temperature. This effect was quite significant at higher temperature, but disappeared almost completely at lower temperature.

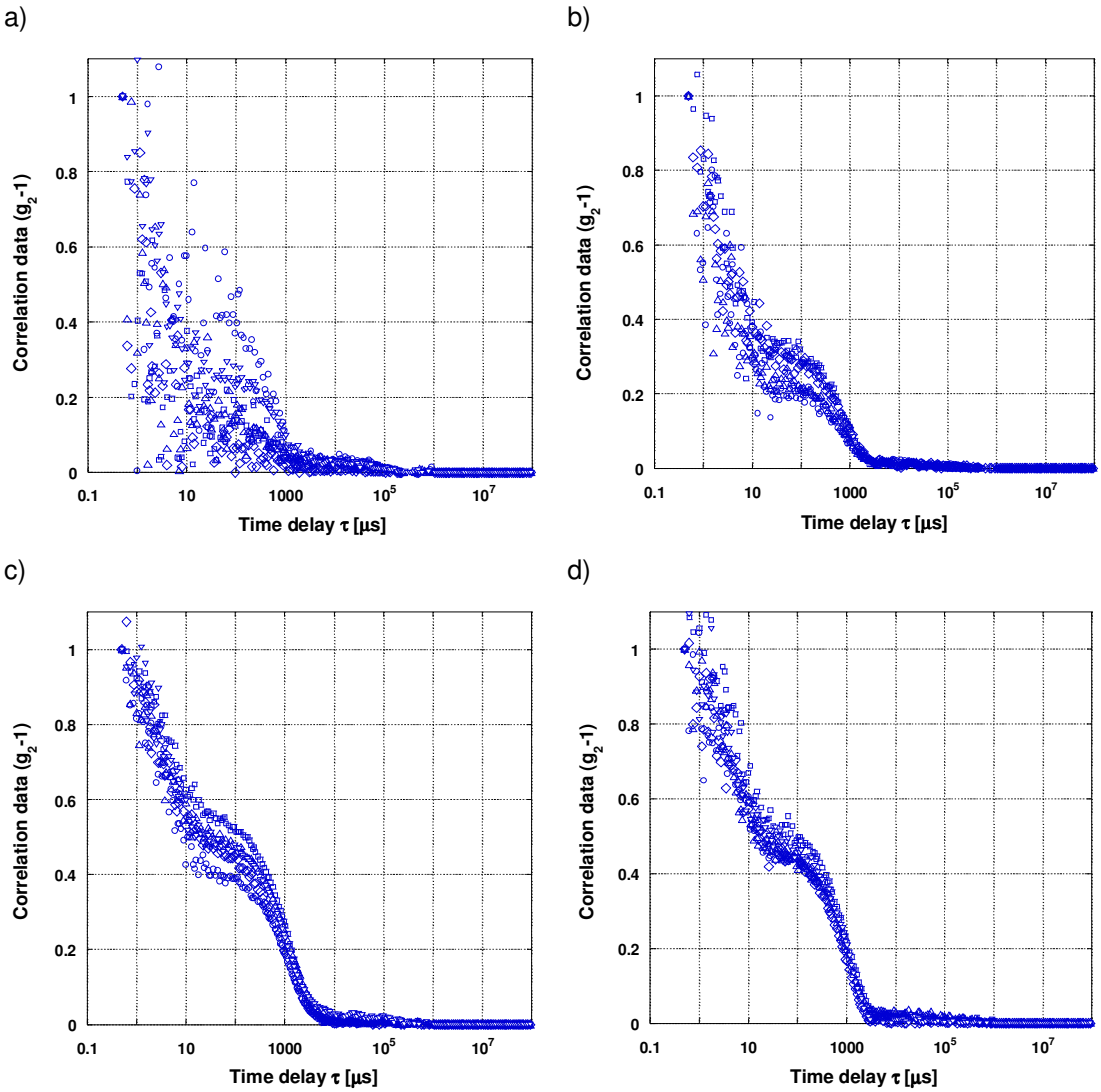

Figure 7.2 Light scattering autocorrelation functions g_2-*1*, C_{Val} **=16mg/ml**, **COOLING CRYSTALLISATION**, 45°C, b) 35°C, c) 30°C, d) 25°C, 2-propanol/water, 1:1, v/v.

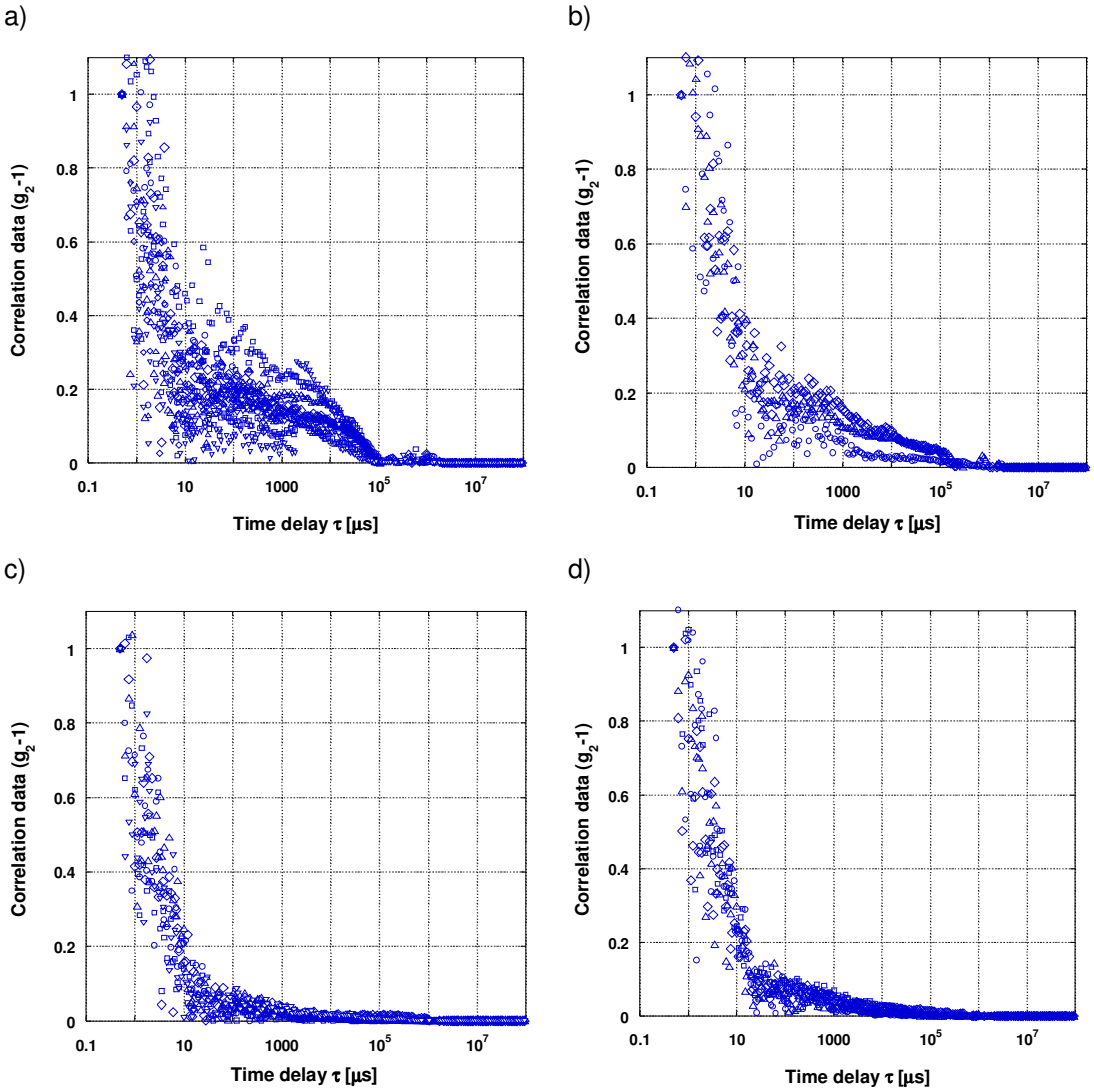

Figure 7.3 Light scattering autocorrelation functions g_2-*1*, **COOLING CRYSTALLISATION** of solvent 2-propanol/water, 1:1, v/v, a) 40˚C, b) 30˚C, c) 25˚C, d) 20˚C.

Using the Stokes-Einstein equation and parameters obtained from fitting the correlation data $ln(g_1)$ using first and second order functions the hydrodynamic diameters of clusters and droplets were calculated, (solvent viscosity table in Appendix Table 11.2). Figure 7.4 shows average hydrodynamic diameter of clusters and droplets measured the temperature range from 35℃ to 15℃ and three different concentrations: 19, 25 and 27mg/ml.

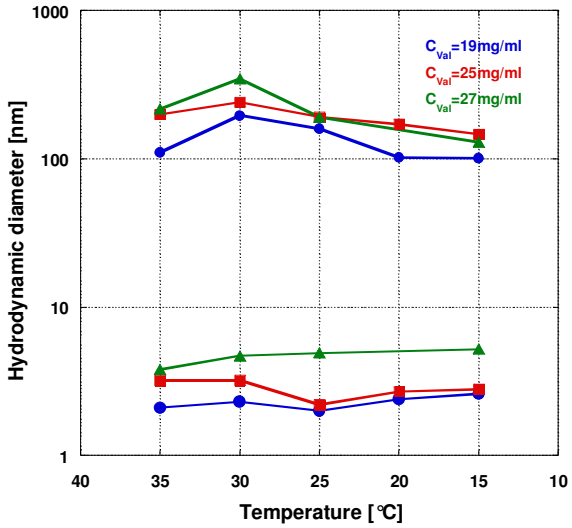

Figure 7.4 Average hydrodynamic diameter of clusters and droplets, **COOLING CRYSTALLISATION**, **first order fit**, C_{Val} =19mg/ml, C_{Val} =25mg/ml and C_{Val} =27mg/ml, 2-propanol/water, 1:1, v/v.

The size of clusters increased with valine concentration in from around 1.5nm for a sample with valine concentration 19mg/ml, to 5.2nm for 27mg/ml, however the clusters size was almost constant over the temperature range 35°C - 15°C. The droplets diameter increased with the valine concentration in the crystallising solution and reached a maximum size at around 30°C (Figure 7.4).

Table 7.1 Mean clusters and droplet hydrodynamic diameters with different D,L-valine concentrations at temp. from 35-15°C, **COOLING CRYSTALLISATION**, **first order fit**, 2-propanol/water, 1:1, v/v.

Temperature [°C]	D,L-valine CONCENTRATION					
	19 mg/ml		**25mg/ml**		**27mg/ml**	
	Hydrodynamic **CLUSTERS** diameter [nm]	Estimated **DROPLETS** diameter [nm]	Hydrodynamic **CLUSTERS** diameter [nm]	Estimated **DROPLETS** diameter [nm]	Hydrodynamic **CLUSTERS** diameter [nm]	Estimated **DROPLETS** diameter [nm]
35	**1.5** (±0.9)	**119** (±62)	**3.2** (±1.1)	**200** (±26)	**3.8** (±1.1)	**217** (±7)
30	**2.0** (±0.5)	**220** (±35)	**3.2** (±0.6)	**241** (±15)	**4.7** (±0.7)	**347** (±8)
25	**2.0** (±0.4)	**156** (±21)	**2.2** (±0.4)	**191** (±9)	**4.9** (±0.7)	**216** (±9)
20	**2.4** (±0.5)	**77** (±8)	**2.7** (±0.4)	**171** (±12)	-	-
15	**2.6** (±0.5)	**74** (±8)	**2.8** (±0.4)	**147** (±9)	**5.2** (±0.7)	**130** (±11)

Because all antisolvent crystallisation samples were prepared at 25°C the behaviour of samples during cooling crystallisation at the same temperature (25°C) was carefully examined. Table 7.2 summaries the estimated diameters of nanodispersions for different D,L-valine concentrations calculated at 25°C. The size of nanodroplets at 25°C increases with concentration of valine in the samples (except the 16mg/ml sample). The droplet diameter within 18.5 and 19mg/ml solutions is around 150nm. With increasing valine concentration to 25mg/ml the droplet size was around 200nm for 27mg/ml diameter or even larger (200-300nm) depending on the fitting method.

Table 7.2 Mean clusters and droplet hydrodynamic diameters with different D,L-valine concentrations at 25°C, **COOLING CRYSTALLISATION**, 2-propanol/water, 1:1, v/v.

Concentration [mg/ml]	**COOLING CRYSTALLISATION Temperature 25°C**			
	Hydrodynamic **CLUSTERS** diameter [nm]	Hydrodynamic **DROPLETS** diameter [nm]	Hydrodynamic **CLUSTERS** diameter [nm]	Hydrodynamic **DROPLETS** diameter [nm]
	1-st order fit	**2-nd order fit**	**1-st order fit**	**2-nd order fit**
16	**4.1** (±0.9)	**2.5** (±0.7)	**243** (±14)	**266** (±51)
18.5	**2.0** (±0.6)	**1.4** (±0.7)	**159** (±60)	**162** (±118)
19	**2.0** (±0.4)	**1.2** (±0.3)	**156** (±21)	**160** (±60)
19	**2.1** (±0.4)	**1.3** (±0.3)	**144** (±16)	**149** (±51)
25	**2.2** (±0.4)	**1.4** (±0.4)	**191** (±9)	**188** (±21)
27	**4.9** (±0.7)	**2.8** (±0.5)	**216** (±9)	**330** (±40)

The nanodroplets formed in cooled solutions were of similar average size to those observed in magnetically mixed solutions (especially samples with low valine concentrations), but had a noticeably narrower size distribution (100-300nm). On storage over many hours there was no change in the average size or size distribution of the nanodroplets and similar results were obtained even at high supersaturations (Figure 7.5). First order fit size distribution attached in Appendix Figure 11.12. Thus, in the absence of agitation, valine-rich nanodroplets form a metastable phase with no sign of coalescence or setting.

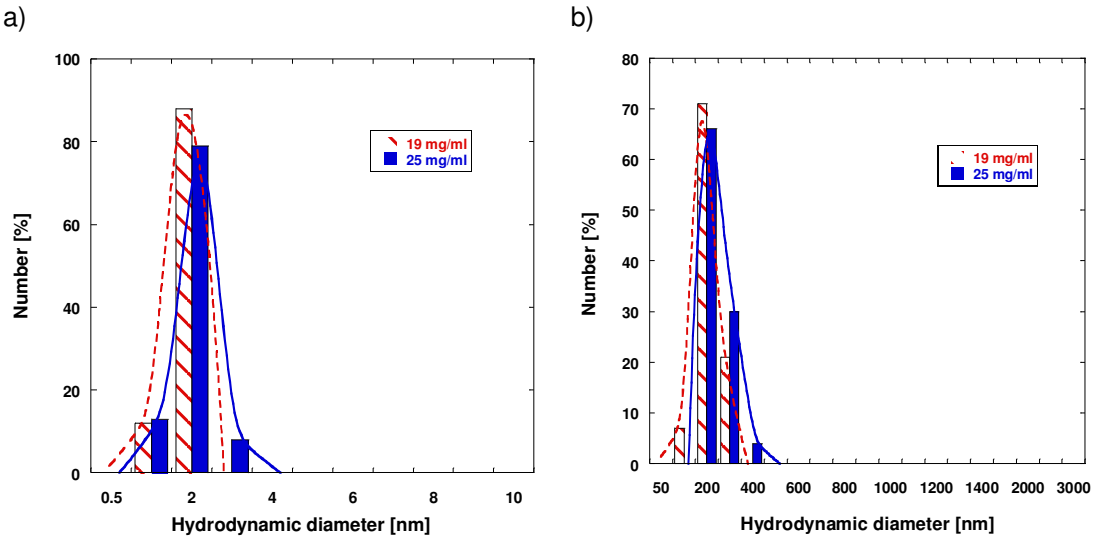

Figure 7.5 Nanodispersions estimated size distribution, **COOLING CRYSTALLISATION**, 2-propanol/water, 1:1, v/v, **second order fit**, C_{Val} =19 and 25mg/ml at 25ºC, a) clusters, b) droplets.

Previously nanodroplets were observed in samples prepared by mixing at concentrations below the solubility limit of valine crystals. This could have been a mixing artefact or else be an indication that the valine-rich phase was actually thermodynamically stable over a certain composition range. If stable such a phase must exist in equilibrium with a crystalline valine phase. To test this possibility a 19mg/ml solution of valine was prepared from filtered aqueous valine and 2-propanol at 50°C, cooled and held for 12 hours at 12°C, whereupon large valine crystals could be observed. The sample was then reheated until the components redissolved (> 35°C). DLS measurements were made during cooling, on standing at 12°C and again on heating. It was observed that at 35°C or below nanodroplets were invariably observed. Thus, even in solutions equilibrated for 12 hours, with valine crystals present, the valine-rich liquid phase persisted. It could be argued that this was because exchange of material with the valine nanodroplets was very slow compared to crystal growth. However, as shown in Figure 7.6 and Table 7.3 during both the cooling and heating cycles the size of the nanodroplets was observed to vary. (Autocorrelation functions graphs attached in Appendix Fig.11.13). Furthermore, the size observed at a particular temperature during cooling and heating was almost identical suggesting that the system remained in equilibrium. The reversible appearance of the nanodroplets at a specific temperature and their coexistence with valine crystals was clearly indicative that the inhomogeneous phase, comprised of valine-rich nanodroplets dispersed within a solution of concentrated valine, could well be the most thermodynamically stable over a range of valine concentrations. However, if this were the case, it should of course be possible to generate the inhomogeneous liquid phase from both sides of the phase boundary.

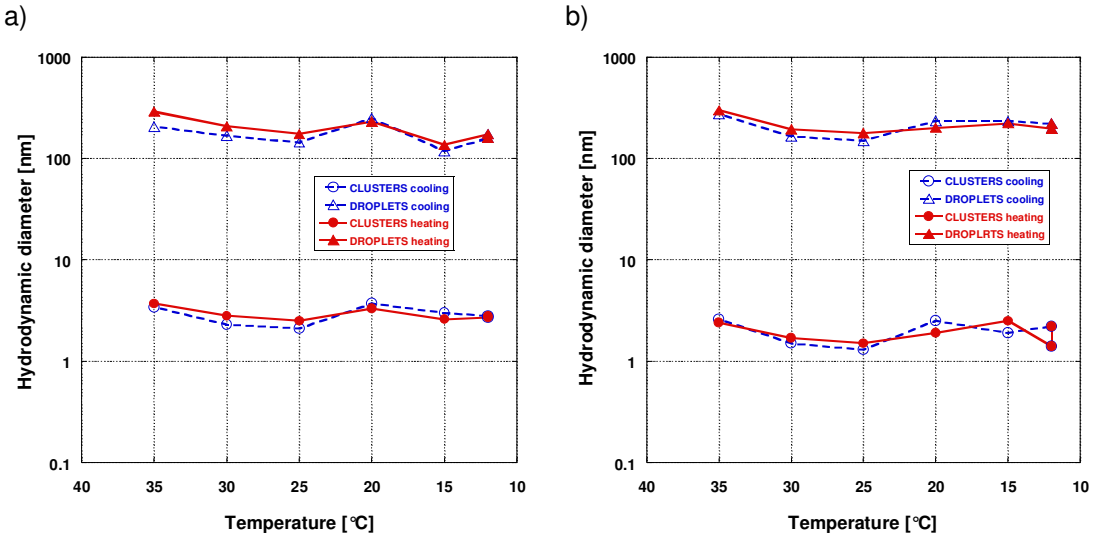

Figure 7.6 Average hydrodynamic diameters of clusters and droplets, **COOLING-HEATING EXPERIMENT**, 2-propanol/water, 1:1, v/v, C_{Val} **=19mg/ml**, a) first order fit, b) second order fit.

Table 7.3 Mean clusters and droplets hydrodynamic diameter with D,L-valine concentration C_{Val}**=19mg/ml**, **COOLING-HEATING EXPERIMENT**, 2-propanol/water, 1:1, v/v.

Temperature [℃]	D,L-valine CONCENTRATION			
	Hydrodynamic **CLUSTERS** diameter [nm]	Hydrodynamic **DROPLETS** diameter [nm]	Hydrodynamic **CLUSTERS** diameter [nm]	Hydrodynamic **DROPLETS** diameter [nm]
	1-st order fit	**2-nd order fit**	**1-st order fit**	**2-nd order fit**
35 (cooling)	**3.4** (±0.5)	**2.6** (±0.6)	**205** (±13)	**273** (±50)
30 (cooling)	**2.3** (±0.5)	**1.5** (±0.3)	**167** (±18)	**164** (±39)
25 (cooling)	**2.1** (±0.4)	**1.3** (±0.3)	**144** (±16)	**149** (±51)
20 (cooling)	**3.7** (±0.4)	**2.5** (±0.4)	**248** (±11)	**235** (±30)
15 (cooling)	**3.0** (±0.7)	**1.9** (±0.7)	**118** (±10)	**233** (±90)
12 (cooling)	**2.8** (±0.5)	**2.2** (±0.7)	**159** (±12)	**220** (±77)
12 (after 12h)	**2.7** (±1.7)	**1.4** (±1.0)	**174** (±50)	**197** (±85)
15 (heating)	**2.6** (±0.4)	**2.5** (±0.4)	**136** (±11)	**222** (±93)
20 (heating)	**3.3** (±0.6)	**1.9** (±0.4)	**231** (±13)	**200** (±21)
25 (heating)	**2.5** (±0.4)	**1.5** (±0.2)	**174** (±14)	**177** (±42)
30 (heating)	**2.8** (±0.5)	**1.7** (±0.3)	**208** (±22)	**194** (±53)
35 (heating)	**3.7** (±0.7)	**2.4** (±0.4)	**288** (±19)	**297** (±32)

However, there remains the possibility that the crystal growth had not completely finished after 12 hours, and 12 hours is not enough time to observe all the metastable nanodroplets disappear. Because it will be always hard to appraise the point when a crystallisation process is finished a different experiment was carried out to capture, whether the nanodroplets might be stable.

A 23 mg/ml solution was prepared at 50ºC from filtered solutions, checked to ensure it contained no scattering particles and cooled for 24 hours in the DLS cell. This resulted in formation of a significant number of visible crystals stuck to the base of the cell. The supernatant above the crystals again contained nanodroplets but this time was carefully removed, without disturbing the crystals, and replaced with a slightly under-saturated filtered (0.2µm PTFE) valine solution (14.2 mg/ml, Figure 7.7 and 7.8). DLS analysis showed a weak signal from nanodroplets still remained so the supernatant was again removed and replaced with filtered under-saturated solution. DLS analysis showed that this treatment lowered the concentration of nanodroplets below the detectable limit.

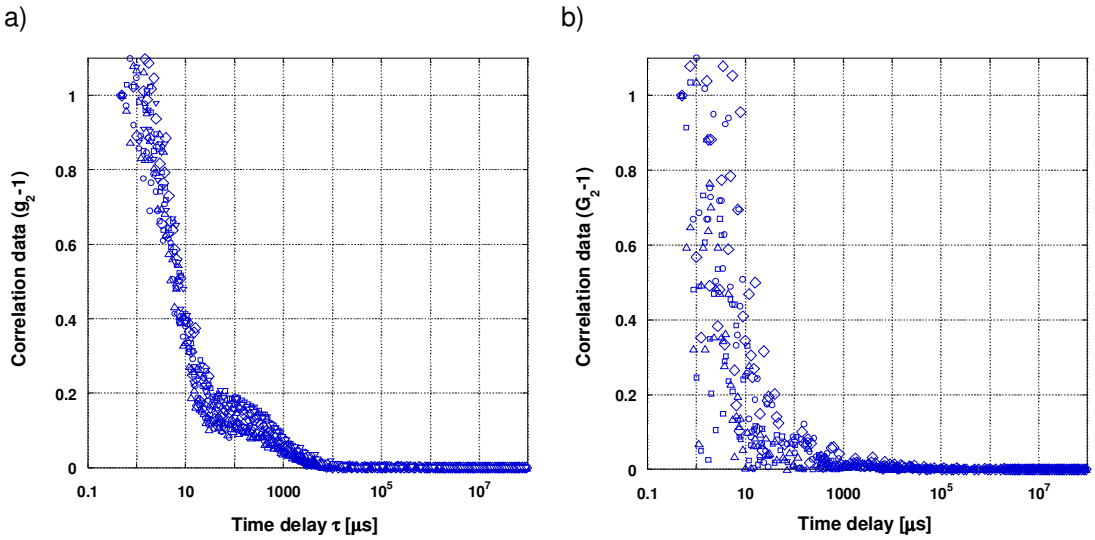

Figure 7.7 Light scattering autocorrelation functions g_2-*1*, of C_{Val}**=14.2 mg/ml** D,L-valine/2-propanol/water solution a) without filtration, b) filtered (0.2μm PTFE)-measured immediately after filtration.

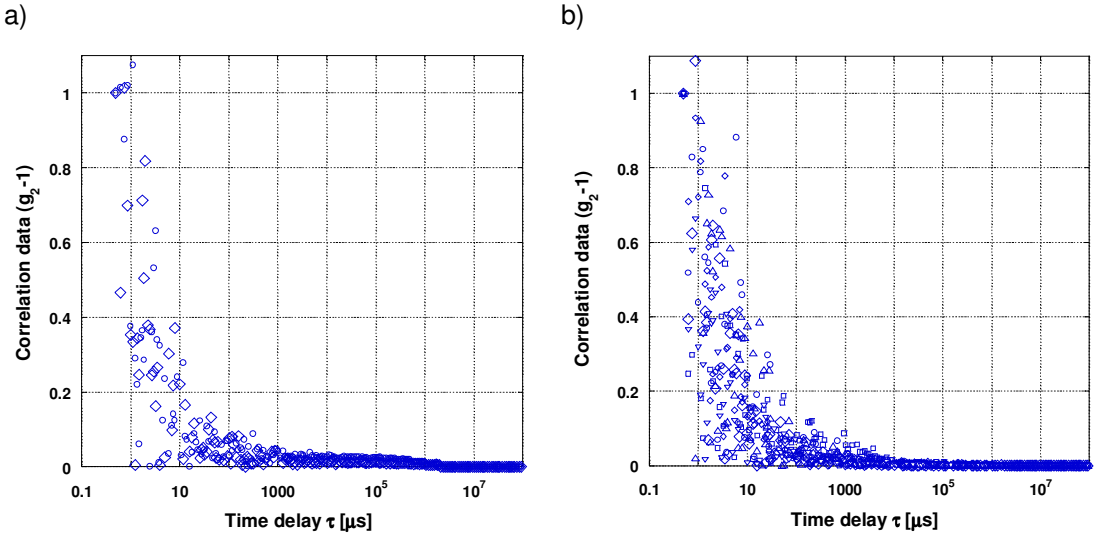

Figure 7.8 Light scattering autocorrelation functions g_2-*1*, of C_{Val}**=14.2 mg/ml** D,L-valine/2-propanol/water filtered solution (0.2μm PTFE) a) 2 hours after filtration, b) 24 hours after filtration.

Crystals were still clearly present at the bottom of the cell out of the optical path. The system was then left undisturbed at 25°C for 24 hours, after that DLS analysis showed a very weak fluctuated signal for nanodroplet (Figure 7.9a). The undisturbed cell was then gradually heated in the DLS whereupon strong constant signals consistent with the presence

of nanodroplets started to be observed. On holding the sample at a constant temperature these signals reduced slightly but then increased again when the temperature was ramped up further. On reaching 35°C the shape of the DLS signal was clearly very similar to that obtained on cooling but still less intense (Figure 7.9b). The appearance of the nanodroplet signal on heating seems counter-intuitive since it would be expected that the solubility of valine should increase under these conditions. However, it is certainly consistent with the source of the nanodroplets being the valine crystals lying outside of the beam in the base of the cell. Diffusion of nanodroplets away from the surface of the crystals would be expected to be extremely slow in a stationary cell and therefore heating will be required to provide a convection current to transport nanodroplets into the beam. The overall scheme of thiese experiments is depicted in Figure 7.10.

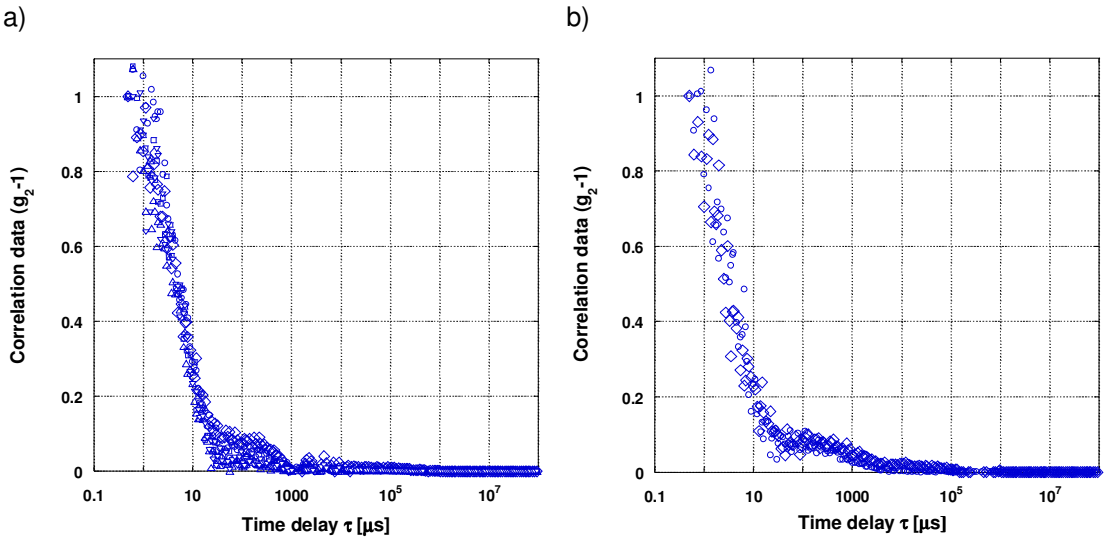

Figure 7.9 Light scattering autocorrelation functions g_2-*1*, of C_{Val}**=14.2 mg/ml** D,L-valine/2-propanol/water filtered solution with D,L-valine microcrystals, after 24h keeping at 25°C, a) 25°C, b) 35°C.

Further support for this transport limitation was obtained by gentle rocking of the DLS cell to homogenise the mixture without dislodging the crystals. Immediately a much stronger signal was observed for the nanodroplets (200-300 nm) and this could still be observed after a further 2 weeks equilibration (Figure 7.11). Thus, a stable inhomogeneous phase, comprised of valine-rich nanodroplets dispersed within a solution of concentrated valine is generated directly on cooling a near-saturated solution and on heating an undersaturated solution, both in the presence of valine crystals. Autocorrelation functions for those experiments are show in Appendix (11.14).

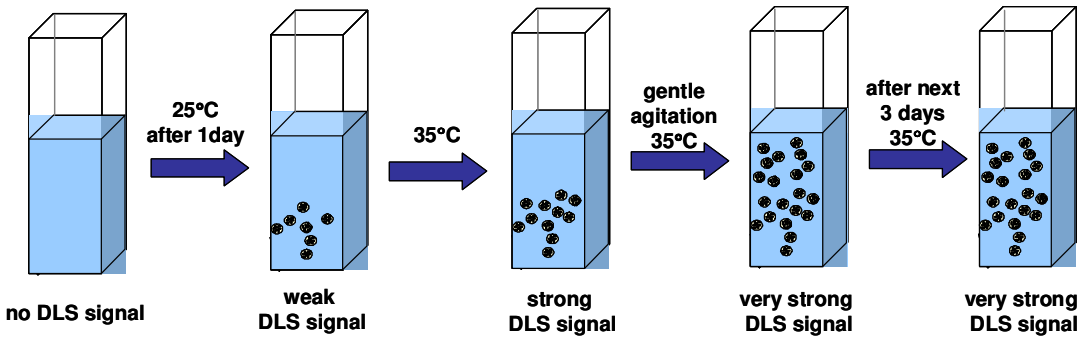

Figure 7.10 Schema of D,L-valine microcrystals dissolving process in slightly undersaturated solution.

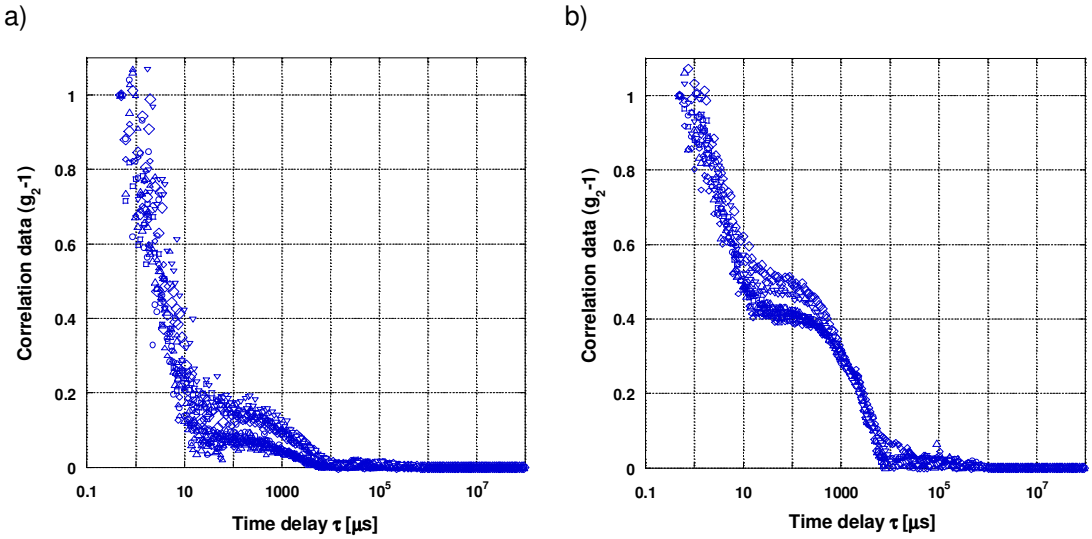

Figure 7.11 Light scattering autocorrelation functions g_2-*1*, of C_{Val}**=14.2 mg/ml** D,L-valine/2-propanol/water filtered solution with D,L-valine microcrystals, after 5days keeping at 25˚C, a) 35˚C, b) 35˚C after shaking.

From this experiment it can definitely be concluded that valine-rich nanodroplets dispersed in valine solution are the thermodynamically-stable state of matter over a range of compositions. The presence of intermediate liquid-like clusters on crystallisation pathways has been proposed by a number of authors ***(Galkin and Vekilov 2000; Galkin and Vekilov 2001; Chattopadhyay et al. 2005; Erdemir et al. 2007; Vekilov 2009).*** but generally they have been considered to be metastable and short-lived and therefore difficult to characterise. The stable sub-visible liquid droplets observed in this work were long-lived and easily detected by dynamic light scattering but nevertheless still proved to be difficult to characterise further. The mass of valine in the valine-rich liquid phase could be estimated

from NMR and the size of particles determined by DLS but because the number of particles was an untractable unknown their composition could not be determined from this information.

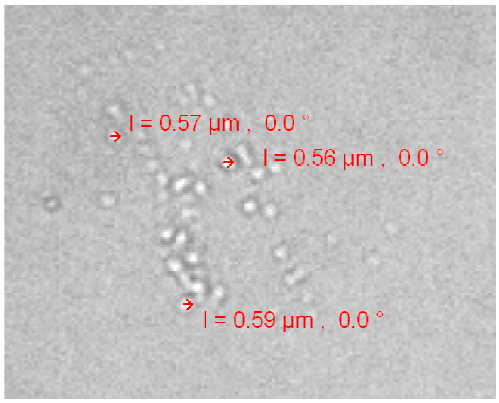

Figure 7.12 Picture of nanodroplets, D,L-valine cooling crystallization sample, **C_{val}=19mg/ml**, 2-propanol/water, 1:1, v/v.

Interestingly, filtration of the mixture using a wide range of filters and pore-sizes resulted in almost complete loss of the valine-rich liquid-phase onto the filter. This left behind a supernatant that was molecularly saturated in valine but sub-saturated with respect to crystallisation. If this had not been recognised it would of course have confounded the monitoring of the nanodroplets by DLS. Conventional protocols invariably involve filtration at the point of measurement.

The above stable liquid nanodroplets phase conclusions have relied heavily on DLS data. To prove corroborating evidence for the presence of nanodroplets intermediates optical microscopy with oil immersed lens was used. The minimum size range for this technique is close to 300nm and so gentle agitation was applied to a cooled supersaturated valine solution to induce some coalescence prior to introduction into the sampling capillary. Under these conditions it was possible to directly image valine-rich nanodroplets in the size range 300-500nm with in the valine solution (Figure 7.12). Interestingly the concentration of imaged nanodroplets appeared to be greater close to the capillary walls suggesting perhaps that coalescence may be faster in this region.

8. COOLING CRYSTALLISATION of glycine.

In this chapter we report studies of the cooling crystallisation of glycine from aqueous solution, using Nuclear Magnetic Resonance (NMR), Dynamic Light Scattering (DLS) and Scanning Electron Microscopy (SEM). The formation of molecular clusters in aqueous glycine solutions was reported previously by Myerson et al. ***(Chattopadhyay et al. 2005; Erdemir et al. 2007)*** who were using Small Angle X-ray Scattering (SAXS). The authors investigated the cooling crystallisation of glycine aqueous solutions at several different concentrations and concluded that glycine molecular clusters existed in saturated and undersaturated solutions.

Studies of supersaturated aqueous solution of glycine by measuring freezing point depression and diffusivity were reported by Huang et al. ***(Huang et al. 2008).*** The authors concluded that glycine supersaturated solution mostly contains monomers, up to 70% with the rest of the glycine molecules estimated to exist as dimers.

In our studies we used the same glycine concentrations as in previously reported research: 230mg/ml and 270mg/ml (concentrations per ml of water), and undersaturated as well as supersaturated solutions were monitored using DLS and NMR

The solubility data for glycine in water (H_2O) and deuterium oxide (D_2O) at different temperatures were taken from the work of Jelinska-Kazimerczuk (Figure 8.1) ***(Jelinska-Kazimierczuk and Szydlowski 1996)***. The aqueous solution with a glycine concentration of 230mg/ml reaches the saturation equilibrium at 23°C, while for the concentration of 270mg/ml the saturation temperature is: 31°C. The glycine solution in deuterium oxide and a glycine concentration of 270mg/ml will reach the saturation point at 36°C according to the reported data ***(Jelinska-Kazimierczuk and Szydlowski 1996).***

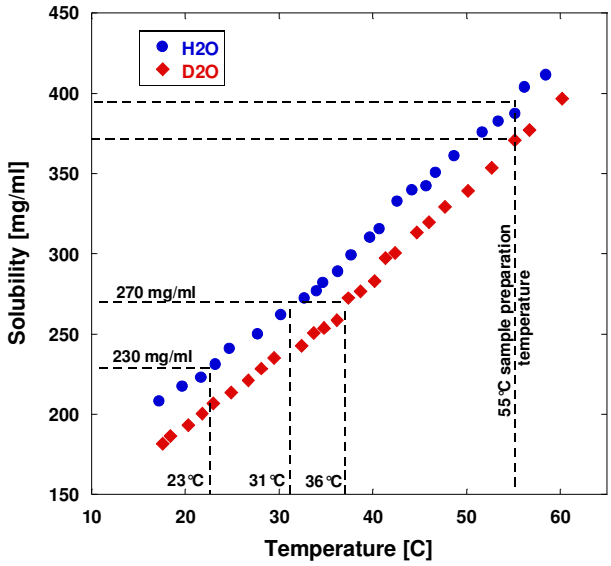

Figure 8.1 Solubility of glycine in water (H_2O) and deuterium oxide (D_2O) at different temperatures. Data from: **M.Jelinska-Kazimierczuk, J.Szydlowski;** Journal of Solution Chemistry, 25(12), 1996.

In the undisturbed, cooled sample the crystallisation process is very slow and the glycine solution remained transparent for more than 24 hours. Large crystals were typically observed only after 2 days of keeping the solution at 23°C.

8.1 ^{1}H Nuclear Magnetic Resonance (NMR)

The cooling crystallisation of glycine from aqueous solution was monitored using NMR. As mentioned before, the nuclear relaxation rate is faster for a substance in solution are considerably shorter than in the solid phase and therefore solution-phase NMR allows one to selectively determine the amount of solute remaining in the liquid phase throughout a cooling crystallisation process. Samples were prepared by dissolving glycine in deuterium oxide at 55°C, and transferred to a preheated (55°C) NMR tube in which a small internal tube was present containing an internal reference standard (TSP) of a known concentration. The reference allowed the absolute concentration of glycine remaining in solution to be monitored throughout the cooling crystallisation process. Meyrosn et al. suggested that the small molecular clusters which existed in the supersaturated solution rearrange during crystallisation process to form liquid-like larger clusters and finally glycine microcrystals ***(Chattopadhyay et al. 2005; Erdemir et al. 2007).*** In this study, we used NMR to monitor the concentration of glycine in solution during 5 hours of the crystallisation process.

The glycine concentration as a function of temperature is shown in Figure 8.2. The results show that the glycine concentration remained approximately constant throughout the cooling experiment.

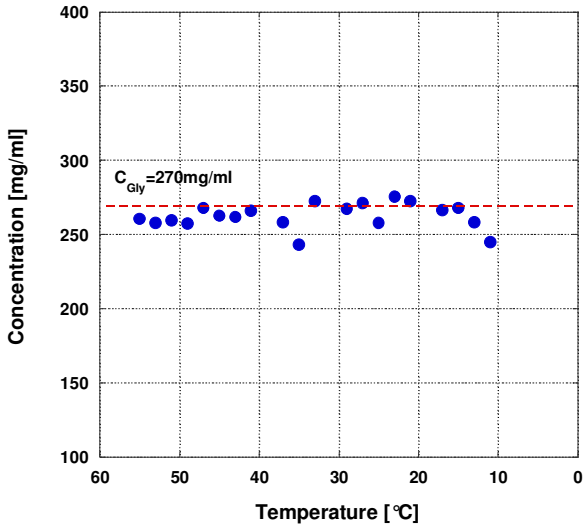

Figure 8.2 Kinetics of cooling crystallisation process of glycine from deuterium oxide solution, temperature range 55°C-10°C, C_{Gly} **=270mg/ml**.

The typical ^{1}H NMR spectrum obtained for glycine in deuteried solvent (D_2O) is shown in Figure 8.3. The spectrum contains peaks corresponds to all hydrogen atoms present in investigated sample (H_2O, glycine, TSP). Carefull investigation of glycine-hydrogen peak shows a typical shift with temperature (estimated on the basis of the standard TSP peak at 0ppm) and a small peak deformation at temperatures slightly below the glycine saturation temperature (Figure 8.4).

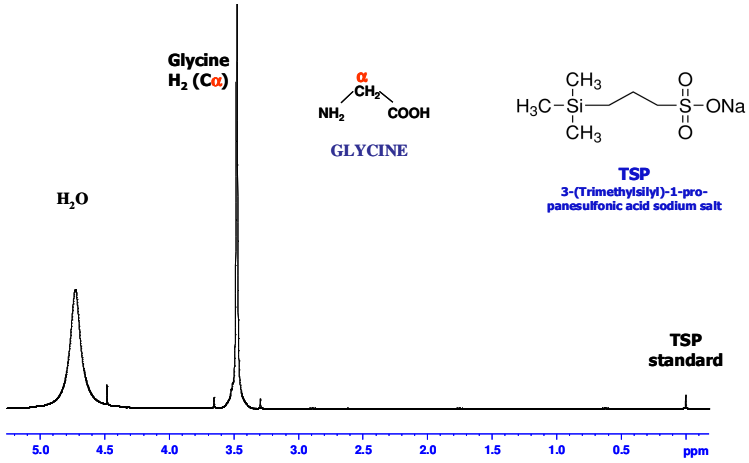

Figure 8.3 ^{1}H NMR spectrum of cooling crystallization of glycine, C_{Gly} **=270mg/ml**, temp. 30°C.

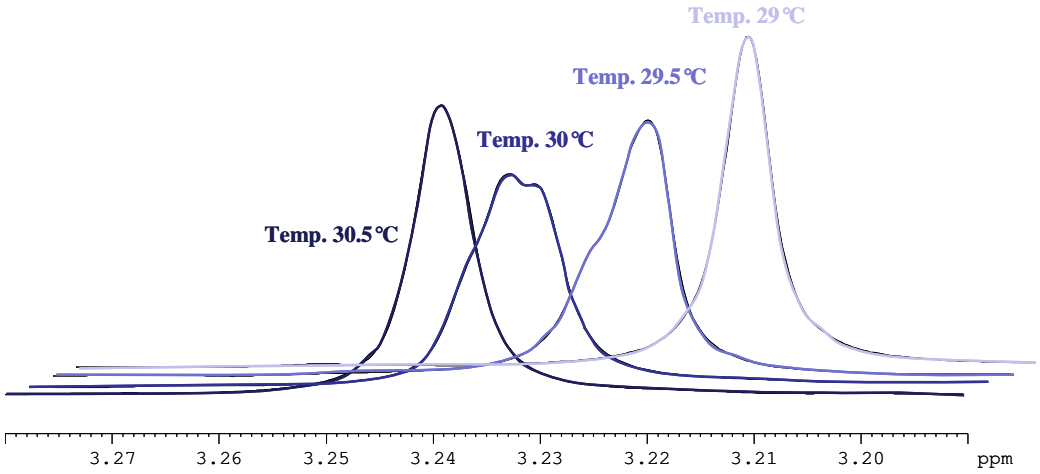

Figure 8.4 ^{1}H NMR spectrum, glycine peak ~3.2ppm, at temperature range 30.5-29°C, C_{Gly}=270mg/ml.

The small deformation of the glycine peak in the sample with solute concentration C_{Gly}=270mg/ml was seen at temperature around 30°C which disappearanced later at 29°C. This could be couse by the formation of moleculer clusters in glycine supersaturated solution. However, furthure careful peak investigation is required.

8.2 Diffusion Ordered Spectroscopy (DOSY)

DOSY measurement was carried out using deuterated solvent and samples prepared similarly to the NMR kinetics experiments. Diffusion measurements were preformed during a few hours of the cooling crystallisation process alternated with the NMR kinetics experiments. The diffusion coefficient was not changed throughout cooling crystallisation and showed quite broad peaks indicating the presence of the some glycine monomers as well as some molecular clusters (Figure 8.5). The diffusion coefficient signals for water and TSP standard are narrow with a diffusion coefficient was around $6.31 \cdot 10^{-9}$ m^2/s for water and $2.51 \cdot 10^{-9}$ m^2/s for TSP.

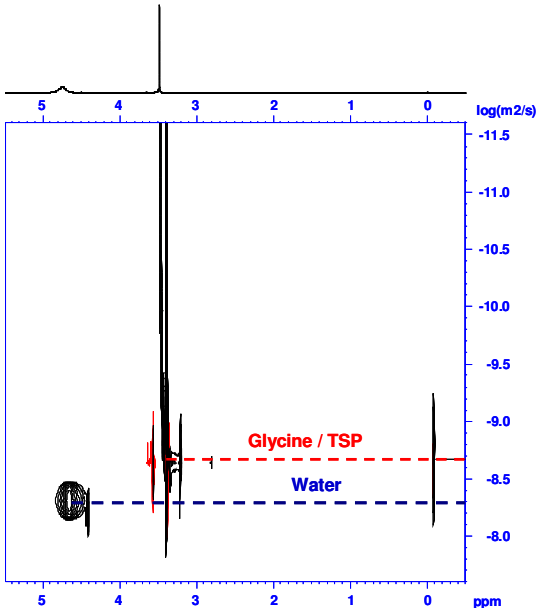

Figure 8.5 Diffusion coefficient measurement (DOSY), C_{Gly} = **270mg/ml**, at 50°C, solvent – deuterium oxide D_2O.

The diffusion coefficient for glycine was more difficult to estimate. For diffusion coefficient $10^{-8.65}$ log m^2/s where most of signal is located the calculated diameter of glycine is around 3.9 Å which corresponds to glycine monomer d=3.8 Å estimated on basis of crystal structure of hen egg white lysozyme ***(Sauter et al. 2001).*** The hydrodynamic diameter was calculated from the Stokes-Einstein equation: $d_H = \frac{k_B \cdot T}{3\pi\eta D}$ where k_B =1.38·10^{-23} J/K (Boltzman's constant), T=323K (absolute temperature), η=0.000547Pa·s (viscosity of solvent) – D_2O at 50°C and D=2.239 ·10^{-9} m^2/s = $10^{-8.65}$ m^2/s (diffusion coefficient). (Solvents H_2O and D_2O viscosity table in Appendix Table 11.3).

However, the signal from glycine is quite broad and showed larger diffusion coefficients with values up to 1000 times smaller, this corresponds to radii up to 1000 times larger than the monomer which may indicate the existence some much larger molecular clusters and even liquid-like nanodroplets.

The DOSY NMR studies indicated that clusters exist in both undersaturated and supersaturated glycine solutions, and they are present in what appears to be a liquid-like phase. If small molecular clusters are present in glycine solutions it should be possible using dynamic light scattering to investigate they size.

8.3 Dynamic Light Scattering (DLS)

DLS is a good technique for monitoring particles with sizes from about a nanometer to a few micrometers. Thus, by using DLS it should be possible to monitor the formation or presence of glycine molecular clusters in aqueous solution. All DLS samples were prepared using hydrogen oxide or deuterium oxide as a solvent at 55°C, filtered using 0.2 μm PP filter and transferred to a preheated DLS cuvette. The DLS cell was also preheated to 55°C and the temperature was then gradually reduced to 15°C during the cooling process.

The autocorrelation functions observed from glycine aqueous solution during cooling crystallisation immediately showed two exponential decays regions. This indicated the existence of not only small molecular clusters, but also of larger species, with a size corresponding to a few hundred nanometers. These species were present in solution from the beginning of the cooling experiment at a temperature at about 50°C, where the solution with a concentration at 230mg/ml or 270mg/ml is undersaturated (according to solubility data ***(Jelinska-Kazimierczuk and Szydlowski 1996)***). The solution phase NMR data showed that all glycine was in the liquid phase, so presumably the second detected species are liquid-like domeins. Figure 8.6 shows the autocorrelation function g_2*-1* obtained during cooling crystallisation experiment of glycine aqueous solution of 270mg/ml glycine concentration and over a temperature range from 50°C to 20°C. Two scattering species of a few and few hundreds nanometers were observed in the crystallising glycine solution from 50°C. A small third decay was observed at 50°C which is probably due to solution movement induced by not complete temperature equilibration of the sample. This effect disappeared at lower temperatures. DLS of control sample (deionised water filtered by 0.2μm PP filter) were also done and only very weak signal due to solvent fluctuations were observed (Figure 8.7).

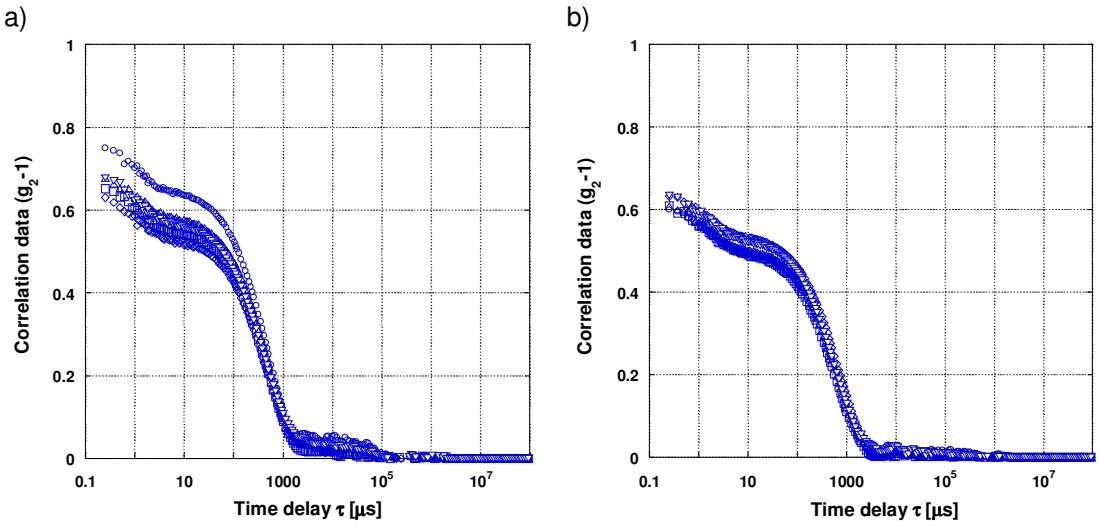

Figure 8.6 Light scattering autocorrelation functions g_2-*1*, C_{Gly}=270mg/ml, solvent – water (H_2O), COOLING CRYSTALLISATION, a) 40°C, b) 25°C.

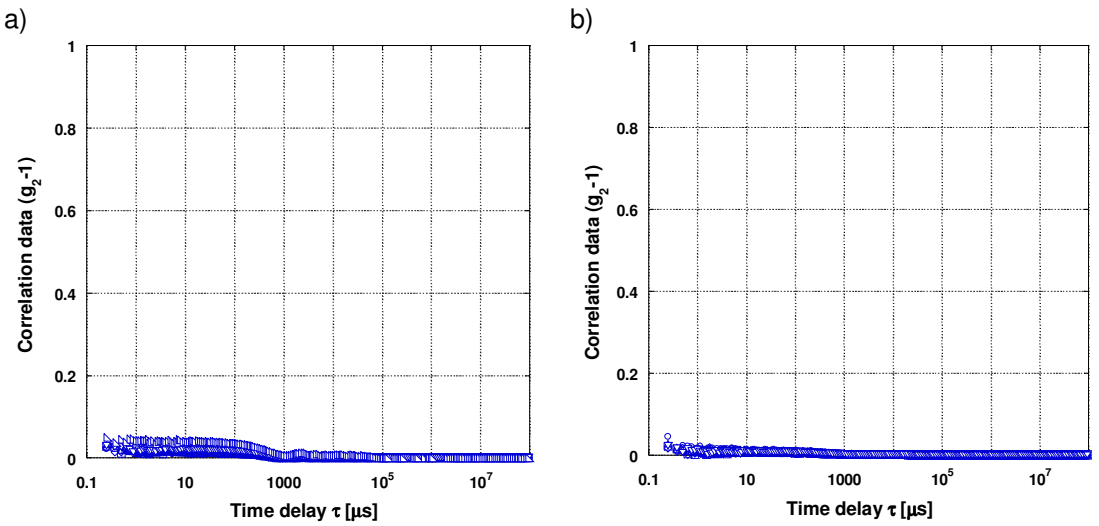

Figure 8.7 Light scattering autocorrelation functions *g2-1*, **solvent – water (H2O),** COOLING CRYSTALLISATION, a) 40°C, b) 25°C.

The cooling crystallisation of glycine with a concentration 270mg/ml from deuterated aqueous solution also was monitored using DLS. The formation of γ-glycine polymorph from deuterated aqueous solution at neutral pH instead of α-glycine which is crystallised form neutral aqueous solution has been reported ***(Hughes et al. 2007; Hughes and Harris 2009; Itaka 1961; Weissbuch et al. 2005)***. Because all NMR experiments were done in deuterated solvents, it was important to establish the presence of the same nano-size species during cooling crystallisation of glycine from deuterium oxide solutions.

The autocorrelation functions g_2-*1* presents in Figure 8.8 show similar results with two kinds of nanospecies in crystallised solutions over the whole range of tested temperatures (55℃ – 20℃). The control DLS experiment for cooled deuterium oxide was carried out, and an example of autocorrelation functions shows in Figure 8.9. No scattering species were observed in pure solvent. The autcorrelation functions for glycine nanodroplets and control solvent cooling experiment for the investigated temperature range are attached in Appendix Figure 11.15-11.19.

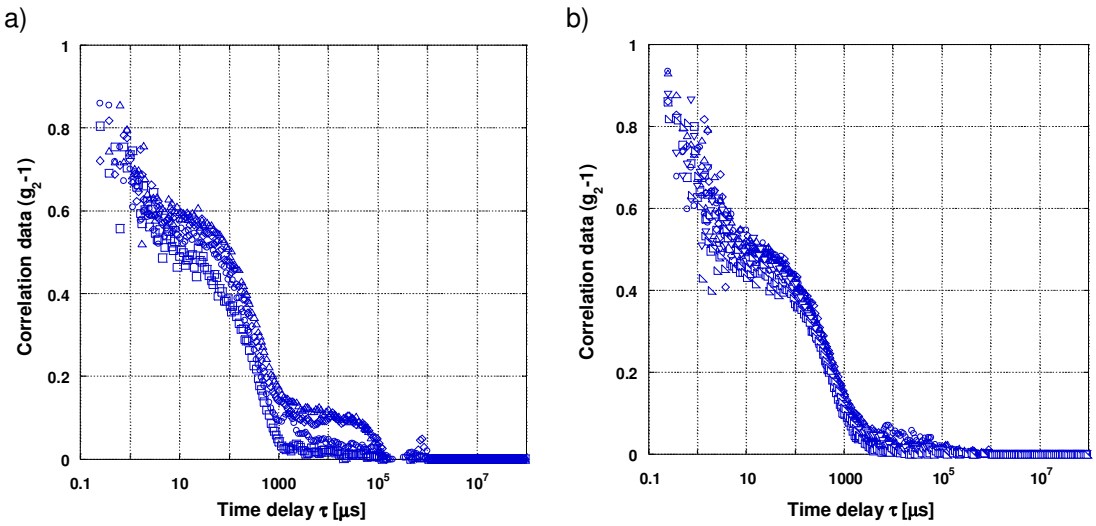

Figure 8.8 Light scattering autocorrelation functions g_2-*1*, C_{Gly}=270mg/ml, solvent – deuterium oxide (D_2O), COOLING CRYSTALLISATION, a) 45˚C, b) 25˚C

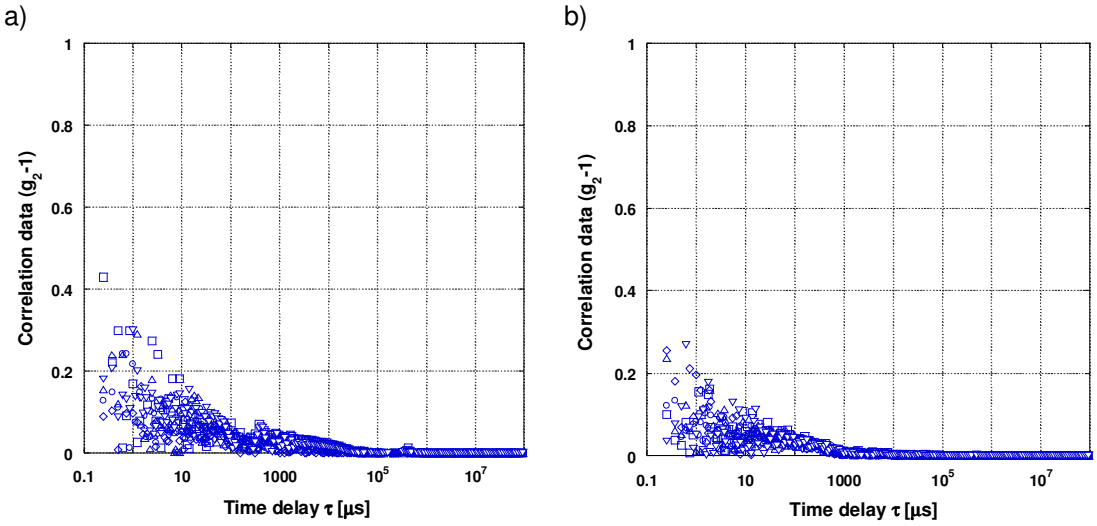

Figure 8.9 Light scattering autocorrelation functions g_2-*1*, solvent – **deuterium oxide (D_2O),** COOLING CRYSTALLISATION, a) 45˚C, b) 25˚C.

The size of clusters and liquid nanodroplets were calculated as in the previous experiments by separate fitting of two exponential decay parts of the autocorrelation functions $ln(g_1)$, see Experimental Techniques chapter for more details. The viscosity of hydrogen oxide and deuterium oxide at different temperatures were taken from work of Cho ***(Cho et al. 1999).*** The results show that the size of clusters and droplets increased with glycine concentration in the crystallising samples. This difference is larger in the case of the clusters than the droplets. The deuterated solvent does not change the hydrodynamic diameter of clusters however the droplets formed from deuterium oxide solution are larger compared to droplets detected in aqueous solution. The hydrodynamic diameter of clusters and droplets calculated by first and second order fitting of autocorrelation function $ln(g_1)$ at different temperatures show Tables 8.1 -8.3.

Table 8.1 Mean clusters and droplets diameter at glycine concentration **230mg/ml**, **COOLING CRYSTALLISATION** from H_2O solution.

Temperature [°C]	**GLYCINE CONCENTRATION, C_{Gly} =230mg/ml – H_2O**			
	Hydrodynamic **CLUSTERS** diameter [nm]		Hydrodynamic **DROPLETS** diameter [nm]	
	1-st order fit	**2-nd order fit**	**1-st order fit**	**2-nd order fit**
50	**1.7** (±1.1)	**1.7** (±0.6)	**228** (±22)	**304** (±141)
40	**2.3** (±0.8)	**1.0** (±0.5)	**220** (±98)	**232** (±107)
30	**1.9** (±0.6)	**1.2** (±0.6)	**229**(±47)	**203** (±114)
25	**2.2** (±0.6)	**1.0** (±0.5)	**237** (±32)	**240** (±81)
20	**1.8** (±0.5)	**1.0** (±0.5)	**224** (±28)	**243** (±80)
15	**1.7** (±0.5)	**1.1** (±0.5)	**232** (±30)	**272** (±99)

Table 8.2 Mean clusters and droplets diameter of glycine concentration **270mg/ml**, **COOLING CRYSTALLISATION** from H_2O solution.

Temperature [°C]	**GLYCINE CONCENTRATION, C_{Gly} =270mg/ml – H_2O**			
	Hydrodynamic **CLUSTERS** diameter [nm]		Hydrodynamic **DROPLETS** diameter [nm]	
	1-st order fit	**2-nd order fit**	**1-st order fit**	**2-nd order fit**
40	**9.5** (±2.1)	**5.5** (±1.1)	**390** (±13)	**423** (±38)
35	**8.9** (±1.7)	**5.6** (±1.0)	**354** (±13)	**370** (±22)
30	**8.1** (±1.7)	**5.2** (±0.9)	**323** (±14)	**348** (±28)
25	**7.4** (±1.8)	**5.4** (±0.8)	**322** (±10)	**328** (±15)
20	**6.5** (±0.9)	**4.3** (±0.6)	**277** (±5)	**292** (±9)
15	**4.4** (±1.4)	**3.3** (±0.8)	**248** (±12)	**246** (±25)

Table 8.3 Mean clusters and droplets diameter of glycine concentration **270mg/ml**, **COOLING CRYSTALLISATION** from deuterated D_2O solution.

Temperature [°C]	**GLYCINE CONCENTRATION, C_{Gly} =270mg/ml – D_2O**			
	Hydrodynamic **CLUSTERS** diameter [nm]		Hydrodynamic **DROPLETS** diameter [nm]	
	1-st order fit	**2-nd order fit**	**1-st order fit**	**2-nd order fit**
55	**5.8** (±1.6)	**3.4** (±1.4)	**337** (±37)	**316** (±98)
50	**10.4** (±2.4)	**5.6** (±1.4)	**503** (±15)	**495** (±33)
45	**9.1** (±5.9)	**3.9** (±1.0)	**514** (±28)	**469** (±45)
30	**9.5** (±2.0)	**5.1** (±1.3)	**488** (±10)	**431** (±12)
25	**8.5** (±4.8)	**4.1** (±2.7)	**424** (±24)	**375** (±36)
20	**6.4** (±2.9)	**3.5** (±1.8)	**385** (±24)	**288** (±34)

The hydrodynamic diameters of molecular clusters and droplets as a function of temperature for different glycine concentrations in crystallising solutions (230mg/ml and 270mg/ml) and two different solvents (hydrogen oxide and deuterium oxide) are plotted in Figure 8.10. The graphs show clearly that the glycine concentration has a big impact on the size of molecular clusters and liquid droplets. With decreasing temperature the hydrodynamic diameter of the nanospecies decreases. Using deuterium oxide instead of hydrogen oxide does not affect cluster size however larger droplets are formed.

a) b)

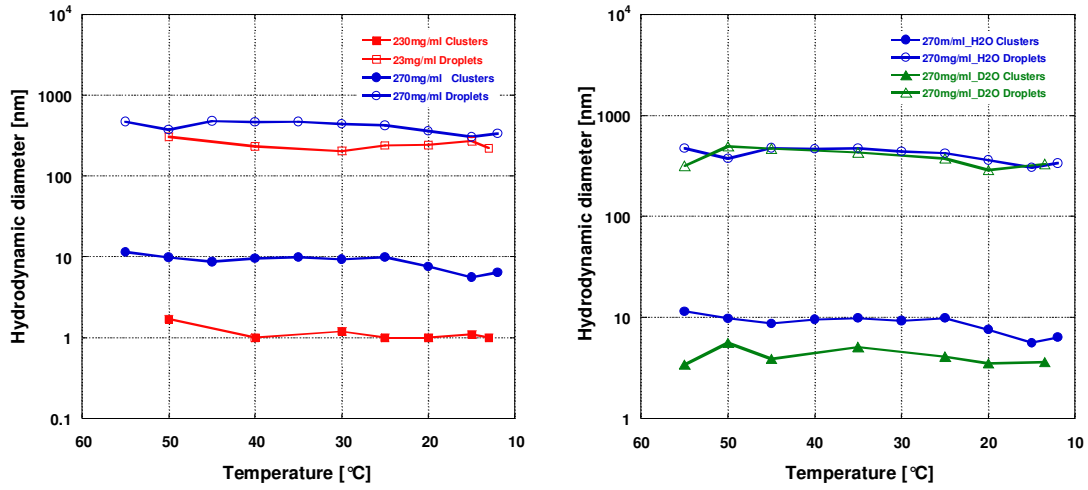

Figure 8.10 Average hydrodynamic diameters of clusters and droplets as a function of temperature, **COOLING CRYSTALLISATION**, **second order fit**, a) solvent - water (H_2O) C_{Gly} =230mg/ml and 270mg/ml, b) C_{Gly} =270mg/ml, solvent -deuterium oxide (D_2O).

The cluster and droplet size distribution diagrams calculated at 25℃ (supersaturated conditions) are plotted in Figure 8.11. The data shows a narrow size distribution of droplets for high and low glycine concentration samples, and larger droplets are presented in the deuterated crystallising solution. The cluster distributions for the same concentration solutions but different solvents (natural and deuterated) are very similar (Figure 8.11b). The size distribution of clusters for two glycine concentrations 230mg/ml and 270mg/ml have a completely different range. Larger clusters appear to be formed in samples of higher glycine concentration but this could be influenced by decay from droplets, and real the size may be much smaller (see Experimental Techniques Chapter).

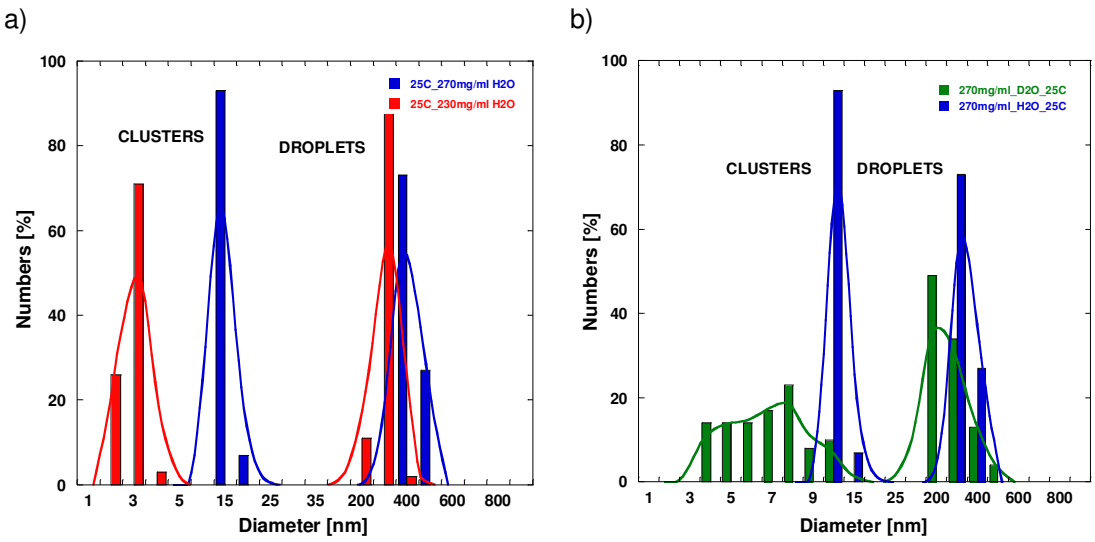

Figure 8.11 Nanodispersions estimated size distribution at 25°C, **COOLING CRYSTALLISATION, second order fit**, a) solvent - water (H_2O) C_{Gly} =230mg/ml and 270mg/ml, b) C_{Gly} =270mg/ml, solvent -deuterium oxide (D_2O).

As mentioned before in the experimental techniques chapter, the particle size in DLS is calculated on the basis of the scattering intensity signal which is proportional to the second power of particle mass. So, DLS technique can monitor even a very small population of larger clusters, whereas different analytical techniques such as PFG or DOSY in which the results are obtained on the basis of particle number will not show the presence of a small population of larger particles in the value of the average diffusion coefficient measurement.

8.4 Scanning Electron Microscopy (SEM)

For checking the structure of the final glycine microcrystal morphology Scanning Electron Microscopy was used. All SEM samples were prepared by cooling crystallisation of natural and deuterated aqueous solution of glycine from 55℃ to 23°, samples were filtered after being kept at 23℃ for two days. The pictures of glycine crystals crystallised form aqueous solution and deuterated solution show Figure 8.12a and 8.12b respectively.

The glycine crystals obtained from natural aqueous solution are more compact and mostly formed α-glycine polymoph. However, a few long needles β-glycine polymorph were formed, probably due to some shaking which induced β-polymoph formation ***(Mahajan and Kirwan 1993; Mahajan and Kirwan 1994).*** The glycine crystals obtained from deuterated aqueous solution appear to be less compact, and with rough surfaces like mesocrystals. A large number of small spherical crystals or amorphous particles were also formed as well as small, short needles crystals (β-glycine).

a) b)

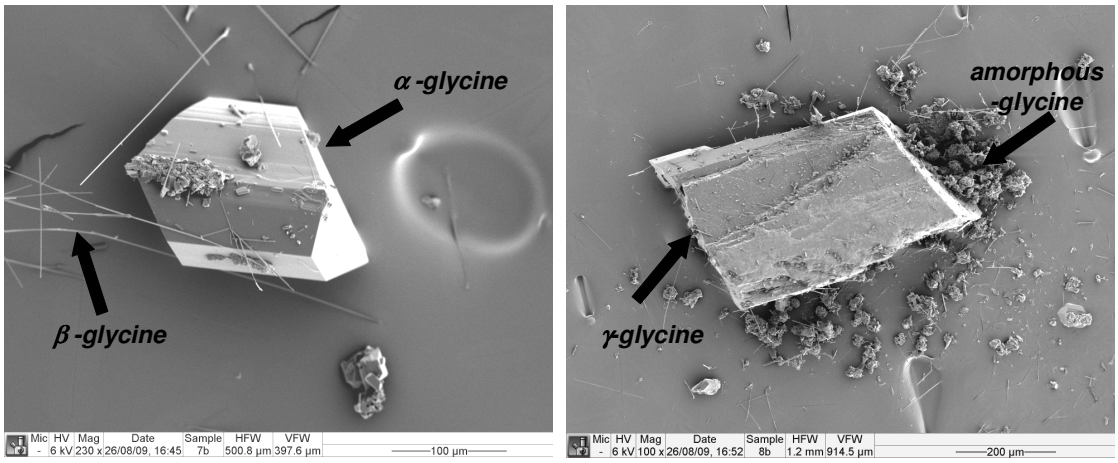

Figure 8.12 SEM pictures of glycine microcrystals, **COOLING CRYSTALLISATION**, **C_{Gly} = 270mg/ml**, crystallised from a) natural aqueous solution (H_2O), b) deuterated aqueous solution (D_2O).

In this study nuclear magnetic resonance (NMR), diffusion ordered spectroscopy (DOSY) and dynamic light scattering (DLS) were used for monitoring the formation of glycine microcrystals from supersaturated aqueous solution during cooling crystallisation process. The results revealed the formation of intermediate species (solute-rich liquid nanodroplets) with the size depends on sample supersaturation.

9. CONCLUSIONS.

The aim of thesis was to investigate the nucleation mechanism of crystal formation during antisolvent or cooling crystallisation of simple organic molecules (D,L-valine and glycine).

The antisolvent crystallisation process of the amino acid D,L-valine from 2-propanol/water solutions was monitored using a number of complementary techniques, such as spectrophotometry, nuclear magnetic resonance (NMR) and dynamic light scattering (DLS), has revealed the presence of a non-classical crystallisation pathway. The nucleation mechanism of anitisolvent crystallisation was found to involve formation of sub-micron valine-rich liquid nanodroplets.

A proposed phase diagram for valine in mixed solvent systems is illustrated schematically in Figure 9.1. The diagram has some features commonly associated with a simple lyotropic liquid crystal. Passing along the dotted horizontal line a-b, at lower concentrations (left) valine is present as a fully homogeneous molecular solution. A critical aggregation concentration is then reached at point (1). Above this point the lowest energy state for the valine/water/2-propanol mixtures is a dispersion of valine-rich nanodroplets suspended within the valine solution. As more valine is added, this inhomogeneous state of matter remains the most thermodynamically stable until an upper composition limit is reached at point (2). If the inhomogeneous distribution of valine was not recognised, this would be simply identified as the molecular solubility limit. Actually, it is the composition above which any additional valine will be thermodynamically more stable in the crystalline phase than in dispersed valine-rich-nanodroplets. It could also be pictured as corresponding to the maximum volume fraction of the valine-rich liquid phase that can be stably dispersed as nanodroplets within the molecular valine solution. As further valine is added, more nanodroplets will be produced but these will be metastable relative to conversion to the crystalline state (3). If there were no kinetic barriers, valine crystals would indeed be expected to directly precipitate from this valine-rich liquid phase. Similarly, if excess valine crystals were dissolved in a valine solution of concentration (1), nanodroplets should be observed.

Direct evidence for the later situation was obtained in the DLS experiments, in which stable nanodroplets were observed to coexist with valine crystals during cooling-heating and valine crystals dissolving experiments. In the 12 hour cooling experiment the stable nanodroplets were observed coexisting with valine crystals after 10 hours of equilibration at 12°C. It could

be argued that this was because the crystallisation kinetics for this system was very slow, so the process did not reach complete equilibrium, and observed nanodroplets were metastable. However, additional experiments with valine crystals immersed in slightly undersaturated valine/water/2-propanol filtered solution at 25°C and subsequent heating to 35°C (where crystals were still present) were also carried out. The nanodroplets appeared in such solution after 24 hours while keeping the samples at 25°C and there is no other way those could form but by dissolving of valine crystals. DLS measurements showed a stronger signal when samples were heated up to 35°C or after gentle shaking of the samples. This is presumably due to nanodroplets formation and accumulation at the crystals surface which is the most faveourable place for them to stay. They can then only be removed from the crystals and transported into the DLS laser beam by a very slow diffusion process. Because stable liquid nanodroplets have size of hundreds of nanometers, this is a very slow process. The heating or gentle shaking helps to disperse the stable nanodroplets throughout the solution. This experiment gives direct evidence of existence liquid nanodroplets.

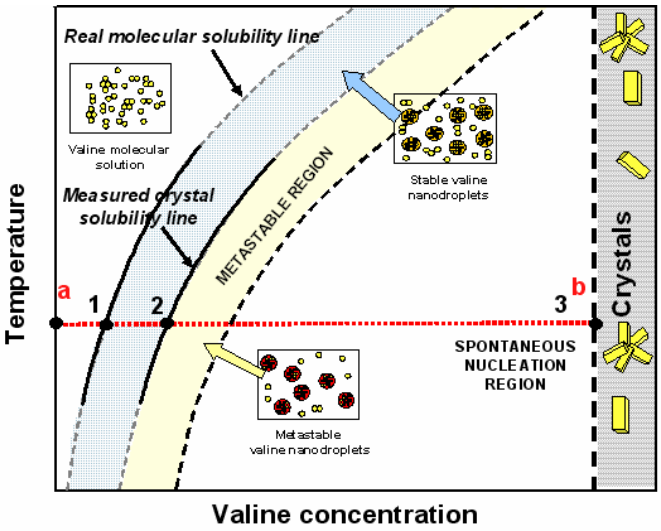

Figure 9.1 Phase diagram of three component system D,L-valine/2-proanol/water.

With this insight into the phase behaviour of valine solutions in place, it becomes straightforward to understand why the rate of crystallisation is affected by the intensity of mixing. Since valine-rich nanodroplets are spontaneously generated as a stable phase below the saturation limit, they will always constitute a metastable phase in a supersaturated valine solution, however this is produced. Application of intense mixing leads to shear, induced coalescence, as was observed by DLS for the magnetically stirred and, in particular, the

vortexed solutions. The longer the mixing is applied for, the greater the degree of coalescence. Once nanodroplets reach a critical size, in the range 700-1200nm, they become key intermediates on the rapid crystallisation pathway. Hence, the more of them are initially formed, the greater the number of microcrystals produced. This behaviour was observed by spectrophotometry and NMR with the vortexed samples, generating significantly more crystals than stirred samples. The critical liquid nanodroplet size probably depends on the solvent ratio in the supersaturated solutions as well as on the solute nature.

Figure 9.2 shows pictorial interpretation of crystal nucleation and growth process samples prepared using vortexer and magnetic mixer. The samples prepared using vortexer contained more droplets above the critical size which then crystallised and consumed more valine during crystal growth process, as was detected using NMR.

The large number of nucleated crystals produced more turbid solutions, which gave stronger spectrophotometry signal and finally more valine microscrystals are produced (SEM).

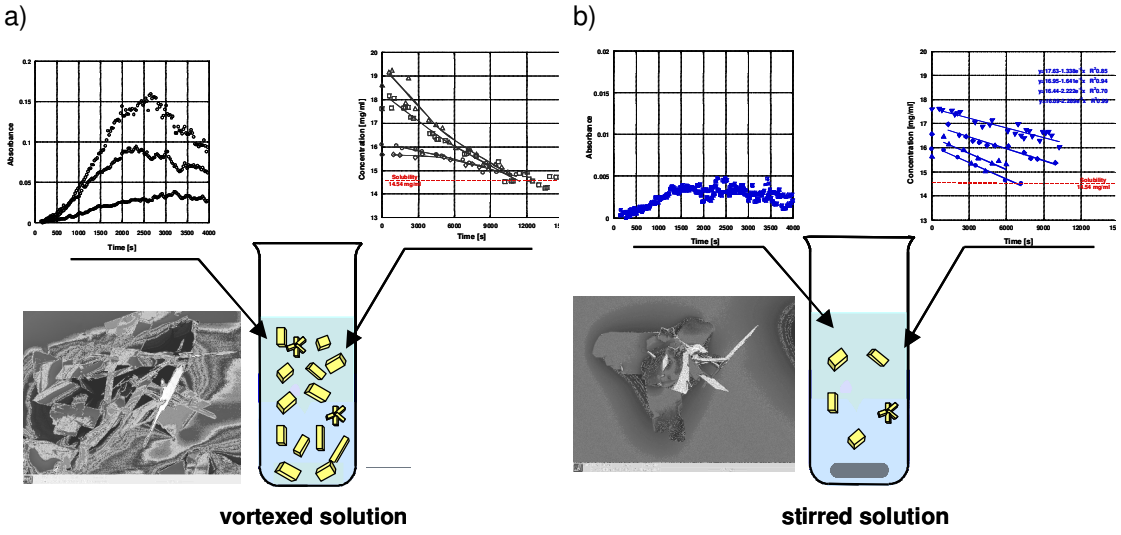

Figure 9.2 Effect of mixing on two steps crystallisation process of valine from 2-propanol/water solution, a) vortexing and b) magnetic mixer stirring

On the other hand, magnetic stirring produced a smaller number of droplets above the critical size and this able to nucleate crystals (assuming the same crystal growth rate as in the vortexed samples). Less valine was consumed during the same processing time. As was clearly seen using NMR spectroscopy the transfer of valine molecules from solution into crystals is determined by the number of crystal forming nanodroplets. Stirred samples, even with higher supersaturation, how it was shown does not have simple as many nanodroplets above the critical size which can form crystals and the rate of crystal formation becomes constant or even decreases with supersaturation. The stirred samples are less turbid, as was

detected by spectrophotometry, and a smaller number of larger valine microcrystals are formed. However, both of these types of mixing showed similar induction times values, which is defined as the time when the first visible crystals are detected in solutions. The induction times for these samples were not very different, but the number of detected crystals was larger in vortexed than in stirred samples.

The continuous process of antisolvent crystallisation of D,L-valine was investigated using the Confined Impinging Jet CIJ mixer. The CIJ mixer is designed to achieve the rapid micromixing of two liquid streams which promote the crystal nucleation process in highly supersaturated solutions. In a fast precipitation process rapid mixing is required in a time less than the nucleation and growth time of nanoparticles in order to produce small final particles size with a narrow size distribution.

In our study we did not work with high supersaturations of solute and the crystal formation kinetics was not very rapid. However, as is already known from our batch crystallisation experiments, the mixing conditions have a large influence on nucleation, crystal growth kinetics and final microcrystal size even in low supersaturation systems, where liquid-liquid phase separation occurs. DLS measurements of supersaturated valine solutions produced using the CIJ mixer revealed quite narrow liquid nanodroplet size distribution with an average diameter between 300nm and 500nm. As has been discussed above, the nanodroplets presumably need to reach a certain critical size before crystal nucleation occurs which is in the range 700-1200nm for a solvent ratio of 2-propanol/water equal to 1:1.

The nanodroplets prepared by micromixing are mostly below that size range and compared to batch systems they are between those in vortexed and stirred samples. However, the CIJ mixed samples gave stronger DLS signals, which could indicate that a larger number of nanodroplets were formed.

The induction times of CIJ mixed samples were extended especially for higher valine concentration solutions (C_{Val}=18mg/ml) which made it possible for longer DLS monitoring of crystallising samples. The larger number of final valine microcrystals formed compared to stirred samples, indicate that more liquid nanodroplets above critical size were produced using CIJ mixing.

9.1 Cooling crystallisation of D,L-valine

In supersaturated solutions prepared by cooling, the metastable nanodroplets formed were all in the range of 100-300nm. Crystallisation occurred from these solutions, but induction times were around 500 times longer than for vortexed samples and only a small number of large crystals were produced. Throughout this crystallisation process nanodroplets were always present, consistent with them forming a stable phase in equilibrium with the crystals. No direct evidence was obtained for the involvement of nanodroplets in the crystallisation process but it would appear likely that nucleation would take place from the valine-rich phase. Possibly adsorption of nanodroplets onto the vial surface provides an alternate albeit slower coalescence pathway which then triggers crystal nucleation and growth. This could be consistent with the finding that the valine crystals in cooled solutions are often found bound to the side of the vial. Figure 9.3 provides a pictorial summary of the proposed rapid homogeneous and slow heterogeneous crystallisation pathways.

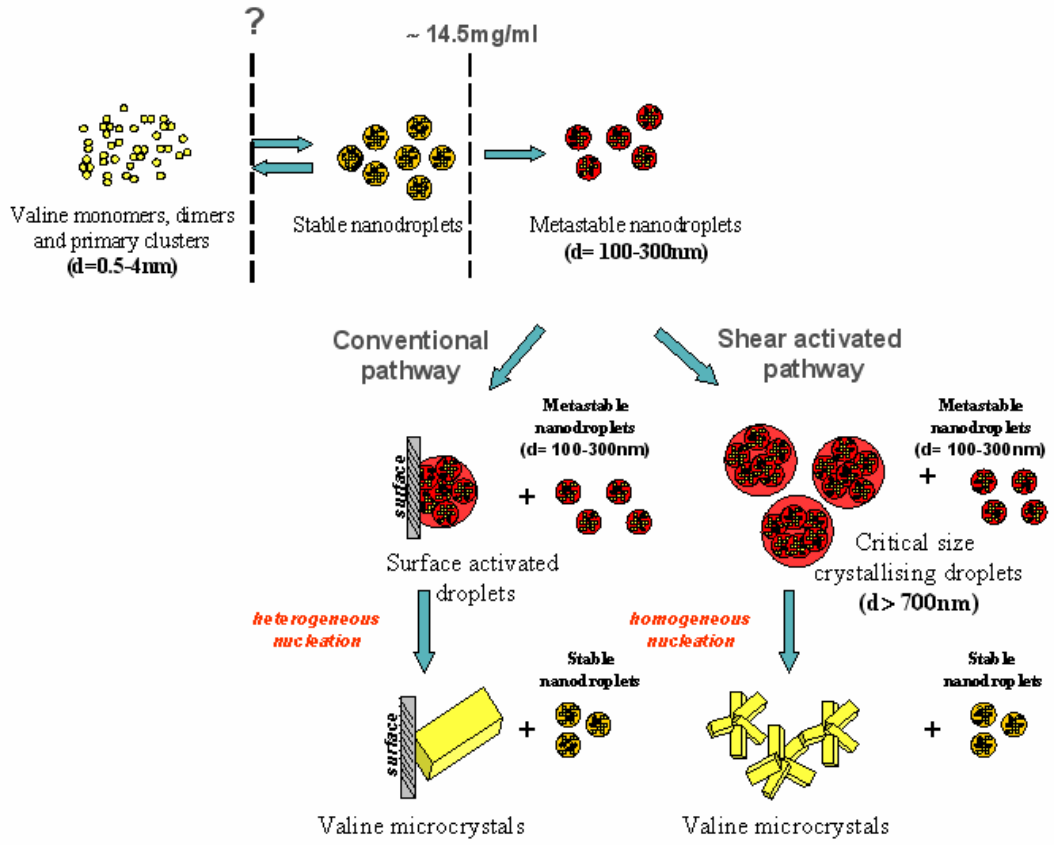

Figure 9.3 Proposed two-steps pathway of antisolvent crystallisation of amino acid (valine) via primary liquid droplets formation: homogeneous and heterogeneous nucleation.

Because it has not yet been possible to determine the composition of the valine-rich nanodroplets, it is not yet clear why they need to be coalesced to above critical size before the onset of rapid crystallisation. Borrowing from the classical theory, it can be speculated that smaller droplets may not actually contain sufficient valine to be able to form stable crystals. This could certainly be the case if the nanodroplets contain a significant volume fraction of solvent so that any crystals produced were only tens of nanometers in size. The observed critical nanodroplet size would then correspond to the volume which contains just sufficient valine to be able to form a stable growing crystal. In this model it can be imagined that valine-rich nanodroplets of all sizes intermittently sample the crystalline phase and most commonly simply reform and go back to the liquid phase. An opposite line of argument would be that the probability of a nucleation event occurring within smaller nanodroplets will be almost negligible. Only once a critical volume has been reached will nucleation be feasible. Possibly both arguments have some validity so that these effects may reinforce each other. A rapid cross-over from metastable nanodroplets to crystal inducing nanodroplets may then occur as both the critical mass of valine is reached and nucleation becomes increasingly likely.

It is of course tempting to speculate that other solute systems might exhibit similar phase behaviour. Certainly, because the nanodroplets are not visible to the naked eye, it would be easy to miss them. As shown here, very careful DLS studies are required that avoid all filtration of solutions except under highly undersaturated conditions. This is clearly much easier to achieve in a mixed solvent system where the two composites can be filtered separately. In the valine system investigated here, stable nanodroplets formed over a fairly wide concentration range and consequently provided a strong DLS signal. It is easy to imagine that in other systems the corresponding stable solute-rich liquid phase might only form over a more narrow concentration range. This could make it much more difficult to observe experimentally. However, the possibility that other crystallising systems pass through an intermediate phase of thermodynamically stable, solute-rich, nanodroplets presents a paradigm shift that clearly deserves further investigation. In this regard it is interesting to note that preliminary experiments have shown that similar nanodroplet phases also exist for two other amino-acids, glycine and histidine.

9.2 Cooling crystallisation of glycine

In this study diffusion ordered spectroscopy (DOSY) and dynamic light scattering (DLS) were used for monitoring the formation of glycine microcrystals from supersaturated aqueous solution during cooling crystallisation process.

The presence of glycine molecular clusters in under- and supersaturated aqueous solutions of glycine was previously widely reported ***(Chattopadhyay et al. 2005; Erdemir et al. 2007)***. The authors reported that glycine in under-and supersaturated solution exsist mostly as small molecular clusters (dimers, trimers). Other scientists ***(Hamad et al. 2008; Huang et al. 2008)*** concluded that glycine exsits mostly as a monomer in such solutions and only small populations of clusters were found. Our DLS and DOSY results revealed some population of glycine molecular clusters in crystallising solutions, but the accurate size and fraction of the clusters can not be accurately determined from those experiments.

The most interesting result was the presence of the second population of larger liquid-based species found to be present in supersaturated as well as in undersaturated solutions. Average diameter of these liquid nanodroplets was around 200-500nm and was found to depend on glycine concentration in samples.

Previously published Small Angle X-ray Scattering data for the same cooling crystallisation system clearly shows that some species larger than a few nanometers are present in the crystallising solutions. The data corresponding to larger particles actually was not properly fitted (increasing shoulder for values of q below $q \cong 3 Å^{-1}$) and the authors instead concentrated only on small glycine molecular clusters formation (Figure 9.4)***(Chattopadhyay et al. 2005)***. SAXS results at low q values are consistent with the glycine liquid-nanodroplets which were clearly seen using DLS.

The liquid nanodroplet formation process in three component systems (D,L-valine (glycine, histidine)/2-propanol/water) seems to be easier to explain and understand then that in two component solutions (glycine/water). The key for understanding this phenomena could be that glycine in aqueous solution existes in two forms: $CH_2(NH_2)(COOH)$ and $CH_2(NH_3)^+(COO)^-$ (zwitterions). The isoelectric point (IEP) of glycine is 5.97 and is defined as the pH of an aqueous solution of an amino acid at which the molecules on average have no net charge. In other words, the positively charged groups are exactly balanced by the negatively charged groups. The presence of $CH_2(NH_2)(COOH)$ and $CH_2(NH_3)^+(COO)^-$ forms in solution could assist liquid-liquid separation which leads to liquid-nanodroplets formation.

The glycine cooling experiments were done with undisturbed cooled samples and mixing effects on the crystallisation process has not been tested. In non-mixed samples large glycine crystals were formed after 2days, similar to valine cooling experiments.

10. FURTHER WORK.

Although promising progress has been done, there remains, as ever, planty more research to undertake. The following points are suggested as being crucial to the further understanding of the nucleation mechanism of amino acids and small molecules.

1. Further study of stable solute-rich liquid nanodroplets in undersaturated and supersaturated solutions of D,L-valine using DLS, SLS and NMR to constract a more precise phase diagram of valine-2-propanol-water system.

2. Investigation the composition and role of the valine-rich stable liquid phase in crystals nucleation using microanalitical techniques.

3. XRD and mass spectroscopy study of the valine (rhombohedral-shaped plates and needle-like crystals) and glycine (needle-like and spherical) crystals to obtain exact microcrystals structure and composition.

4. Study of nucleation mechanism of different amino acids (e.g. tryptophan, phenyloalanine, tyrosine) using DLS, NMR and fluorescence spectroscopy.

5. Further investigation of liquid stable nanodroplets in undersaturated and supersaturated aqueous solution of glycine using small angle X-ray scattering, which is able to give information about size, structure and interaction of nanomolecules.

6. Study of the liquid phase composition and nucleation mechanism of crystals formation during antisolvent and cooling crystallisation prepared using different antisolvents (more and less polar).

7. Further study of mixing influence on nucleation mechanism of amino acids and different small molecules.

11. APPENDIX.

11.1 Induction times, 2-propanol/water, 1:1, v/v

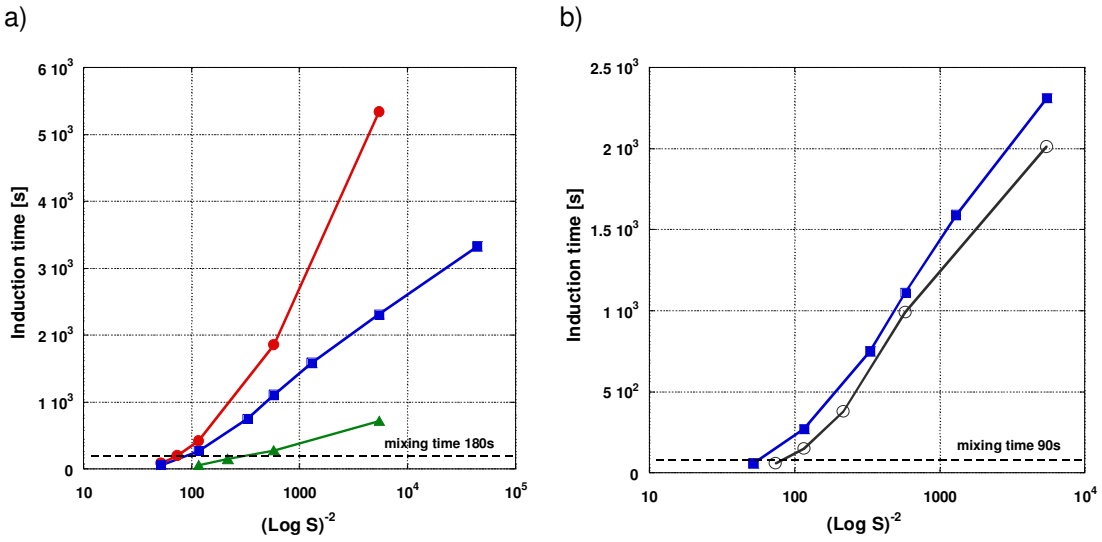

Figure 11.1 Plot of induction times t_{ind} as a function of initial supersaturation $\log(S)^{-2}$ for D,L-valine: a) **magnetic mixer**, mixing time: 60s (red circles), 90s (blue squares), 180s (green triangles), b) **mixing time 90s**, magnetic mixer (blue squares), vortexer (opened black circles), 2-propanol/water, 1:1, v/v.

11.2 Autocorrelation function – undersaturated solution -9mg/ml

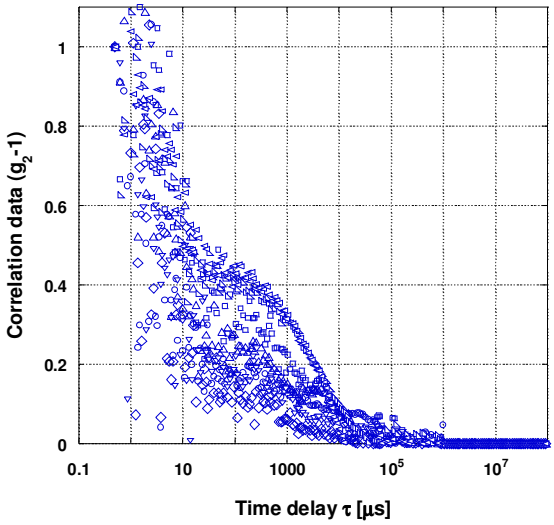

Figure 11.2 Autocorrelation function g_2-*1*, C_{Val} **=9mg/ml**, undersaturated solution, 2-propanol/water, 1:1, v/v.

11.3 Hydrodynamic diameters clusters-droplets vs D,L-valine concentration

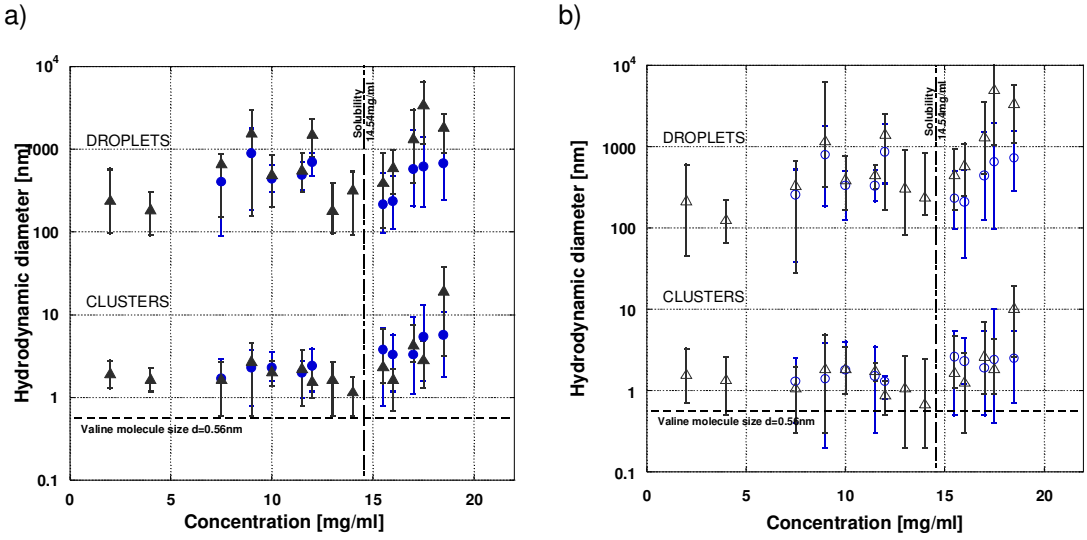

Figure 11.3 Nanoprecursors (clusters and droplets) hydrodynamic diameter as a function of valine concentration with size distribution, blue symbols - magnetic mixer 90s, black symbols - vortexer 90s, a) **first order fit**, b) **second order fit**, 2-propanol/water, 1:1, v/v.

11.4 Clusters – droplets size distribution

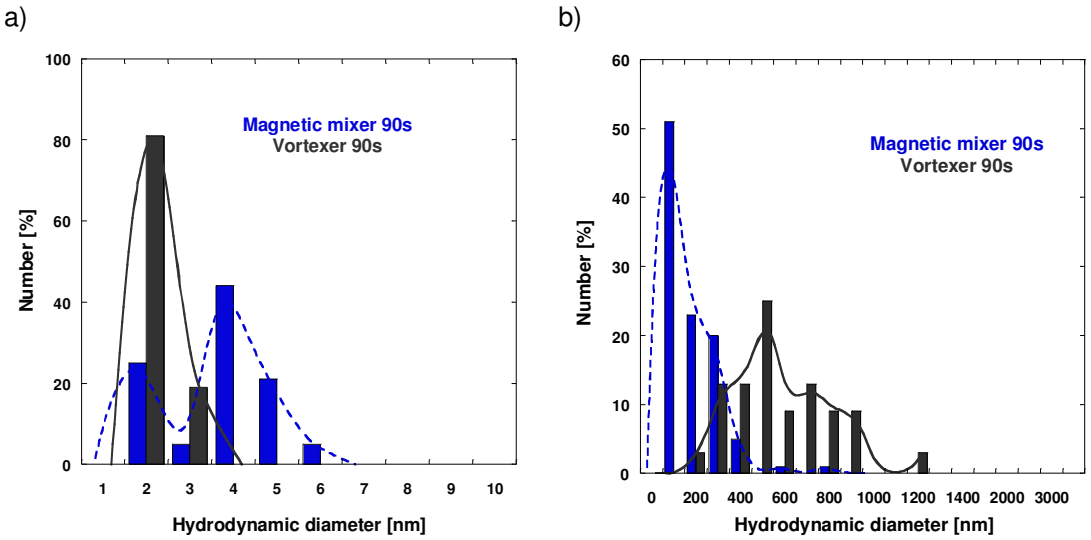

Figure 11.4 Nanodispersions estimated size distribution, **C $_{Val}$=16mg/ml**, 2-propanol/water, 1:1, v/v, **first order fit** a) CLUSTERS, b) DROPLETS.

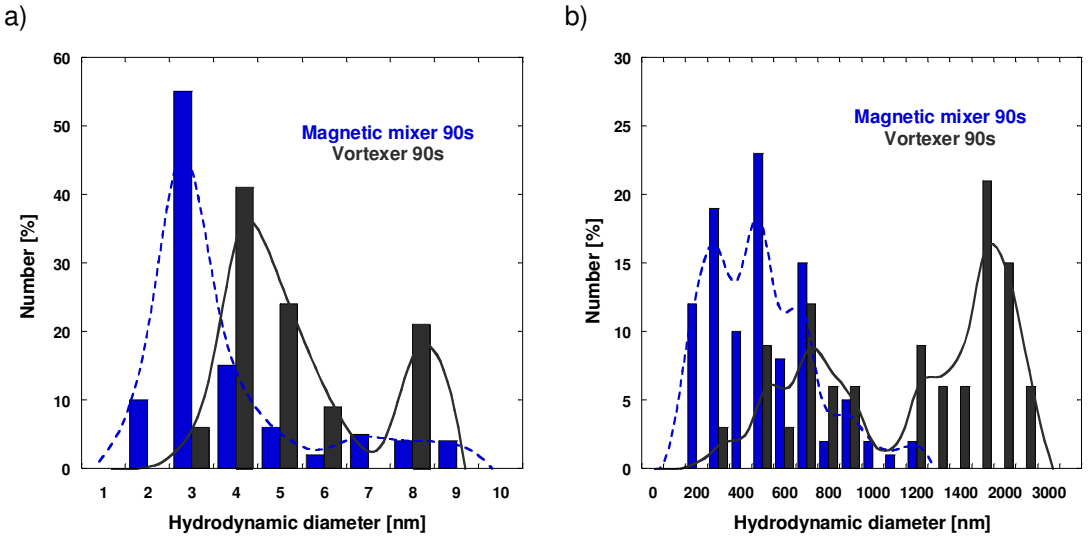

Figure 11.5 Nanodispersions estimated size distribution, **C $_{Val}$=17mg/ml**, 2-propanol/water, 1:1, v/v, **first order fit** a) CLUSTERS, b) DROPLETS.

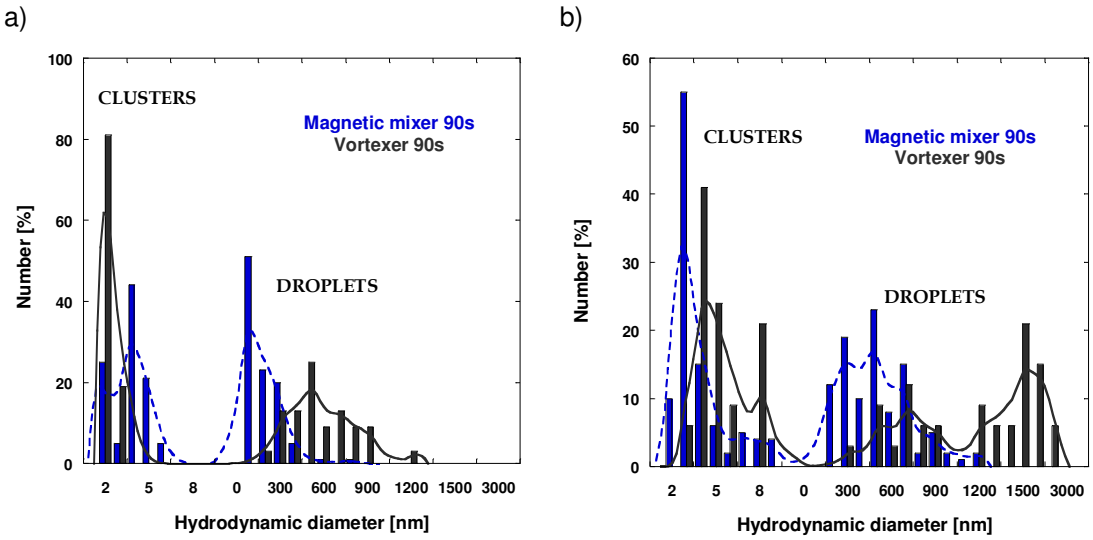

Figure 11.6 Nanodispersions estimated size distribution, 2-propanol/water, 1:1, v/v, **first order fit** a) 16mg/ml, b) 17mg/ml.

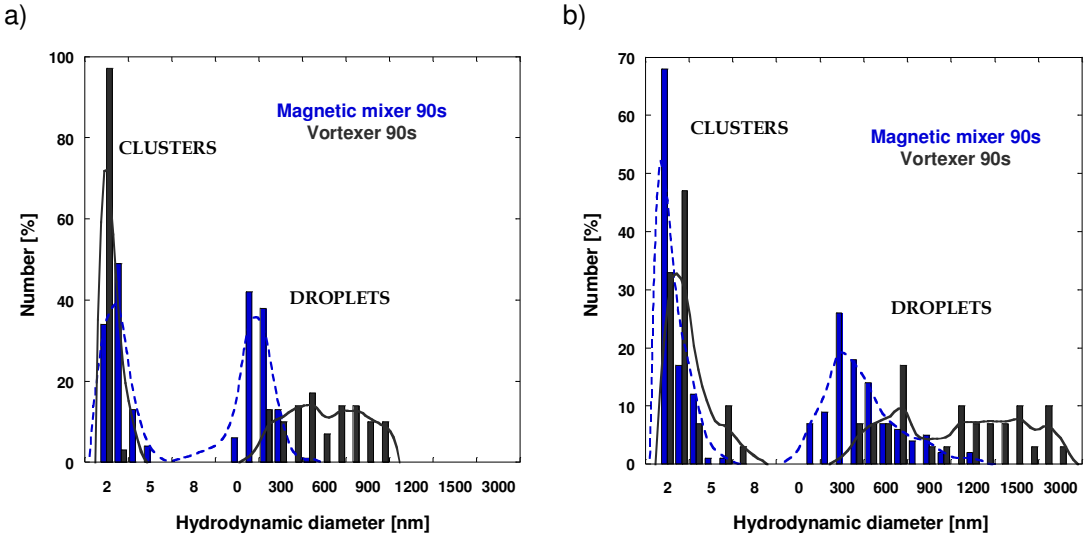

Figure 11.7 Nanodispersions estimated size distribution, 2-propanol/water, 1:1, v/v, **second order fit** a) 16mg/ml, b) 17mg/ml.

11.5 SEM pictures of D,L-valine microcrystals surface

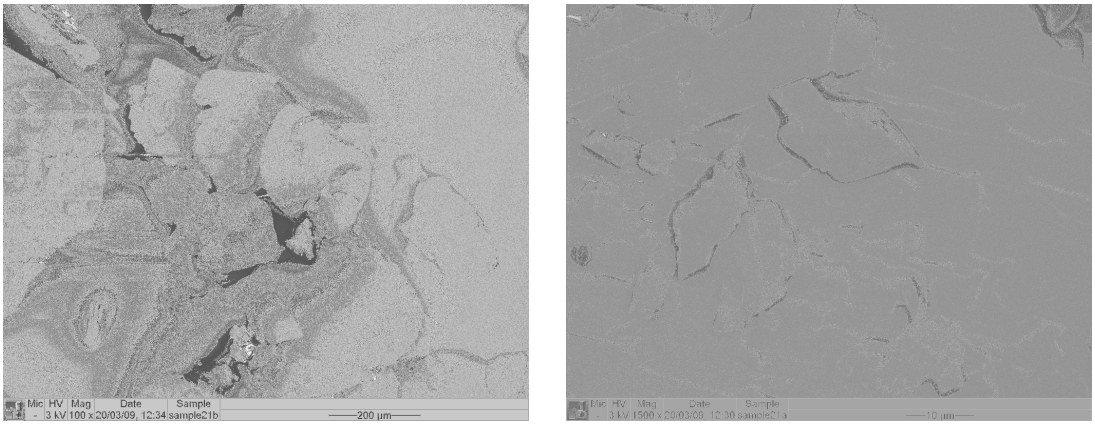

Figure 11.8 SEM images of the surface of D,L-valine microcrystals prepared by dissolving excess of valine in 2-propanol/water, 1:1, v/v solvents.

11.6 COOLING CRYSTALLISATION – 2propanol/water, 1:1, v/v

11.6.1 19 mg/ml, 2-propanol/water, 1:1, v/v, cooling crystallisation

a)

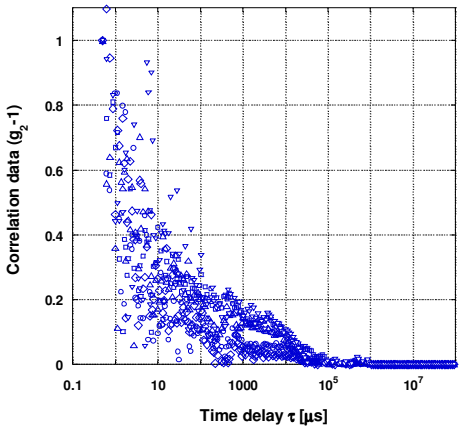

b)

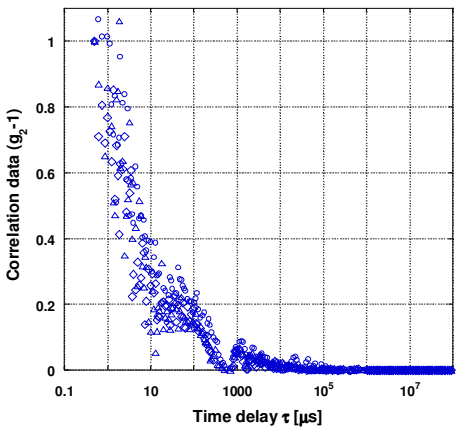

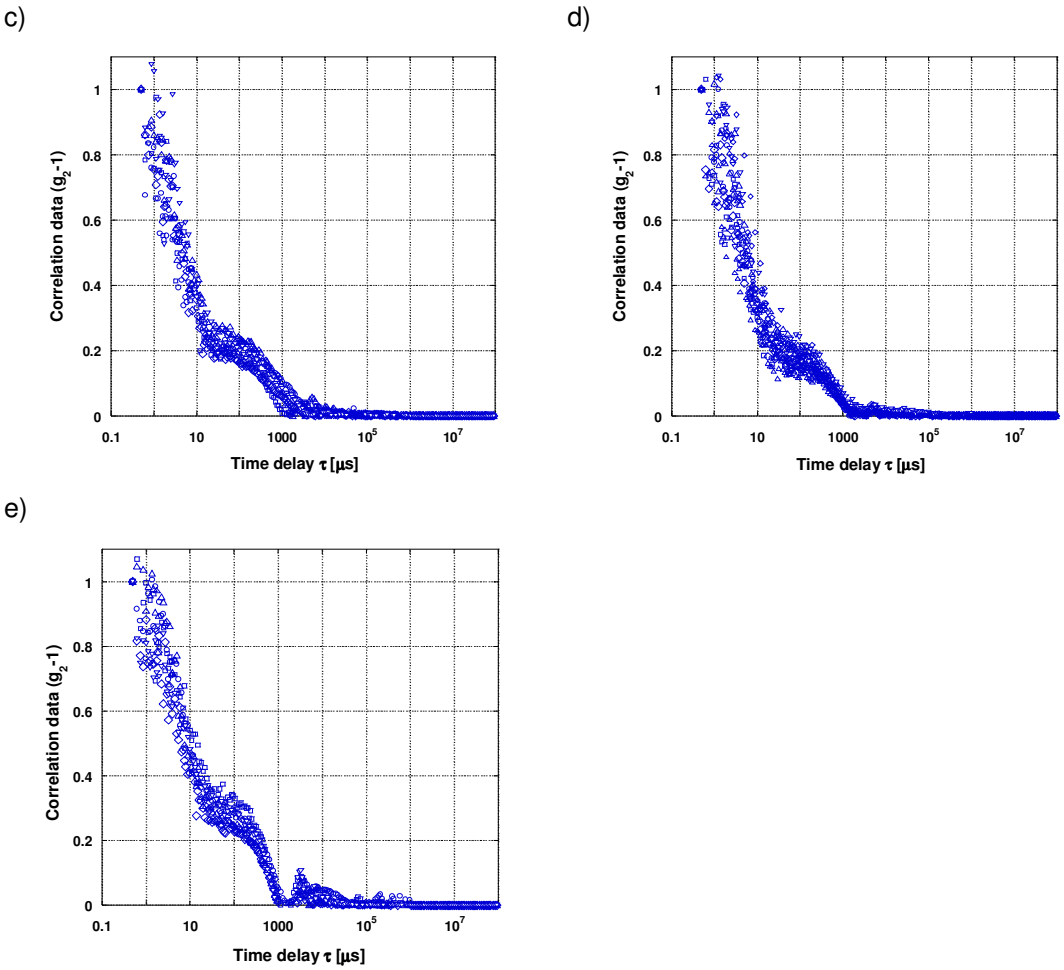

Figure 11.9 Light scattering autocorrelation functions g_2-*1*, C_{Val} **=19mg/ml**, **COOLING CRYSTALLISATION**,a) 50°C, b) 35°C, c) 30°C, d) 25°C, e) 20°C, 2-propanol/water, 1:1, v/v.

11.6.2 25 mg/ml, 2-propanol/water, 1:1, v/v, cooling crystallisation

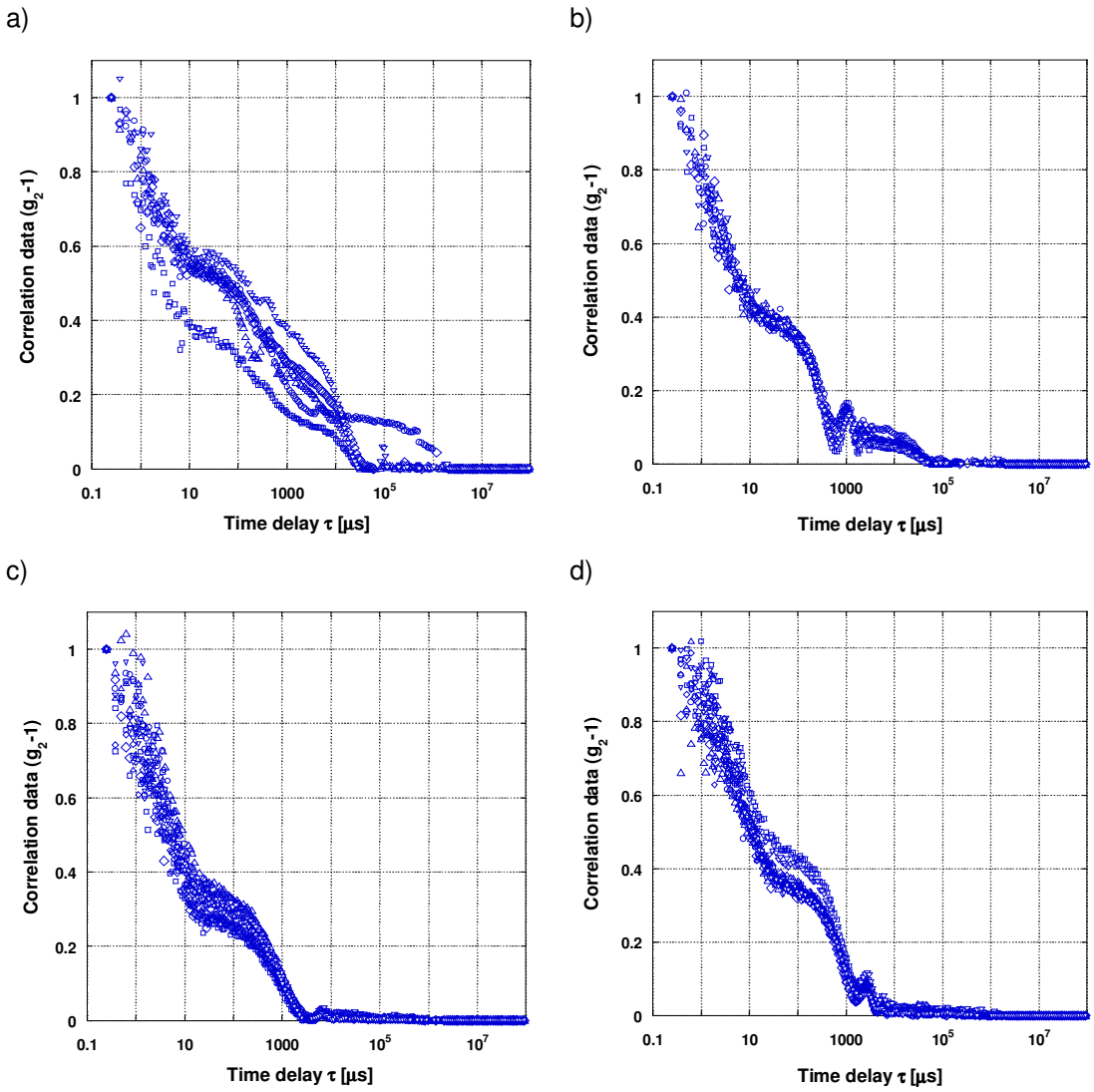

Figure 11.10 Light scattering autocorrelation functions g_2-*1*, C_{Val} **=25mg/ml**, **COOLING CRYSTALLISATION**, a)50˚C, b) 35˚C, c) 25˚C, d) 15˚C, 2-propanol/water, 1:1, v/v.

11.6.3 27 mg/ml, 2-propanol/water, 1:1, v/v, cooling crystallisation

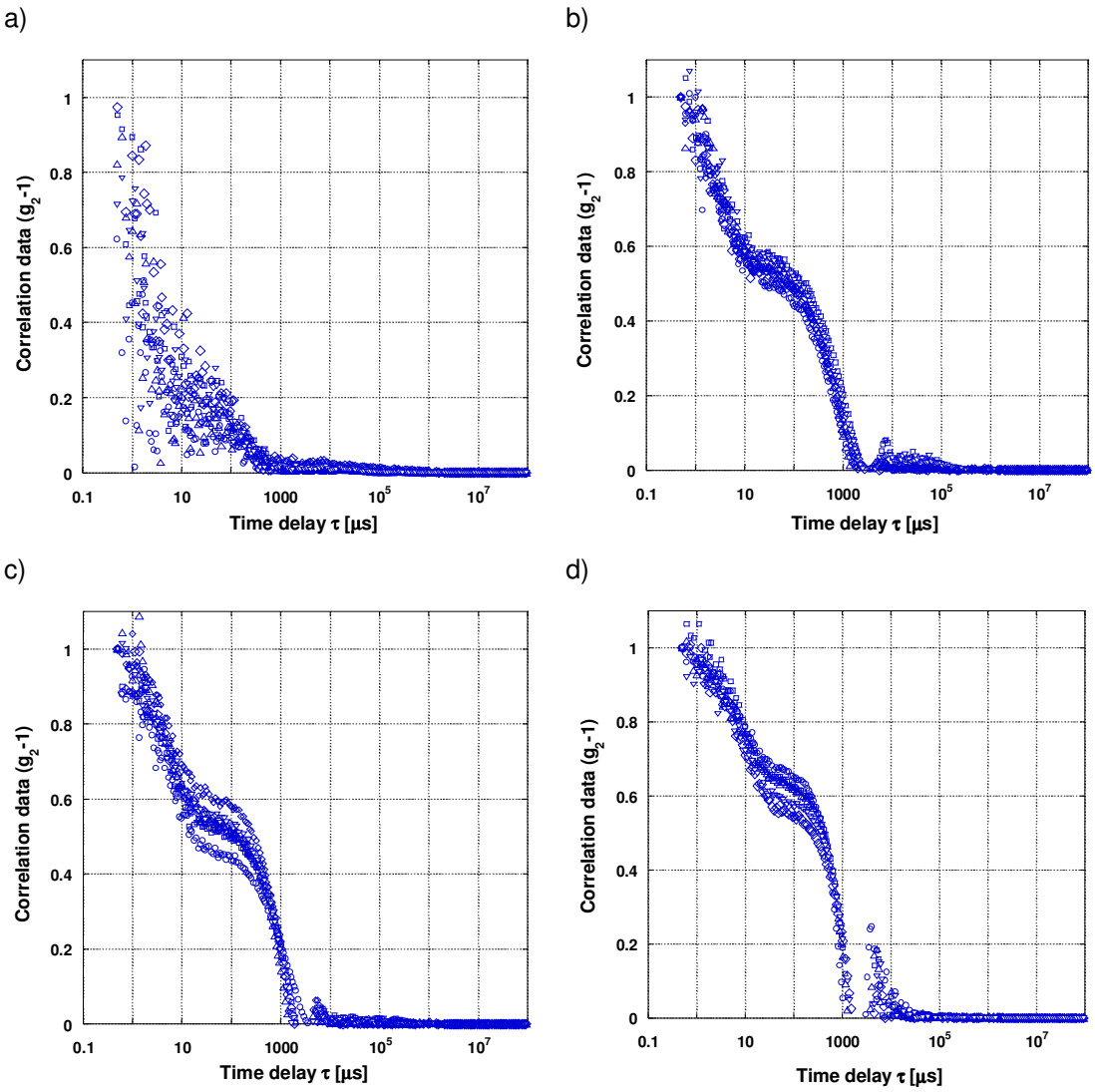

Figure 11.11 Light scattering autocorrelation functions g_2-*1*, C_{Val} **=27mg/ml**, **COOLING CRYSTALLISATION**, a)50°C, b) 40°C, c) 25°C, d) 15°C, 2-propanol/water, 1:1, v/v.

11.6.4 Nanodispersions size distribution - cooling crystallisation

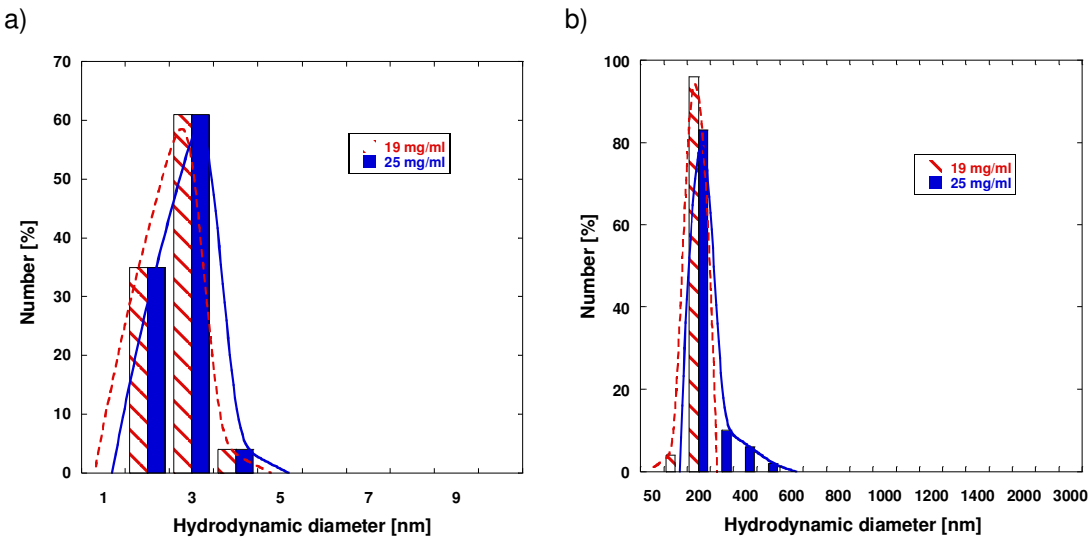

Figure 11.12 Nanodispersions estimated size distribution, **COOLING CRYSTALLISATION**, 2-propanol/water, 1:1, v/v, **first order fit**, C_{Val} =19 and 25mg/ml, a) clusters, b) droplets.

11.6.5 19 mg/ml, 2-propanol/water, 1:1, v/v, cooling - heating experiments

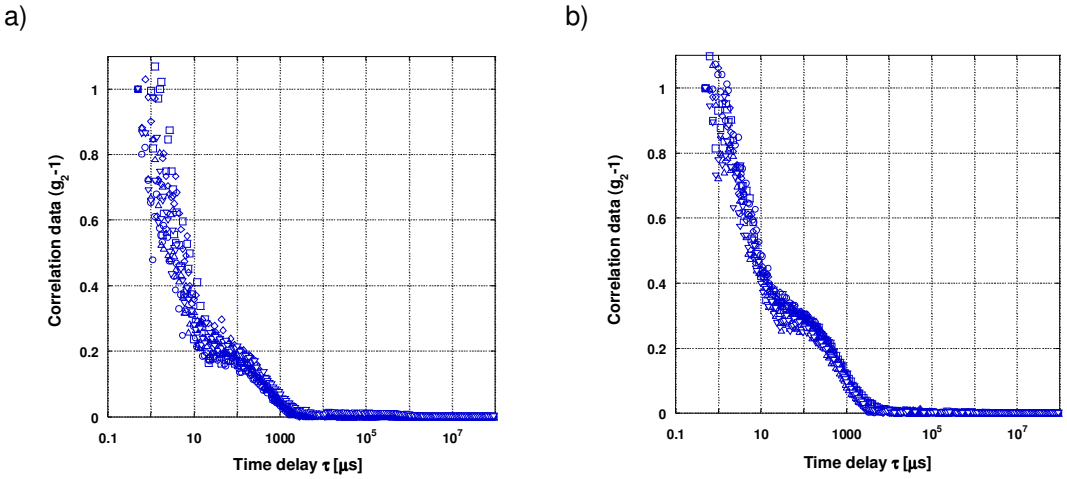

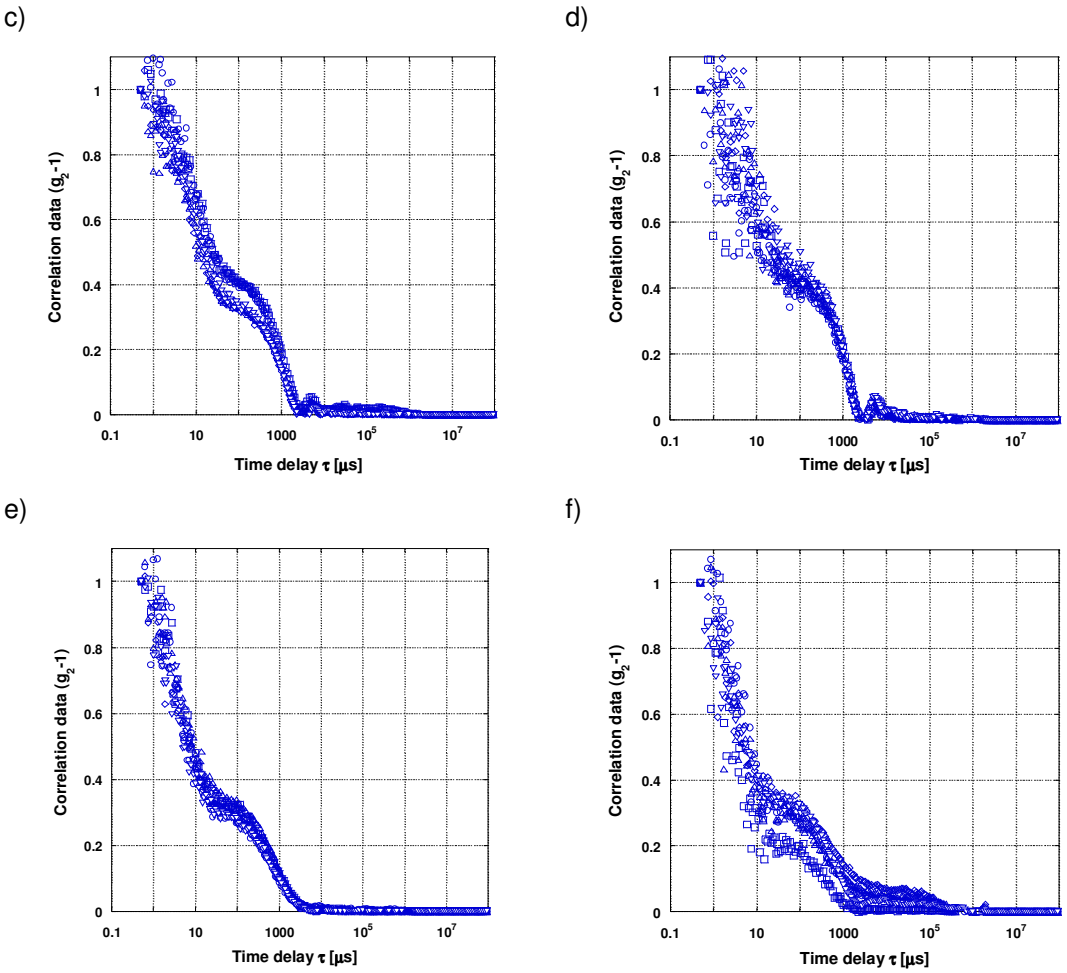

Figure 11.13 Light scattering autocorrelation functions *g_2-1*, **C_{Val} =19mg/ml**, **COOLING – HEATING EXPERIMENT**, a) 35˚C -cooling, b) 25˚C -cooling, c)12˚C -cooling, d) 12˚C –after 12hours, e) 25˚C – heating, f) 35˚C - heating, 2-propanol/water, 1:1, v/v.

11.6.6 D,L-valine microcrystals with 14.2mg/ml D,L-valine/2-propanol/water

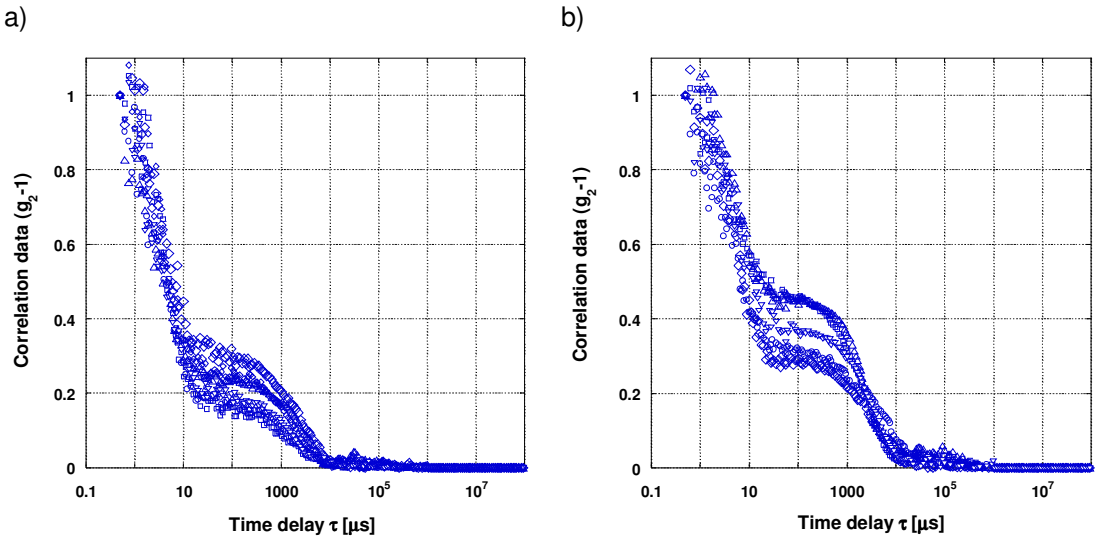

Figure 10.14 Light scattering autocorrelation functions g_2-*1*, of C_{Val}**= 14.2 mg/ml** D,L-valine/2-propanol/water filtered solution with D,L-valine microcrystals, after 4days keeping at 25°C and 3 days at 35°C,a) 35°C, b) 25°C.

11.7 COOLING CRYSTALLISATION – Glycine

11.7.1 270mg/ml glycine -DLS aqueous (H_2O) solution

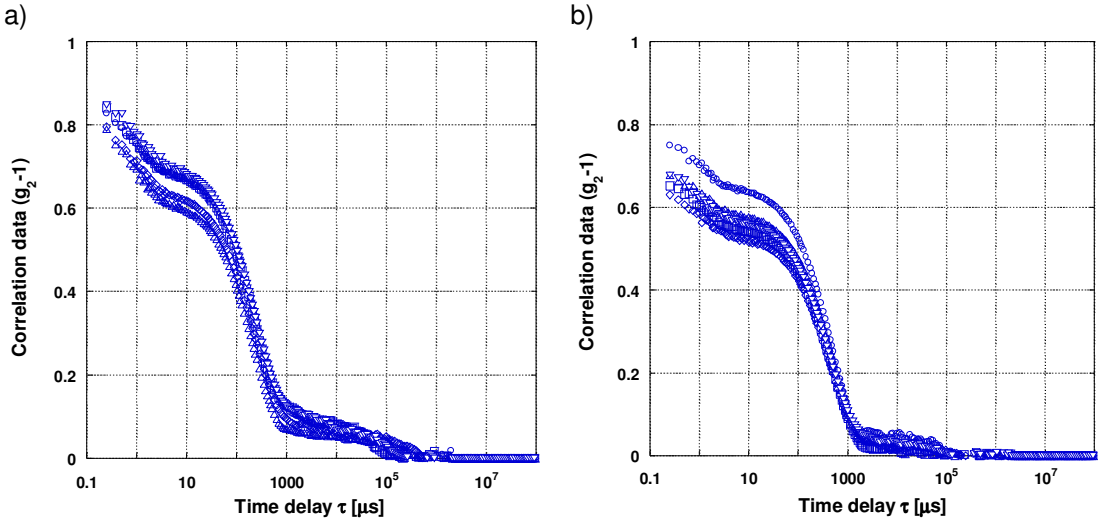

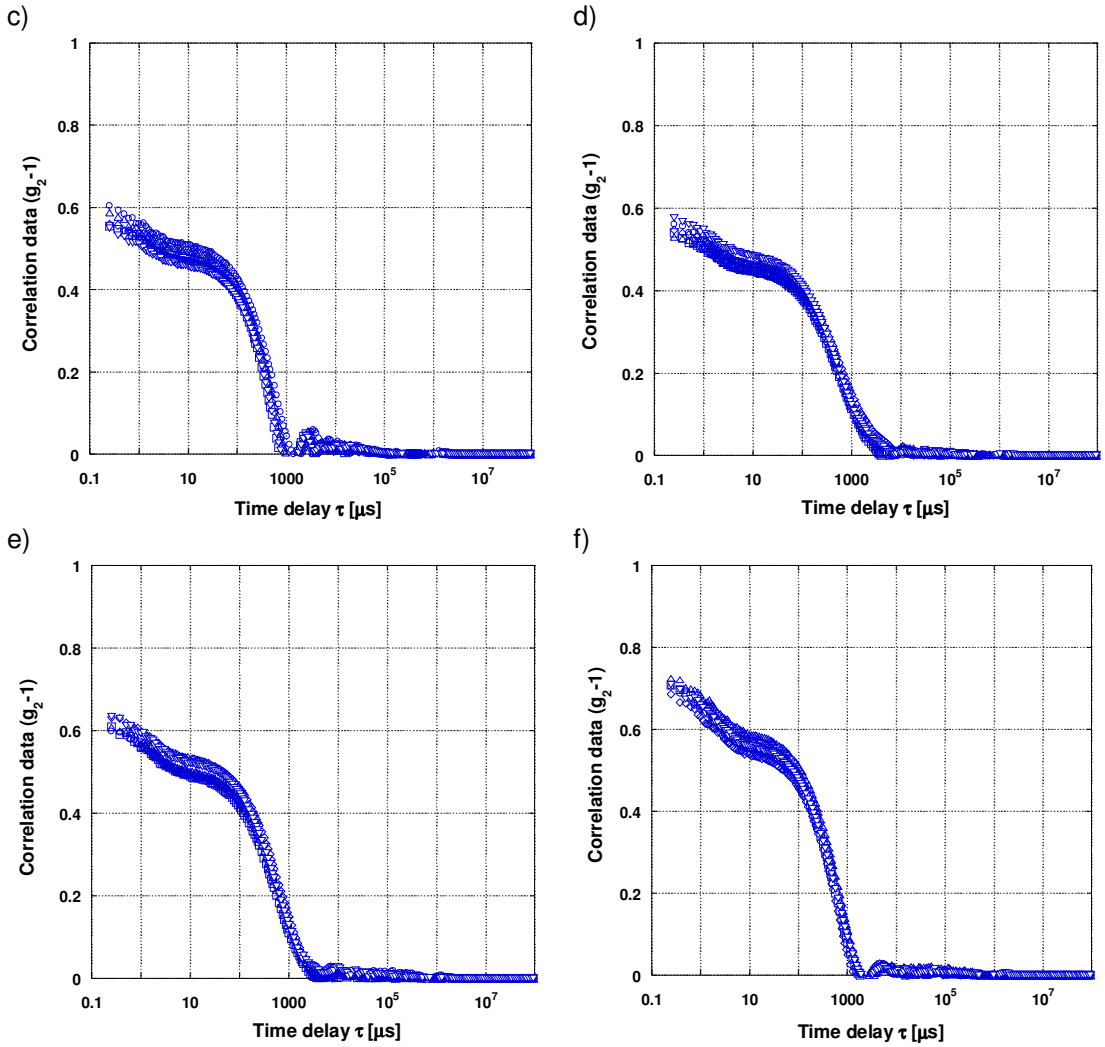

Figure 11.15 Light scattering autocorrelation functions g_2-*1*, $\mathbf{C_{Gly}}$**=270mg/ml**, solvent – water (H_2O), **COOLING CRYSTALLISATION**, a) 50°C, b) 40°C, c) 35°C, d) 30°C, e) 25°C, f) 20°C.

11.7.2 Water (H_2O) - DLS

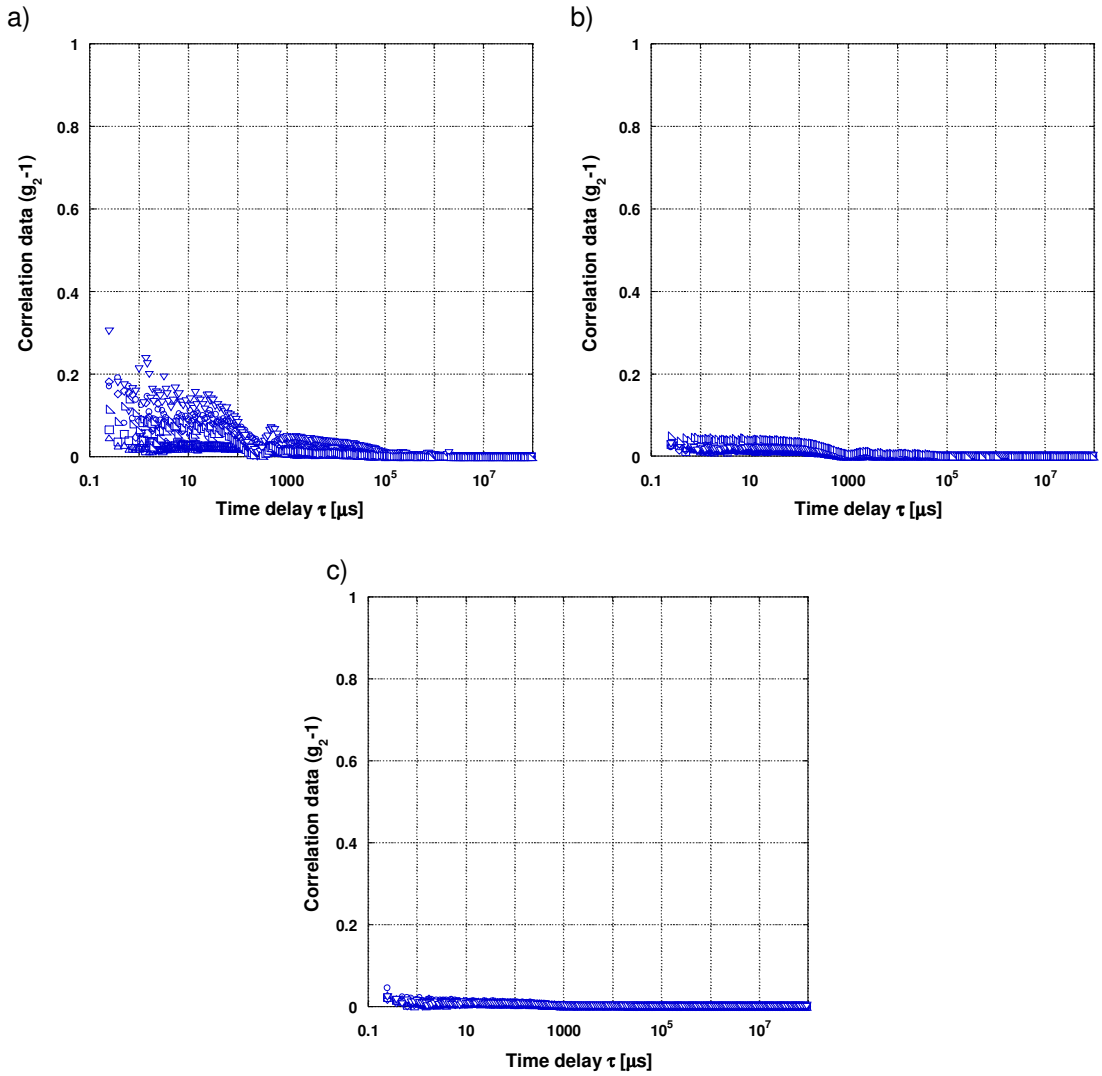

Figure 11.16 Light scattering autocorrelation functions *g_2-1*, **solvent - water (H_2O)**, COOLING CRYSTALLISATION, a) 55°C, b) 40°C, c) 25°C.

11.7.3 270mg/ml glycine -DLS aqueous (D_2O) solution

a)

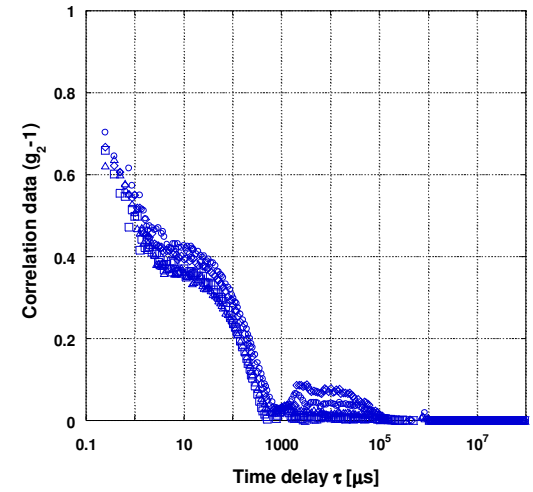

b)

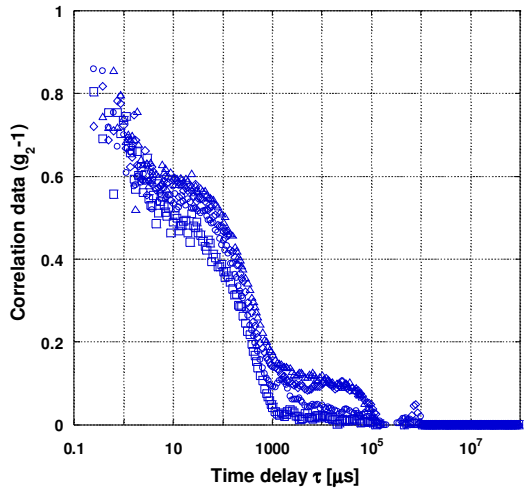

c)

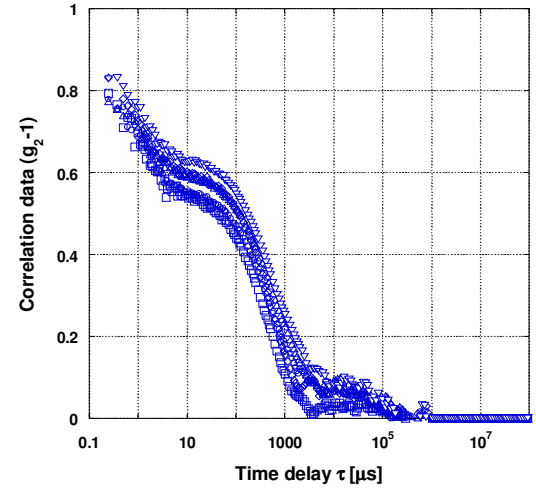

d)

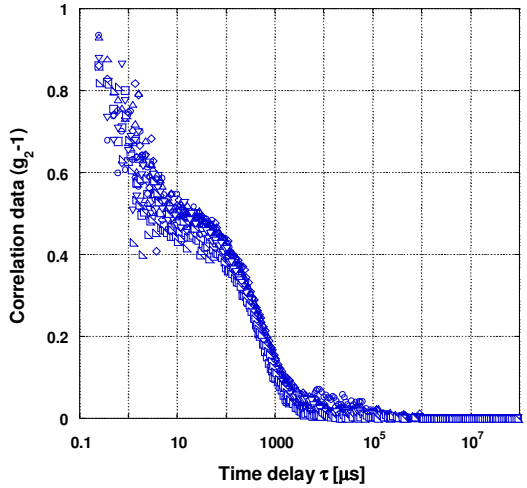

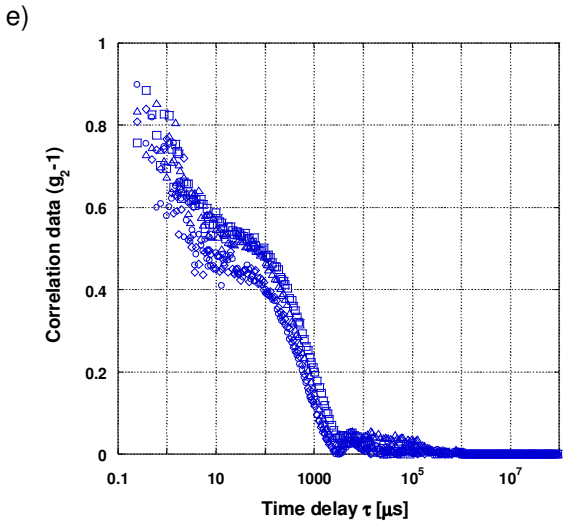

Figure 11.17 Light scattering autocorrelation functions g_2-*1*, C_{Gly}**=270mg/ml**, solvent – deuterium oxide (D_2O), **COOLING CRYSTALLISATION**, a) 55°C, b) 45°C, c) 35°C, d) 25°C, e) 20°C.

11.7.4 Deuterium Oxide (D_2O) - DLS

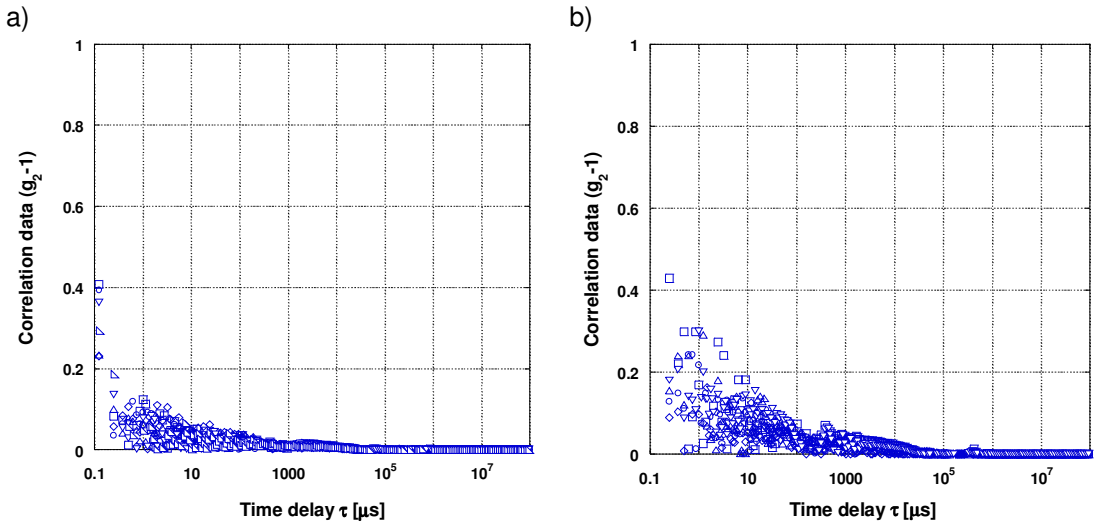

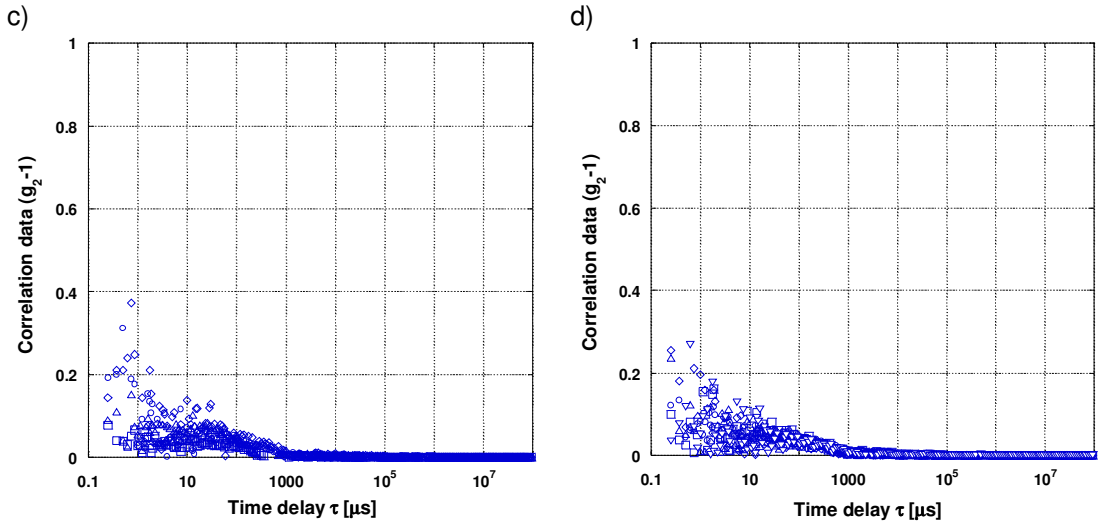

Figure 11.18 Light scattering autocorrelation functions *g_2-1*, solvent – deuterium oxide (D_2O), COOLING CRYSTALLISATION, a) 55°C, b) 45°C, c) 35°C, d) 25°C.

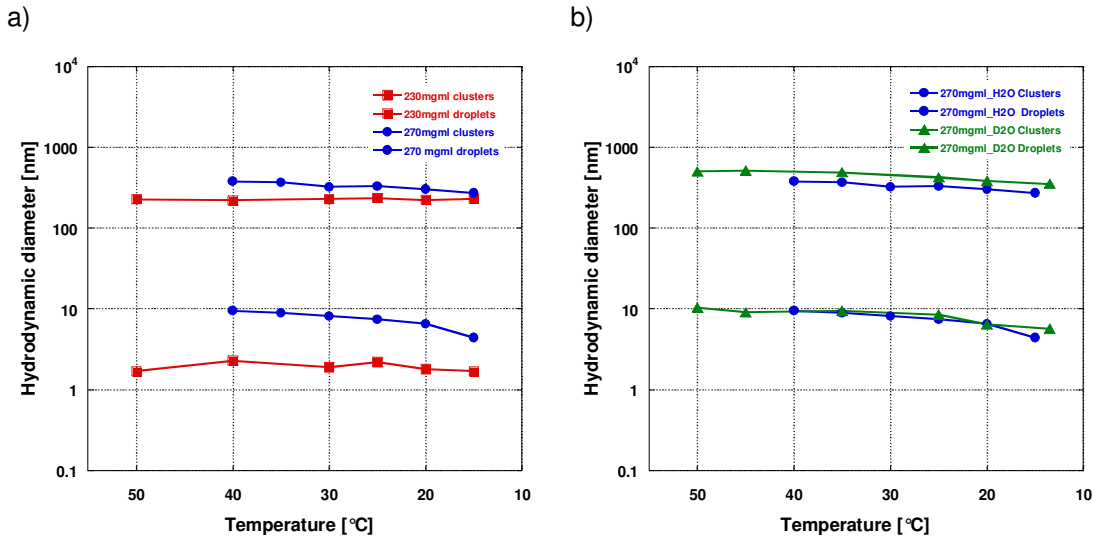

Figure 11.19 Average hydrodynamic diameters of clusters and droplets as a function of temperature, **COOLING CRYSTALLISATION**, **first order fit**, a) solvent - water (H_2O) C_{Gly} =230mg/ml and 270mg/ml, b) C_{Gly} =270mg/ml, solvent -deuterium oxide (D_2O).

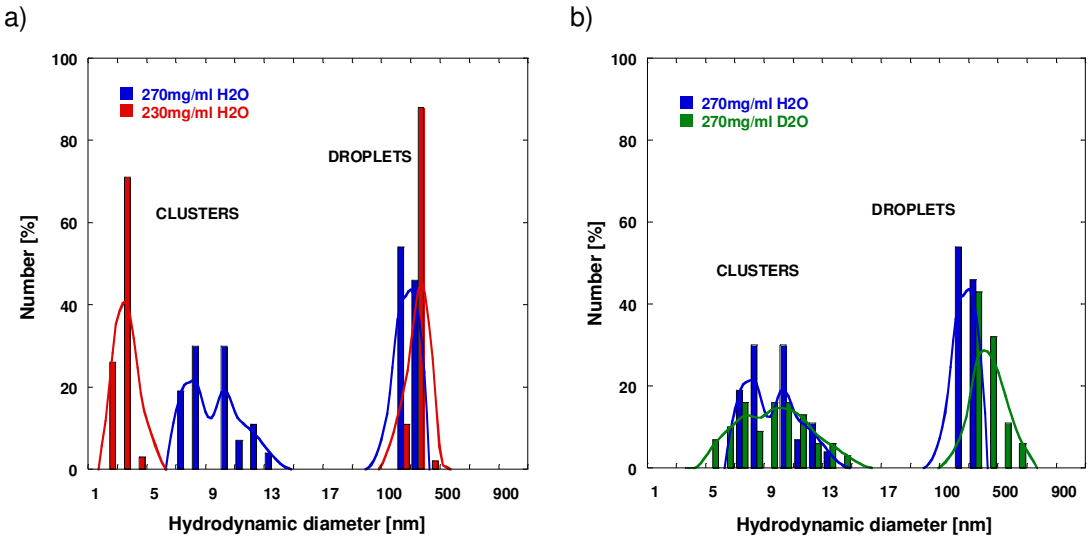

Figure 11.20 Nanodispersions estimated size distribution at 25°C, **COOLING CRYSTALLISATION**, **first order fit**, a) solvent - water (H_2O) C_{Gly} =230mg/ml and 270mg/ml, b) C_{Gly} =270mg/ml, solvent - deuterium oxide (D_2O).

11.8 Solvent viscosity and refractive index data.

Table 11.1 Viscosity and refractive index of 2-propanol/water solvent, different ratios at 25°C.

Solvent ratio 2-propanol:water	Viscosity [Pa·s] $\cdot 10^{-3}$	Refractive index
1:1	3.30	1.365
1:3	2.10	1.350
3:1	3.10	1.369
9:1	3.00	1.366

Table 11.2 Viscosity of 2-propanol/water, solvent 1:1, at different temperature.

Temperature [°C]	Viscosity [Pa·s] $\cdot 10^{-3}$
50	1.37
45	1.54
40	1.86
35	2.23
30	2.47
25	3.30
20	3.71
15	4.32

Table 11.3 Viscosity of H_2O and D_2O at different temperature.

Temperature [°C]	H_2O viscosity [Pa·s] $\cdot 10^{-3}$	D_2O viscosity [Pa·s] $\cdot 10^{-3}$
50	0.548	0.652
45	0.559	0.714
40	0.653	0.787
35	0.719	0.873
30	0.797	0.975
25	0.890	1.100
20	1.002	1.251
15	1.138	1.440

REFERENCES

Akers MJ, Milton N, Byrn SR, Nail SL. 1995. Pharmaceutical Research 12(10):1457-1461.

Akitt JW. 1992. NMR and chemistry. An introduction to modern NMR sceptroscopy.: Chaman&Hall.

Asakura T, Ishida M. 1989. Journal of Colloid and Interface Science 130(1):184-189.

ASTM_Standards. 2003. Annual Book of ASTM Standards, Water and Environment Technology. Standard test method for turbidity of water.

Atkins PW. 1986. Physical Chemistry: Oxford University Press.

Baldyga J, Bourne JR. 1999. Turbulet mixing in chemical reactions: John Wiley & Sons.

Bernstein J, Davey RJ, Henck JO. 1999. Angew. Chem.Int.Ed. 38(23):3440-3461.

Boldyreva EV, Drebushchak VA, Drebushchak TN, Paukov IE, Kovalevskaya YA, Shuova ES. 2003. Journal of Thermal Analysis and Calorimetry 73(2):409-418.

Bonnett PE, Carpenter KJ, Dawson S, Davey RJ. 2003. Chemical Communications 6:698-699.

Bourne JR, Kozicki F, Rys P. 1981. Chemical Engineering Science 36(10):1643-1648.

Brown W. 1993. Dynamic Light Scattering. The method and some applications.: Oxford Science Publications.

Canat D. 1991. Nulcear Magnetic Resonance concepts and methods.: John WIey&Sons.

Carteau D, Pianet I, Brunerie P, Guillemat B, Bassani DM. 2007. Langmuir 23(7):3561-3565.

Chattopadhyay S, Erdemir D, Evans JMB, Ilavsky J, Amenitsch H, Segre CU, Myerson AS. 2005. Crystal Growth & Design 5(2):523-527.

Chen HL, Hwang JC, Yang JM, Wang RC. 1998. Polymer 39(26):6983-6989.

Chiarella RA, Gillon AL, Burton RC, Davey RJ, Sadiq G, Auffret A, Cioffi M, Hunter CA. 2007. Faraday Discussions 136(179-193).

Cho CH, Urquidi J, Singh S, Robinson GW. 1999. Journal of Physical Chemistry B 103(11):1991-1994.

Cölfen H, Mann S. 2003. Angewandte Chemie 42(21):2350-2365.

Dalhus B, Gorbitz CH. 1996. Acta Crystallographica C 52:1759-1761.

Davey RJ, Allen K, Blagden N, Cross WI, Lieberman HF, Quayle MJ, Righini R, Seton L, Tiddy GJT. 2002a. Crystal Engineering Communications:257-264.

Davey RJ, Garside J. 2000. From Molecules to Crystallisers. An indroduction to crystallisation.: Oxford University Press.

Davey RJ, Liu W, Quayle MJ, Tiddy GJT. 2002b. Crystal Growth & Design 2(4):269-272.

Deneau E, Steele G. 2005. Organic Process Research & Development 9(6):943-950.

Ding X, Stringfellow TC, Robinson JR. 2004. Journal of Pharmaceutical Sciences 93(5):1351-1358.

Drews TO, Katsoulakis MA, Tsapatsis M. 2005. Journal of Physical Chemistry B 109:23879-23887.

Erdemir D, Chattopadhyay S, Guo L, Ilavsky J, Amenitsch H, Segre CU, Myerson AS. 2007. Physical Review Letters 99(11):115702/1-115702/4.

Erdemir D, Lee AY, Myerson AS. 2009. Accounts of Chemical Research 42(5):621-629.

Filobelo LF, Galkin O, Vekilov PG. 2005. Journal of Chemical Physics 123(1):014904/1-014904/7.

Finsy R. 1994. Advances in Colloid and Interface Science 52:79-143.

Flick EW. 1998. Industrial solvents handbook: William Andrew Publishing / Noyes.

Fokin VM, Zanotto ED. 2000. Journal of Non-Crystalline Solids 265(1-2):105-112.

Galkin O, Vekilov PG. 2000. Journal of American Chemical Society 122(1):156-163.

Galkin O, Vekilov PG. 2001. Journal of Crystal Growth 232(1-4):63-76.

Gavi E, Marchisio DL, Barresi AA. 2007. Chemical Engineering Science 62(8):2228-2235.

Georgalis Y, Kierzak AM, Saenger W. 2000. Journal of Physical Chemistry B 104(15):3405-3406.

Gidalevitz D, Feidenhans'l R, Matlis S, Smilgies DM, Christensen MJ, Leiserowitz L. 1997. Angew. Chem.Int.Ed.Engl. 24:4476-4481.

Gliko G, Neumaier N, Pan W, Haase I, Fisher M, Bacher A, Weinkauf W, Vekilov PG. 2005. Journal of American Chemical Society 127(10):3433-3438.

Gliko G, Pan W, Katsonis P, Neumaier N, Galkin O, Weinkauf S, Vekilov PG. 2007. Journal of Physical Chemistry B 111(12):3106-3114.

Haas C, Drenth J. 1999. Journal of Crystal Growth 196(2-4):388-394.

Hamad S, Hughes CE, Catlow CRA, Harris KDM. 2008. Journal of Physical Chemistry B 112(24):7280-7288.

Hamada K, Taka S, Lijima T, Mnina S. 1986. Journal of the Chemical Society 1(82):3141-3148.

Harwood LM, Claridge TDW. 1997. Introduction to organic spectroscopy.: Oxford University Press.

Heijna MCR, van Enckevort WJP, Vlieg E. 2007. Physical Review E 76(1):011604/1-011604/7.

Huang J, Stringfellow TC, Yu L. 2008. Journal of American Chemical Society 130(42):13973-13980.

Hughes CE, Hamad S, Harris KDM, Catlow CRA, Griffiths PC. 2007. Faraday Discussions 136:71-89.

Hughes CE, Harris KDM. 2009. New Journal of Chemistry 33(4):713-716.

Huo R, Wehrnes R, van Duynhoven J, Buydens LMC. 2003. Analitica Chimica Acta 490(1-2):231-251.

ISO13321. 1996. Internatrional Standard. Particle szie analysis- Photon correlation spectroscopy. First edition ed.

Itaka Y. 1961. Acta Cryst. 14:1-10.

Jelinska-Kazimierczuk M, Szydlowski J. 1996. Journal of Solution Chemistry 25(12):1175-1184.

Johnson BK, Prud'homme RK. 2003. AIChE 49(3):2264-2282.

Jones AG. 2002. Crystallization Process Systems: Butterworth-Heinemann.

Kashchiev D, Vekilov PG, Kolomeisky AB. 2005. Journal of Chemical Physics 122(24):244706/1-244706/6.

Kazakevich YV, LoBrutto R. 2007. HPLC for Pharmaceutical Scientists.: Wiley.

Kimura M. 2006. Crystal Growth & Design 6(4):854-860.

Kreiner M, Amarima Fernandes JF, O'Farrell N, Halling PJ, Parker MC. 2005a. Journal of Molecular Catalysis B 33(3-6):65-72.

Kreiner M, Fuglevand G, Moore BD, Parker MC. 2005b. Chemical Communications 21:2675-2676.

Kreiner M, Moore BD, Parker MC. 2001. Chemical Communications 12:1096-1097.

Lafferrere L, Hoff C, Veesler S. 2004a. Crystal Growth & Design 4(6):1175-1180.

Lafferrere L, Hoff C, Veesler S. 2004b. Journal of Crystal Growth 269(2-4):550-557.

Li M, Schnablegger H, Mann S. 1999. Letters to Nature 402:393-395.

Linder P, Zember T, Pusey PN. 2002a. Neutron, X-rays and light scattering methods to soft condensed matter. Dynamic Light Scattering.: Elsevier Science B.V.

Linder P, Zember T, Pusey PN. 2002b. Neutron, X-rays and light scattering methods to soft condensed matter. Introduction to Scattering experiments.: Elsevier Science B.V.

Lomakin A, Asherie N, Benedek GB. 2003. PANAS 100(18):10254-10257.

Lutsko JF, Nicolis G. 2006. Physical Review Letters 96(4):046102/1-046102/4.

Ma Y, Cölfen H, Antonietti M. 2006. Journal of Physical Chemistry B 110(22):10822-10828.

Mahajan AJ, Kirwan DJ. 1993. Journal of Physics D: Applied Physics 26(8B):B176-B180.

Mahajan AJ, Kirwan DJ. 1994. Journal of Crystal Growth 144(3-4):281-295.

Mallikarjunan M, Thyagaraja RS. 1969. Acta Crystallographica B 25:296-303.

Mann S, Heywood BR, Rajam S, Birchall JD. 1988. Letters to Nature 334(6184).

Marchisio DL, Rivautella J, Barresi AA. 2006. AIChE 52:1877-1881.

Medina DD, Mastai Y. 2008. Crystal Growth & Design 8(10):3646-3651.

Meyer VR. 2004. Practical High Preformance Liquid Chromatography.: Wiley.

Moreno A, Mas-Oliva J, Soriano-Garcia M, Salvador CO, Bolanos-Garcia VM. 2000. Journal of Molecular Structure 519:243-256.

Mullin JW. 1993. Crystallization: Third edition, Butterworth Heinemann.

Mullin JW, Leci CL. 1969. Philosophical Magazine 19:1075-1077.

Murugesan M, Cunningham D, Martinez-Albertos JL, Vercelj RM, Moore BD. 2005. Chemical Communications 21:2677-2679.

Myerson AS, Lo PY. 1990. Journal of Crystal Growth 99(1-4):1048-1052.

Niederberger M, Cölfen H. 2006. Physical Chemistry Chemical Physics 8(28):3271-3287.

Niimura N, Minezaki Y, Ataka M, Katsura T. 1995. Journal of Crystal Growth 154(1-2):136-144.

Onuma K, Kanzaki N. 2007. Journal of Crystal Growth 304(2):452-459.

Oxtoby DW, Kashchiev DA. 1994. Journal of Chemical Physics 100(10):7665-7771.

Parkinson JA. 2003. Advance methods in NMR spectroscopy. An introductory postgraduate lecture course at Strathclyde University.

Paul EL, Atiemo-Obeng VA, Kresta SM. 2004. Handbook of Industrial Mixing. Science and Practice.: Wiley-Interscience.

Paul EL, Treybal RE. 1971. AIChE 17(3):718-731.

Poznanski J, Szymanski J, Basinska T, Slomkowski S, Zielenkiewicz W. 2005. Journal of Molecular Liquids 212:21-26.

Price WS, Tsuchiya F, Arata Y. 1999. Journal of American Chemical Society 121(49):11503-11512.

Price WS, Tsuchiya F, Arata Y. 2001. Biophysical Journal 80(3):1585-1590.

Rein den Wolde P, Frenkel D. 1997. Science 277(5334):1975-1978.

Sauter C, Otalora F, Gavira JA, Vidal O, Giege R, Garcia-Ruiz JM. 2001. Acta Crystallographica D 57:1119-1126.

Schwahn D, Ma Y, Cölfen H. 2007. Journal of Physical Chemistry Letters C 111(8):3224-3227.

Shikii K, Sakamoto TC, Seki H, Utsumi H, Yamaguchi K. 2004. Thetrahedron 60(15):3487-3492.

Soh YS, Kim JH, Gryte CC. 1995. Polymer 36(19):3711-3717.

Sorensen TJ, Sontum PC, Samseth J, Thorsen G, Malthe-Sorenssen D. 2003. Chemical Engineering&Technology 26(3):307-312.

Spitaleri A, Hunter CA, McCabe JF, Packer MJ, Cockroft SL. 2004. Crystal Engineering Communications 6:489-493.

Talanquer V, Oxtoby DW. 1998. Journal of Chemical Physics 109(1):223-227.

Variny M, Alvarez de Miguel S, Moore BD, Sefcik J. 2008. Journal of Dispersion Science and Technology 29:617-620.

Veesler S, Lafferrere L, Garcia E, Hoff C. 2003. Organic Process Research & Development 7(6):983-989.

Veesler S, Revalor E, Bottini O, Hoff C. 2006. Organic Process Research & Development 10:841-845.

Vekilov PG. 2009. Interdisciplinary Transport Phenomena 1161:377-386.

Vekshin NL. 2002. Phitonics of biopolymers: Springer.

Vos J. 2006. Understanding the formation mechanism of protein coated microcrystals.

Wadsworth HM. 1990. Handbook of statistical methods for engineers and scientists.: Library of Congress Cataloging-in-Publication Data.

Waizumi K, Eguchi T. 2005. Chemistry Letters 34(12):1654-1655.

Wang X, Gillian JM, Kirwan DJ. 2006. Crystal Growth & Design 6(10):2214-2227.

Wang X, Kirwan DJ. 2006. Crystal Growth & Design 6(10):2228-2240.

Wang X, Ponder CS, Kirwan DJ. 2005. Crystal Growth & Design 5(1):85-92.

Weissbuch I, Torbeev VY, Leiserowitz L, Lahav M. 2005. Angew. Chem.Int.Ed. 44(21):3226-3229.

Xu AW, Ma Y, Cölfen H. 2007. Journal of Materials Chemistry 17(5):415-449.

Yalkowsky SH, He Y. 2003. Handbook of aqueous solubility data.: CRC Press.